

**INTELLIGENT DIAGNOSIS AND SMART
DETECTION OF CRACK IN A STRUCTURE
FROM ITS VIBRATION SIGNATURES**



Harish Chandra Das

Intelligent Diagnosis and Smart Detection of Crack in a Structure from its Vibration Signatures

Thesis Submitted to the

*Department of Mechanical Engineering
National Institute of Technology, Rourkela*

for award of the degree

of

Doctor of Philosophy

by

Harish Chandra Das

under the guidance of

Prof. Dayal R. Parhi

&

Prof. R.C.Kar



**Department of Mechanical Engineering
National Institute of Technology Rourkela
Orissa (India)-769008
December 2009**

Declaration

I hereby declare that this submission is my own work and that, to the best of my knowledge and belief, it contains no material previously published or written by another person nor material which to a substantial extent has been accepted for the award of any other degree or diploma of the university or other institute of higher learning, except where due acknowledgement has been made in the text.

(Harish Chandra Das)

Date:

Certificate

This is to certify that the thesis entitled, “Intelligent Diagnosis and Smart Detection of Crack in a Structure from its Vibration Signatures”, being submitted by Mr. Harish Chandra Das to the Department of Mechanical Engineering, National Institute of Technology, Rourkela, for the partial fulfillment of award of the degree Doctor of Philosophy, is a record of bona fide research work carried out by him under our supervision and guidance.

This thesis in our opinion, is worthy of consideration for award of the degree of Doctor of Philosophy in accordance with the regulation of the institute. To the best of our knowledge, the results embodied in this thesis have not been submitted to any other University or Institute for the award of any degree or diploma.

Prof. D.R. Parhi
(Supervisor)

Prof. R.C. Kar
(Co-Supervisor)

ROURKELA

Acknowledgements

I would like to express my gratitude to all those people who made this research possible and those who have made my experience in the Institute one that I will always remember fondly. First and foremost I wish to thank my supervisor, Prof. Dayal R. Parhi, Professor of Mechanical Engineering, N.I.T, Rourkela, for kindly providing me an opportunity to work under his supervision and guidance. His patience, stimulating suggestions and encouragement helped me in all the time of research for and writing of this thesis.

I wish to thank my second supervisor, Dr. R.C. Kar for his priceless suggestions and for directing the PhD on to the right track. He has been supportive since the days I began working on this research.

I am thankful to Prof. Sunil Kumar Sarangi, Director of National Institute of Technology, for giving me an opportunity to work under the supervision of Prof. Dayal R. Parhi. I am thankful to Prof. R.K. Sahoo, Head of the Department, Department of Mechanical Engineering, for his moral support and valuable suggestions regarding the research work.

I express my deepest gratitude to Prof. Manojranjan Nayak, President, Siksha O Anusandhan University, Bhubaneswar, Orissa, who gave me the opportunity of pursuing this research work .His constant inspiration, encouragement and valuable advice have profoundly contributed to the completion of the present thesis.

I am thankful to Mr. Amiya kumar Dash, research scholar, who has helped me a lot in compilation of this thesis.

Finally I would like to thank my wife, Mrs. Lipika Das, for all her support and encouragement. I thank my daughter, Ms. Barsha Das and son Mr. Adarsh Das, for giving me so much joy now and so much to look forward to.

Synopsis

In recent years, there has been a growing interest in the development of structural health monitoring for vibrating structures, especially crack detection methodologies and on-line diagnostic techniques. In the current research, methodologies have been developed for damage detection of a cracked cantilever beam using analytical, fuzzy logic, neural network and fuzzy neuro techniques. The presence of a crack in a structural member introduces a local flexibility that affects its dynamic response. For finding out the deviation in the vibrating signatures of the cracked cantilever beam the local stiffness matrices are taken into account. Theoretical analyses have been carried out to calculate the natural frequencies and mode shapes of the cracked cantilever beam using local stiffness matrices. Strain energy release rate has been used for calculating the local stiffness of the beam. The fuzzy inference system has been designed using the first three relative natural frequencies and mode shapes as input parameters. The output from the fuzzy controller is relative crack location and relative crack depth. Several fuzzy rules have been developed using the vibration signatures of the cantilever beam. A Neural Network technique using multi layered back propagation algorithm has been developed for damage assessment using the first three relative natural frequencies and mode shapes as input parameters and relative crack location and relative crack depth as output parameters. Several training patterns are derived for designing the Neural Network. A hybrid fuzzy-neuro intelligent system has been formulated for fault identification.

The fuzzy controller is designed with six input parameters and two output parameters. The input parameters to the fuzzy system are relative deviation of first three natural frequencies and first three mode shapes. The output parameters of the fuzzy system are initial relative crack depth and initial relative crack location. The input parameters to the neural controller are relative deviation of first three natural frequencies and first three mode shapes along with the interim outputs of fuzzy controller. The output parameters of the fuzzy-neuro system are final relative crack depth and final relative crack location. A series of fuzzy rules and training patterns are derived for the fuzzy and neural system respectively to predict the final crack location and final crack depth. To diagnose the crack in the vibrating structure multiple

adaptive neuro-fuzzy inference system (MANFIS) methodology has been applied. The final outputs of the MANFIS are relative crack depth and relative crack location. Several hundred fuzzy rules and neural network training patterns are derived using natural frequencies, mode shapes, crack depths and crack locations.

The proposed research work aims to broaden the development in the area of fault detection of dynamically vibrating structures. This research also addresses the accuracy for detection of crack location and depth with considerably low computational time. The objective of the research is related to design of an intelligent controller for prediction of damage location and severity in a uniform cracked cantilever beam using AI techniques (i.e. Fuzzy, neural, adaptive neuro-fuzzy and Manfis).

Table of Contents

Declaration.....	iii
Certificate	iv
Acknowledgements	v
Synopsis.....	vi
Contents	viii
List of Tables	xii
List of Figures.....	xiii
List of Symbols	xxvi
1 INTRODUCTION	1
1.1 Background and Motivation	1
1.2 Aims & Objectives of this Research	3
1.3 Outline of the Research Work	6
2 LITERATURE REVIEW	8
2.1 Introduction	8
2.2 History and Development of Dynamic Analysis of Cracked Structure	9
2.2.1 <i>Structural Vibration and its Analysis</i>	10
2.2.2 <i>Dynamics of Cracked Structures</i>	11
2.3 Effect of Different Parameters on Dynamic Response of Cracked Structures	12
2.4 Dynamic Characteristics of Beam with Transverse Crack	13
2.5 Damage Diagnosis by Artificial Intelligence Technique	26
2.5.1 <i>Fuzzy Logic Technique for Damage Diagnosis</i>	27
2.5.1.1 <i>Fuzzy History</i>	27
2.5.1.2 <i>Application of Fuzzy Logic</i>	28
2.5.1.3 <i>Application of Fuzzy Logic for Fault Diagnosis</i>	28
2.5.2 <i>Neural Network Technique for Damage Diagnosis</i>	30
2.5.2.1 <i>Neural Network History</i>	31

2.5.2.2	<i>Application of Neural Network</i>	31
2.5.2.3	<i>Application of Neural Network for Fault Diagnosis</i>	33
2.5.3	<i>Neuro-Fuzzy Technique for Damage Diagnosis</i>	38
2.5.3.1	<i>Neuro-Fuzzy Technique History</i>	38
2.5.3.2	<i>Application of Neuro-Fuzzy Technique</i>	39
2.5.3.3	<i>Appilication of Neuro-Fuzzy Technique for Fault Diagnosis</i>	39
2.5.4	<i>Multiple Adaptive Neuro Fuzzy Inference Technique (MANFIS) for Damage Diagnosis</i>	40
2.5.4.1	<i>MANFIS History</i>	40
2.5.4.2	<i>Application of MANFIS</i>	41
2.5.4.3	<i>Application of MANFIS for Fault Diagnosis</i>	41
3	ANALYSIS OF DYNAMIC CHARACTERISTICS OF BEAM WITH TRANSVERSE CRACK	44
3.1	Introduction	44
3.2	Dynamic Characteristics of a Cantilever Beam with a Transverse Crack	45
3.2.1	<i>Theoretical Analysis</i>	45
3.2.1.1	<i>Local Flexibility of a Cracked Cantilever Beam under Bending and Axial Loading</i>	45
3.2.1.2	<i>Free Vibration Analysis of the Cracked Cantilever Beam</i>	49
3.2.1.3	<i>Forced Vibration analysis of Cracked Cantilever Beam</i>	52
3.2.2	<i>Numerical Analysis</i>	53
3.2.2.1	<i>Results of Numerical Analysis</i>	53
3.3	Analysis of Experimental Results	129
3.3.1	<i>Experimental Results</i>	129
3.3.2	<i>Comparison among the Results of Numerical and Experimental Analyses</i>	134
3.4	Discussions	135
3.5	Summary	137
4	ANALYSIS OF FUZZY LOGIC TECHNIQUE FOR CRACK DETECTION	138
4.1	Introduction	138
4.2	Fuzzy Inference System	140
4.2.1	<i>Membership Functions</i>	140
4.2.2	<i>Fuzzy Logic Controllers (FLC) and Fuzzy Reasoning Rules</i>	142

4.2.3	<i>Defuzzification</i>	143
4.3	Analysis of the Fuzzy Controller used for Crack Detection	144
4.3.1	<i>Fuzzy Mechanism for Crack Detection</i>	144
4.3.2	<i>Fuzzy Controller for Finding out Crack Depth and Crack Location</i>	145
4.3.3	<i>Results of Fuzzy Controller</i>	146
4.4	Discussions	147
4.5	Summary	157
5	ANALYSIS OF ARTIFICIAL NEURAL NETWORK FOR CRACK DETECTION	158
5.1	Introduction	158
5.2	Neural Network Technique	161
5.2.1	<i>Design of Neural Network</i>	161
5.2.2	<i>Activation Function</i>	163
5.2.2.1	<i>Threshold Activation Function</i>	164
5.2.2.2	<i>Ramping Activation Function</i>	164
5.2.2.3	<i>Hyperbolic Tangent Activation Function</i>	165
5.2.3	<i>Modeling of Back Propagation Neural Network</i>	165
5.3	Analysis of Neural Network Controller used for Crack Detection	166
5.3.1	<i>Neural Controller Mechanism for Crack Detection</i>	167
5.3.2	<i>Neural Controller for Finding out Crack Depth and Crack Location</i>	171
5.4	<i>Results of Neural Controller</i>	175
5.5	Discussions	175
5.6	Summary	176
6	ANALYSIS OF HYBRID FUZZY-NEURO SYSTEM FOR CRACK DETECTION	177
6.1	Introduction	177
6.2	Analysis of Fuzzy-Neuro Controller	178
6.2.1	<i>Analysis of the Fuzzy Segment of Fuzzy-Neuro Controller</i>	179
6.2.2	<i>Analysis of the Neural Segment of Fuzzy-Neuro Controller</i>	183
6.2.3	<i>Results of Fuzzy-Neuro Controller</i>	184
6.3	Discussions	187
6.4	Summary	187

7 ANALYSIS OF MANFIS FOR CRACK DETECTION	188
7.1 Introduction	189
7.2 Analysis of Multiple Adaptive Neuro-Fuzzy Inference System for Crack Detection	190
7.3 Results of MANFIS Controller	197
7.4 Discussions	200
7.5 Summary	200
8 ANALYSIS AND DESCRIPTION OF EXPERIMENTAL SETUP	201
8.1 Description of Instruments used in the Experimental Analysis	201
8.2 Experimental Set-up	204
8.3 Experimental Procedure	207
8.4 Experimental Results and Discussions	207
9 RESULTS & DISCUSSIONS	209
9.1 Introduction	209
9.2 Discussions of Results	209
10 CONCLUSIONS AND FURTHER WORK	213
10.1 Contributions	213
10.2 Conclusions	214
10.3 Applications	215
10.4 Scope for Future Work	216
REFERENCES	217
PUBLISHED PAPERS	240

List of Tables

Table 3.3.1	Comparison of results between numerical and experimental analyses...	135
Table 4.3.1	Description of fuzzy linguistic terms.....	151
Table 4.3.2	Examples of twenty fuzzy rules being used in fuzzy controller.....	152
Table 4.3.3	Comparison of results between triangular, gaussian and trapezoidal fuzzy controller, numerical analysis and experimental analysis.....	156
Table 5.3.1	Examples of the training patterns for training of the neural network controller.....	171
Table 5.3.2	Comparison of results between neural controller, fuzzy controller, numerical analysis and experimental analysis.....	174
Table 6.2.1	Comparison of the results of the fuzzy-neuro controllers with the results of numerical and experimental analyses.....	185
Table 6.2.2	Comparison of the results of the fuzzy-neuro controllers with the results of neural and fuzzy controllers.....	186
Table 7.3.1	Comparison of the results of the MANFIS with the results of numerical and experimental analysis	198
Table 7.3.2	Comparison of the results of the MANFIS with the results of fuzzu-neuro, neural and fuzzy controller analysis	199

List of Figures

Fig. 3.2.1	Geometry of beam, (a) cantilever beam, (b) cross-sectional view of the beam. (c) segments taken during integration at the crack section.....	45
Fig. 3.2.2	Relative crack depth (a_1/W) vs. dimensionless compliance ($\ln(\overline{C_{xy}})$)....	48
Fig. 3.2.3	Beam model.....	49
Fig.3.2.4 (a)	Relative amplitude vs. relative distance from the fixed end (1 st mode of vibration), $a_1/W=0.1$, $L_1/L=0.0256$	54
Fig. 3.2.4(a1)	Magnified view of Fig. 3.2.4(a) at the vicinity of the crack location.....	54
Fig.3.2.4 (b)	Relative amplitude vs. relative distance from the fixed end (2 nd mode of vibration), $a_1/W=0.1$, $L_1/L=0.0256$	55
Fig. 3.2.4(b1)	Magnified view of Fig. 3.2.4(b) at the vicinity of the crack location.....	55
Fig.3.2.4 (c)	Relative amplitude vs. relative distance from the fixed end (3 rd mode of vibration), $a_1/W=0.1$, $L_1/L=0.0256$	56
Fig. 3.2.4(c1)	Magnified view of Fig. 3.2.4(c) at the vicinity of the crack location.....	56
Fig.3.2.5 (a)	Relative amplitude vs. relative distance from the fixed end (1 st mode of vibration), $a_1/W=0.2$, $L_1/L=0.0256$	57
Fig. 3.2.5(a1)	Magnified view of Fig. 3.2.5(a) at the vicinity of the crack location.....	57
Fig.3.2.5 (b)	Relative amplitude vs. relative distance from the fixed end (2 nd mode of vibration), $a_1/W=0.2$, $L_1/L=0.0256$	58
Fig. 3.2.5 (b1)	Magnified view of Fig. 3.2.5(b) at the vicinity of the crack location.	58
Fig.3.2.5 (c)	Relative amplitude vs. relative distance from the fixed end (3 rd mode of vibration), $a_1/W=0.2$, $L_1/L=0.0256$	59
Fig. 3.2.5(c1)	Magnified view of Fig. 3.2.5(c) at the vicinity of the crack location.....	59
Fig.3.2.6 (a)	Relative amplitude vs. relative distance from the fixed end (1 st mode of vibration), $a_1/W=0.3$, $L_1/L=0.0256$	60
Fig. 3.2.6(a1)	Magnified view of Fig. 3.2.6(a) at the vicinity of the crack location.....	60

Fig.3.2.6 (b)	Relative amplitude vs. relative distance from the fixed end (2 nd mode of vibration), $a_1/W=0.3$, $L_1/L=0.0256$	61
Fig. 3.2.6(b1)	Magnified view of Fig. 3.2.6(b) at the vicinity of the crack location.....	61
Fig.3.2.6 (c)	Relative amplitude vs. relative distance from the fixed end (3 rd mode of vibration), $a_1/W=0.3$, $L_1/L=0.0256$	62
Fig. 3.2.6(c1)	Magnified view of Fig. 3.2.6(c) at the vicinity of the crack location.....	62
Fig.3.2.7 (a)	Relative amplitude vs. relative distance from the fixed end (1 st mode of vibration), $a_1/W=0.4$, $L_1/L=0.0256$	63
Fig. 3.2.7(a1)	Magnified view of Fig. 3.2.7(a) at the vicinity of the crack location.....	63
Fig.3.2.7 (b)	Relative amplitude vs. relative distance from the fixed end (2 nd mode of vibration), $a_1/W=0.4$, $L_1/L=0.0256$	64
Fig. 3.2.7(b1)	Magnified view of Fig. 3.2.7(b) at the vicinity of the crack location.....	64
Fig.3.2.7 (c)	Relative amplitude vs. relative distance from the fixed end (3 rd mode of vibration), $a_1/W=0.4$, $L_1/L=0.0256$	65
Fig. 3.2.7(c1)	Magnified view of Fig. 3.2.7(c) at the vicinity of the crack location.....	65
Fig.3.2.8 (a)	Relative amplitude vs. relative distance from the fixed end (1 st mode of vibration), $a_1/W=0.1$, $L_1/L=0.0513$	66
Fig. 3.2.8(a1)	Magnified view of Fig. 3.2.8 (a) at the vicinity of the crack location....	66
Fig.3.2.8 (b)	Relative amplitude vs. relative distance from the fixed end (2 nd mode of vibration), $a_1/W=0.1$, $L_1/L=0.0513$	67
Fig. 3.2.8(b1)	Magnified view of Fig. 3.2.8 (b) at the vicinity of the crack location...	67
Fig. 3.2.8 (c)	Relative amplitude vs. relative distance from the fixed end (3 rd mode of vibration), $a_1/W=0.1$, $L_1/L=0.0513$	68
Fig. 3.2.8 (c1)	Magnified view of Fig. 3.2.8 (c) at the vicinity of the crack location.....	68
Fig.3.2.9 (a)	Relative amplitude vs. relative distance from the fixed end(1 st mode of vibration), $a_1/W=0.2$, $L_1/L=0.0513$	69
Fig. 3.2.9 (a1)	Magnified view of Fig. 3.2.9 (a) at the vicinity of the crack location....	69

Fig.3.2.9 (b)	Relative amplitude vs. relative distance from the fixed end (2 nd mode of vibration), $a_1/W=0.2$, $L_1/L=0.0513$	70
Fig. 3.2.9(b1)	Magnified view of Fig. 3.2.9 (b) at the vicinity of the crack location...	70
Fig.3.2.9 (c)	Relative amplitude vs. relative distance from the fixed end (3 rd mode of vibration), $a_1/W=0.2$, $L_1/L=0.0513$	71
Fig. 3.2.9 (c1)	Magnified view of Fig. 3.2.9 (c) at the vicinity of the crack location.....	71
Fig.3.2.10 (a)	Relative amplitude vs. relative distance from the fixed end (1 st mode of vibration), $a_1/W= 0.3$, $L_1/L=0.0513$	72
Fig. 3.2.10 (a1)	Magnified view of fig. 3.2.10 (a) at the vicinity of the crack location.	72
Fig.3.2.10 (b)	Relative amplitude vs. relative distance from the fixed end (2 nd mode of vibration), $a_1/W=0.3$, $L_1/L=0.0513$	73
Fig. 3.2.10 (b1)	Magnified view of Fig. 3.2.10 (b) at the vicinity of the crack location...	73
Fig.3.2.10 (c)	Relative amplitude vs. relative distance from the fixed end (3 rd mode of vibration), $a_1/W=0.3$, $L_1/L=0.0513$	74
Fig. 3.2.10 (c1)	Magnified view of Fig. 3.2.10 (c) at the vicinity of the crack location....	74
Fig.3.2.11 (a)	Relative amplitude vs. relative distance from the fixed end (1 st mode of vibration), $a_1/W=0.4$, $L_1/L=0.0513$	75
Fig. 3.2.11 (a1)	Magnified view of Fig. 3.2.11 (a) at the vicinity of the crack location....	75
Fig. 3.2.11 (b)	Relative amplitude vs. relative distance from the fixed end (2 nd mode of vibration), $a_1/W=0.4$, $L_1/L=0.0513$	76
Fig. 3.2.11(b1)	Magnified view of Fig. 3.2.11 (b) at the vicinity of the crack location...	76
Fig.3.2.11 (c)	Relative amplitude vs. relative distance from the fixed end (3 rd mode of vibration), $a_1/W=0.4$, $L_1/L=0.0513$	77
Fig. 3.2.11 (c1)	Magnified view of Fig. 3.2.11 (c) at the vicinity of the crack location.	77
Fig.3.2.12 (a)	Relative amplitude vs. relative distance from the fixed end (1 st mode of vibration), $a_1/W=0.1$, $L_1/L=0.1795$	78
Fig. 3.2.12 (a1)	Magnified view of Fig. 3.2.12 (a) at the vicinity of the crack location...	78

Fig. 3.2.12 (b)	Relative amplitude vs. relative distance from the fixed end (2 nd mode of vibration), $a_1/W=0.1$, $L_1/L=0.1795$	79
Fig. 3.2.12 (b1)	Magnified view of Fig. 3.2.12 (b) at the vicinity of the crack location..	79
Fig. 3.2.12 (c)	Relative amplitude vs. relative distance from the fixed end (3 rd mode of vibration), $a_1/W=0.1$, $L_1/L=0.1795$	80
Fig. 3.2.12 (c1)	Magnified view of Fig. 3.2.12 (c) at the vicinity of the crack location...	80
Fig.3.2.13 (a)	Relative amplitude vs. relative distance from the fixed end (1 st mode of vibration), $a_1/W=0.2$, $L_1/L=0.1795$	81
Fig. 3.2.13 (a1)	Magnified view of Fig. 3.2.13 (a) at the vicinity of the crack location..	81
Fig. 3.2.13 (b)	Relative amplitude vs. relative distance from the fixed end (2 nd mode of vibration), $a_1/W=0.2$, $L_1/L=0.1795$	82
Fig. 3.2.13(b1)	Magnified view of Fig. 3.2.13 (b) at the vicinity of the crack location...	82
Fig.3.2.13 (c)	Relative amplitude vs. relative distance from the fixed end (3 rd mode of vibration), $a_1/W=0.2$, $L_1/L=0.1795$	83
Fig. 3.2.13 (c1)	Magnified view of Fig. 3.2.13 (c) at the vicinity of the crack location....	83
Fig.3.2.14 (a)	Relative amplitude vs. relative distance from the fixed end (1 st mode of vibration), $a_1/W=0.3$, $L_1/L=0.1795$	84
Fig. 3.2.14 (a1)	Magnified view of Fig. 3.2.14 (a) at the vicinity of the crack location...	84
Fig.3.2.14 (b)	Relative amplitude vs. relative distance from the fixed end (2 nd mode of vibration), $a_1/W=0.3$, $L_1/L=0.1795$	85
Fig. 3.2.14(b1)	Magnified view of Fig. 3.2.14(b) at the vicinity of the crack location....	85
Fig.3.2.14 (c)	Relative amplitude vs. relative distance from the fixed end (3 rd mode of vibration), $a_1/W=0.3$, $L_1/L=0.1795$	86
Fig. 3.2.14(c1)	Magnified view of Fig. 3.2.14(c) at the vicinity of the crack location.....	86
Fig.3.2.15 (a)	Relative amplitude vs. relative distance from the fixed end (1 st mode of vibration), $a_1/W=0.4$, $L_1/L=0.1795$	87
Fig. 3.2.15 (a1)	Magnified view of Fig. 3.2.15 (a) at the vicinity of the crack location...	87

Fig.3.2.15 (b)	Relative amplitude vs. relative distance from the fixed end (2 nd mode of vibration), $a_1/W=0.4$, $L_1/L=0.1795$	88
Fig. 3.2.15(b1)	Magnified view of Fig. 3.2.15(b) at the vicinity of the crack location....	88
Fig.3.2.15 (c)	Relative amplitude vs. relative distance from the fixed end (3 rd mode of vibration), $a_1/W=0.4$, $L_1/L=0.1795$	89
Fig. 3.2.15(c1)	Magnified view of Fig. 3.2.15(c) at the vicinity of the crack location.....	89
Fig.3.2.16 (a)	Relative amplitude vs. relative distance from the fixed end (1 st mode of vibration), $a_1/W=0.1$, $L_1/L=0.2564$	90
Fig. 3.2.16(a1)	Magnified view of Fig. 3.2.16(a) at the vicinity of the crack location.....	90
Fig.3.2.16 (b)	Relative amplitude vs. relative distance from the fixed end (2 nd mode of vibration), $a_1/W=0.1$, $L_1/L=0.2564$	91
Fig. 3.2.16(b1)	Magnified view of Fig. 3.2.16(b) at the vicinity of the crack location....	91
Fig. 3.2.16 (c)	Relative amplitude vs. relative distance from the fixed end (3 rd mode of vibration), $a_1/W=0.1$, $L_1/L=0.2564$	92
Fig. 3.2.16 (c1)	Magnified view of Fig. 3.2.16 (c) at the vicinity of the crack location....	92
Fig.3.2.17 (a)	Relative amplitude vs. relative distance from the fixed end (1 st mode of vibration), $a_1/W=0.2$, $L_1/L=0.2564$	93
Fig. 3.2.17 (a1)	Magnified view of Fig. 3.2.17 (a) at the vicinity of the crack location....	93
Fig.3.2.17 (b)	Relative amplitude vs. relative distance from the fixed end (2 nd mode of vibration), $a_1/W=0.2$, $L_1/L=0.2564$	94
Fig. 3.2.17(b1)	Magnified view of Fig. 3.2.17(b) at the vicinity of the crack location....	94
Fig. 3.2.17 (c)	Relative amplitude vs. relative distance from the fixed end (3 rd mode of vibration), $a_1/W=0.2$, $L_1/L=0.2564$	95
Fig. 3.2.17 (c1)	Magnified view of Fig. 3.2.17 (c) at the vicinity of the crack location....	95
Fig.3.2.18 (a)	Relative amplitude vs. relative distance from the fixed end (1 st mode of vibration), $a_1/W=0.3$, $L_1/L=0.2564$	96
Fig. 3.2.18 (a1)	Magnified view of Fig. 3.2.18 (a) at the vicinity of the crack location....	96

Fig.3.2.18 (b)	Relative amplitude vs. relative distance from the fixed end (2 nd mode of vibration), $a_1/W=0.3$, $L_1/L=0.2564$	97
Fig. 3.2.18(b1)	Magnified view of Fig. 3.2.18 (b) at the vicinity of the crack location...	97
Fig. 3.2.18 (c)	Relative amplitude vs. relative distance from the fixed end (3 rd mode of vibration), $a_1/W=0.3$, $L_1/L=0.2564$	98
Fig. 3.2.18 (c1)	Magnified view of Fig. 3.2.18 (c) at the vicinity of the crack location...	98
Fig.3.2.19 (a)	Relative amplitude vs. relative distance from the fixed end (1 st mode of vibration), $a_1/W=0.4$, $L_1/L=0.2564$	99
Fig. 3.2.19 (a1)	Magnified view of Fig. 3.2.19 (a) at the vicinity of the crack location..	99
Fig.3.2.19 (b)	Relative amplitude vs. relative distance from the fixed end (2 nd mode of vibration), $a_1/W=0.4$, $L_1/L=0.2564$	100
Fig. 3.2.19(b1)	Magnified view of Fig. 3.2.19(b) at the vicinity of the crack location....	100
Fig.3.2.19 (c)	Relative amplitude vs. relative distance from the fixed end (3 rd mode of vibration), $a_1/W=0.4$, $L_1/L=0.2564$	101
Fig. 3.2.19 (c1)	Magnified view of Fig. 3.2.19 (c) at the vicinity of the crack location....	101
Fig.3.2.20 (a)	Relative amplitude vs. relative distance from the fixed end (1 st mode of vibration), $a_1/W=0.1$, $L_1/L=0.3846$	102
Fig. .3.2.20 (a1)	Magnified view of Fig. 3.2.20 (a) at the vicinity of the crack location....	102
Fig.3.2.20 (b)	Relative amplitude vs. relative distance from the fixed end (2 nd mode of vibration), $a_1/W=0.1$, $L_1/L=0.3846$	103
Fig. 3.2.20(b1)	Magnified view of Fig. 3.2.20 (b) at the vicinity of the crack location...	103
Fig.3.2.20 (c)	Relative amplitude vs. relative distance from the fixed end (3 rd mode of vibration), $a_1/W=0.1$, $L_1/L=0.3846$	104
Fig. 3.2.20 (c1)	Magnified view of Fig. 3.2.20 (c) at the vicinity of the crack location....	104
Fig.3.2.21 (a)	Relative amplitude vs. relative distance from the fixed end (1 st mode of vibration), $a_1/W=0.2$, $L_1/L=0.3846$	105
Fig. 3.2.21 (a1)	Magnified view of Fig. 3.2.21 (a) at the vicinity of the crack location..	105

Fig.3.2.21 (b)	Relative amplitude vs. relative distance from the fixed end (2 nd mode of vibration), $a_1/W=0.2$, $L_1/L=0.3846$	106
Fig. 3.2.21 (b1)	Magnified view of Fig. 3.2.21 (b)at the vicinity of the crack location....	106
Fig.3.2.21(c)	Relative amplitude vs. relative distance from the fixed end (3 rd mode of vibration), $a_1/W=0.2$, $L_1/L=0.3846$	107
Fig. 3.2.21(c1)	Magnified view of Fig. 3.2.21(c) at the vicinity of the crack location...	107
Fig.3.2.22 (a)	Relative amplitude vs. relative distance from the fixed end (1 st mode of vibration), $a_1/W=0.3$, $L_1/L=0.3846$	108
Fig. 3.2.22 (a1)	Magnified view of Fig. 3.2.22 (a) at the vicinity of the crack location....	108
Fig.3.2.22 (b)	Relative amplitude vs. relative distance from the fixed end (2 nd mode of vibration), $a_1/W=0.3$, $L_1/L=0.3846$	109
Fig. 3.2.22 (b1)	Magnified view of Fig. 3.2.22 (b) at the vicinity of the crack location...	109
Fig.3.2.22 (c)	Relative amplitude vs. relative distance from the fixed end (3 rd mode of vibration), $a_1/W=0.3$, $L_1/L=0.3846$	110
Fig. 3.2.22 (c1)	Magnified view of Fig. 3.2.22 (c) at the vicinity of the crack location....	110
Fig.3.2.23 (a)	Relative amplitude vs. relative distance from the fixed end (1 st mode of vibration), $a_1/W=0.4$, $L_1/L=0.3846$	111
Fig. 3.2.23 (a1)	Magnified view of Fig. 3.2.23 (a) at the vicinity of the crack location....	111
Fig.3.2.23 (b)	Relative amplitude vs. relative distance from the fixed end (2 nd mode of vibration), $a_1/W=0.4$, $L_1/L=0.3846$	112
Fig. 3.2.23(b1)	Magnified view of Fig. 3.2.23(b) at the vicinity of the crack location....	112
Fig.3.2.23 (c)	Relative amplitude vs. relative distance from the fixed end (3 rd mode of vibration), $a_1/W=0.4$, $L_1/L=0.3846$	113
Fig. 3.2.23 (c1)	Magnified view of Fig. 3.2.23 (c) at the vicinity of the crack location....	113
Fig.3.2.24 (a)	Relative amplitude vs. relative distance from the fixed end (1 st mode of vibration), $a_1/W=0.1$, $L_1/L=0.5128$	114
Fig. 3.2.24 (a1)	Magnified view of Fig. 3.2.24 (a) at the vicinity of the crack location....	114

Fig.3.2.24 (b)	Relative amplitude vs. relative distance from the fixed end (2 nd mode of vibration), $a_1/W=0.1$, $L_1/L=0.5128$	115
Fig. 3.2.24(b1)	Magnified view of Fig. 3.2.24 (b) at the vicinity of the crack location...	115
Fig.3.2.24 (c)	Relative amplitude vs. relative distance from the fixed end (3 rd mode of vibration), $a_1/W=0.1$, $L_1/L=0.5128$	116
Fig. 3.2.24 (c1)	Magnified view of Fig. 3.2.24 (c) at the vicinity of the crack location....	116
Fig. 3.2.25(a)	Relative amplitude vs. relative distance from the fixed end (1 st mode of vibration), $a_1/W=0.2$, $L_1/L=0.5128$	117
Fig. 3.2.25(a1)	Magnified view of Fig. 3.2.25(a) at the vicinity of the crack location.....	117
Fig. 3.2.25(b)	Relative amplitude vs. relative distance from the fixed end (2 nd mode of vibration), $a_1/W=0.2$, $L_1/L=0.5128$	118
Fig. 3.2.25(b1)	Magnified view of Fig.3.2.25 (b) at the vicinity of the crack location....	118
Fig. 3.2.25(c)	Relative amplitude vs. relative distance from the fixed end (3 rd mode of vibration), $a_1/W=0.2$, $L_1/L=0.5128$	119
Fig. 3.2.25(c1)	Magnified view of Fig. 3.2.25(c) at the vicinity of the crack location.....	119
Fig.3.2.26(a)	Relative amplitude vs. relative distance from the fixed end (1 st mode of vibration), $a_1/W=0.3$, $L_1/L=0.5128$	120
Fig. 3.2.26(a1)	Magnified view of Fig. 3.2.26(a) at the vicinity of the crack location.....	120
Fig.3.2.26 (b)	Relative amplitude vs. relative distance from the fixed end 2 nd mode of vibration), $a_1/W=0.3$, $L_1/L=0.5128$	121
Fig. 3.2.26(b1)	Magnified view of Fig. 3.2.26(b) at the vicinity of the crack location...	121
Fig. 3.2.26(c)	Relative amplitude vs. relative distance from the fixed end (3 rd mode of vibration), $a_1/W=0.3$, $L_1/L=0.5128$	122
Fig. 3.2.26(c1)	Magnified view of Fig. 3.2.26(c) at the vicinity of the crack location.....	122
Fig. 3.2.27(a)	Relative amplitude vs. relative distance from the fixed end (1 st mode of vibration), $a_1/W=0.4$, $L_1/L=0.5128$	123
Fig. 3.2.27(a1)	Magnified view of Fig. 3.2.27(a1) at the vicinity of the crack location...	123

Fig.3.2.27 (b)	Relative amplitude vs. relative distance from the fixed end (2 nd mode of vibration), $a_1/W=0.4$, $L_1/L=0.5128$	124
Fig. 3.2.27(b1)	Magnified view of Fig. 3.2.27(b) at the vicinity of the crack location....	124
Fig. 3.2.27(c)	Relative amplitude vs. relative distance from the fixed end (3 rd mode of vibration), $a_1/W=0.4$, $L_1/L=0.5128$	125
Fig. 3.2.27(c1)	Magnified view of fig. Fig. 3.2.27(c) at the vicinity of the crack location.....	125
Fig. 3.2.28 (a)	Three dimensional cum contour plot for relative first natural frequency..	126
Fig.3.2.28 (b)	Three dimensional cum contour plot for relative second natural frequency.....	126
Fig. 3.2.28 (c)	Three dimensional cum contour plot for relative third natural frequency.....	127
Fig. 3.2.29 (a)	Three dimensional cum contour plot for relative 1 st mode shape difference.....	127
Fig. 3.2.29 (b)	Three dimensional cum contour plot for relative 2 nd mode shape difference.....	128
Fig. 3.2.29 (c)	Three dimensional cum contour plot for relative 3 rd mode shape difference.....	128
Fig. 3.3.1	Schematic block diagram of experimental set-up.....	129
Fig.3.3.2 (a)	Relative amplitude vs. relative distance from the fixed end (1 st mode of vibration), $a_1/W=0.4$, $L_1/L=0.026$	130
Fig.3.3.2 (b)	Relative amplitude vs. relative distance from the fixed end (2 nd mode of vibration), $a_1/W=0.4$, $L_1/L=0.026$	130
Fig.3.3.2 (c)	Relative amplitude vs. relative distance from the fixed end (3 rd mode of vibration), $a_1/W=0.4$, $L_1/L=0.026$	131
Fig.3.3.3 (a)	Relative amplitude vs. relative distance from the fixed end (1 st mode of vibration), $a_1/W =0.3$, $L_1/L =0.05128$	131
Fig.3.3.3 (b)	Relative amplitude vs. relative distance from the fixed end (2 nd mode of vibration), $a_1/W =0.3$, $L_1/L =0.05128$	132

Fig.3.3.3(c)	Relative amplitude vs. relative distance from the fixed end (3 rd mode of vibration), $a_1/W = 0.3$, $L_1/L = 0.05128$	132
Fig.3.3.4 (a)	Relative amplitude vs. relative distance from the fixed end (1 st mode of vibration), $a_1/W = 0.4$, $L_1/L = 0.05128$	133
Fig.3.3.4 (b)	Relative amplitude vs. relative distance from the fixed end (2 nd mode of vibration), $a_1/W = 0.4$, $L_1/L = 0.05128$	133
Fig.3.3.4 (c)	Relative amplitude vs. relative distance from the fixed end (3 rd mode of vibration), $a_1/W = 0.4$, $L_1/L = 0.05128$	134
Fig. 4.2.1(a)	Triangular membership function.....	141
Fig.4.2.1 (b)	Gaussian membership function.....	141
Fig.4.2.1(c)	Trapezoidal membership function.....	141
Fig. 4.2.2	Schematic diagram of the fuzzy logic controller for crack detection.....	143
Fig. 4.3.1(a)	Triangular fuzzy controller.....	148
Fig. 4.3.1(b1)	Triangular membership functions for relative natural frequency for first mode of vibration.....	148
Fig. 4.3.1(b2)	Triangular membership functions for relative natural frequency for second mode of vibration.....	148
Fig. 4.3.1(b3)	Triangular membership functions for relative natural frequency for third mode of vibration.....	148
Fig. 4.3.1(b4)	Triangular membership functions for relative mode shape difference for first mode of vibration.....	148
Fig. 4.3.1(b5)	Triangular membership functions for relative mode shape difference for second mode of vibration.....	148
Fig. 4.3.1(b6)	Triangular membership functions for relative mode shape difference for third mode of vibration.....	148
Fig. 4.3.1(b7)	Triangular membership functions for relative crack depth.....	148
Fig. 4.3.1(b8)	Triangular membership functions for relative crack location.....	148
Fig. 4.3.2(a)	Gaussian fuzzy controller.....	149

Fig. 4.3.2(b1)	Gaussian membership functions for relative natural frequency for first mode of vibration.....	149
Fig. 4.3.2(b2)	Gaussian membership functions for relative natural frequency for second mode of vibration.....	149
Fig. 4.3.2(b3)	Gaussian membership functions for relative natural frequency for third mode of vibration.....	149
Fig. 4.3.2(b4)	Gaussian membership functions for relative mode shape difference for first mode of vibration.....	149
Fig. 4.3.2(b5)	Gaussian membership functions for relative mode shape difference for second mode of vibration.....	149
Fig. 4.3.2(b6)	Gaussian membership functions for relative mode shape difference for third mode of vibration.....	149
Fig. 4.3.2(b7)	Gaussian membership functions for relative crack depth.....	149
Fig. 4.3.2(b8)	Gaussian membership functions for relative crack location.....	149
Fig. 4.3.3(a)	Trapezoidal fuzzy controller.....	150
Fig. 4.3.3(b1)	Trapezodial membership functions for relative natural frequency for first mode of vibration.....	150
Fig. 4.3.3(b2)	Trapezodial Membership functions for relative natural frequency for second mode of vibration.....	150
Fig. 4.3.3(b3)	Trapezodial membership functions for relative natural frequency for third mode of vibration.....	150
Fig. 4.3.3(b4)	Trapezodial membership functions for relative mode shape difference for first mode of vibration.....	150
Fig. 4.3.3(b5)	Trapezodial membership functions for relative mode shape difference for second mode of vibration.....	150
Fig. 4.3.3(b6)	Trapezodial membership functions for relative mode shape difference for third mode of vibration.....	150
Fig. 4.3.3(b7)	Trapezodial membership functions for relative crack depth.....	150
Fig. 4.3.3(b8)	Trapezodial membership functions for relative crack location.....	150

Fig.4.3.4	Resultant values of relative crack depth and relative crack location from triangular fuzzy controller when Rules 1 and 19 of Table 4.3.2 are activated.....	153
Fig. 4.3.5	Resultant values of relative crack depth and relative crack location from gaussian fuzzy controller when Rules 1 and 19 of Table 4.3.2 are activated.....	154
Fig. 4.3.6	Resultant values of relative crack depth and relative crack location from trapezoidal fuzzy controller when Rules 1 and 19 of Table 4.3.2 are activated.....	155
Fig. 5.2.1	Model of a neuron.....	163
Fig.5.2.2	Threshold activation function.....	164
Fig.5.2.3	Ramping activation function.....	164
Fig.5.2.4	Hyperbolic tangent activation function.....	165
Fig. 5.2.5	Architecture of feed forward multilayer neural network trained by back-propagation algorithm.....	166
Fig. 5.3.1	Multi layer neural network controller.....	172
Fig. 5.3.2	Ten-layer neural network controller for crack detection.....	173
Fig.6.2.1	Triangular fuzzy-neuro controller for crack detection.....	180
Fig.6.2.2	Gaussian fuzzy-neuro controller for crack detection.....	181
Fig.6.2.3	Trapezoidal fuzzy-neuro controller for crack detection.....	182
Fig. 7.2.1	Bell-shaped membership function.....	192
Fig. 7.2.2	Multiple ANFIS (MANFIS) controller for crack detection.....	195
Fig. 7.2.3	Adaptive Neuro Fuzzy Inference System (ANFIS) for crack detection..	196
Fig. 8.1	View of complete assembly of the experimental set-up.....	204
Fig.8.2 (a)	Concrete foundation with beam specimen.....	205
Fig.8.2 (b)	Vibration indicator (PULSE labShop software) with lap top.....	205
Fig.8.2 (c)	Vibration exciter.....	205

Fig.8.2 (d)	Vibration pick-up (accelerometer).....	206
Fig.8.2 (e)	Vibration analyser.....	206
Fig.8.2 (f)	Function generator.....	206
Fig.8.2 (g)	Power amplifier.....	207
Fig.8.2	View of the instruments used in the experimental set-up.....	207

List of Symbols

a_1	= depth of crack
A	= cross-sectional area of the beam
$A_i \ i = 1 \text{ to } 12$	= unknown coefficients of matrix A
B	= width of the beam
B_1	= vector of exciting motion
C_u	= $\left(\frac{E}{\rho}\right)^{1/2}$
C_y	= $\left(\frac{EI}{\mu}\right)^{1/2}$
E	= Young's modulus of elasticity of the beam material
f_{md}	= Relative first mode difference
f_{nf}	= Relative first natural frequency
$F_i \ i = 1, 2$	= experimentally determined function
i, j	= variables
J	= strain-energy release rate
$K_{1,i} \ i = 1, 2$	= Stress intensity factors for P_i loads
\bar{K}_u	= $\frac{\omega L}{C_u}$
\bar{K}_y	= $\left(\frac{\omega L^2}{C_y}\right)^{1/2}$
K_{ij}	= local flexibility matrix elements
L	= length of the beam

L_1	= location (length) of the crack from fixed end
M_i $i=1,4$	= compliance constant
P_i $i=1,2$	= axial force ($i=1$), bending moment ($i=2$)
Q	= stiff-ness matrix for free vibration.
Q_1	= stiff-ness matrix for forced vibration
rcd	= Relative crack depth
rcL	= Relative crack location
smd	= Relative second mode difference
snf	= Relative second natural frequency
tmd	= Relative third mode difference
tnf	= Relative third natural frequency
u_i $i=1,2$	= normal functions (longitudinal) $u_i(x)$
x	= co-ordinate of the beam
y	= co-ordinate of the beam
Y_0	= amplitude of the exciting vibration
y_i $i=1,2$	= normal functions (transverse) $y_i(x)$
W	= depth of the beam
ω	= natural circular frequency
β	= relative crack location $\frac{L_1}{L}$
μ	= $A\rho$
ρ	= mass-density of the beam
ξ_1	= relative crack depth $\frac{a_1}{W}$

- \vee = Aggregate (union)
- \wedge = Minimum (min) operation
- \forall = For every

Chapter 1

INTRODUCTION

Research has been carried out in recent years for crack detection of dynamically vibrating structures from its modal parameters. A brief description about the methodologies that have been adapted for fault diagnosis has been given in the current chapter. At first background and motivation in the field of vibration analysis of damaged structures has been outlined. The second part of this chapter describes the aims and objective of the research. Finally the details of each chapter of the thesis for the current investigation have been explained in the third part of this chapter.

1.1 Background and Motivation

Most of the researches in the area of crack identification are done to avoid catastrophic failure of structures or engineering systems. Researchers from different domain of engineering stream have shown their interest to find out a potential tool for damage detection. On line condition monitoring, prediction and identification of cracks in structural systems as well as in mechanical components are the areas of application of the crack detection methodologies. A number of non destructive testing (NDT) techniques with lower order accuracy have been developed so far. Techniques developed for damage prediction in the field of structural health monitoring with practical applications have been demonstrated in very limited research work with very low success rate.

It has been observed that the presence of cracks in structures or in machine members lead to operational problem as well as premature failure. A number of researchers throughout the world are working on structural dynamics and particularly on dynamic characteristics of structures with crack. Due to presence of crack the dynamic characteristics of structure changes. These signatures comprise of natural frequencies; the amplitude responses due to vibration and the mode shapes. Cracks present a serious threat to proper performance of structures and machines. Most of the failures are due to material fatigue. For this reason

methods used for early detection and localization of cracks have been the subject of intensive research since several years. Since last two decades a number of experiments and theories have been developed to elucidate the phenomenon and determine the crack effect on dynamic structures.

Beams are one of the most commonly used structural elements in numerous engineering applications and experience a wide variety of static as well as dynamic loads. Cracks may develop in beam-like structures due to such loads. Considering the crack as a significant form of such damage, its modelling is an important step in studying the behavior of damaged structures. Knowing the effect of crack on stiffness, the beam or shaft can be modeled using either Euler-Bernoulli or Timoshenko beam theories. The beam boundary conditions are used along with the crack compatibility relations to derive the characteristic equation relating the natural frequency, the crack depth and location with the other beam properties. Beam type structures are commonly used in steel construction and machinery industries. The current study is based on crack detection for structural health monitoring in regard to change in natural frequencies and mode shapes of the beam.

Fatigue cracks are a potential source of catastrophic structural failure. To avoid failure caused by cracks, many researchers have performed extensive investigations to develop structural integrity monitoring techniques. Most of these techniques are based on vibration measurements and analysis because vibration based methods can offer an effective and convenient way to detect fatigue cracks. Generally, vibration based methods can be classified into two categories: linear and nonlinear approaches. Linear approaches detect the presence of cracks in a target object by monitoring changes in the resonant frequencies in the mode shapes or in the damping factors. Depending on the assumptions, the type of analysis, the overall beam characteristics and the kind of loading or excitation, a number of research papers containing a variety of different approaches have been reported in the relevant literature. In recent years, transport engineering has experienced serious advances characterized mainly by parameters like higher speeds and weights of vehicles. These parameters make the transportation problem more complex. With a race towards high speed, high power and lightweight in rotating machinery design and operation often impose severe stress and environmental condition upon rotors. As rotating machinery is designed to operate

at higher mechanical efficiency; operating speed, power, and load are increased as weight and dimensional tolerances are decreased. High torsional and radial loads, together with a complex pattern of rotor motion, can create a severe mechanical stress condition that may eventually lead to development of a crack in the shaft. The presence of a transverse crack in shaft/rotor incurs a potential risk of destruction or collapse. This produces high costs of production and maintenance. Detection of a crack in its early stages may save the rotor/beam for use after repair. By monitoring the system, depending upon the type and severity of the crack, it may be possible in some cases to extend the use of a flawed rotor without risking a catastrophic failure, while arrangements are being made for a replacement rotor. The method will also improve safety by helping to prevent major rotor failure. For the time being, the research on cracked rotor is still at the theoretical stage. With a well known fact the dynamic behavior of a structure changes due to presence of crack. There are two types of problems related to this topic: the first may be called direct problem and the second called inverse problem. The direct problem is to determine the effect of damages on the structural dynamic characteristics, while the inverse problem is to detect, locate and quantify the extent of the damages. In the past two decades, both the direct and the inverse problems have attracted many researchers.

A direct procedure is difficult for crack identification and unsuitable in some particular cases, since they require minutely detailed periodic inspections, which are very costly. In order to avoid these costs, researchers are working on more efficient procedure in crack detection through vibration analysis.

1.2 Aims and Objectives of this Research

It is required that structures must safely work during its service life but, damages initiate a breakdown period on the structures. Cracks are among the most encountered damage types in the structures. It is an established fact that dynamic behavior of structures changes due to presence of crack in them. It has been observed that the presence of cracks in structures or in machine members lead to operational problem as well as premature failure. A number of investigators round the globe are working on structural dynamics and particularly on dynamic characteristics of structures with crack. Due to presence of cracks the dynamic

characteristics of structure changes. The change in dynamic behavior has been utilized by the researchers as one of the criteria of fault diagnosis for structures. Major characteristics of the structure which undergo change due to presence of crack are; natural frequencies, the amplitude responses due to vibration and the mode shapes.

Scientific study on the changes in these characteristics can be widely utilized for the identification of crack in structures. In general fault detection in structures can be more specific with the help of these information.

In the current investigation, a number of literatures published till now have been surveyed, reviewed and analyzed. It is felt that, the results presented by the researchers have not been utilized so far in a systematic way for engineering applications. Although information on some aspect are available but it is not exhaustive for real applications. A systematic attempt has been made in the present study to investigate the dynamic behavior of cracked cantilever beam structure using theoretical analysis, experimental analysis and artificial intelligence techniques for damage diagnosis of cracked structure. The dynamic responses of the system are used for crack prediction.

The phases of the process plan for the present investigation are as follows:

1. At first theoretical, free and forced vibration analyses of the cracked cantilever beam have been addressed.
2. Experimental analysis is done to obtain the relative values of first, second and third modal natural frequencies and mode shapes.
3. Training of the developed controllers has been done using artificial intelligence techniques with series of data obtained from theoretical and experimental analysis. These controllers predict relative values of crack depth and crack length from the three inputs such as relative values of first, second, third natural frequencies and mode shapes.

For developing the analytical expressions on dynamic characteristics of structures, a single transverse crack in the structure has been considered in the theory and the analyses are presented in detail in subsequent chapters.

In all these theories, the presence of a transverse crack in the structure has been considered. This crack introduces local flexibility at the vicinity of the crack location. Boundary conditions are derived from the strain energy equation using castigliano's theorem. Presence of crack also reduces the stiffness of the structure which has been derived from stiffness matrix, the details of which have been presented in the respective sections. For dynamic behavior of beam with a transverse crack, Timoshenko beam theory with modified boundary conditions due to presence of crack, have been used to find out the theoretical expressions for natural frequencies and mode shapes for the beam. The first three relative value of first, second, third natural frequencies and mode shapes obtained from theoretical analysis are used as input parameters to the controller (fuzzy, neural network, fuzzy-neuro, MANFIS controller) for crack identification. The outputs from the controller are relative crack location and relative crack depth.

In the last stage of the investigation the effect of crack depth and crack location on the modal values of natural frequencies and mode shapes are obtained with a very convincing manner. Results obtained from the theoretical, fuzzy, fuzzy-neuro, manfis and experimental analysis are compared and a close agreement has been found. Suitable numerical methods are used in order to solve the theoretical equations developed. Useful conclusions are drawn from the numerical results of respective sections. The results from the various methodologies mentioned above are validated using the developed experimental set up.

From the vibration analysis of a cracked structure the crack characteristics can be detected. Smart method can be developed for on line condition monitoring of damaged structure with the help of artificial intelligence techniques. The system can be developed using fuzzy logic and neural network techniques. Fuzzy system has the advantage of capturing the imprecise nature of human knowledge and reasoning processes. The neural network has a different approach for designing of the intelligent system because of its tremendous learning capability. These two innovative modeling approaches share some common characteristics such as i) they assume parallel operations, ii) they are well known for their fault tolerance capabilities . Researchers from different field of engineering applications have integrated the capabilities of neural network and fuzzy logic techniques to develop a hybrid method, which has a better capability than the independent methods. This is one of the most important

reasons for carrying out the research work to develop a hybrid technique for crack detection. Multiple Adaptive Neuro-Fuzzy Inference System (MANFIS) has also been devised for crack diagnosis.

In the current investigation work has been done to develop methodologies with the aid of artificial intelligence techniques for crack detection in various structural members.

1.3 Outline of the Research Work

The research work as outlined in this thesis is broadly divided into ten chapters. Following the introduction, Chapter two presents the literature review of previous work on structural vibration and its analysis, effect of different parameters on dynamic response of cracked structures, dynamic characteristics of beam with transverse crack, crack detection by artificial intelligence technique such as fuzzy logic, neural network, fuzzy neuro, multi adaptive neuro-fuzzy inference system (MANFIS).

Chapter three analyses the dynamics characteristics of beam with a transverse crack using the expression of strain energy release rate and strain energy density function. The local flexibilities generated due to the presence of crack have been evaluated. The free and forced vibration analyses have been performed to compute the vibration characteristics of the cracked cantilever beam. The results and discussions of the numerical analysis have also been presented in this chapter. Finally, the results of experimental and numerical analyses have been compared for validation of theoretical analysis.

Chapter four defines the concept of the fuzzy logic and outlines the methodology used to design an intelligent fuzzy logic controller for prediction of relative crack location and relative crack depth using the relative deviations of first three natural frequencies and first three mode shapes. The results obtained from the developed fuzzy controller have been validated with the results from experimental analysis.

Chapter five discusses the neural network technique being used for crack detection in vibrating structures. Comparisons of the results from numerical, fuzzy controller, neural controller and experimental analyses have been presented.

In Chapter six the application of hybrid intelligent system (fuzzy neuro controller) for crack detection has been discussed. The analysis of fuzzy and neural segment of the fuzzy-neuro controller has been presented. Comparisons of results of the numerical, fuzzy, neural, fuzzy-neuro and experimental analysis have been discussed.

Chapter seven discusses the concept of the multiple adaptive neuro fuzzy inference system (MANFIS) and outlines the methodology for prediction of relative crack location and relative crack depth using deviations of vibration signatures of cracked beam. The results of the numerical, fuzzy, neural, fuzzy-neuro, MANFIS and experimental analysis have been discussed.

In chapter eight the details of the developed experimental set-up for vibration analysis along with the specifications of the different equipments used are presented. Finally the experimental results are discussed. Chapter nine summarizes the findings of all chapters discussed above.

Finally in Chapter ten contributions, conclusions of this research and future directions for further investigation have been discussed. The developed methodologies are found to be suitable for fault diagnosis of vibrating structures.

Chapter 2

LITERATURE REVIEW

This chapter reviews the work related to the analyses of crack in dynamic structures and the development of crack diagnosis tool in damaged structures. The progress made in the last few decades in the field of crack diagnosis of dynamically vibrating structures has been described. This chapter also presents a literature review of past and recent developments in area of crack identification and prediction with the aid of artificial intelligence techniques.

2.1 Introduction

A significant amount of research has been published in many aspects related to crack detection. This section discusses the contributions that cover structural vibration and its analysis, dynamics of cracked structures, fault identification methodologies and artificial intelligence technique that helps to design an intelligent controller for crack identification. A large number of researchers have used the free and forced vibration analysis for developing algorithm for crack detection. The ultimate goal of this research is to establish new methodologies which will predict the crack location and its intensity in a dynamically vibrating structure by the help of artificial intelligence technique with considerably less computational time and high precision. This chapter summarizes the past work, mostly in computational methods for structures, and discusses possible directions for research.

Another challenge in literature review is that even the perception of what constitutes progress varies widely in the research community. The representations would be difficult to extend to different structural and mechanical member for crack detection, where the systems work in various environments (i.e. with noise, chaos, uncertainty). Despite these challenges, the next section reviews and highlights some of the interesting, important and experimental milestones. This chapter provides details survey report within important aspects of what the researchers have worked in the area of vibration analysis and planning for methodologies to identify crack using fuzzy logic, neural network, neuro-fuzzy and MANFIS technique.

2.2 History and Development of Dynamic Analysis of Cracked Structure

The development of techniques for crack identification in real-world environments constitutes one of the major trends in the current research on fault diagnosis. Some of the researchers have analyzed the dynamic response of cracked structure during last few decades.

Ayre et al. [1] have developed a method for calculating the natural frequencies of continuous beams of uniform span length by vibration analysis. Miles [2] has carried out analysis of beams on many supports using vibration parameters. Bollinger et al. [3] have presented a method for analysis and prediction of the static and dynamic behavior of machine tool spindle systems using finite difference technique. Gladwell [4] has analysed a large structural system using component mode synthesis method, for vibration analysis and shown the effectiveness of component mode synthesis method with reference to other approaches. Mercer et al. [5] have developed a transfer matrix method for the prediction of natural frequencies and normal modes of a row of skin-stringer panels. They have also presented few examples. Watrasiewicz [6] has applied Wavefront reconstruction interferometry to mechanical vibration analysis and validated the results with experimental results. Lin et al. [7] have briefly surveyed the use of transfer matrix method for analyzing the dynamic behavior of beam structures. Chun [8] has considered the free vibration of a beam hinged at one end by a rotational spring (with a constant spring constant) and the other end free. Lee [9] has evaluated the eigenfrequencies for the fundamental mode of a beam hinged at one end by a rotational spring by vibration analysis. Thomas et al. [10] have used straight beam finite elements for the analysis of the vibration of curved beams and concluded that the proposed method gives superior results than a solid 20 node isoparametric element. Venkateswara et al. [11] have revealed that the Galerkin finite element method is very accurate and even with a one element idealization of the beam the fundamental frequencies coincide up to five significant figures.

Broadly the development of dynamic analysis of cracked structure can be divided into two parts 1) structural vibration and its analysis 2) Dynamics of cracked structures.

2.2.1 Structural Vibration and its Analysis

The development of vibration theory, as a subdivision of mechanics, came as a natural result of the development of the basic sciences i.e. mathematics and mechanics. The sciences are founded in the middle of the first millennium B.C. by the ancient Greek philosophers. The term vibration has been used from Vedic times of India, approximately 10,000 B.C.. Pythagoras of Somas (570-497 B.C.) has conducted several vibration experiments with hammers, springs, pipes, and shells. He established the first vibration research laboratory. Moreover, he has invented the monochord, a purely scientific instrument to conduct experimental research in the vibration of taut strings and to set a standard for vibration measurements.

Extensive experimental results are available for the vibrating strings since Pythagoras times. Daniel Bernoulli has explained the experimental results using the principle of superposition of the harmonics and has introduced the idea of expressing the response as a sum of the simple harmonics. The problem of the vibrating string is solved mathematically first by Lagrange considering it as sequence of small masses. The wave equation is introduced by D'Alembert in a memoir to the Berlin Academic. He has used it in his memoir also for longitudinal vibration of air columns in pipe organs. Experimental results for the same problem are obtained by Pythagoras. Euler obtained the differential equation for the lateral vibration of bars and he has determined the functions that we now call normal functions and the equation that we now call frequency equation for beams with free, clamped or simply supported ends, while Daniel Bernoulli has supplied him with experimental verification. The first systematic treatise on vibration has been written by Rayleigh [12]. He has formalized the idea of normal functions. He has introduced systematically the energy and approximate methods in vibration analysis, without solving differential equations. This idea has been further developed by Ritz [13]. Timoshenko theory accounts for rotary inertia and the correction due to shear deformation of the lateral vibration of beam. Donaldson [14] has presented the importance of vibration as a flanking path in airborne noise insulation and the reduction of airborne noise transmitted through panels damped by friction. Henderson et al. [15] have formulated analytical techniques, based on transfer matrix methods, and presented for the analysis of the forced vibrations of cylindrically curved multi-span structures with

various examples. Tottenham et al. [16] have used the matrix progression method to determine eigenvalues and eigenvectors for the free vibration problem of thin circular cylindrical shells. Petyt et al. [17] have calculated the frequencies and modes of vibration of a five bay curved beam on hinged supports using the finite element displacement method, which are confirmed experimentally. Gorman [18] has proposed method to calculate the first five frequencies and modal shapes for the entire family of beams regardless of the location of the intermediate support following free lateral vibration of double-span uniform beams.

2.2.2 Dynamics of Cracked Structures

The problem on crack is the central problem of science for several decades. The mechanics of fracture as an independent branch of the mechanics of deformable solids has originated quite recently. Galileo Galilei is rightly considered the founder of fracture mechanics. He has stated that the breaking load is independent of the length of a tension bar and is directly proportional to its cross sectional area. In general the first stage of the investigation on fracture mechanics, is associated with the names of Galileo Galilei, Robert Hooke, Charles Augustin de Coulomb, Barre de Saint Venant and Otto mohr. Their investigation is characterized by extensive studies of deformation properties of solids and by the development of various failure criteria termed strength theories. These theories state that fracture occurs at the moment when at a certain point of a body a particular combination of parameters, such as stress, strain. etc., reaches its critical value. In this approach the process of fracture propagation through the volume of the body is completely ignored, which is justified only in cases where the development of defects causing failure takes place in a small vicinity of the critical region.

Irwin [19] first has studied about cracked beam for finding out local flexibilities of the beam at crack location. Later Tada [20] has developed theories for strain energy density function with the help of stress intensity function at the crack section. With the light of above theory Pafelias [21], Gasch [22] and Henry et al. [23] have analyzed the dynamic behavior of a simple cracked rotor. Also Mayes et al. [24] have analyzed the vibrational behavior of a rotating shaft system containing a transverse crack. Freud et al. [25] have analysed the dynamic fracture of a beam or plate in plane bending. Subsequently Adeli et al. [26] have

analyzed the effect of axial force for dynamic fracture of a beam or plate in pure bending. Dentsoras et al. [27] in their investigation they have taken coupling effect of various type of vibration (such as bending vibration, torsional vibration and longitudinal vibration) for analysis of dynamic behavior of cracked beam. Wong et al. [28] have diagnosed the fracture damage in structures by modal frequency method. Also Nian et al. [29], Quain et al. [30], Ismail et al. [31] and Sekhar et al. [32] have used the vibrational diagnosis approach for detection of structural fault. Sorkin et al. [33] have evaluated the performance of different methodologies for detecting the initiation and propagation of cracks by cyclic loading of the structure with particular attention to the requirements for high-performance ship structures. Rao et al. [34] have developed a finite element model to analyse three typical problems pertaining to the vibrations of initially stressed thin shells of revolution. Wood [35] has reviewed significant factors leading to the development of damage tolerance criteria and illustrate the role of fracture mechanics in the analysis and testing aspects necessary to satisfy the necessary requirements to prevent damage from growing to catastrophic size prior to detection in aircrafts.

2.3 Effect of Different Parameters on Dynamic Response of Cracked Structures

The effect of crack parameters on the dynamic response of the cracked structure can be further established with the review of the following published papers.

Dimarogonas et al. [36] have studied the dynamic response of a cracked cantilever shaft due to the local flexibility generated at the crack section. The results from the analytical solution are validated using developed experimental setup. Nonlinear vibration of beams made of functionally graded materials (FGMs) containing an open edge crack has been studied by Kitipornchai et al. [37] based on Timoshenko beam theory and von Kármán geometric nonlinearity. The cracked section is modeled as a mass less elastic rotational spring. It is found that the intact and cracked FGM beams show different vibration behavior. Rizos et al. [38] has determined the crack location and its depth in a cantilever beam from the vibration modes. Analytical results are used to relate the measured vibration modes to the crack location and depth. It is stated that the crack location can be found and depth can be estimated with satisfactory accuracy. Ostachowicz et al. [39] have assumed an open and

closed crack with triangular disk finite elements. They have analyzed the forced vibrations of the beam, the effects of the crack locations and sizes on the vibrational behavior and discussed a basis for crack identification.

2.4 Dynamic Characteristics of Beam with Transverse Crack

The dynamic characteristics of the cracked structures such as natural frequencies and mode shapes are dependent on the crack depth and its position. Following review discusses on the effect of crack on vibrating structure.

Shen et al. [40, 41] have proposed an identification procedure to determine the crack characteristics by measuring the difference between natural frequencies and mode shapes. They have tested the method for simulated damage in the form of one-side or symmetric cracks in a simply supported Bernoulli-Euler beam to evaluate the sensitivity of the solution of damage identification. The crack can be simulated by an equivalent spring, connecting the two segments of the beam, as stated by Narkis [42]. Analysis of this approximate model results in algebraic equations which relate the natural frequencies of beam and crack characteristics. The robustness of the proposed method is confirmed by comparing it with the results from finite element calculations. Müller et al. [43] have proposed a model to detect the crack and establish a clear relation between shaft cracks in turbo rotors and induced phenomena in vibrations. This model is designed to estimate the nonlinear effects. Different crack identification techniques have been discussed briefly by Dimarogonas [44] and they have found that crack in a structural member introduce a local flexibility which affect its vibration response. Tsai et al. [45] have investigated diagnostic method of determining the position and size of a transverse open crack on a stationary shaft without disengaging it from the machine system assuming the crack as a joint of a local spring. To obtain the dynamic characteristics of a stepped shaft and a multidisc shaft the transfer matrix method is employed by them on the basis of Timoshenko beam theory. Gounaris et al. [46] have proposed a method for crack identification in beams assuming the crack to be always open and the method is based on eigenmodes of the structure. In this paper they have co-related the mode differences with crack depth and location. A cracked Euler-Bernoulli cantilevered beam with an edge crack has been formulated by Chondros and Dimarogonas [47, 48] for

vibration analysis. Yokoyama et al. [49] have studied the vibration characteristics of a uniform Bernoulli-Euler beam with a single edge crack using a modified line-spring model. They have determined the natural frequencies and the corresponding mode shapes for uniform beams having edge cracks of different depths at different positions. Kisa et al. [50] present a novel numerical technique applicable to analyze the free vibration analysis of uniform and stepped cracked beams with circular cross section using finite element and component mode synthesis methods. To reveal the accuracy and effectiveness of the offered method, a number of numerical examples are demonstrated for free vibration analysis of beams. Damage detection in vibrating beam systems has been done by Fabrizio et al. [51] by measuring the natural frequencies to locate and quantify the damage. Xia et al. [52] have presented a technique for damage identification by selecting a subset of measurement points and corresponding modes. They have used two factors for measuring the damage, the sensitivity of a residual vector to the structural damage and the sensitivity of the damage to the measured noise. A new method of vibration-based damage identification in structures exhibiting axial and torsional responses has been proposed by Duffey et al. [53]. The method has been derived to detect and localize linear damage in a structure using the measured modal vibration parameters. Cracked beam element method for structural analysis has been used by Viola et al. [54] for detection of crack location. The local flexibility introduced by cracks changes the dynamic behavior of the structure and by examining this change, crack position and magnitude can be identified. In order to model the structure a special finite element for a cracked Timoshenko beam has been developed. Effect of the cracks on the stiffness matrix and consistent mass matrix are investigated and the cracks in the structure were identified using the modal data. Theoretical and experimental dynamic behavior of different multi-beams systems containing a transverse crack has been performed by Saavedra and Cuitino [55]. Yang et al. [56] have developed an energy-based numerical model to investigate the influence of cracks on structural dynamic characteristics during the vibration of a beam with open crack. Upon the determination of strain energy in the cracked beam, the equivalent bending stiffness over the beam length is computed. Gounaris et al. [57] have used a method for rotating cracked shafts to identify the depth and the location of a transverse surface crack. A local compliance matrix of different degrees of freedom is used to model the transverse crack in the shaft of circular cross section, based on available expressions of the

stress intensity factors and the associated expressions for the strain energy release rates. Fernandez-saez et al. [58] have presented simplified method of evaluating the fundamental frequency for the bending vibrations of cracked Euler–Bernoulli beams. Their method is based on the well-known approach of representing the crack in a beam through a hinge and an elastic spring, by adding polynomial functions to that of the un-cracked beam. This approach is applied to simply supported beams with a cracked section in any location of the span. Yang et al. [59] have developed a method to detect the onset and progression of surface cracks in rotary shafts. They have used a wavelet -based algorithm effective in identifying the nonlinear dynamical characteristics of a model-based, cracked rotor. Saavedra et al. [60] have presented a theoretical and experimental dynamic analysis of a rotor-bearing system with a transversely cracked shaft by modeling a cracked cylindrical shaft using finite element. They have proposed a simplified opening and closing crack model and the analysis is being done using Hilbert, Hughes, and Taylor integration method (HHT) implemented in Matlab platform. Kim et al. [61] have derived a new algorithm to predict locations and severities of damage in structures using modal characteristics. They have reviewed two existing algorithms and formulated a new algorithm by eliminating the erratic assumptions and limitations in those existing algorithm. As described by them this new proposed method has been applied to a two span continuous beam and the results shown an improved accuracy in crack location and severity estimation. An analysis has been performed by Patil et al. [62] for the detection of multiple cracks using frequency measurements. Their method is based on transverse vibration modeling through transfer matrix method and representation of a crack by rotational spring. The procedure gives a linear relationship explicitly between the changes in natural frequencies of the beam and the damage parameters. Darpe et al. [63] have studied a simple Jeffcott rotor with two transverse surface cracks. The stiffness of such a rotor is derived based on the concepts of fracture mechanics. Subsequently, the effect of the interaction of the two cracks on the breathing behavior and on the unbalance response of the rotor is studied. Zheng et al. [64] have presented a tool for vibrational stability analysis of cracked hollow beams. According to them each crack is assigned with a local flexibility coefficient which is a function of depth of crack. They have used least squared method to device the formulae for shallow cracks and deep cracks. Zou et al. [65] have presented a slightly modified version of local flexibility of Dimarogonas [2] which is more suitable for

theoretical model. According to them there are extensive research on the vibrational behavior of the cracked rotor and use of response characteristics to detect crack. Owolabi et al. [66] have done experimental investigations with two sets of aluminum beams with a view to detect, quantify, and determine the effect of cracks and locations. According to them the damage detection depends on the measured changes in the first three natural frequencies and the corresponding amplitudes. Identification of location and severity of damage in structures using frequency response function (FRF) data have been formulated by Hwang et al. [67]. To verify the proposed method, examples for simple cantilever and a helicopter rotor blade are numerically demonstrated. A method for crack identification in double-cracked beams based on wavelet analysis has been presented by Loutridis et al. [68] using continuous wavelet transform. The location of the crack is determined by the sudden changes in the spatial variation of the transformed response. A comprehensive analysis of the stability of a cracked beam subjected to a follower compressive load is presented by Wang [69]. The beam is fixed at its left end and restrained by a translational spring at its right end. The vibration analysis on such cracked beam is conducted to identify the critical compression load for flutter or buckling instability based on the variation of the first two resonant frequencies of the beam. Kishen et al. [70] have studied the fracture behavior of cracked beams and columns using finite element analysis. Assuming that failure occurs due to crack propagation when the mode I stress intensity factor reaches the fracture toughness of the material, the failure load of cracked columns are determined for different crack depths and slenderness ratios. Hwang et al. [71] have presented method to identify the locations and severity of damage in structures using frequency response function data. Dharmaraju et al. [72] have used Euler–Bernoulli beam element and finite element modeling for crack identification. The transverse surface crack is considered to remain open. The present identification algorithms have been illustrated through numerical examples. Khiem et al. [73] have formulated a method to detect multiple cracks of beams by analyzing natural frequencies in the form of a non-linear optimization problem, then solving by using the MATLAB functions. They have applied spring model of crack to establish the frequency equation based on the dynamic stiffness for the multiple cracked beam. Kyricazoglou et al. [74] have presented method to detect the damage in composite laminates by measuring and analyzing the slope deflection curve of composite beams in flexure. They have provided the damage mechanism and location of

damage from comparison of dynamic results with the dynamic response from the damaged laminates. They suggested that slope deflection curve is a promising technique for detection initial damage in composites. Zheng et al. [75] have used finite element method to find out the natural frequencies and mode shapes of a cracked beam. They have used overall additional flexibility matrix instead of local additional flexibility matrix to find out the stiffness matrix. According to them the overall additional matrix gives more accurate result to calculate the natural frequencies. Mackerle [76] has reviewed the finite-element methods along with electrical, magnetic and electromagnetic methods, sonic methods, mechanical methods, optical methods, condition monitoring methods applied for the non-destructive evaluation of materials. Wang et al. [77] have investigated the bending and torsional vibration of a fiber reinforced composite cantilever with a surface crack. Their analysis concluded that changes in natural frequencies and the corresponding mode shapes depends on both crack location and material properties. Cerri et al. [78] have proposed a method to detect the structural damage affecting a narrow zone of a doubly hinged plane circular arch by measuring natural frequencies. Nobile et al. [79] have applied S-theory to determine crack initiation and direction for cracked T-beams and circumferentially cracked pipes. As stated by them they have used strain energy density factor(s) which is a function of stress intensity factor. According to them the strain energy density theory has the ability to describe the multi scale feature of material damage and in dealing with mixed mode crack propagation problem. A model-based fault diagnosis methodology for nonlinear systems is presented by Luh et al. [80]. Their simulation results show that it can detect and isolate actuator faults, sensor faults, and system component faults efficiently. A formulation has been developed by Chondros [81] for the torsional vibration analysis of a cylindrical shaft with a circumferential crack. The work is compared with existing methods. Structural damage detection using transfer matrix method has been performed by Escobar et al. [82] for locating and estimating structural damage. A robust fault detection method has been formulated by McAdams et al. [83] for the damage assessment of turbine blades considering impact of crack damage and manufacturing variation. The changes in the transverse vibration and associated eigenfrequencies of the beams are considered. They have observed that changes in fault detection monitoring signals caused by geometric variation are small with those caused by damage and impending failure. For beams containing multiple cracks and subjected to axial

force a new method has been proposed by Binici [84] which used a set of end conditions as initial parameters for determining the mode shape functions. Analysis for detection of the location and size of the cracks has been performed by Chang et al. [85]. The proposed analysis is able to calculate both the positions and depths of multi-cracks from spatial wavelet based method. First, the mode shapes of free vibration and natural frequencies of the multiple cracked beams are obtained. Then the mode shapes are analyzed by wavelet transformation to get the positions of the cracks. The elastic characteristics of a cantilevered composite panel of large aspect ratio and with an edge crack are investigated by Wang et al. [86]. The fundamental mode shapes of the cracked cantilever are used to study the crack. It is observed that the analysis may help the development of an online diagnosis tool. Crack identification in beam using dynamic response has been proposed by Law et al. [87]. The crack is modeled following the Dirac delta function. The dynamic responses are calculated based on modal superposition. The proposed identification algorithm is also verified experimentally from impact hammer tests on a beam with a single crack. Cam et al. [88,90] have performed a study to obtain information about the location and depth of the cracks in cracked beam. Their study suggested determining the location and depth of cracks by analyzing the vibration signals. Sekhar [89] applied the theory of model based identification in a rotor system with two cracks. They have analysed the detection and monitoring of slant crack in the rotor system using mechanical impedance. Loutridis et al. [91] have presented a new method for crack detection in beams based on instantaneous frequency and empirical mode decomposition. The dynamic behavior of a cantilever beam with a breathing crack under harmonic excitation is investigated both theoretically and experimentally. Patil et al. [92] have utilized a method for prediction of location and size of multiple cracks based on measurement of natural frequencies and verified experimentally for slender cantilever beams with two and three normal edge cracks. Their analysis is based on energy method and representation of a crack by a rotational spring. The equation of motion and corresponding boundary conditions has been developed by Behzad et al. [93] for forced bending vibration analysis of a beam with an open edge crack. A uniform Euler-Bernoulli beam and Hamilton principle have been used in this analysis. They have stated that there is an agreement between the theoretical results and finite element results. Nahvi et al. [94] have proposed method based on measured frequencies and mode shapes of the beam. In their experimental set up

they have used a hammer as an exciter and the responses are obtained in an accelerometer assuming the crack to be an open crack. To identify the crack location and depth the intersection of contours of the normalized frequency with the constant modal natural frequency planes are used. Leontios et al. [95] have presented a new method of crack detection in beams based on Kurtosis. As stated by them the location of the crack has been determined by the abrupt changes in spatial variation of the analyzed response and the size of the crack is calculated by the estimation of Kurtosis. In this work the proposed method has been validated by experiments on crack Plexiglas beams. Vibration analysis of an axially loaded cracked Timoshenko beam have been performed by Mei et al. [96] considering axial loading, shear deformation and rotary inertia criteria. The transmission and reflection matrices for various discontinuities of an axially loaded Timoshenko beam are derived. These matrices are combined to provide a concise and systematic approach for both free and forced vibration analyses of beams with cracks and sectional changes. Chasalevris and Papadopoulos [97] have studied the dynamic behavior of a cracked beam with two transverse surface cracks. Each crack is characterized by its depth, position and relative angle. A local compliance matrix of two degrees of freedom, bending in the horizontal and the vertical planes is used to model the rotating transverse crack in the shaft and is calculated based on the available expressions of the stress intensity factors and the associated expressions for the strain energy release rates. The natural frequencies have been obtained by Loya et al. [98] for Timoshenko cracked beams with different boundary conditions by modeling the beam as two segments connected by two mass less springs. The results show that the method provides simple expressions for calculating the natural frequencies of cracked beams and it gives good results for shallow cracks. Humar et al. [99] have studied the vibration based damage detection method and tried to find number of difficulties present in those damage identification methods. According to them vibration frequencies, mode shapes and damping are directly affected by the physical change in the structure including its stiffness. Vibration based structural damage detection in flexural members using multi criteria approach has been presented by Shih et al. [100]. In the analysis computer simulation techniques have been developed and applied for damage assessment in beams and plates. In addition to changes in natural frequencies, two methods, called the modal flexibility and the modal strain energy method have been applied which are based on the vibration characteristics of the structure.

Dash and chatterjee [101] have studied the fracture toughness of the epoxy composites using numerical technique. Harsha [102] has presented a model for investigating structural vibrations in rolling element bearings due to radial internal clearance using the vibration parameters and the Hertzian elastic contact deformation theory. Panda et al. [103] have investigated the nonlinear planar vibration of a pipe conveying pulsatile fluid subjected to principal parametric resonance in the presence of internal resonance. A numerical technique based on the global-local hybrid spectral element (HSE) method is proposed by Hu et al. [104] to study wave propagation in beams containing damages in the form of transverse and lateral cracks. This method is employed to investigate the behaviors of wave propagation in beams containing multiple transverse cracks and lateral cracks. Yang et al. [105] have discussed on the free and forced vibration of Euler–Bernoulli beams containing open edge cracks subjected to an axial compressive force and a concentrated transverse load moving along the longitudinal direction. Analytical solutions of natural frequencies and dynamic deflections are obtained for cantilever beams. It is found that the natural frequencies decreases and the dynamic deflection increases due to the presence of the edge crack and the axial compressive force. Yoona et al. [106] have investigated the influence of two open cracks on the dynamic behavior of a double cracked simply supported beam both analytically and experimentally. The equation of motion is derived by using the Hamilton’s principle and analyzed by numerical method. The simply supported beam is modeled by the Euler-Bernoulli beam theory. A combined analytical and experimental study has been conducted by Wang et al. [107] to develop efficient and effective damage detection techniques for beam-type structures. In combination with the uniform load surface (ULS), two new damage detection algorithms, i.e., the generalized fractal dimension (GFD) and simplified gapped-smoothing (SGS) methods, have been proposed for prediction of damage location and size successfully. The results from the proposed algorithm are experimentally validated. Lissenden et al. [108] have focused on the relationship between a crack and load, which propagated due to bending loads, and the torsional stiffness of the shaft. They have used a 3-D finite element model of a shaft section with a crack to predict the effect of a crack on stiffness. Al-Said [109] has proposed an algorithm based on a mathematical model to identify crack location and depth in an Euler-Bernoulli beam carrying a rigid disk. As stated by him, the lateral vibration of the beam has been described in the mathematical model using

Lagrange's equation. He has used mode shapes for two uniform beams connected by mass less torsional spring as trial function for the proposed method. The presented method utilizes the natural frequencies to estimate the crack location and depth. Kisa et al. [110] have presented a numerical technique to analyze the free vibration of uniform and stepped cracked beam of circular cross section. They have used finite element and component mode synthesis methods for the analysis and computed the flexibility matrix taking into account inertia forces and calculated the inverse of the compliance matrix by following appropriate expression for stress intensity factor and strain energy release rate. Karthikeyan et al. [111] have followed a method for crack location and size from the free and forced response of the beam. They have used Finite Element Method for free and forced vibration analysis of the open transverse surface crack beam. Orhan [112] has studied the free and forced vibration analysis of a cracked beam to identify the crack in a single- and two-edge cracks cantilever beam. Darpe [113] has presented a method using both the typical nonlinear breathing phenomenon of the crack and the coupling of bending-torsional vibrations to detect fatigue transverse cracks in rotating shafts. Viola et al. [114] have investigated the in-plane linear dynamic behavior of multi-stepped and multi-damaged circular arches. They have proposed analytical and numerical solutions for multi-stepped arches in damaged and undamaged configurations by adapting Euler characteristics exponent procedure for analytical solutions and focused on generalized differential quadrature method, generalized differential quadrature element for numerical solutions. According to them the convergence and stability characteristics of the generalized differential quadrature element techniques are investigated and the stability of the numerical procedure is found to be very good. Sinha [115] has proposed the higher order spectra tools for the identification of presence of harmonics in a signal which is a typical case of a non linear dynamic behavior in case of a mechanical system. He has found that for a misaligned rotating shaft or a cracked shaft, they are going to generate higher harmonics exhibiting non linear behavior. He has concluded that the results from higher order spectra tools are encouraging and suggested the use of the tool for condition monitoring of rotating machinery. Peng et al. [116,117,137] have used nonlinear output frequency response functions (NOFRFs), to explain the occurrence of the nonlinear phenomena when a cracked structure is subjected to sinusoidal excitations. They have also applied finite element model to analyze the crack induced nonlinear response of a beam by

using NOFRF concept. From this research study it has been concluded that NOFRF concept can be used in fault diagnosis of mechanical structures. Tandon et al. [118] have compared the condition monitoring techniques available for rolling element bearing namely vibration, stator current, acoustic emission and shock pulse method. They have concluded that acoustic emission proved to be the best among them. Friswell [119] has given an overview of the use of inverse method in the detection of crack location and size by using vibration data. He has suggested that the uncertain parameters associated with the model have to be identified. A number of problems with this method have been discussed for health monitoring, including modeling error, environmental efforts, damage localization and regularization. Yan et al. [120] have presented a general summary and review of vibration-based structural damage detection techniques. Various structural damage detection methods based on structural dynamic characteristic parameters are summarized and evaluated. The principle of intelligent damage diagnosis and its application prospects in structural damage detection are introduced. Naniwadekar et al. [121] have presented a technique based on measurement of change in natural frequencies and modeling of crack by rotational spring to detect a crack with straight front in different orientations in a section of straight horizontal steel hollow pipe. Variation of rotational spring stiffness with crack size and orientation has been obtained experimentally by deflection and vibration methods. The method is found to be very robust. Trendafilova et al. [122] have dealt with vibration-based fault detection in structures and suggests a viable methodology based on principal component analysis (PCA) and a simple pattern recognition (PR) method. The suggested damage detection methodology is based purely on the analysis of the vibration response of the structure. Courtney et al. [123] have used the bispectrum signal processing technique to analyze the nonlinear response of a sample to continuous excitation at two frequencies. The increased nonlinearity due to defects such as fatigue cracks is detected. Flexural wave propagation characteristics have been used by Park [124] for identification of damage in beam structures. The results from the proposed method are validated by the experimental analysis. The locations of damage on the beam structures with different magnitudes are identified accurately using the developed method. Different methodologies for crack detection for multi-crack structures have been analyzed by Sekhar [125] and the respective influences, identification methods in vibrating structures such as beams, rotors, pipes etc. are discussed. Waveform fractal method has been proposed by Qiao

et al. [126] for mode shape-based damage identification of beam-type structures. In their analysis a mathematical solution using waveform fractal dimension to higher mode shapes for crack identification has been demonstrated. The applicability and effectiveness of the applied method is validated by an experimental program on damage identification of a cracked composite cantilever beam using smart piezoelectric sensors/actuators. To calculate the natural frequencies and normal mode shapes of uniform isotropic beam element have been developed by Li et al. [127] using dynamic stiffness matrix based on trigonometric shear deformation theory. The numerical results obtained are compared to the available solutions wherever possible and validate the accuracy and efficiency of the present approach. Ostachowicz [128] has proposed Spectral finite element method for crack detection in structures using fracture mechanics, elastic wave propagations and applications of Lamb waves. The results obtained indicated that the current approach is capable of detecting cracks of very small size, even in the presence of measurement errors. Damage identification based on Lamb wave measurements have been introduced by Grabowska et al. [129]. The usage of wavelet transformation with propagating Lamb waves are for distinguishing between different types of damage. Reddy et al. [130] have presented fractal finite element based continuum shape sensitivity analysis for a multiple crack system in a homogeneous, isotropic, and two dimensional linear-elastic body subjected to mixed-mode loading conditions. The best feature of this method is that the stress intensity factors and their derivatives for the multiple crack system can be obtained efficiently. Hearndon et al. [131] have developed a method to study the influence of crack on dynamic properties of a cantilever beam subjected to bending with the help of Euler-Bernoulli and Timoshenko theories. A finite element model based on the response of the cracked beam element under static load has been proposed by them to compute the influence of crack location and size on the structural stiffness. In this work they have revealed that the experimental and computational natural frequencies decreases with increasing crack length. Al-said [132] has developed a crack identification algorithm to identify crack location and depth in a stepped cantilever beam carrying concentrated masses. According to him in vibration analysis the difference between the natural frequencies are used to locate the crack position and depth. As stated by him the advantage of the algorithm is to identify the crack by monitoring a single natural frequency system. According to him the advantage of the algorithm is to identify the

crack by monitoring a single natural frequency system. The robustness of the algorithm has been tested from an experimental work and from finite element analysis in this paper. Shin et al. [133] have presented vibration analysis of circular arches of variable cross section as they are widely used in modern architectural and structural requirements. In this study generalized differential quadrature method and differential transformation method have been applied by them for deriving governing equation of motion and for obtaining natural frequencies for different boundary conditions and the results are compared with previously published work. Cerri et al. [134] have presented a comparison of the experimental results of the dynamic behavior of a circular arch in undamaged and several damaged configuration with those obtained by analytical methods. In this work they have proposed an identification procedure by measuring natural frequencies and natural vibration modes and validated the results experimentally. Ebersbach et al. [135] have suggested an expert system for condition monitoring of fixed plant, laboratory and industry testing by using vibration analysis which will allow a great analysis and enable the technician to perform routine analysis. As described by them the expert system incorporates tri axial and demodulated frequency and the time domain vibration data analysis algorithms for high accuracy fault detection. Babu et al. [136] have addressed the problem of multi-crack assessment for rotors and described that solutions comprising of parameters characterizing the cracks are more complicated. They have developed a new technique called amplitude deviation curve, or slope deviation curve, which is a modification of the operational deflection shape. Yaghin et al. [138] have used the theory of wavelet analysis including continuous and discrete wavelet transform followed by its application to structural health monitoring. According to them by using the frequency analysis response of dam with ABAQUS software, crack detection has been done in dam structure under Wavelet analyzing in MATLAB software. Bayissa et al. [139] have presented a new method for damage identification based on the statistical moments of the energy density function of the vibration responses in time-frequency domain. According to them the major advantage of this method is that the time-frequency analysis conducted using the wavelet transform provides a tool to characterize deterministic as well as random responses and can be used to detect slight changes in the response of local vibration. Finally they have suggested that the proposed method is more sensitive to damage than the other methods. A solution to the free vibration problem of a stepped column with cracks is presented by Sukla

[140]. The open cracks at step changes in the cross-section of the column or at the intermediate points of the uniform segments are represented by mass less rotational springs. The proposed approach measures the vibration parameters assuming the column consists of an arbitrary number of uniform segments. Dilena et al. [141] have shown that the natural frequency and anti resonant frequency contains certain generalized fourier coefficients of the stiffness variation due to damage. According to them the results of numerical simulations on rods with localized or diffused cracks are in good agreement with theory. Mazanoglu et al. [142] have followed energy based method for vibration identification of non-uniform Euler – Bernoulli beams having open cracks. They have estimated the distribution of energy consumed by considering strain change at the cracked beam surface and the stress field due to angular displacement of beam because of bending. Rayleigh – Ritz approximation method has been adapted by them for analysis of beam with crack. Lee [143] has presented a method to identify crack in a beam by modeling the cracks as rotational springs. Newton-Rapson method has been adapted by him to identify the locations and sizes of the double as well as triple cracks in a cantilever beam. He has concluded that the detected crack locations and sizes are in excellent agreement with the actual ones. Faverjon et al. [144] have presented a damage assessment technique for detection of size of the open crack in beams. They have used constitutive relation error updating method for identification of crack location and size of the beam. According to them even if noise has been added to the simulation the algorithm can identify the crack location and size with satisfactory precision. He et al. [145] have presented a method to calculate the stress intensity factor and local flexibility matrix for cracked pipes by dividing the cracked pipe into series of these annuli. They have described that the calculation of local flexibility matrix for cracked pipes have been calculated experimentally without calculating the Stress intensity factor. Further the results from their method have been compared with the experimental results to verify the effectiveness of the method. Douka et al. [146] have presented the influence of two transverse open cracks on the anti resonances of a double cracked cantilever beam both analytically and experimentally. They have shown that the shift in the anti resonances of the cracked beam can be used as additional information for crack identification in double cracked beam. The results of experiments performed by them on Plexiglas beams for crack location and severity are in good agreement with theoretical predictions. Labuschagne et al. [147] have considered three

different linear theories: Euler – Bernoulli, Timo Shenko and Two dimensional elasticity for three models of cantilever beams. Using natural frequencies and modes as the basis, they concluded that the Timo Shenko theory is close to the two dimensional theory for practical purpose, but the applicability of Euler – Bernoulli theory is limited. Gan et al. [148] have developed a clonal selection programming (CSP)-based fault detection system to perform induction machine fault detection and analysis. The extracted features are inputs of a CSP-based classifier for fault identification and classification. The proposed CSP-based machine fault diagnostic system has been intensively tested with unbalanced electrical faults and mechanical faults operating at different rotating speeds. Ribeiro et al. [149,150] have used transmissibility concept for a structure and observed the response when the structure is excited at a given set of coordinates for fault detection.

2.5 Damage Diagnosis by Artificial Intelligence Technique

Intelligence is the computational part of the ability to achieve goals in the world. The aim of artificial intelligence is to develop algorithms that allow machines to perform tasks that involve cognition when performed by humans. The word “cognition” comes from the latin word “cognitio”, which means “knowledge”. Cognitive sciences concern thinking, perception, reasoning, creation of meaning, and other functions of a human mind. As cracks pose as a potential cause of failure for mechanical or structural systems, the early detection of it will save the systems from catastrophic failure and also save a lot amount of finance involved in it. Algorithms have been developed which can predict the crack location and its severity of a system before hand using different Artificial Intelligence techniques. Since the algorithms use Artificial Intelligence techniques they can be used as non destructive testing methodology for early detection of crack in dynamically vibrating structures. McCarthy [151] has stated that Artificial intelligence is the science and engineering of making intelligent machines, especially intelligent computer programs. It is related to the similar task of using computers to understand human intelligence, but AI does not have to confine itself to methods that are biologically observable.

2.5.1 Fuzzy Logic Technique for Damage Diagnosis

The fuzzy logic technique is one of the AI methods which can be used for damage diagnosis in the domain of dynamically vibrating structures. It is very much evident that the crack can be detected from the vibration analysis of the cracked structure but to develop a methodology/controller for on line condition monitoring of damaged structure artificial intelligence techniques has to be adapted. To design an intelligent controller fuzzy logic play vital role. This is due to the fact that fuzzy if-then rules are well suited for capturing the imprecise nature of human knowledge and reasoning processes. Fuzzy sets are functions that map a value, which might be a member of a set, to a number between zero and one, indicating its actual degree of membership .Fuzzy logic is based on the idea that all things admit of degrees. A degree of zero means that the value is not in the set and a degree of one means that the value is completely representative of the set. Fuzzy logic modeling is primarily based on fuzzy sets and fuzzy if-then rules proposed by Zadeh [152] which are closely related to perception and cognitive science.

2.5.1.1 Fuzzy History

About 300 B.C., the Greek scholar Aristotle developed binary logic. Aristotle thought that the world was made up of opposites, for example male versus female, hot versus cold, dry versus wet, active versus passive. Everything has to be A or not-A, it can't be both. Subsequently with this idea a new technique was developed wick accommodate the uncertainty of the problem and gives the solution i.e. fuzzy logic. Fuzzy logic is based on the idea that A can equal not-A. That means that something can contain a part of its opposite. Negoitã [153] has dealt with a new clustering technique using the concept of fuzzy set [152]. A membership function is proposed and a method to select the cluster elements is derived using the separation theorem of the fuzzy sets. Kandel [154] has discussed two theorems, which are the basis of a new technique that generates the complete set of fuzzy implicants, and used for the minimization of fuzzy functions.

2.5.1.2 Application of Fuzzy Logic

The fuzzy logic method can be used in a wide spectrum of industrial application as well as in domestic appliances such as shower heads, rice cookers, vacuum cleaners etc. The application of fuzzy approach is further expressed with the review of following published papers.

Fox [155] has studied the use of fuzzy logic in medical diagnosis and raised a broad range of issues in connection to the role of information-processing techniques in the development of medical computing. Gologlu [156] has presented a set-up planning module as part of a feature-based process planning system with the aid of artificial intelligence. Zimmermann [157] has applied fuzzy linear programming approach for solving linear vector maximum problem. The solutions are obtained by fuzzy linear programming. These are found to be efficient solutions then the numerous models suggested to solve the vector maximum problem. Wada et al. [158] have proposed a fuzzy control method with triangular type membership functions using an image processing unit to control the level of granules inside a hopper. They have stated that the image processing unit can be used as a detecting element and with the use of fuzzy reasoning methods good process responses are obtained. Fuzzy finite element method for static analysis of engineering systems has been done by Rao et al. [159] using an optimization-based scheme taking fuzzy parameters into consideration. A fuzzy arithmetical approach has been used by Hanss et al. [160] for the solution of finite element problems involving uncertain parameters. Boutros et al. [161] have reported a simple, effective and robust fusion approach based on fuzzy logic and sugeno-style inference engine. Using this method, four condition-monitoring indicators, developed for detection of transient and gradual abnormalities, are fused into one single comprehensive fuzzy fused index (FFI) for reliable machinery health assessment. This approach has been successfully tested and validated in two different practical applications.

2.5.1.3 Application of Fuzzy Logic for Fault Diagnosis

In this section a number of journal papers related to fault diagnosis using fuzzy technique has been reviewed and described.

A fuzzy finite element approach has been proposed by Akpan et al. [162] for modeling smart structures with imprecise parameters. A simple method for diagnosis of railway wheel defects using fuzzy-logic has been proposed by Skarlatos et al. [163]. The method is based on vibration measurements at different train speeds on healthy wheels and wheels with known defects. To facilitate the implementation of the method fuzzy-logic is adopted. Liu et al. [164] have described a new method of grinding burn identification with highly sensitive acoustic emission (AE) techniques. The wavelet packet transform is used to extract features from AE signals and fuzzy pattern recognition is employed for optimizing features and identifying the grinding status. Experimental results show that the accuracy of grinding burn recognition is satisfactory. Parhi et al. [165] have designed a mobile robot navigation system using fuzzy logic. Fuzzy rules embedded in the controller of a mobile robot enable it to avoid obstacles in a cluttered environment that includes other mobile robots. Angelov et al. [166] have presented a systematic classification of the data-driven approaches for design of fuzzy systems. The condition monitoring of a lab-scale, single stage, gearbox using different non-destructive inspection methodologies and the processing of the acquired waveforms with advanced signal processing techniques have been presented by Loutas et al. [167]. Acoustic emission (AE) and vibration measurements with fuzzy method are utilized for this purpose. The experimental setup has been used for validation of results from the proposed method. As stated by the author the system can be used for the early diagnosis of natural wear in gear systems. Saravanan et al. [168] have used decision tree for selecting best statistical features that will discriminate the fault conditions of the gear box from the signals extracted to determine the condition of an inaccessible gear in an operating machine. A rule set is formed from the extracted features and fed to a fuzzy classifier. A fuzzy classifier is built and tested with representative data. A fuzzy finite element method has been used by Chen et al. [169] for vibration analysis of imprecisely defined systems by using a search based algorithm. The fuzzy approach enhances the computational efficiency for identifying the system dynamic responses. Pawar et al. [170,174] have used a genetic fuzzy system and finite element model of a cantilever beam to find the location and extent of damage. Using these changes in frequencies, a fuzzy system is generated and the rule-base and membership functions are optimized by genetic algorithm. The genetic fuzzy system gives very good results for hinge less helicopter rotor blade for frequency as well as mode shape-based data. Taha et al. [171]

have introduced a method to improve pattern recognition and damage detection by supplementing Intelligent Structural Health Monitoring (ISHM) with fuzzy sets. Bayesian updating is used to demarcate levels of damage into fuzzy sets accommodating the uncertainty associated with the ambiguous damage states. The new techniques are examined to provide damage identification using data simulated from finite element analysis of a pre-stressed concrete bridge. Packianather et al. [172] have proposed a method for identification of defects in wood veneer using neural network. Dwivedy et al. [173] have discussed about application of AI techniques in various engineering problems. Kim et al. [175] have presented a computer assisted crack diagnosis system for reinforced concrete structures. The system presented adapts fuzzy set theory to reflect fuzzy conditions, for crack symptoms and characteristics which are difficult to treat using crisp sets. The inputs to the system are mostly linguistic variables of the crack and some numeric data about concrete and environmental conditions. An attempt has been made by Sasmal et al. [176] to develop a systematic procedure and formulations for condition evaluation of existing bridges using analytic hierarchy process in a fuzzy environment. Fuzzy logic approach has been used to take care of the uncertainties and imprecision in the bridge observations. Chandrashekhar et al. [177] have shown that geometric and measurement uncertainty cause considerable problem in damage assessment which can be alleviated by using a fuzzy logic-based approach for damage detection. Monte Carlo simulation (MCS) is used to study the changes in the damage indicator due to uncertainty in the geometric properties of the beam. The paper brings together the disparate areas of probabilistic analysis and fuzzy logic to address uncertainty in structural damage detection.

2.5.2 Neural Network Technique for Damage Diagnosis

The human brain is very complex, nonlinear and parallel computer. There are billions of neurons and trillions of connections between them. The interest in neural network stems from the wish of understanding principles leading in some manner to the comprehension of the basic human brain functions, and to building the machines that are able to perform complex tasks. Neural network theory revolves around the idea that certain key properties of biological neurons can be extracted and applied to simulations, thus creating a simulated brain. The neural network technique can be used for damage diagnosis in vibrating cracked

structures. For on line condition monitoring of damaged structure artificial intelligence techniques has to be adapted. To design an intelligent controller neural network play vital role.

2.5.2.1 Neural Network History

The modern era of neural network research is credited with the work done by neuro-physiologist, Warren McCulloch and young mathematical prodigy Walter Pitts in 1943[179]. They wrote a paper on how neurons might work, and they designed and built a primitive artificial neural network using simple electric circuits. They are credited with the McCulloch-Pitts Theory of Formal Neural Networks. The next major development in neural network technology have arrived in 1949 with Donald Hebb [180]. A major point brought forward from his research, described how neural pathways are strengthened each time they were used. As we shall see, this is true of neural networks, specifically in training a network. Years later, John von Neumann thought of imitating simplistic neuron functions by using telegraph relays or vacuum tubes. This led to the invention of the von Neumann machine.

2.5.2.2 Application of Neural Network

This section describes the review of literature from the application area of neural network in various fields.

Little et al. [181] have solved a linearized version of the model and explicitly showed that the capacity of the memory is related to the number of synapses rather than the number of neurons. In addition, they have shown that in order to utilize this large capacity, the neural network must store the major part of the information in memory to generate patterns which evolve with time. Urban et al. [182] have described the development of enhanced, high speed data reduction algorithms using artificial neural networks (ANN). The networks are trained using computed data and subsequently give values of film parameters in the millisecond time regime. Athanasiu et al. [183] have used an artificial neural network (ANN) with local connectivity as a track identifier for high energy physics experiments. The performance of the ANN is evaluated with data of the experiment, with very encouraging results. Sette et al. [185] have presented a method to simulate a complex production process using a neural

network and the optimization by genetic algorithm for quality control of the end product in a manufacturing environment. They have used the genetic algorithm with a sharing function and a Pareto optimization to optimize the input parameters for obtaining the best yarns. According to them the results from this method are considerably better than current manual machine intervention. Mohanty et al. [186] have proposed a method for classification of remotely sensed data using an artificial neural network (ANN) approach. Taib et al. [187] have applied an artificial neural network (ANN) for the analysis of the response of an optical fibre pH sensor. A three layer feed forward neural network is used and network training is performed using the recursive prediction error (RPE) algorithm. An application of the method has been demonstrated. Kermanshahi [188] have applied two artificial neural networks, a recurrent neural network (RNN) and a three-layer feed-forward back-propagation (BP) for long-term load forecasting. In this study, total system load forecast reflecting current and future trends, tempered with good judgement which is the key to all planning and indeed financial success is carried out for nine utilities in Japan. Ghiassi et al. [190] have presented a dynamic neural network model for forecasting time series events that uses a different architecture than traditional models. To assess the effectiveness of this method, they have forecasted a number of standard benchmarks in time series research from forecasting literature. Results show that this approach is more accurate and performs significantly better than the traditional neural network. Hines et al. [191] have focused on the implementation of methods and the development of methods for next generation plants and space reactors. As stated by them the advanced techniques are expected to become increasingly important for current generation nuclear power plants. Song et al. [192] have presented a method for comparison of logistic regression and artificial neural network for computer-aided diagnosis on breast sonograms. They have concluded that there is no difference in performance between logistic regression and the artificial neural network as measured by the area under the ROC curve. Kadi et al. [193] have attempted to reflect on the work done in the mechanical modeling of fiber-reinforced composite materials using ANN during the last decade. Lucon et al. [194] have utilized artificial neural networks in place of a traditional micromechanical approach to calculate the global elastic properties of composite materials given the local properties and local geometry. This approach is shown to be more computationally efficient than conventional numerical micromechanical approaches. Assaad

et al. [195] have adapted an ensemble method to the problem of predicting future values of time series using recurrent neural networks (RNNs) as base learners. The improvement is made by combining a large number of RNNs, each of which is generated by training on a different set of examples. Carbonneau et al. [196] have investigated the applicability of advanced machine learning techniques, including neural networks, recurrent neural networks, and support vector machines, to forecast distorted demand at the end of a supply chain. Lolas et al. [197] have presented the first module of an expert system, a neural network architecture that could predict the reliability performance of a vehicle at later stages of its life by using only information from a first inspection after the vehicle's prototype production. A case study is presented by them to demonstrate the methodology. Ozerdem et al. [198] have employed an artificial neural network approach to predict the mechanical properties of cast alloys. In artificial neural network (ANN), multi layer perceptron (MLP) architecture with back-propagation algorithm is utilized. ANN system is trained using the prepared training set and has given satisfactory results. Reddy et al. [199] have developed an artificial neural network (ANN) model for the analysis and simulation of the correlation between the mechanical properties and composition and heat treatment parameters of low alloy steels. Panigrahi et al. [200] have used adaptive bacterial foraging algorithm and AI technique for monitoring power system. Sun et al. [201] have formulated and solve the force distribution problem for multi arm systems with flexible-link arms, with particular attention to the non minimum phase character of the system.

2.5.2.3 Application of Neural Network for Fault Diagnosis

The application of neural network for fault diagnosis in different domain of engineering system can be established with the review of literatures as follows.

Uhrig et al. [202] have described methods that deal with power plants or parts of plants that can be isolated. Typically, the measured variables from the plants are analog variables that must be sampled and normalized to expected peak values before they are introduced into neural networks. Specific applications using neural network described by them include: transient identification, plant-wide monitoring, analysis of vibrations, and monitoring of performance and efficiency. Sreedhar et al. [203] have presented an adaptive neural network

for fault detection in nonlinear systems. The scheme used by them provides robust fault detection in the presence of modeling errors and is validated by simulating faults in a section of a thermal power plant model. Uhrig et al. [204] have done a comprehensive study of the application of soft computing technologies, particularly neural networks, fuzzy logic, and genetic algorithms, to the surveillance, diagnostics and operation of nuclear power plants. The benefits of combining the use of neural networks, fuzzy systems and genetic algorithms are illustrated in several applications. Gao et al. [205] have proposed an Elman neural network-based method for fault detection in motor drive systems. They have stated that the Elman neural network has the advantageous time series prediction capability because of its memory nodes, as well as local recurrent connections. The intelligent computational tools of feed forward neural networks and genetic algorithms are used to develop a real-time detection and diagnosis system of specific mechanical, sensor failures in a deep-trough hydroponic system by Ferentinos et al. [206]. Samanta et al. [207] have presented the comparison of the performance of bearing fault detection using three types of artificial neural networks (ANNs), namely, multilayer perceptron (MLP), radial basis function (RBF) network, and probabilistic neural network (PNN). They have used vibration signals of a rotating machine with defective bearings as inputs to all three ANN classifiers for normal or fault recognition. The characteristic parameters along with the selection of input features are optimized using genetic algorithms (GA). According to them the procedure has used the experimental vibration data of a rotating machine with and without bearing faults. The results show the relative effectiveness of three classifiers in detection of the bearing condition. Choi et al. [209] have developed a method to estimate the size of a tooth transverse crack for a spur gear in operation. Zhou et al. [211] have described how the recursive algorithm updates the BRB (Belief Rule Base) system work, so that the updated BRB cannot only be used for pipeline leak detection but also satisfy the given patterns. They have also demonstrated that compared with other methods such as fuzzy neural networks (FNNs), the developed system has a special characteristic of allowing direct intervention of human experts in deciding the internal structure and the parameters of a BRB expert system. Nishith et al. [212] have proposed a method with the application of a counter propagation neural network (CPNN) to detect single faults and their magnitudes in a non isothermal continuous stirred tank reactor (CSTR). Stavroulakis et al. [213] have used soft computing and in particular neural network

techniques for crack detection and identification problems. Elastostatic and elastodynamic excitations are modelled by the BEM. Results of inverse calculations obtained by the back propagation neural network model are presented. Suh et al. [214] have established that a crack has an important effect on the dynamic behavior of a structure. This effect depends mainly on the location and depth of the crack. A neural network technique is developed for identifying the damage occurrence in the side shell of a ship's structure by Zubaydi et al. [215]. The side shell is modeled as a stiffened plate. The input to the network is the autocorrelation function of the vibration response of the structure. The response is obtained using a finite element model of the structure. The results show that the method presented in this work is successful in identifying the occurrence of damage. Kao et al. [216] have employed a novel neural network-based approach for detecting structural damage. The first step, system identification, uses neural system identification networks (NSINs) to identify the undamaged and damaged states of a structural system. The second step, structural damage detection, uses the aforementioned trained NSINs to generate free vibration responses with the same initial condition. Furthermore, numerical and experimental examples demonstrate the feasibility of applying the proposed method for detecting structural damage. Yam et al. [217,218] have presented an integrated method for damage detection of composite structures using their vibration responses, wavelet transform and artificial neural networks (ANN). The ANN are applied to establish the mapping relationship between structural damage and damage status (location and severity). The results show that the method can be applied to online structural damage detection and health monitoring for various industrial structures. Sahin et al. [219] have presented a damage detection algorithm using a combination of global (changes in natural frequencies) and local (curvature mode shapes) vibration-based analysis data as input in artificial neural networks (ANNs) for location and severity prediction of damage in beam-like structures. Different damage scenarios have been introduced by reducing the local thickness of the selected elements at different locations along finite element model (FEM) of the beam structure. Zacharias et al. [220] have proposed a crack detection method by an artificial neural network (ANN) trained exclusively with frequency response spectra from finite-element simulations. The classification fails for some data sets of intact crates, due to experimental conditions not accounted for in the finite-element simulation. Suresh et al. [221] have presented a method considering the flexural vibration in

a cantilever beam having transverse crack. They have computed modal frequency parameters analytically for various crack locations and depths and these parameters are used to train the neural network to identify the damage location and size. Damage assessment in structures from changes in static parameter using neural network have been performed by Maity et al. [222]. The basic strategy applied in their study is to train a neural network to recognize the behaviour of the undamaged structure as well as of the structure with various possible damaged states. When this trained network is subjected to the measured response, it is able to detect any existing damage. Lee et al. [223] have developed a neural networks-based damage detection method using the modal properties, which can effectively consider the modelling errors in the baseline finite element model from which the training patterns are to be generated. Two numerical example analyses on a simple beam and a multi-girder bridge are presented to demonstrate the effectiveness of the proposed method. Yeung et al. [224] have proposed a damage detection procedure, using pattern recognition of the vibration signature and finite element model of a real structure. They have stated that the neural networks may be adjusted so that a satisfactory rate of damage detection may be achieved even in the presence of noisy signals. A new approach for crack detection in beam structures using neural network (Radial Basis Function) have been performed by Li et al. [225]. Damage detection algorithm is presented using a combination of global and local vibration-based analysis data as input in artificial neural networks (ANNs) for location and severity prediction of damage in beam like structures. Finite element analysis has been used to obtain the dynamic characteristics of intact and damaged cantilever steel beams for the first three modes. The results from the proposed method have been validated with the results from experimental analysis. Neural network based damage detection generally consists of a training phase and a recognition phase. The relative sensitivities of structural dynamic parameters are analyzed by He-sheng et al. [226] using neural network. The combined parameters are presented as the input to the neural network, which computed with the change rates of the several natural frequencies and the change ratios of the frequencies. Some numerical simulation examples, such as, cantilever and truss with different damage extends and different damage locations are analyzed. The results indicated that the combined parameters are more suitable for the input patterns of neural networks than the other parameters alone. Choubey et al. [227] have studied to analyze the effect of cracks on natural

frequencies in two vessel structures. Finite element analysis has been used by them to obtain the dynamic characteristics of intact and damaged vessels. The natural frequencies for different modes have been used as input pattern of ANN (artificial neural network) model. The output of the ANN model is a crack size for a particular location. Li et al. [228] have described a new and practical method to estimate the size of a crack on a rotating beam in a laboratory setting. Their paper consists of selecting and validating a sensor and a measurement variable, devising a signal processing method for crack size estimation and carrying out experimental validations. The study employed a diagnostic neural network to map the frequencies to crack size. The experimental results show that the proposed approach can provide reasonably good estimates of the crack size using the indirectly excited acoustic signal. Yu et al. [229] have developed a vibration-based damage detection method for a static laminated composite shell partially filled with fluid and validated by experiment. An artificial neural network (ANN) is trained by them using numerically simulated structural damage index to establish the mapping relationship between the structural damage index and damage status. The damage status is successfully identified using ANN and the method can be applied to online structural damage detection and health monitoring. Wang et al. [230] have presented the numerical simulation and the model experiment upon a hypothetical concrete arch dam for the research of crack detection based on the reduction of natural frequencies. Numerical analysis and model experiment show that the crack occurring in the arch dam will reduce natural frequencies and can be detected by using the statistical neural network based on the information of such reduction. Pawar et al. [231] have proposed spatial Fourier analysis and Neural technique for damage detection in beam. Their study investigated the effect of damage on beams with fixed boundary conditions using Fourier analysis. A finite element model is used to obtain the mode shapes of a damaged beam. It is found that damage caused considerable change in the Fourier coefficients of the mode shapes, which are found to be sensitive to both damage size and location. A neural network is trained to detect the damage location and size using Fourier coefficients as input. Numerical studies showed that damage detection using Fourier coefficients and neural networks has the capability to detect the location and damage size accurately. Reddy et al. [232] have proposed a method for beams with fixed boundary conditions of a damaged fixed beam by using Fourier analysis, for identification of crack location and depth. They have also used

neural network which is trained to detect the damage location and size using fourier coefficients as input. They have studied that the method for damage detection using Fourier coefficients and neural network has the capability to detect the location and damage size even in the presence of noise parameters satisfactorily and accurately. Bakhary et al. [233] have used Artificial Neural Network for damage detection. In their analysis an ANN model is created by applying Rosenblueth's point estimate method verified by Monte Carlo simulation. The statistics of the stiffness parameters are estimated. The probability of damage existence (PDE) is then calculated based on the probability density function of the existence of undamaged and damaged states. The developed approach is applied to detect simulated damage in a numerical steel portal frame model and also in a laboratory tested concrete slab.

2.5.3 Neuro-Fuzzy Technique for Damage Diagnosis

In the field of artificial intelligence, Neuro-Fuzzy refers to combinations of artificial neural networks and fuzzy logic which incorporates the capability of both fuzzy logic and neural network technique. This hybrid method can give better results than the independent techniques. Fuzzy systems have the ability to make use of knowledge expressed in the form of linguistic rules, thus they offer the possibility of implementing expert human knowledge and experience. Usually, tuning parameters of membership functions is a time consuming task. Neural network learning techniques can automate this process, significantly reducing development time, and resulting in better performance. Neuro-fuzzy hybridization results in a hybrid intelligent system that synergizes these two techniques by combining the human-like reasoning style of fuzzy systems with the learning and connectionist structure of neural networks. Hence, this methodology can take the vibration signatures as input parameters and predict the crack location and depth. Jantunen [234] has used Neuro-Fuzzy System for condition monitoring and diagnostic management of mechanical system.

2.5.3.1 Neuro-Fuzzy Technique History

A neuro-fuzzy system is based on a fuzzy system which is trained by a learning algorithm derived from neural network theory. The learning procedure operates on local information, and causes only local modifications in the underlying fuzzy system. The strength of neuro-

fuzzy systems involves two contradictory requirements in fuzzy modeling: interpretability versus accuracy. In practice, one of the two properties prevails. The neuro-fuzzy in fuzzy modeling research field is divided into two areas: linguistic fuzzy modeling that is focused on interpretability, mainly the Mamdani model; and precise fuzzy modeling that is focused on accuracy, mainly the Takagi-Sugeno-Kang (TSK) model.

2.5.3.2 Application of Neuro-Fuzzy Technique

Ichihashi et al. [235] have developed a popular and efficient method of making a decision tree for classification from symbolic data without much computation. Fuzzy reasoning rules in the form of a decision tree, which can be viewed as a fuzzy partition, are obtained by fuzzy ID3. Wang et al. [236] have evaluated the performance of recurrent neural networks (RNNs) and neuro-fuzzy (NF) systems using two benchmark data sets. Through comparison it is found that if an NF system is properly trained, it performs better than RNNs in both forecasting accuracy and training efficiency. The performance of the developed prognostic system is evaluated by using three test cases.

2.5.3.3 Application of Neuro-Fuzzy Technique for Fault Diagnosis

Singh et al. [237] have reviewed the progress made in electrical drive condition monitoring and diagnostic research and development in general and induction machine drive condition monitoring and diagnostic research and development using expert systems, neural network and fuzzy logic, in particular, since its inception. Xu et al. [238] have proposed neuro-fuzzy control strategy, in which the neural-network technique is adopted to solve time-delay problem and the fuzzy controller is used to determine the control current of MR dampers quickly and accurately. They have observed that the control effect of the neuro-fuzzy control strategy is better than that of the bi-state control strategy. A novel integrated classifier has been developed by Wang et al. [239] for real-time machinery health condition monitoring, specifically for gear systems. The diagnostic classification is performed by a neural fuzzy scheme. An online hybrid training technique is adopted based on recursive Levenberg-Marquett and least-squares estimate (LSE) algorithms to improve the classifier convergence and adaptive capability to accommodate different machinery conditions. The viability of this

new monitoring system is verified by experimental tests under different gear conditions. Test results show that the proposed integrated classifier provides a robust problem solving framework. Saridakis et al. [240] have proposed a method using fuzzy logic, genetic algorithm and neural network for considering the dynamic behavior of a shaft with two transverse cracks characterized by position, depth and relative angle. They have concluded that genetic algorithm along with the neural network which form the analytical model for analysis remarkably reduce the computational time without any loss of accuracy. Rafiee et al. [241] have presented an optimized gear fault identification system using genetic algorithm (GA) to investigate the type of gear failures of a complex gearbox system using artificial neural networks (ANNs) with a well-designed structure suited for practical implementations.

2.5.4 Multiple Adaptive Neuro Fuzzy Inference Technique (MANFIS)for Damage Diagnosis

Adaptive neuro-fuzzy inference systems (ANFIS), fusing the capabilities of artificial neural networks and fuzzy inference systems, offer a lot of space for solving different kinds of problems, and are especially efficient in the domain of signal prediction. However, the ANFIS technique is sometimes notated as being computationally expensive. After considering the conventional ANFIS architecture, a new idea came up known as multiple adaptive neuro-fuzzy inference systems (MANFIS) developed with the intention of making the ANFIS technique more efficient with regard to root mean square error (RMSE) and/or computing time by Jovanovic et al. [242]. So this technique can be used for crack diagnosis effectively in cracked structures with multiple ANFIS system.

2.5.4.1 MANFIS History

Fuzzy inference is the process of formulating the mapping from a given input to an output using fuzzy logic. The mapping then provides a basis from which decisions can be made, or patterns discerned. The process of fuzzy inference includes membership functions, fuzzy logic operators, and if-then rules. ANFIS provides a method for the fuzzy modeling procedure to learn information about a dataset, in order to compute the membership function parameters that best allow the associated fuzzy inference system to track the given input/output data. Jang [243] has exhibited the use of ANFIS technique in engineering

application. Random and bootstrap sampling method and ANFIS (Adaptive Network based Fuzzy Inference System) are integrated into En-ANFIS (an ensemble ANFIS) to predict chaotic and traffic flow time series to achieve both high accuracy and less computational complexity for time series prediction by Chen et al. [244]. Hinojosa et al. [245] have presented four modeling methods of microwave devices using multiple neuro-fuzzy inference systems (MANFIS) based on space-mapping (SM) approach.

2.5.4.2 Application of MANFIS

In this section, applications of MANFIS technique in various fields have been established with the literature review of published paper.

Jassar et al. [246] have developed an inferential sensor model, based on adaptive neuro-fuzzy inference system modeling, for estimating the average air temperature in multi-zone space heating systems. This modeling technique has the advantage of expert knowledge of fuzzy inference systems (FISs) and learning capability of artificial neural networks (ANNs). The average air temperature results estimated by using the developed model are strongly in agreement with the experimental results. Domenech et al. [247] have applied fuzzy logic for accurate analog circuit macro model sizing is presented. In the proposed method, multiple adaptive neuro-fuzzy inference systems (MANFIS) are trained to predict the performance characteristics. Zhang et al. [248] have presented an investigation into the use of the delay coordinate embedding technique with adaptive-network-based-fuzzy-inference system (ANFIS) and MANFIS technique to learn and predict the continuation of chaotic signals ahead in time.

2.5.4.3 Application of MANFIS for Fault Diagnosis

The papers presented, the use of MANFIS technique for fault diagnosis has been reviewed and discussed in this section.

Nguyen et al. [249] have developed a bearing diagnostics method using fuzzy inference based on vibration data. Adaptive Network based Fuzzy Inference System (ANFIS) and Genetic Algorithm (GA) has been proposed to select the fuzzy model input and output

parameters. The result is also tested with other set of bearing data to illustrate the reliability of the chosen model. Elbaset et al. [250] have presented an application of ANFIS approach for automated fault detection and classification in transmission lines using measured data from one terminal of the transmission line. The ANFIS design and implementation are aimed at high-speed processing which can provide selection of real-time detection and classification of faults. The ANFIS's are trained and tested using various sets of field data. Ye et al. [251] have presented an online diagnostic algorithm for mechanical faults of electrical machines with variable speed drive systems using wavelet packet decomposition. A new integrated diagnostic system for electrical machine mechanical faults is proposed using multiple adaptive neuro-fuzzy inference Systems (ANFIS). The diagnostic algorithm is validated on a three-phase induction motor drive system. Yeo et al. [252] have proposed an algorithm for fault detection and classification for both low impedance faults and high impedance faults using Adaptive Network-based Fuzzy Inference System (ANFIS). The inputs into ANFIS are current signals only based on Root-Mean-Square values of three-phase currents and zero sequence current. The performance of the proposed algorithm is tested and found to be encouraging. Sadeh et al. [253] have presented an algorithm for locating faults in a combined overhead transmission line with underground power cable using Adaptive Network-Based Fuzzy Inference System (ANFIS). Simulation results confirm that the proposed method can be used as an efficient means for accurate fault location on the combined transmission lines. Razavi-Far et al. [254] have described a neuro-fuzzy networks based scheme for fault detection and isolation of a U-tube steam generator in a nuclear power plant. Experimental results presented in the final part of the paper confirm the effectiveness of this approach. Tran et al. [255] have presented a fault diagnosis method based on adaptive neuro-fuzzy inference system (ANFIS) in combination with decision trees. The crisp rules obtained from the decision tree are then converted to fuzzy if-then rules that are employed to identify the structure of ANFIS classifier. In order to evaluate the proposed algorithm, the data sets obtained from vibration signals and current signals of the induction motors are used. The results indicate that the ANFIS model has potential for fault diagnosis of induction motors. Lei et al. [256,257] have presented a method for fault diagnosis based on empirical mode decomposition (EMD), an improved distance evaluation technique and the combination of multiple adaptive neuro-fuzzy inference systems (ANFISs). Their proposed method is

applied to the fault diagnosis of rolling element bearings, and testing results show that the multiple ANFIS combination can reliably recognize different fault categories and severities.

From the above literature survey, it is found that the vibration signatures of the cracked structure can be calculated by using strain energy release rate and stress intensity factor. Different Artificial Intelligence Techniques can be used for fault detection and condition monitoring of various engineering applications. It is found from the review that the AI techniques are not used potentially for on line condition monitoring of crack in vibrating structures.

So in the subsequent section algorithm have been developed for on line condition monitoring of a cracked cantilever beam using AI techniques such as Fuzzy Logic, Neural Network, Fuzzy Neuro and MANFIS techniques.

Chapter 3

ANALYSIS OF DYNAMIC CHARACTERISTICS OF BEAM WITH TRANSVERSE CRACK

Cracks in vibrating components can initiate catastrophic failures. Therefore, there is the need to understand the dynamic characteristics of cracked structures to save the structure beforehand by detecting the crack location and its intensity. When a structure suffers damage, its dynamic properties change. Specifically, damage due to the crack can cause a stiffness reduction, with an inherent reduction in natural frequencies, an increase in modal damping, and a change in the mode shapes.

3.1 Introduction

Dynamic characteristics of structures with crack have been studied for last four decades intensively. Natural frequencies and modes shapes undergo variation due to presence of crack in terms of its location and intensity. Scientists are focusing their thoughts on various aspects of cracked structures. The current research addresses the investigation of the dynamic behavior of a cracked beam with a transverse crack. The presence of a crack in a structural member introduces a local flexibility that affects its dynamic response. For finding out the deviation in the vibrating signatures of the cracked cantilever beam the local stiffness matrices are taken into account. Theoretical expressions have been developed to calculate the natural frequencies and mode shapes of the cracked cantilever beam using local stiffness matrices. Strain energy release rate has been used for calculating the local stiffnesses of the beam. The local stiffnesses are dependent on the crack depth. Different boundary conditions are outlined which take into account the crack location. Comparisons are made between the numerical results and corresponding experimental results for validation of the established theory.

3.2 Dynamic Characteristics of a Cantilever Beam with a Transverse Crack

3.2.1 Theoretical Analysis

A systematic approach has been adopted in the present investigation to develop theoretical expressions for calculation of natural frequencies and mode shapes of cracked cantilever beam with a transverse crack and to notice the effect of crack on natural frequencies and mode shapes. Experiments have been conducted over cracked cantilever beam specimen for validation of the theory established. Natural frequencies and the mode shapes of the cracked cantilever beam specimen are found out both numerically and experimentally for different relative crack depth and relative crack location from fixed end of the cantilever beam. Remarkable variations in mode shapes are noticed at the vicinity of crack location.

3.2.1.1 Local Flexibility of a Cracked Cantilever Beam under Bending and Axial Loading

A cantilever beam with a transverse surface crack of depth ' a_1 ' on beam of width ' B ' and height ' W ' is considered in the current research. The beam is subjected to axial force (P_1) and bending moment (P_2) (Fig.3.2.1) which gives coupling with the longitudinal and transverse motion. The presence of crack introduces a local flexibility, which can be defined in matrix form, the dimension of which depends on the degrees of freedom. Here a 2x2 matrix is considered.

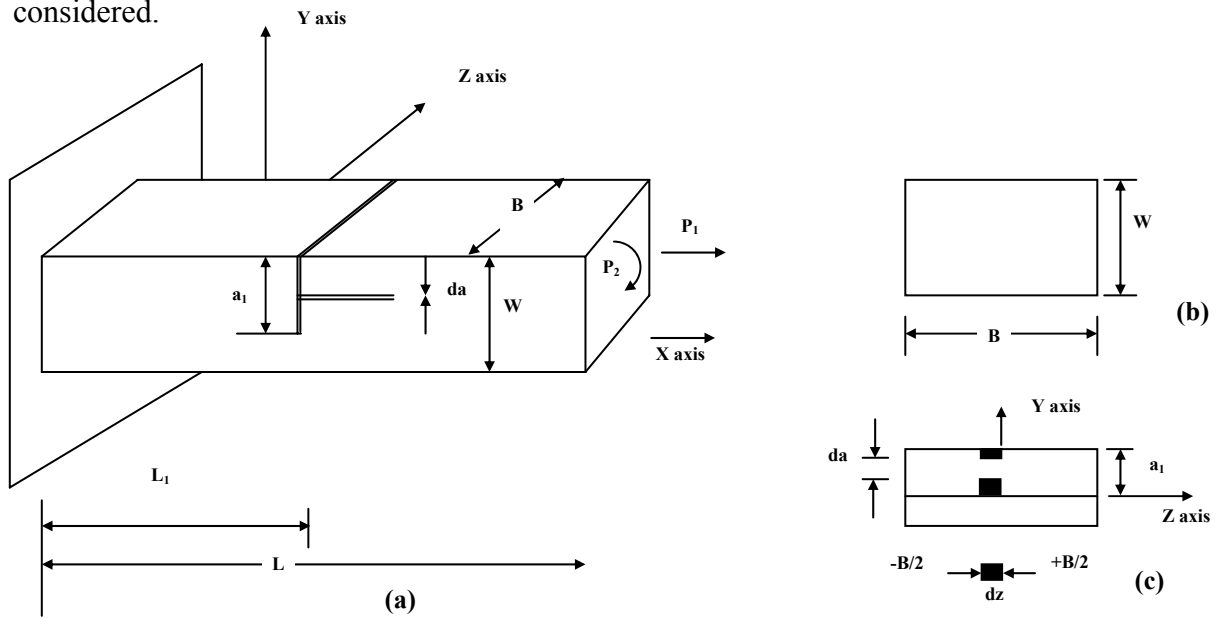


Fig. 3.2.1 Geometry of beam, (a) cantilever beam, (b) cross-sectional view of the beam. (c) segments taken during integration at the crack section

The strain energy release rate at the fractured section can be written as [20];

$$J = \frac{1}{E'} (K_{I1} + K_{I2})^2, \text{ Where } \frac{1}{E'} = \frac{1-\nu^2}{E} \text{ (for plane strain condition);} \quad (3.2.1a)$$

$$= \frac{1}{E} \text{ (for plane stress condition)} \quad (3.2.1b)$$

K_{I1} , K_{I2} are the stress intensity factors of mode I (opening of the crack) for load P_1 and P_2 respectively. The values of stress intensity factors from earlier studies [20] are;

$$K_{I1} = \frac{P_1}{BW} \sqrt{\pi a} (F_1(\frac{a}{W})), K_{I2} = \frac{6P_2}{BW^2} \sqrt{\pi a} (F_2(\frac{a}{W})) \quad (3.2.2)$$

Where expressions for F_1 and F_2 are as follows

$$\left. \begin{aligned} F_1\left(\frac{a}{W}\right) &= \left(\frac{2W}{\pi a} \tan\left(\frac{\pi a}{2W}\right)\right)^{0.5} \left\{ \frac{0.752 + 2.02(a/W) + 0.37(1 - \sin(\pi a / 2W))^3}{\cos(\pi a / 2W)} \right\} \\ F_2\left(\frac{a}{W}\right) &= \left(\frac{2W}{\pi a} \tan\left(\frac{\pi a}{2W}\right)\right)^{0.5} \left\{ \frac{0.923 + 0.199(1 - \sin(\pi a / 2W))^4}{\cos(\pi a / 2W)} \right\} \end{aligned} \right\} \quad (3.2.3)$$

Let U_t be the strain energy due to the crack. Then from Castigliano's theorem, the additional displacement along the force P_i is:

$$u_i = \frac{\partial U_t}{\partial P_i} \quad (3.2.4)$$

$$\text{The strain energy will have the form, } U_t = \int_0^{a_1} \frac{\partial U_t}{\partial a} da = \int_0^{a_1} J da \quad (3.2.5)$$

Where $J = \frac{\partial U_t}{\partial a}$ the strain energy density function.

From (Eqs. 3.2.4 and 3.2.5), thus we have

$$u_i = -\frac{\partial}{\partial P_i} \left[\int_0^{a_1} J(a) da \right] \quad (3.2.6)$$

The flexibility influence co-efficient C_{ij} will be, by definition

$$C_{ij} = \frac{\partial u_i}{\partial P_j} = -\frac{\partial^2}{\partial P_i \partial P_j} \int_0^{a_1} J(a) da \quad (3.2.7)$$

To find out the final flexibility matrix we have to integrate over the breadth 'B'

$$C_{ij} = \frac{\partial u_i}{\partial P_j} = -\frac{\partial^2}{\partial P_i \partial P_j} \int_{-B/2}^{+B/2} \int_0^{a_1} J(a) da dz \quad (3.2.8)$$

Putting the value, strain energy release rate from above, Eq. 3.2.8 modifies as

$$C_{ij} = \frac{B}{E'} \frac{\partial^2}{\partial P_i \partial P_j} \int_0^{a_1} (K_{11} + K_{12})^2 da \quad (3.2.9)$$

Putting $\xi = (a/w)$, $d\xi = \frac{da}{W}$,

We get $da = Wd\xi$ and when $a = 0$, $\xi = 0$; $a = a_1$, $\xi = a_1/W = \xi_1$

From the above condition Eq. 3.2.9 converts to,

$$C_{ij} = \frac{BW}{E'} \frac{\partial^2}{\partial P_i \partial P_j} \int_0^{\xi_1} (K_{11} + K_{12})^2 d\xi \quad (3.2.10)$$

From the Eq. 3.2.10, calculating C_{11} , C_{12} ($=C_{21}$) and C_{22} we get,

$$C_{11} = \frac{BW}{E'} \int_0^{\xi_1} \frac{\pi a}{B^2 W^2} 2(F_1(\xi))^2 d\xi$$

$$= \frac{2\pi}{BE'} \int_0^{\xi_1} \xi (F_1(\xi))^2 d\xi \quad (3.2.11)$$

$$C_{12} = C_{21} = \frac{12\pi}{E'BW} \int_0^{\xi_1} \xi F_1(\xi) F_2(\xi) d\xi \quad (3.2.12)$$

$$C_{22} = \frac{72\pi}{E'BW^2} \int_0^{\xi_1} \xi F_2(\xi) F_2(\xi) d\xi \quad (3.2.13)$$

Converting the influence co-efficient into dimensionless form

$$\overline{C}_{11} = C_{11} \frac{BE'}{2\pi} \quad \overline{C}_{12} = C_{12} \frac{E'BW}{12\pi} = \overline{C}_{21} ; \quad \overline{C}_{22} = C_{22} \frac{E'BW^2}{72\pi} \quad (3.2.14)$$

The local stiffness matrix can be obtained by taking the inversion of compliance matrix. i.e.

$$K = \begin{bmatrix} K_{11} & K_{12} \\ K_{21} & K_{22} \end{bmatrix} = \begin{bmatrix} C_{11} & C_{12} \\ C_{21} & C_{22} \end{bmatrix}^{-1} \quad (3.2.15)$$

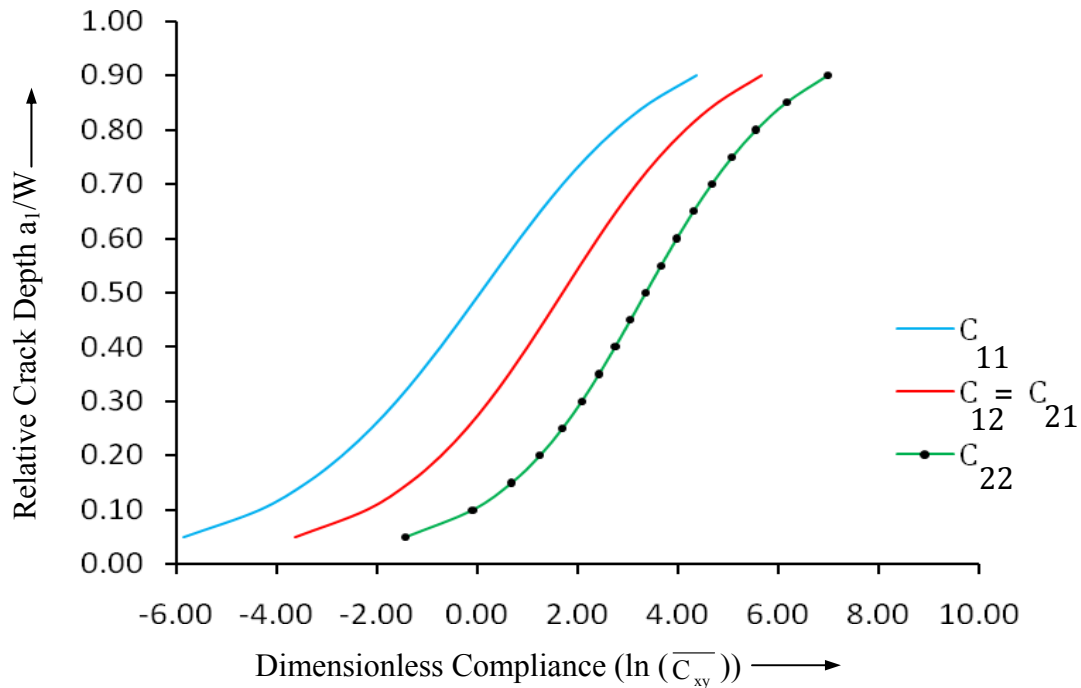


Fig. 3.2.2 Relative crack depth (a_1/W) vs. dimensionless compliance ($\ln(\overline{C}_{xy})$)

Fig. 3.2.2 shows the variation of dimension-less compliances to that of relative crack depth

From Fig. (3.2.2) it can be observed that as the crack depth increases, the compliances (C_{11} , $C_{12}=C_{21}$, C_{22}) also increase.

3.2.1.2 Free Vibration Analysis of the Cracked Cantilever Beam

A cantilever beam of length 'L' width 'B' and depth 'W', with a crack of depth 'a₁' at a distance 'L₁' from the fixed end is considered (Fig. 3.2.1). Taking $u_1(x,t)$ and $u_2(x,t)$ as the amplitudes of longitudinal vibration for the sections before and after the crack and $y_1(x,t)$, $y_2(x,t)$ are the amplitudes of bending vibration for the same sections (Fig. 3.2.3).

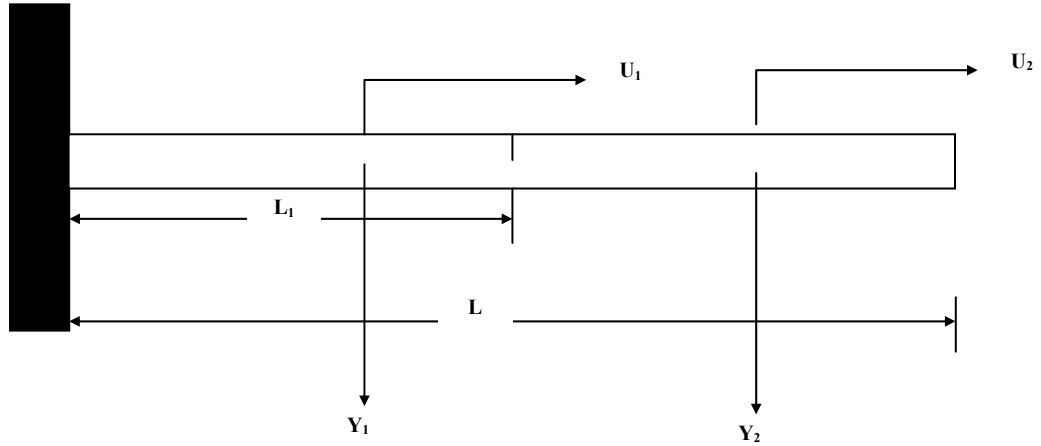


Fig. 3.2.3 Beam model

The normal function for the system can be defined as

$$\bar{u}_1(\bar{x}) = A_1 \cos(\bar{K}_u \bar{x}) + A_2 \sin(\bar{K}_u \bar{x}) \quad (3.2.16a)$$

$$\bar{u}_2(\bar{x}) = A_3 \cos(\bar{K}_u \bar{x}) + A_4 \sin(\bar{K}_u \bar{x}) \quad (3.2.16b)$$

$$\bar{y}_1(\bar{x}) = A_5 \cosh(\bar{K}_y \bar{x}) + A_6 \sinh(\bar{K}_y \bar{x}) + A_7 \cos(\bar{K}_y \bar{x}) + A_8 \sin(\bar{K}_y \bar{x}) \quad (3.2.16c)$$

$$\bar{y}_2(\bar{x}) = A_9 \cosh(\bar{K}_y \bar{x}) + A_{10} \sinh(\bar{K}_y \bar{x}) + A_{11} \cos(\bar{K}_y \bar{x}) + A_{12} \sin(\bar{K}_y \bar{x}) \quad (3.2.16d)$$

Where $\bar{x} = \frac{x}{L}$, $\bar{u} = \frac{u}{L}$, $\bar{y} = \frac{y}{L}$, $\beta = \frac{L_1}{L}$

$$\bar{K}_u = \frac{\omega L}{C_u}, C_u = \left(\frac{E}{\rho}\right)^{1/2}, \bar{K}_y = \left(\frac{\omega L^2}{C_y}\right)^{1/2}, C_y = \left(\frac{EI}{\mu}\right)^{1/2}, \mu = A\rho$$

A_i , ($i=1, 12$) Constants are to be determined, from boundary conditions. The boundary conditions of the cantilever beam in consideration are:

$$\bar{u}_1(0) = 0; \quad 3.2.17(a)$$

$$\bar{y}_1(0) = 0; \quad 3.2.17(b)$$

$$\bar{y}'_1(0) = 0; \quad 3.2.17(c)$$

$$\bar{u}'_2(1) = 0; \quad 3.2.17(d)$$

$$\bar{y}''_2(1) = 0; \quad 3.2.17(e)$$

$$\bar{y}'''_2(1) = 0; \quad 3.2.17(f)$$

At the cracked section:

$$\bar{u}'_1(\beta) = \bar{u}'_2(\beta); \quad 3.2.18(a)$$

$$\bar{y}_1(\beta) = \bar{y}_2(\beta); \quad 3.2.18(b)$$

$$\bar{y}''_1(\beta) = \bar{y}''_2(\beta); \quad 3.2.18(c)$$

$$\bar{y}'''_1(\beta) = \bar{y}'''_2(\beta); \quad 3.2.18(d)$$

Also at the cracked section (due to the discontinuity of axial deformation to the left and right of the crack), we have:

$$AE \frac{du_1(L_1)}{dx} = K_{11}(u_2(L_1) - u_1(L_1)) + K_{12} \left(\frac{dy_2(L_1)}{dx} - \frac{dy_1(L_1)}{dx} \right) \quad (3.2.19)$$

Multiplying both sides of the above equation by $\frac{AE}{LK_{11}K_{12}}$ we get;

$$M_1 M_2 \bar{u}'(\beta) = M_2(\bar{u}_2(\beta) - \bar{u}_1(\beta)) + M_1(\bar{y}'_2(\beta) - \bar{y}'_1(\beta)) \quad (3.2.20)$$

Similarly at the crack section (due to the discontinuity of slope to the left and right of the crack)

$$EI \frac{d^2 y_1(L_1)}{dx^2} = K_{21} (u_2(L_1) - u_1(L_1)) + K_{22} \left(\frac{dy_2(L_1)}{dx} - \frac{dy_1(L_1)}{dx} \right) \quad (3.2.21)$$

Multiplying both sides of the above equation by $\frac{EI}{L^2 K_{22} K_{21}}$ we get,

$$M_3 M_4 \bar{y}_1''(\beta) = M_3 (\bar{u}_2(\beta) - \bar{u}_1(\beta)) + M_4 (\bar{y}'_2(\beta) - \bar{y}'_1(\beta)) \quad (3.2.22)$$

$$\text{Where, } M_1 = \frac{AE}{LK_{11}}, M_2 = \frac{AE}{K_{12}}, M_3 = \frac{EI}{LK_{22}}, M_4 = \frac{EI}{L^2 K_{21}}$$

The normal functions, Eq. {3.2.16} along with the boundary conditions as mentioned above, yield the characteristic equation of the system as:

$$|Q|=0 \quad (3.2.23)$$

Where Q is a 12x12 matrix and is expressed as

$$Q = \begin{bmatrix} 1 & 0 & 1 & 0 & 0 & 0 & 0 & 0 & 0 & 0 & 0 & 0 \\ 0 & 1 & 0 & 1 & 0 & 0 & 0 & 0 & 0 & 0 & 0 & 0 \\ 0 & 0 & 0 & 0 & G_3 & G_4 & -G_7 & -G_8 & 0 & 0 & 0 & 0 \\ 0 & 0 & 0 & 0 & G_4 & G_3 & G_8 & -G_7 & 0 & 0 & 0 & 0 \\ G_1 & G_2 & -G_5 & -G_6 & -G_1 & -G_2 & G_5 & G_6 & 0 & 0 & 0 & 0 \\ G_2 & G_1 & G_6 & -G_5 & -G_2 & -G_1 & -G_6 & G_5 & 0 & 0 & 0 & 0 \\ G_1 & G_2 & G_5 & G_6 & -G_1 & -G_2 & -G_5 & -G_6 & 0 & 0 & 0 & 0 \\ S_1 & S_2 & S_3 & S_4 & -G_2 & -G_1 & G_6 & -G_5 & S_5 & S_6 & S_7 & S_8 \\ 0 & 0 & 0 & 0 & 0 & 0 & 0 & 0 & 0 & 0 & 0 & 0 \\ 0 & 0 & 0 & 0 & 0 & 0 & 0 & 0 & 0 & 0 & -T_8 & T_7 \\ 0 & 0 & 0 & 0 & 0 & 0 & 0 & 0 & -T_6 & T_5 & T_6 & -T_5 \\ S_9 & S_{10} & S_{11} & S_{12} & S_{13} & S_{14} & S_{15} & S_{16} & S_{17} & S_{18} & -T_5 & -T_6 \end{bmatrix} \quad (3.2.24)$$

Where $G_1 = \text{Cosh}(\overline{K}_y \alpha)$, $G_2 = \text{Sinh}(\overline{K}_y \alpha)$, $G_3 = \text{Cosh}(\overline{K}_y)$, $G_4 = \text{Sinh}(\overline{K}_y)$, $G_5 = \text{Cos}(\overline{K}_y \alpha)$,

$G_6 = \text{Sin}(\overline{K}_y \alpha)$, $G_7 = \text{Cosh}(\overline{K}_y)$, $G_8 = \text{Sin}(\overline{K}_y)$,

$T_5 = \text{Cos}(\overline{K}_u \alpha)$, $T_6 = \text{Sin}(\overline{K}_u \alpha)$, $T_7 = \text{Cos}(\overline{K}_u)$, $T_8 = \text{Sin}(\overline{K}_u)$

$$M_{12} = \frac{M_1}{M_2}, M_{34} = \frac{M_3}{M_4}$$

$S_1 = G_2 + M_3 \overline{K}_y G_1$, $S_2 = G_1 + M_3 \overline{K}_y G_2$, $S_3 = -G_6 - M_3 \overline{K}_y G_5$, $S_4 = G_5 - M_3 \overline{K}_y G_6$, $S_5 = \frac{M_{34}}{K_y}$,

$S_6 = \frac{M_{34}}{K_y} T_6$, $S_7 = \frac{-M_{34}}{K_y} T_5$, $S_8 = \frac{-M_{34}}{K_y} T_6$, $S_9 = M_{12} \overline{K}_y G_2$

$S_{10} = M_{12} \overline{K}_y G_1$, $S_{11} = -M_{12} \overline{K}_y G_6$, $S_{12} = M_{12} \overline{K}_y G_5$

$S_{13} = -M_{12} \overline{K}_y G_2$, $S_{14} = -M_{12} \overline{K}_y G_1$,

$S_{15} = M_{12} \overline{K}_y G_6$, $S_{16} = -M_{12} \overline{K}_y G_5$, $S_{17} = T_5 - M_1 \overline{K}_u T_6$, $S_{18} = T_6 + M_1 \overline{K}_u T_5$

This determinant is a function of natural circular frequency (ω_n), the relative location of the crack (L_1/L) and the local stiffness matrix (K) which in turn is a function of the relative crack depth (a_1/W).

3.2.1.3 Forced Vibration Analysis of Cracked Cantilever Beam

If the cantilever beam with transverse crack is excited at its free end by a harmonic excitation ($Y = Y_0 \sin(\omega t)$), the non-dimensional amplitude at the free end may be expressed as $\bar{y}_2(1) = \frac{Y_0}{L} = \bar{y}_0$. Therefore the boundary conditions for the beam remain same as before except the boundary condition $\bar{y}_2''(1) = 0$ which modified as $\bar{y}_2(1) = \bar{y}_0$

The constants A_i , $i=1$, to 12 are then computed from the algebraic condition,

$$Q_1 D = B_1 \tag{3.2.25}$$

Q_1 is the (12 x 12) matrix obtained from boundary conditions as mentioned above,

D is a column matrix obtained from the constants,

B_1 is a column matrix, transpose of which is given by, $B_1^T = [0 \ 0 \ 0 \ \bar{y}_0 \ 0 \ 0 \ 0 \ 0 \ 0 \ 0 \ 0 \ 0]$ (3.2.26)

3.2.2 Numerical Analysis

The numerical analysis is carried out for the cracked cantilever beam to find the relative amplitudes of transverse vibration at different crack location and crack depth. The cracked cantilever beam of the current research has the following dimensions.

Length of the Beam	= 0.8m
Width of the beam	= 0.05m
Height of the Beam	= 0.006m
Relative crack depth (a_1/W)	= Varies from 0.05 to 0.8
Relative crack location (L_1/L)	= Varies from 0.125 to 0.95

3.2.2.1 Results of Numerical Analysis

The relative amplitudes of transverse vibration for first three mode shapes of cracked cantilever beam made of Aluminum are obtained at different crack location and crack depth by numerical solution of (Eqs.3.2.16c and 3.2.161d) of section 3.2.1.2. The results of numerical analysis are presented in Fig. 3.2.4 to Fig. 3.2.27. The relative amplitudes of transverse vibration for first three mode shapes of un-cracked cantilever beam made of Aluminum are also plotted in the corresponding figures for immediate comparison. The three dimensional variation of relative natural frequencies and relative mode shape difference with respect to relative crack location and relative crack depth along with the contour plots are presented in Fig. 3.2.28 to Fig. 3.2.29.

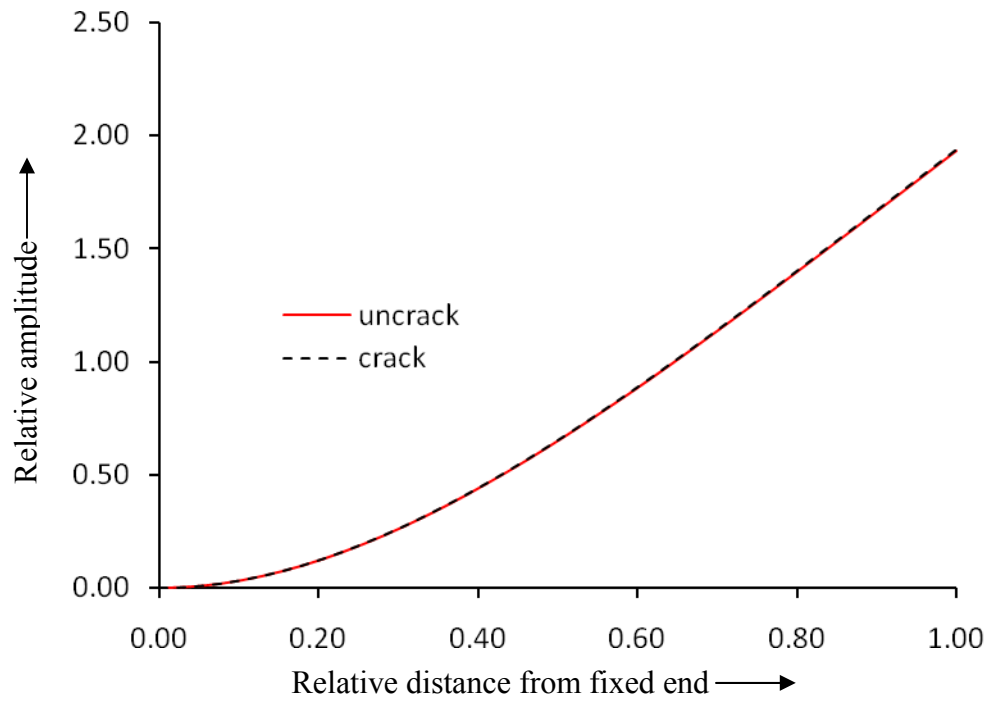


Fig.3.2.4 (a) Relative amplitude vs. relative distance from the fixed end (1st mode of vibration), $a_1/W=0.1$, $L_1/L=0.0256$

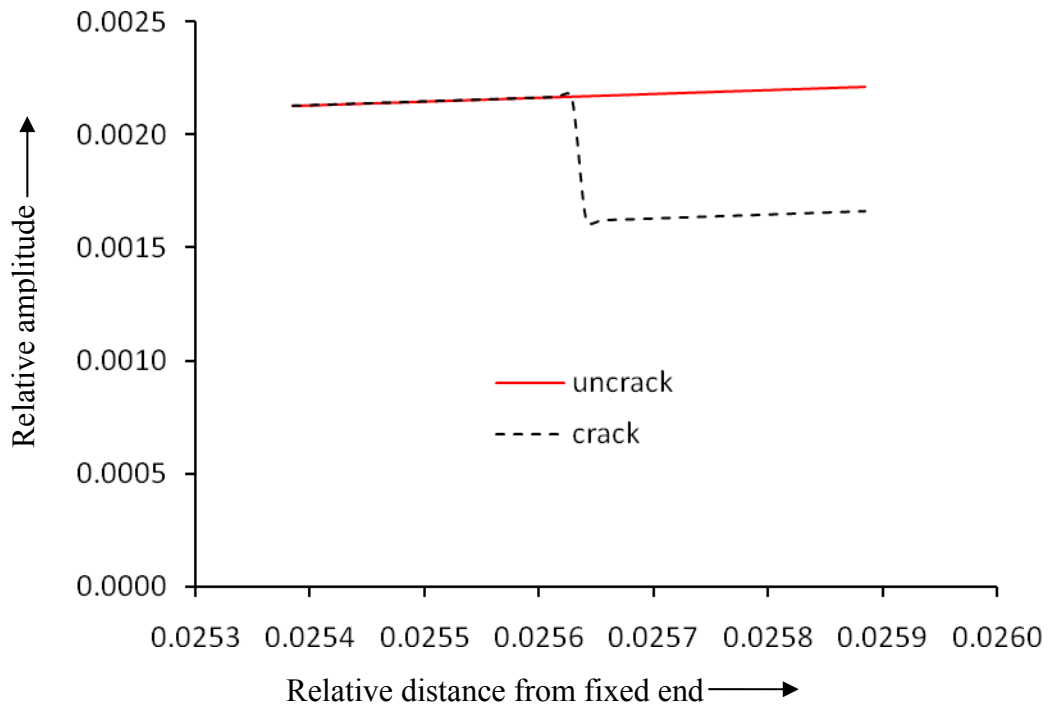


Fig. 3.2.4(a1) Magnified view of Fig. 3.2.4(a) at the vicinity of the crack location.

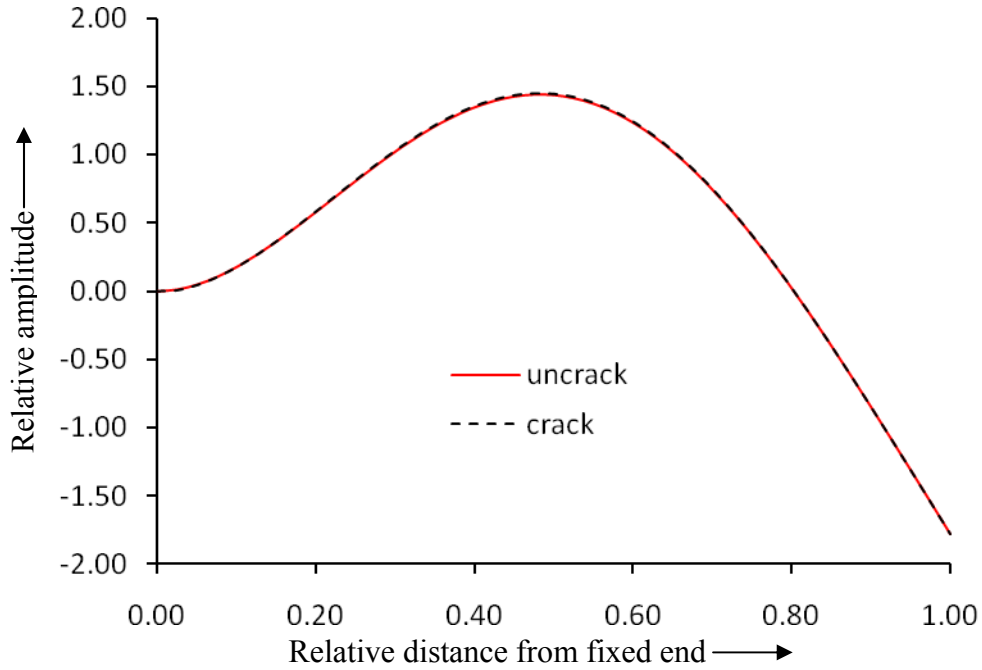


Fig.3.2.4 (b) Relative amplitude vs. relative distance from the fixed end (2nd mode of vibration), $a_1/W=0.1$, $L_1/L=0.0256$

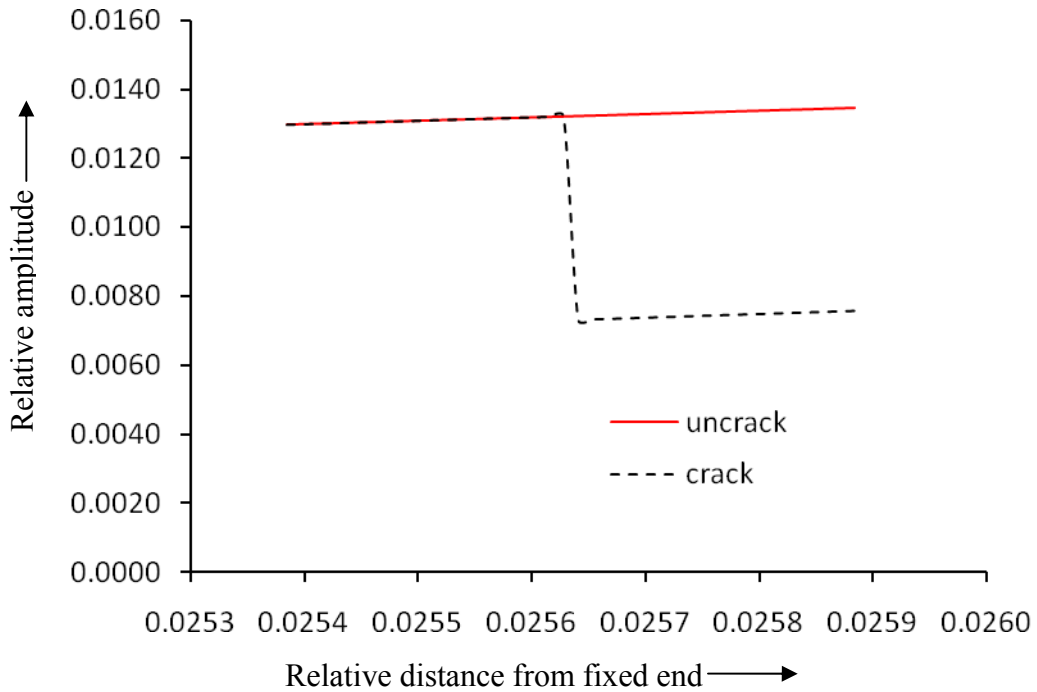


Fig. 3.2.4(b1) Magnified view of Fig. 3.2.4(b) at the vicinity of the crack location.

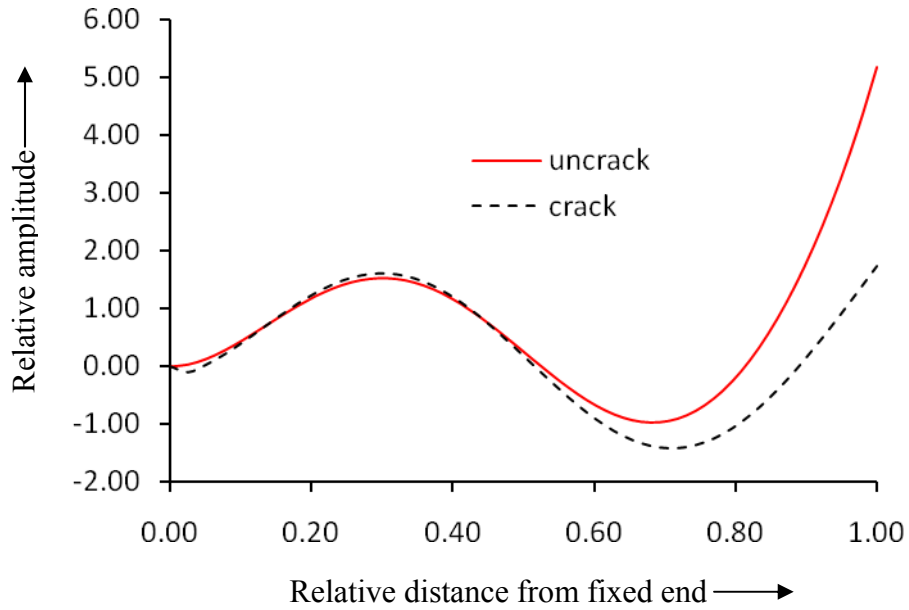


Fig.3.2.4 (c) Relative amplitude vs. relative distance from the fixed end (3rd mode of vibration), $a_1/W=0.1$, $L_1/L=0.0256$

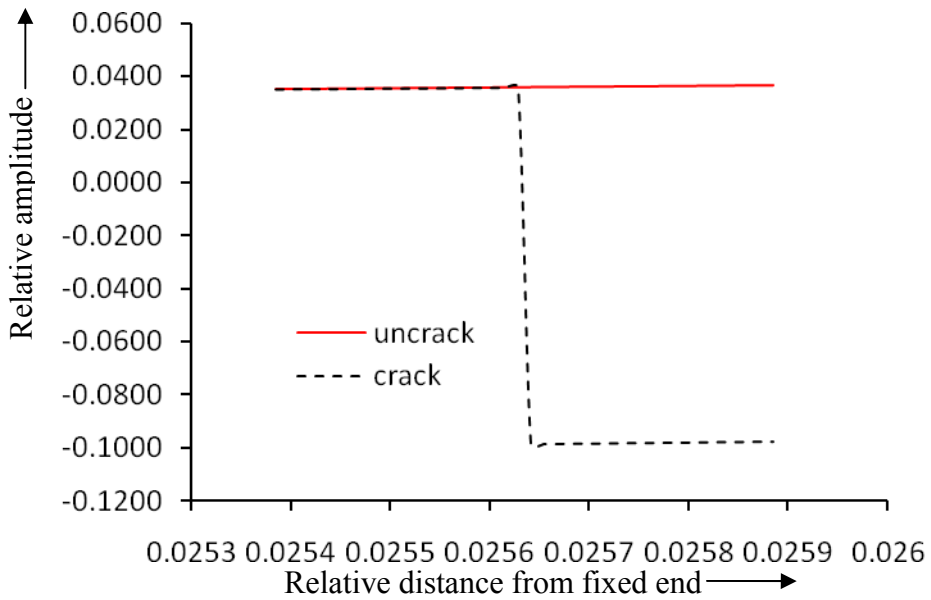


Fig. 3.2.4(c1) Magnified view of Fig. 3.2.4(c) at the vicinity of the crack location.

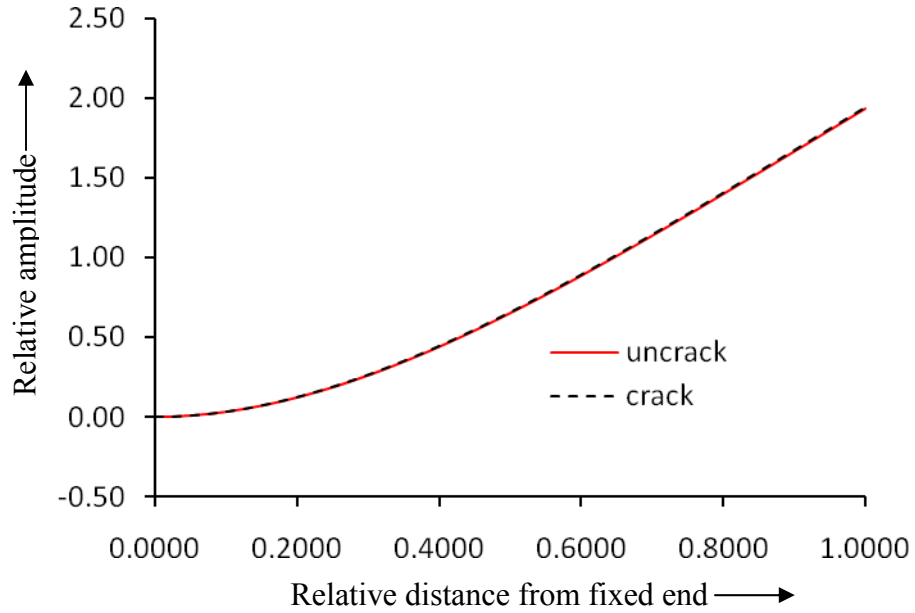


Fig.3.2.5 (a) Relative amplitude vs. relative distance from the fixed end (1st mode of vibration), $a_1/W=0.2$, $L_1/L=0.0256$

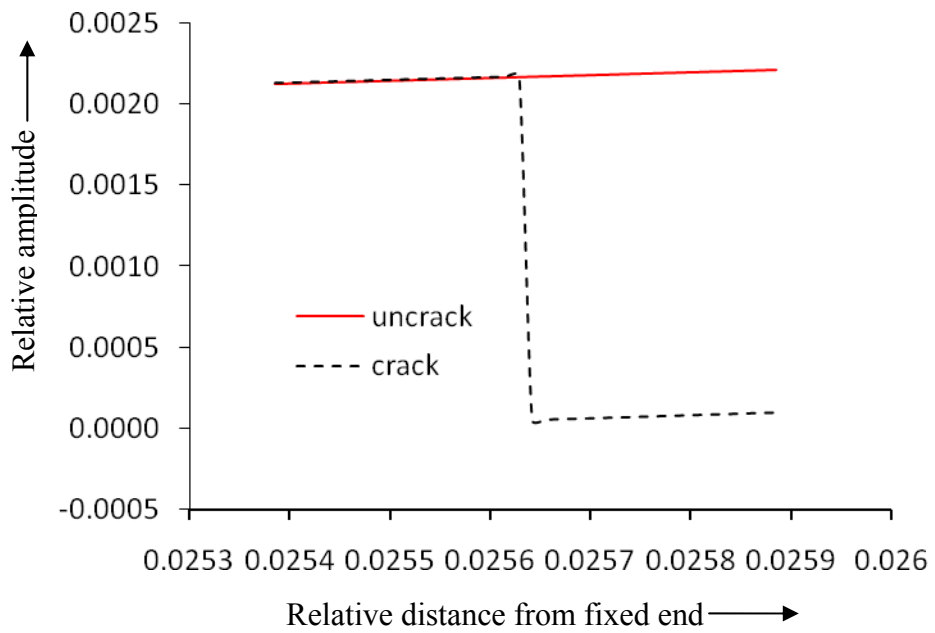


Fig. 3.2.5(a1) Magnified view of Fig. 3.2.5(a) at the vicinity of the crack location.

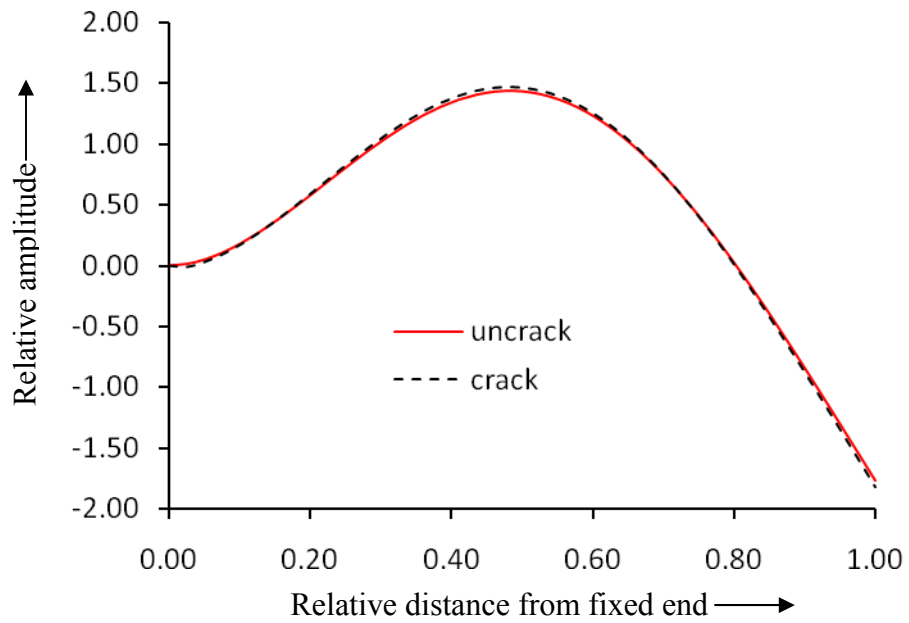


Fig.3.2.5 (b) Relative amplitude vs. relative distance from the fixed end (2nd mode of vibration), $a_1/W=0.2$, $L_1/L=0.0256$

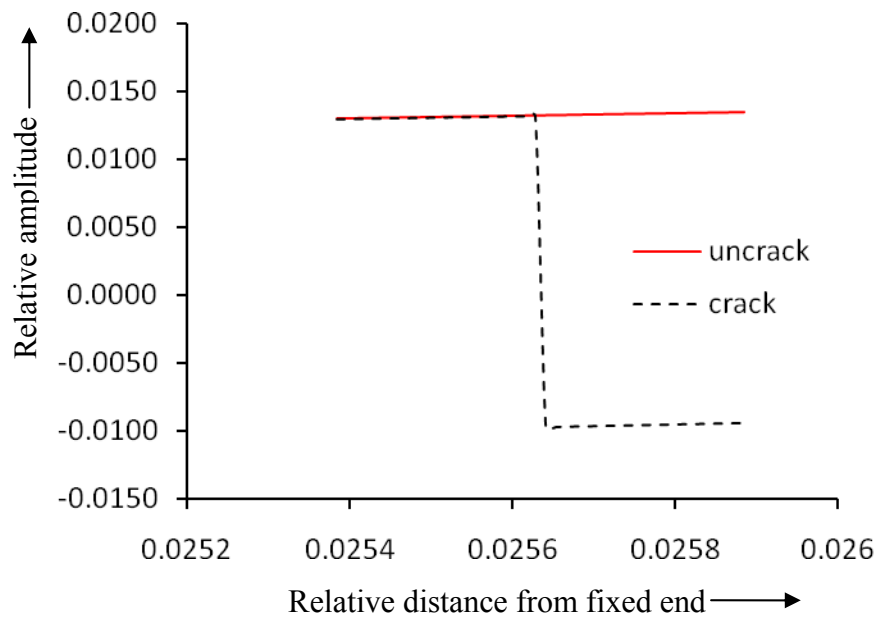


Fig. 3.2.5 (b1) Magnified view of Fig. 3.2.5(b) at the vicinity of the crack location.

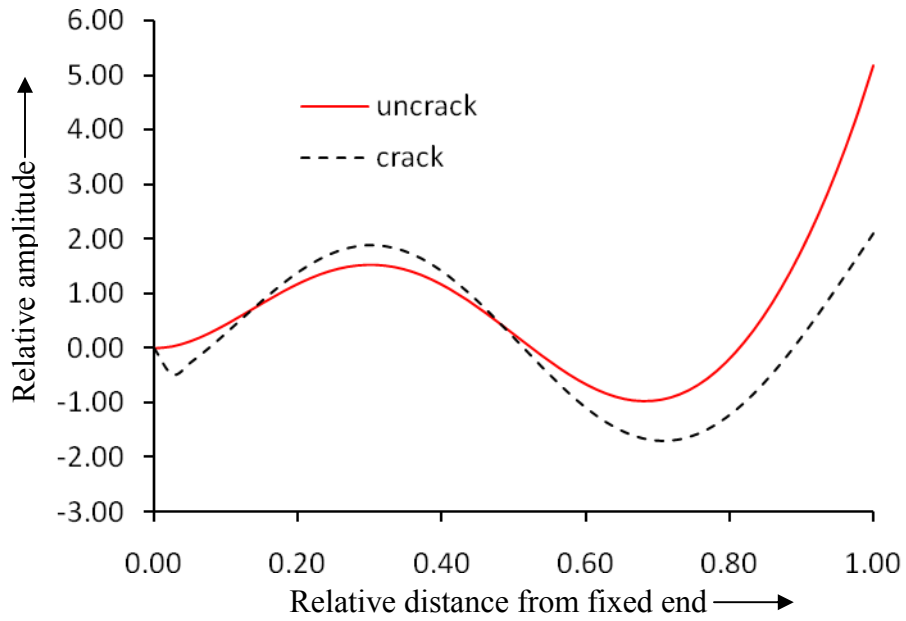


Fig.3.2.5 (c) Relative amplitude vs. relative distance from the fixed end (3rd mode of vibration), $a_1/W=0.2$, $L_1/L=0.0256$

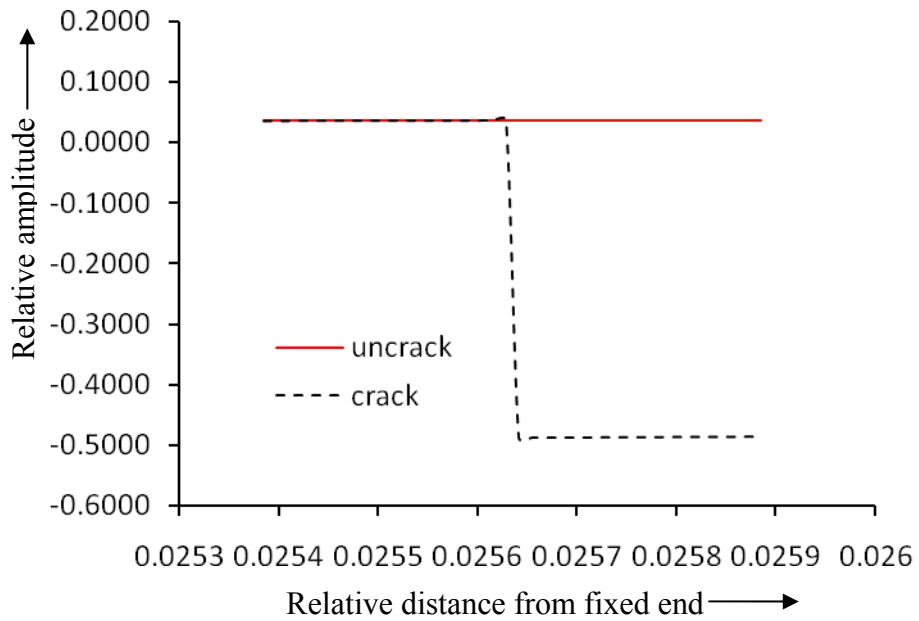


Fig. 3.2.5(c1) Magnified view of Fig. 3.2.5(c) at the vicinity of the crack location.

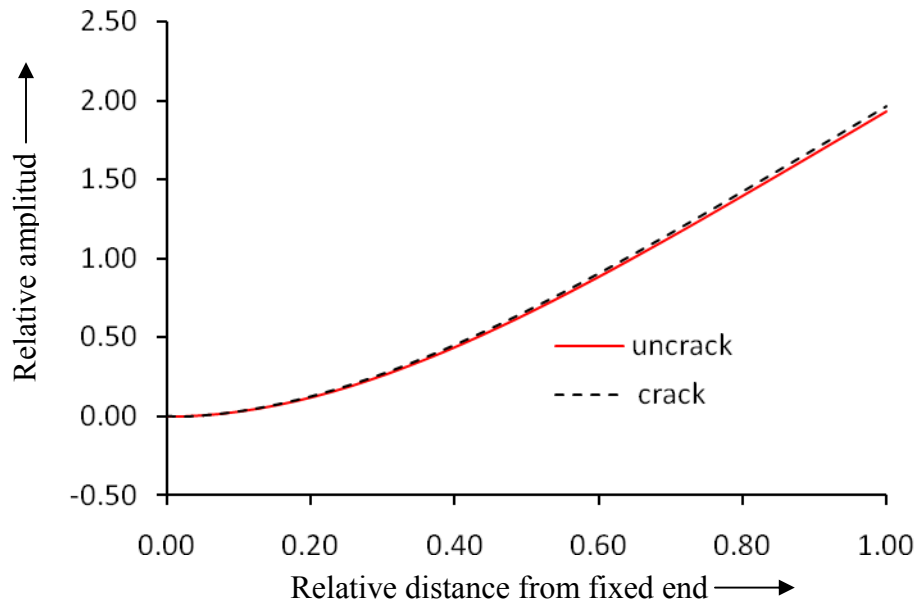


Fig.3.2.6 (a) Relative amplitude vs. relative distance from the fixed end (1st mode of vibration), $a_1/W=0.3$, $L_1/L=0.0256$

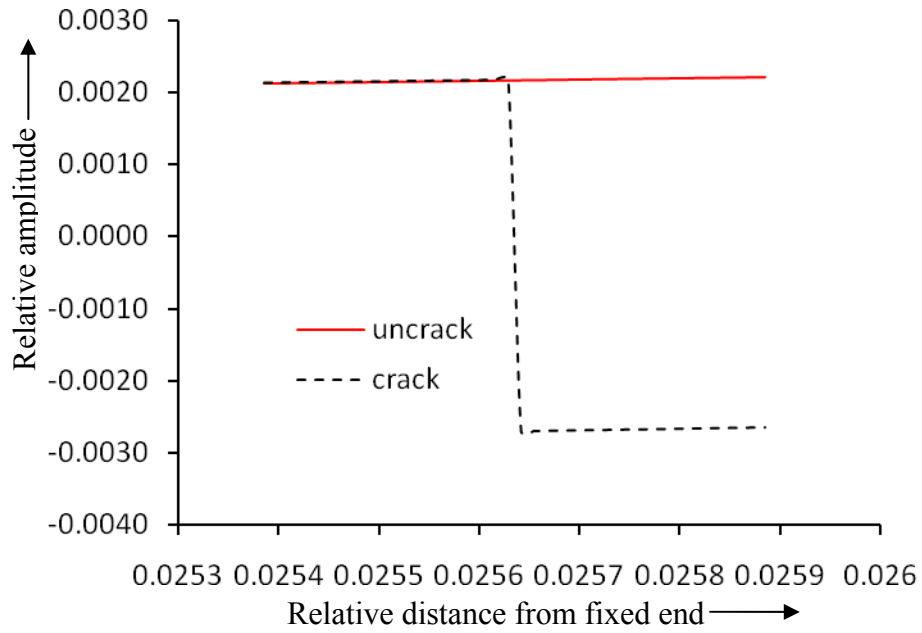


Fig. 3.2.6(a1) Magnified view of Fig. 3.2.6(a) at the vicinity of the crack location.

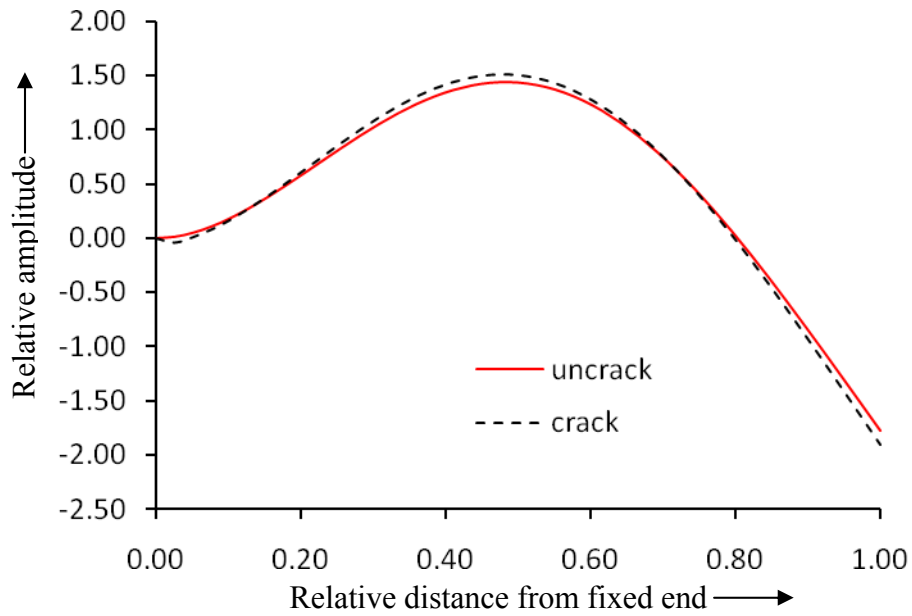


Fig.3.2.6 (b) Relative amplitude vs. relative distance from the fixed end (2nd mode of vibration), $a_1/W=0.3$, $L_1/L=0.0256$

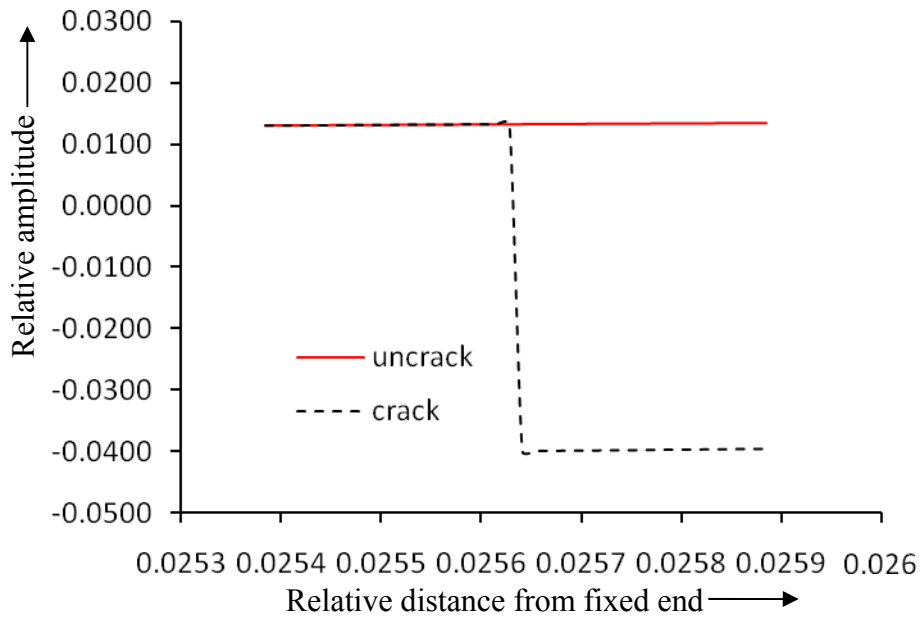


Fig. 3.2.6(b1) Magnified view of Fig. 3.2.6(b) at the vicinity of the crack location.

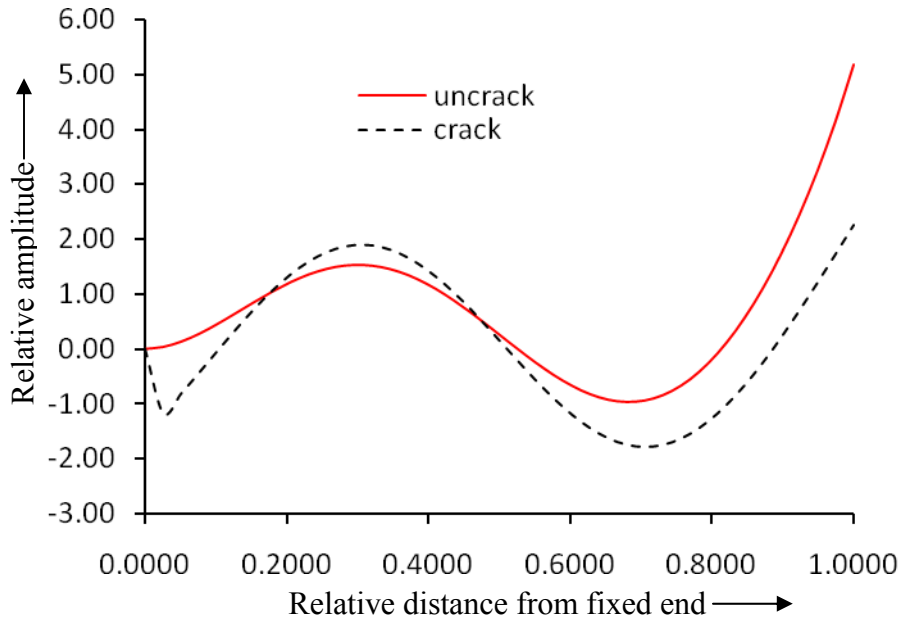


Fig.3.2.6 (c) Relative amplitude vs. relative distance from the fixed end (3rd mode of vibration), $a_1/W=0.3$, $L_1/L=0.0256$

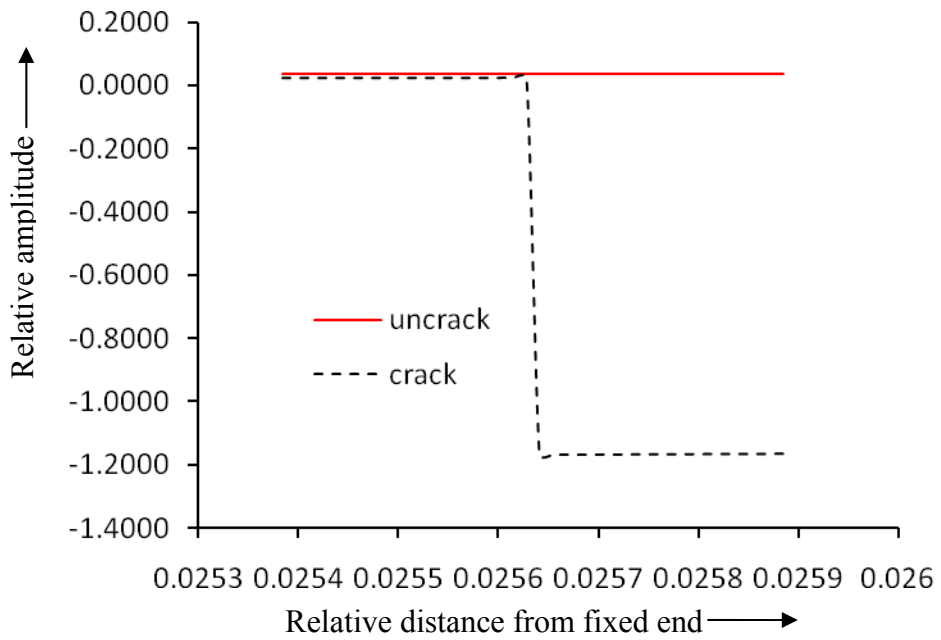


Fig. 3.2.6(c1) Magnified view of Fig. 3.2.6(c) at the vicinity of the crack location.

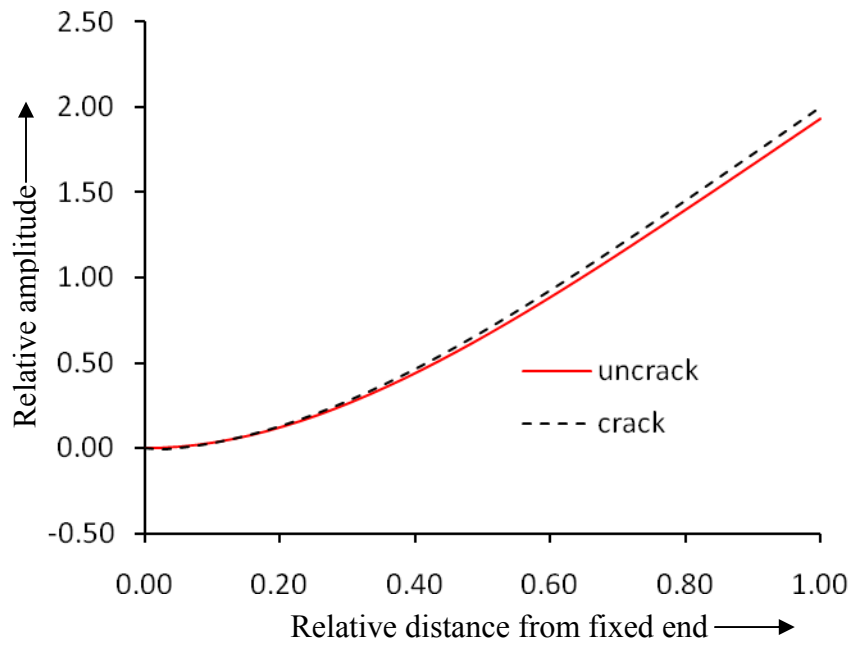


Fig.3.2.7 (a) Relative amplitude vs. relative distance from the fixed end (1st mode of vibration), $a_1/W=0.4$, $L_1/L=0.0256$

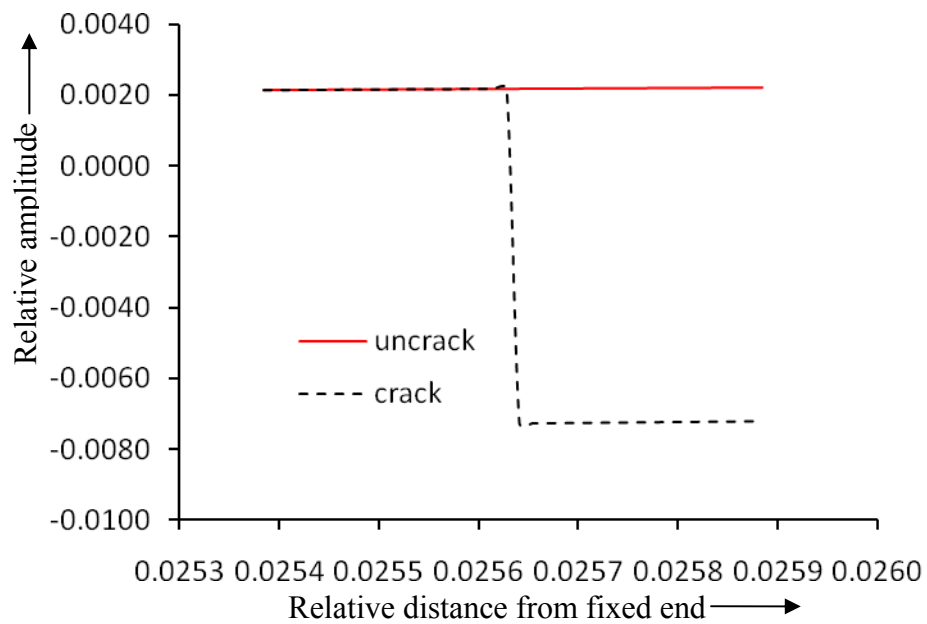


Fig. 3.2.7(a1) Magnified view of Fig. 3.2.7(a) at the vicinity of the crack location.

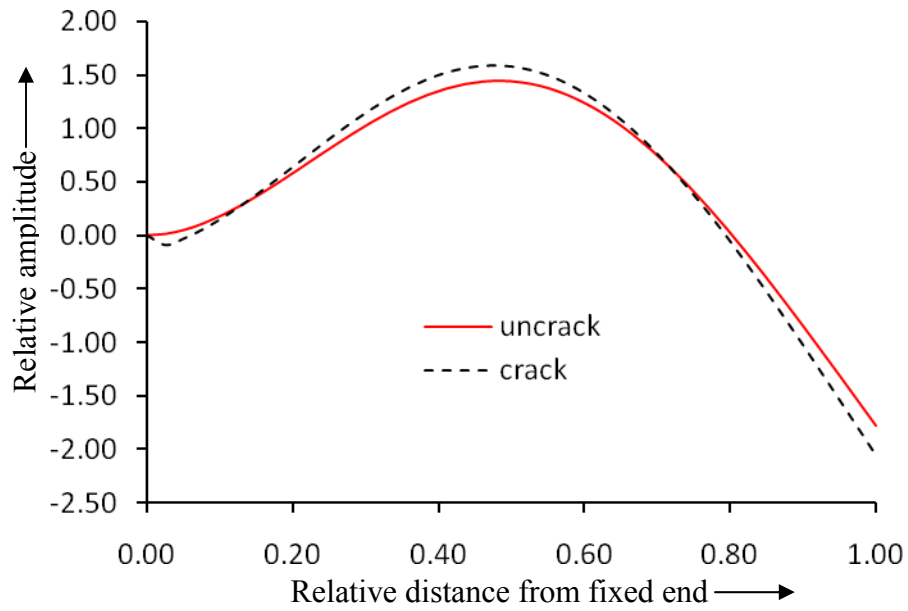


Fig.3.2.7 (b) Relative amplitude vs. relative distance from the fixed end (2nd mode of vibration), $a_1/W=0.4$, $L_1/L=0.0256$

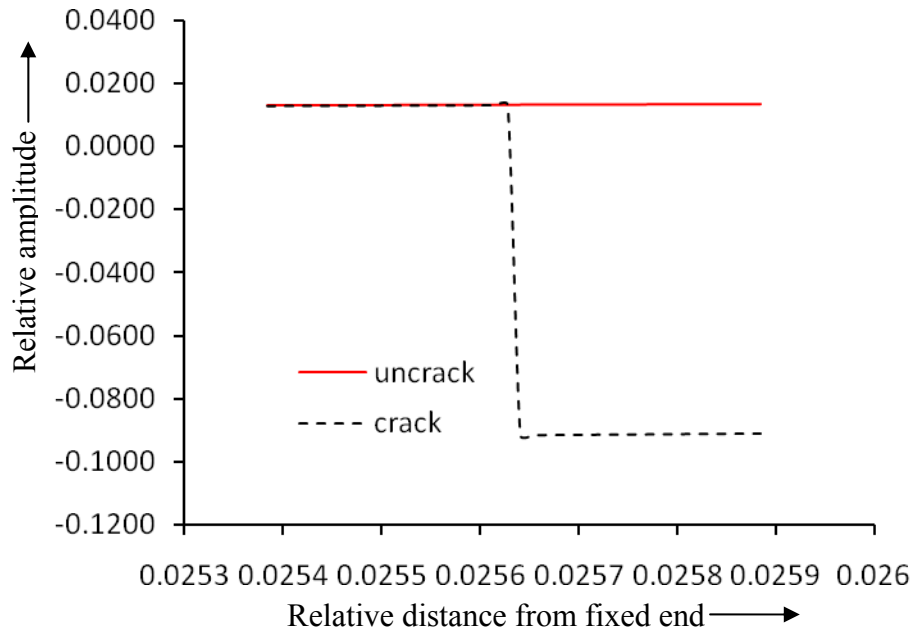


Fig. 3.2.7(b1) Magnified view of Fig. 3.2.7(b) at the vicinity of the crack location.

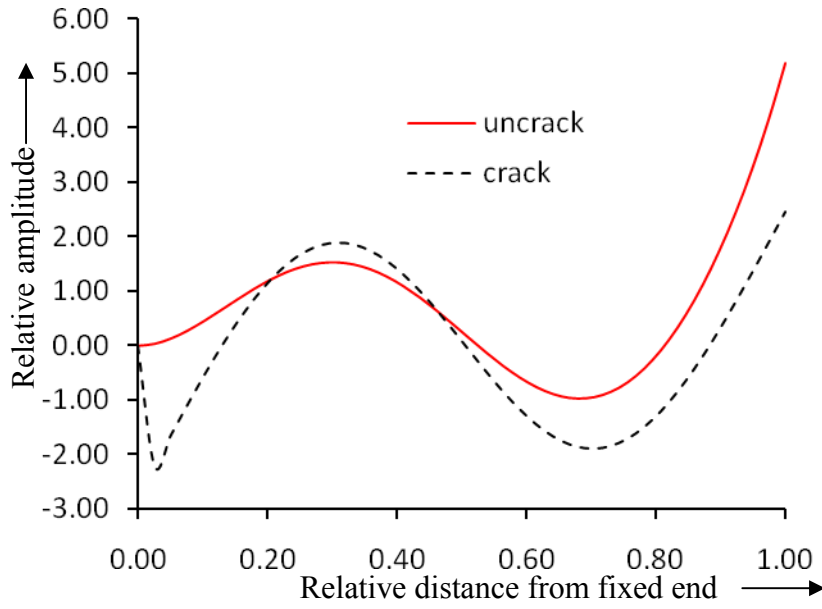


Fig.3.2.7 (c) Relative amplitude vs. relative distance from the fixed end (3rd mode of vibration), $a_1/W=0.4$, $L_1/L=0.0256$

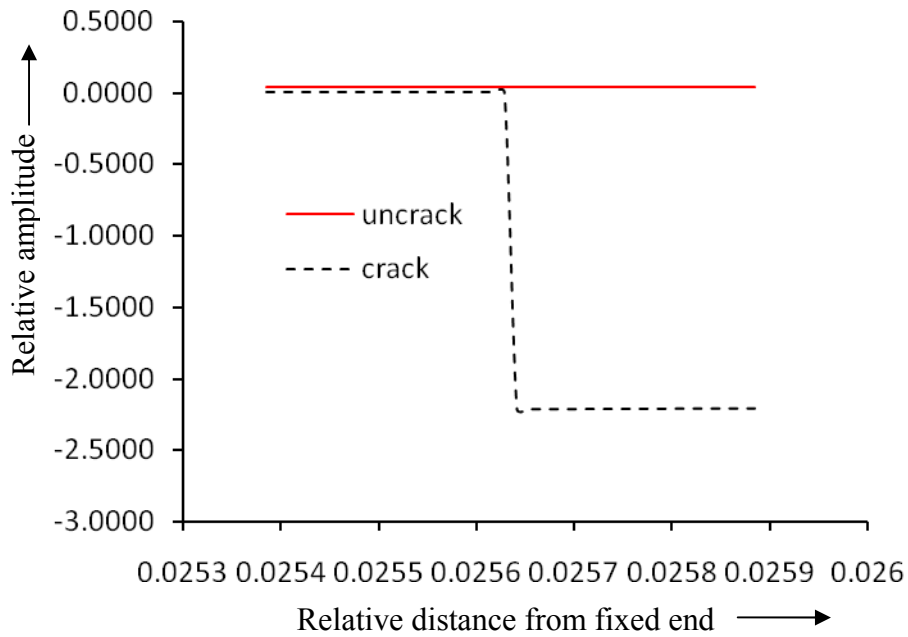


Fig. 3.2.7(c1) Magnified view of Fig. 3.2.7(c) at the vicinity of the crack location.

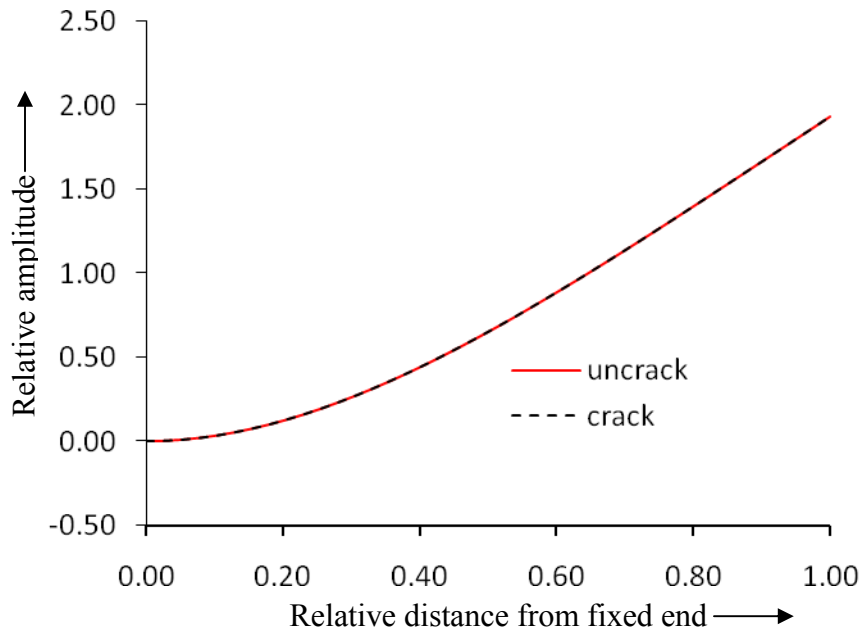


Fig.3.2.8 (a) Relative amplitude vs. relative distance from the fixed end (1st mode of vibration), $a_1/W=0.1$, $L_1/L=0.0513$

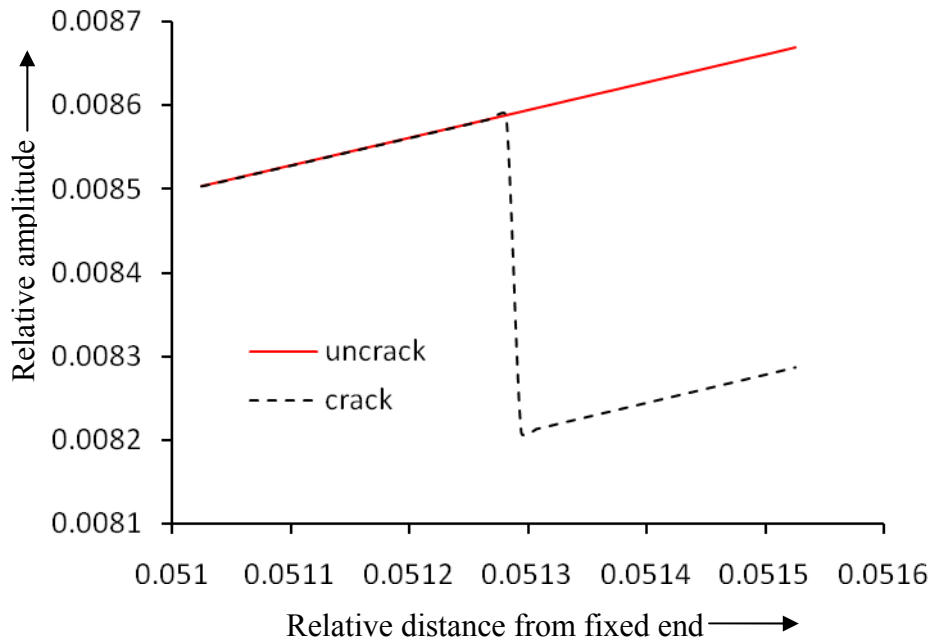


Fig. 3.2.8(a1) Magnified view of Fig. 3.2.8 (a) at the vicinity of the crack location.

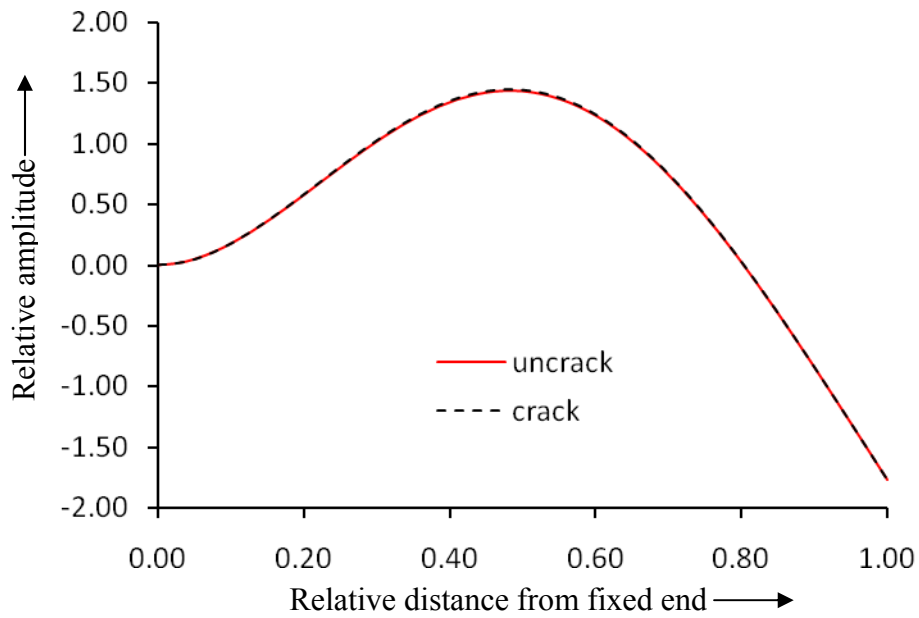


Fig.3.2.8 (b) Relative amplitude vs. relative distance from the fixed end (2nd mode of vibration), $a_1/W=0.1$, $L_1/L=0.0513$

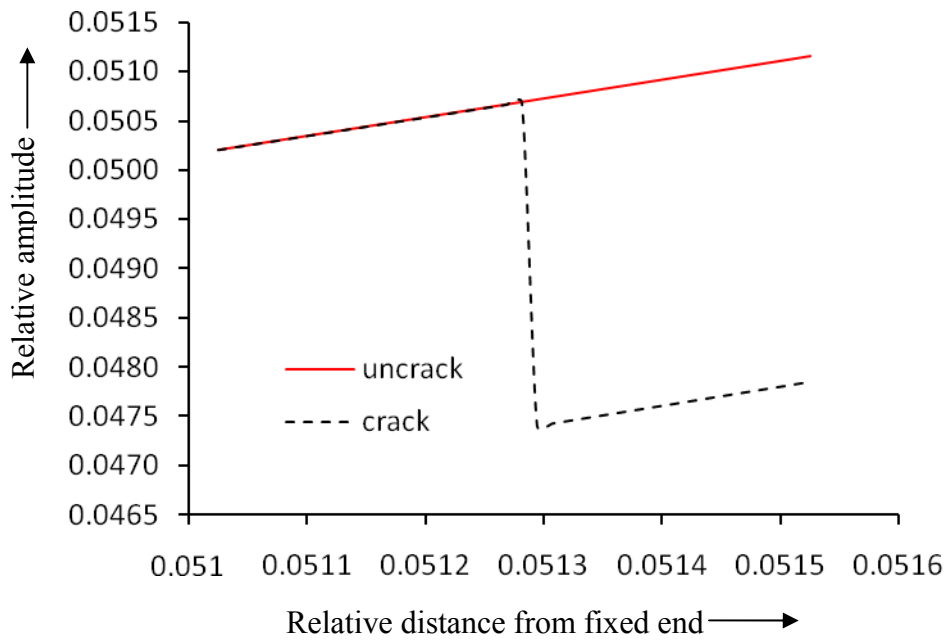


Fig. 3.2.8(b1) Magnified view of Fig. 3.2.8 (b) at the vicinity of the crack location.

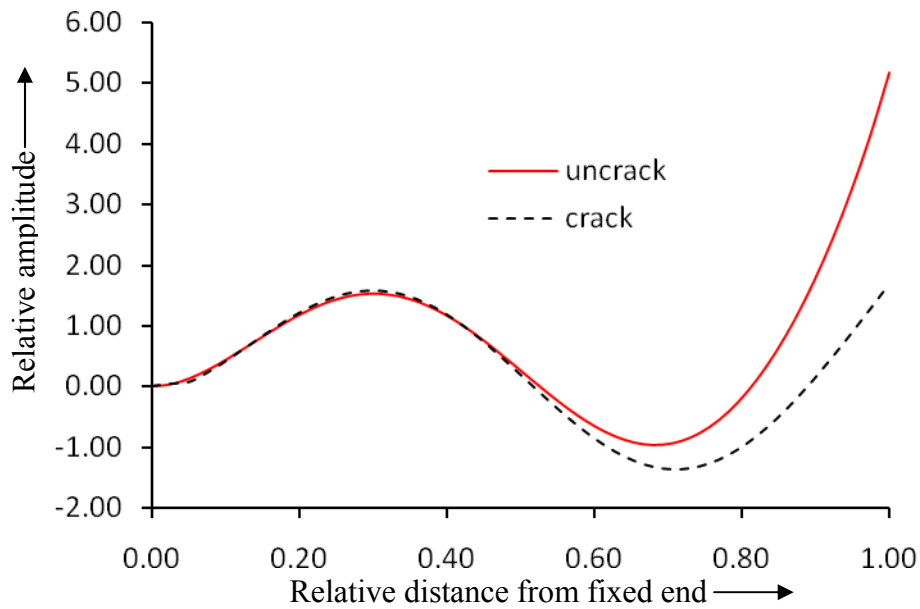


Fig. 3.2.8 (c) Relative amplitude vs. relative distance from the fixed end (3rd mode of vibration), $a_1/W=0.1$, $L_1/L=0.0513$

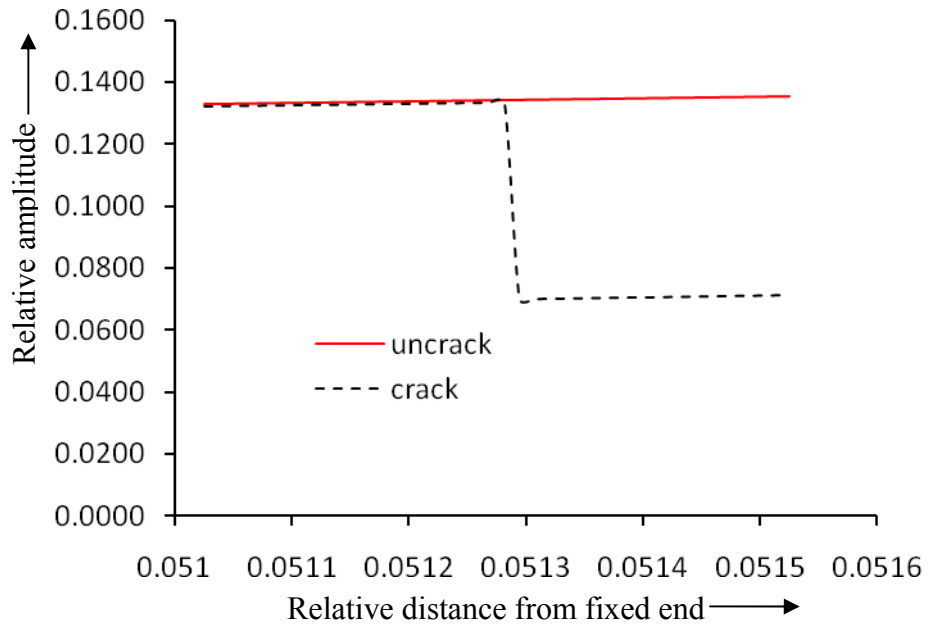


Fig. 3.2.8 (c1) Magnified view of Fig. 3.2.8 (c) at the vicinity of the crack location.

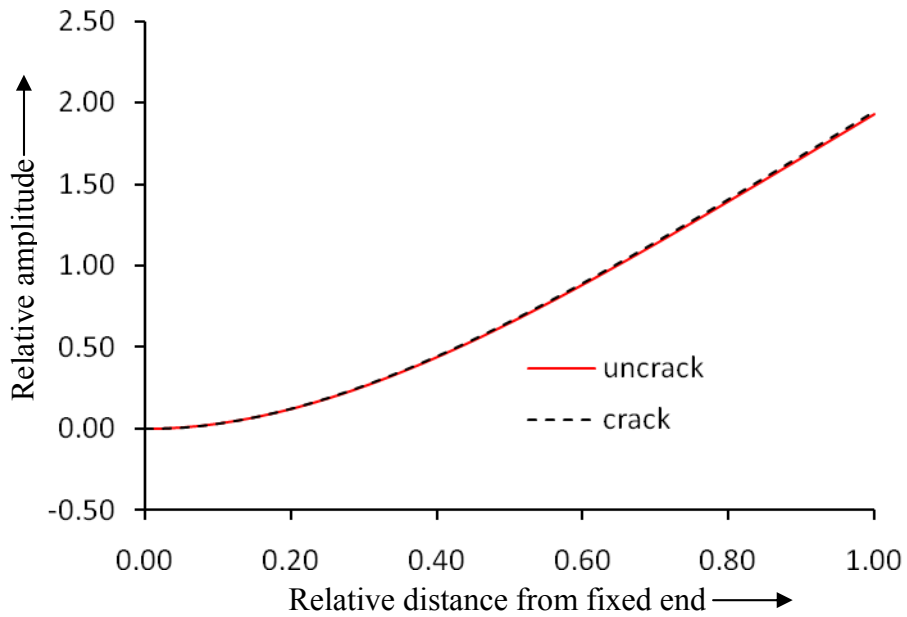


Fig.3.2.9 (a) Relative amplitude vs. relative distance from the fixed end(1st mode of vibration), $a_1/W=0.2$, $L_1/L=0.0513$

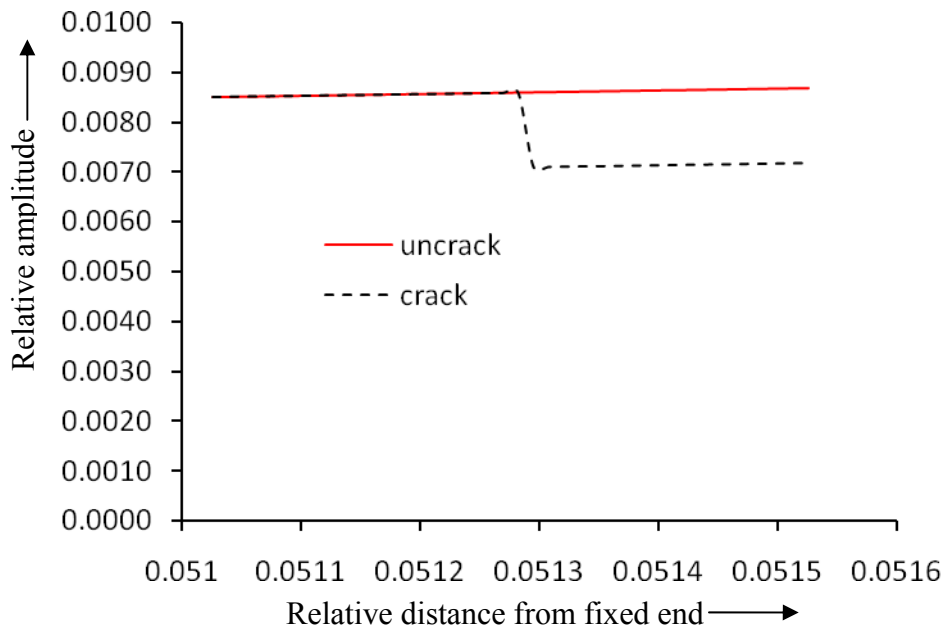


Fig. 3.2.9 (a1) Magnified view of Fig. 3.2.9 (a) at the vicinity of the crack location.

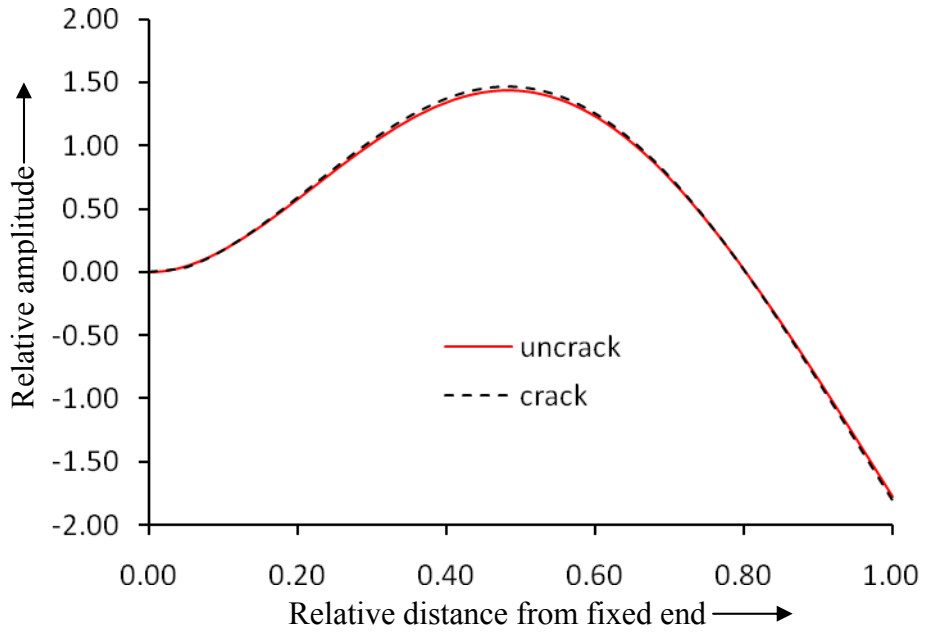


Fig.3.2.9 (b) Relative amplitude vs. relative distance from the fixed end (2nd mode of vibration), $a_1/W=0.2$, $L_1/L=0.0513$

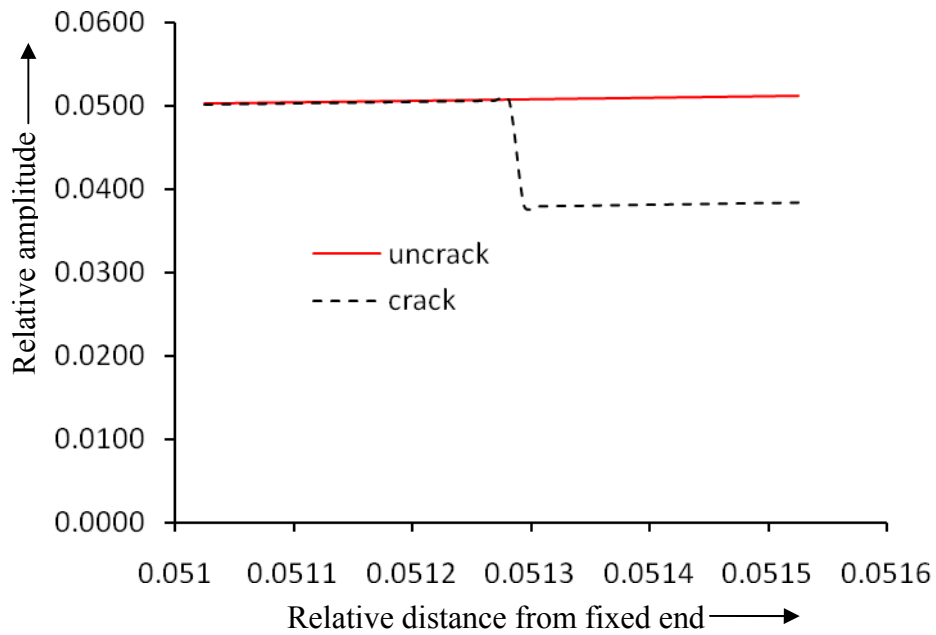


Fig. 3.2.9(b1) Magnified view of Fig. 3.2.9 (b) at the vicinity of the crack location.

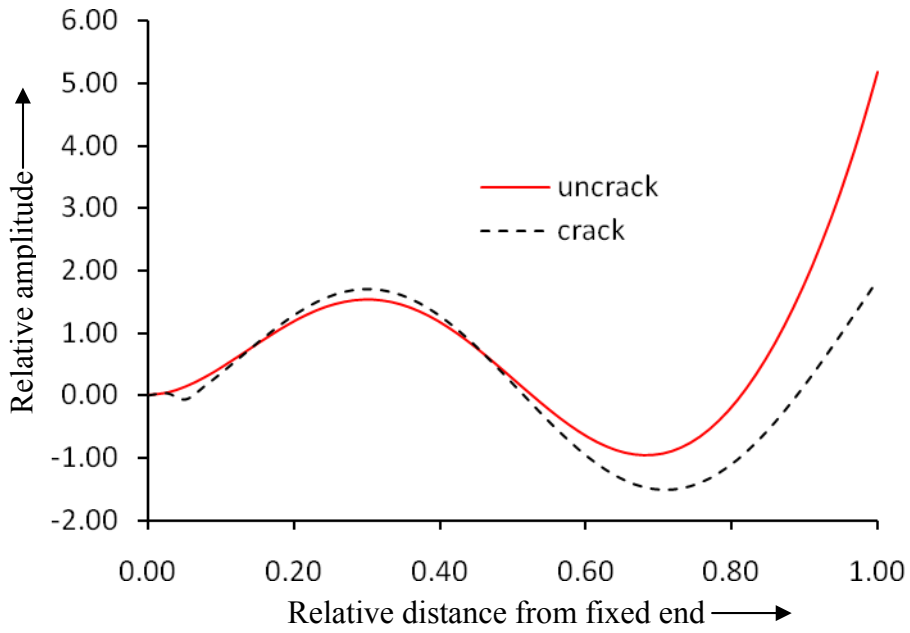


Fig.3.2.9 (c) Relative amplitude vs. relative distance from the fixed end (3rd mode of vibration), $a_1/W=0.2$, $L_1/L=0.0513$

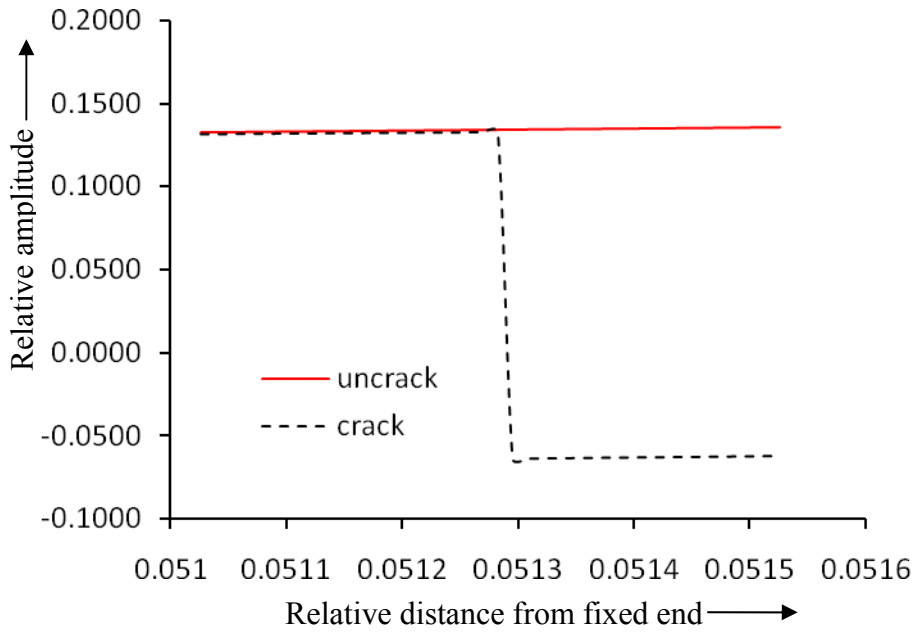


Fig. 3.2.9 (c1) Magnified view of Fig. 3.2.9 (c) at the vicinity of the crack location.

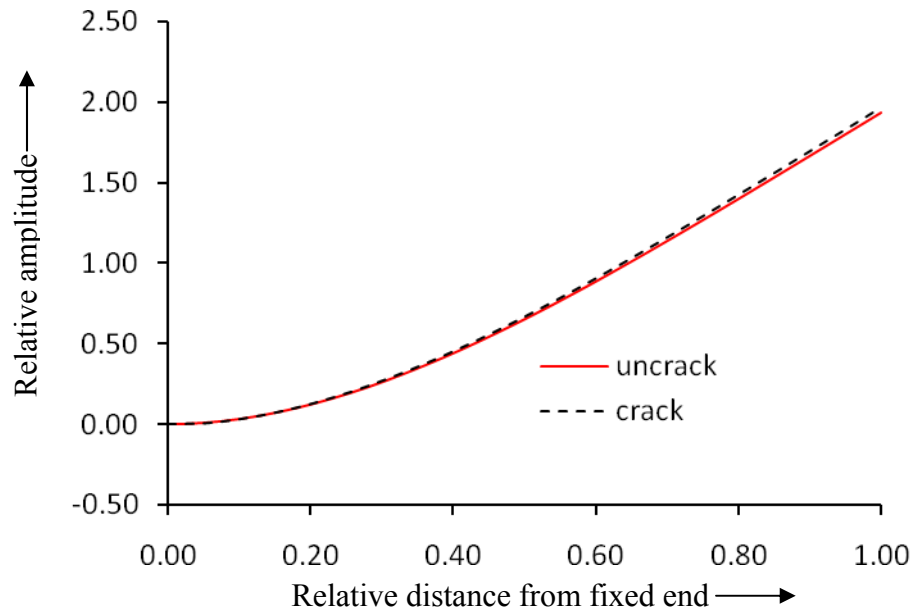


Fig.3.2.10 (a) Relative amplitude vs. relative distance from the fixed end (1st mode of vibration), $a_1/W= 0.3$, $L_1/L=0.0513$

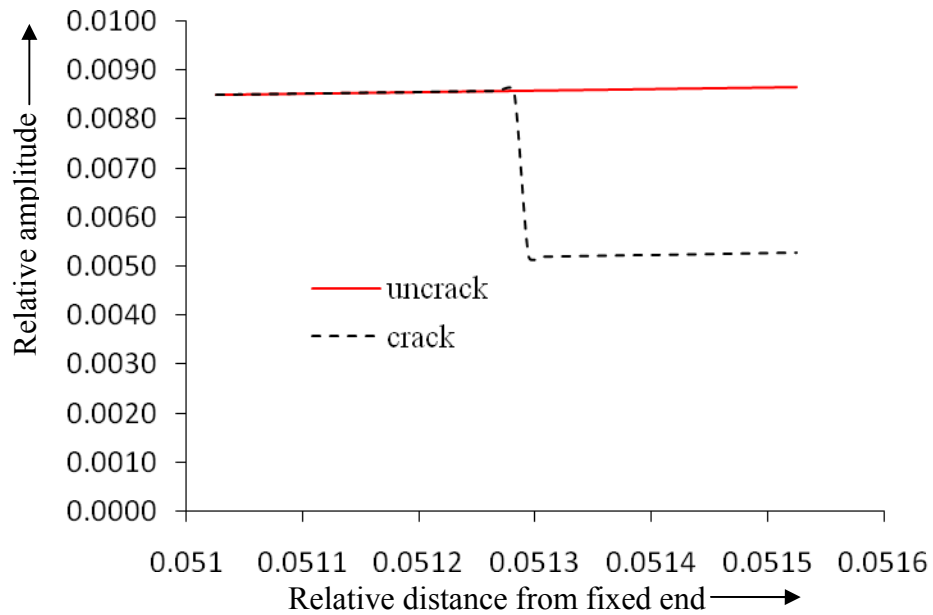


Fig. 3.2.10 (a1) Magnified view of fig. 3.2.10 (a) at the vicinity of the crack location.

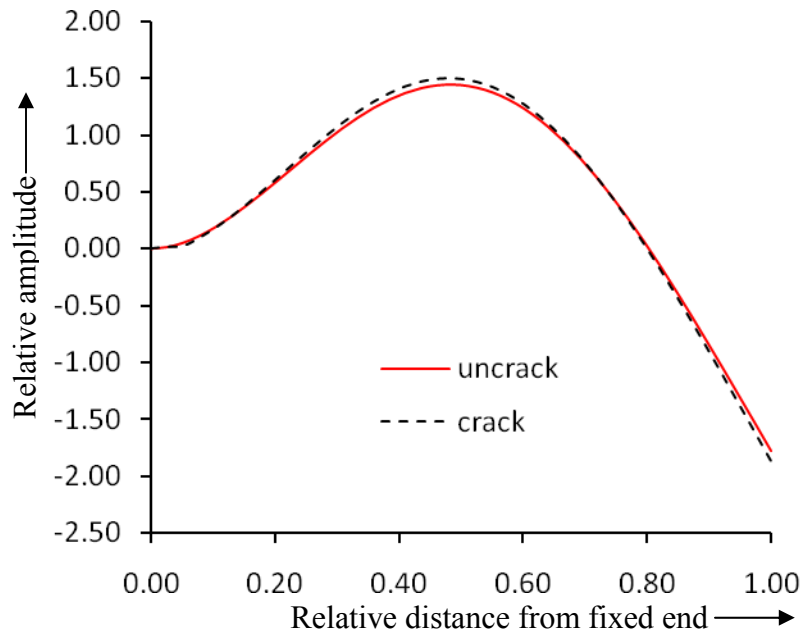


Fig.3.2.10 (b) Relative amplitude vs. relative distance from the fixed end (2nd mode of vibration), $a_1/W=0.3$, $L_1/L=0.0513$

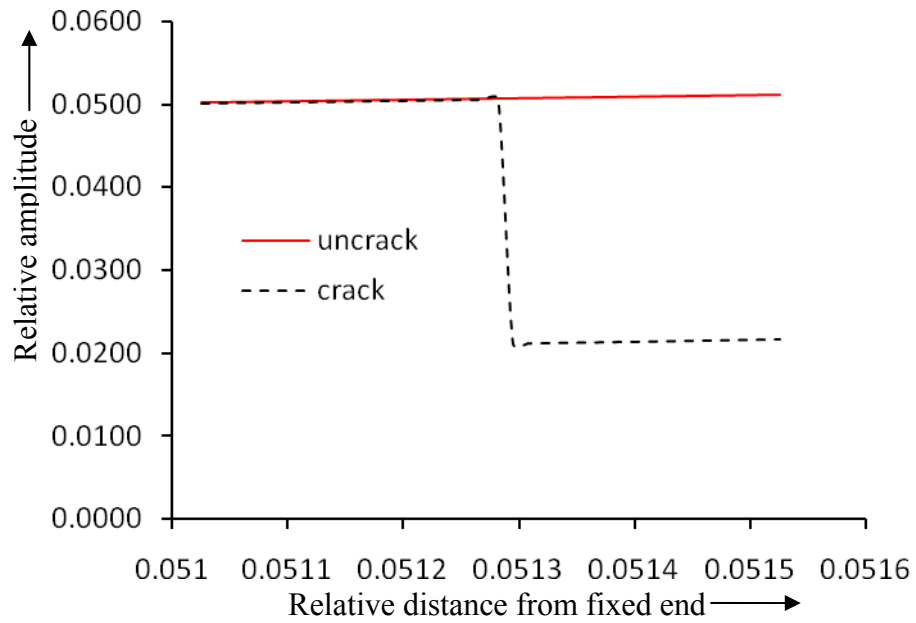


Fig. 3.2.10 (b1) Magnified view of Fig. 3.2.10 (b) at the vicinity of the crack location.

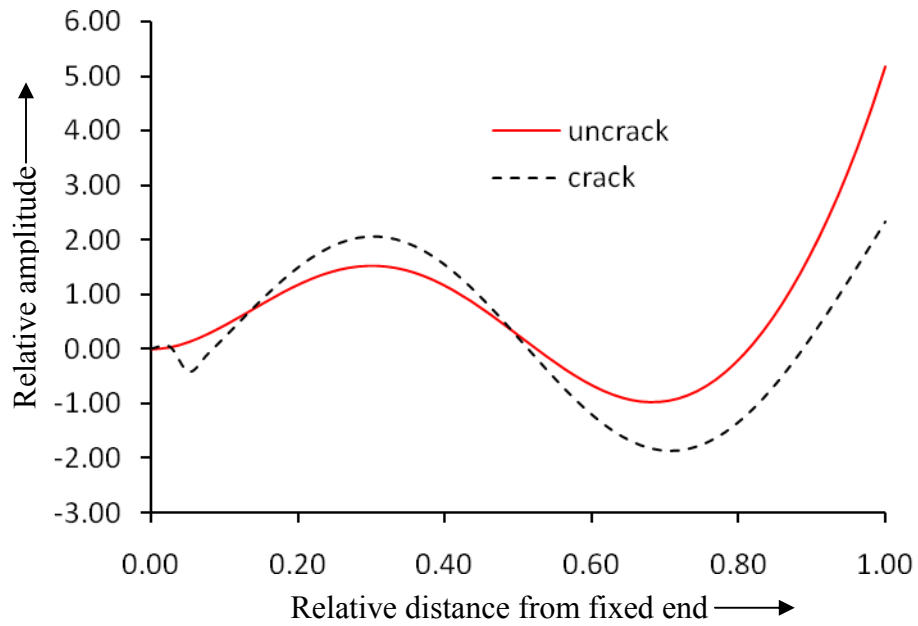


Fig.3.2.10 (c) Relative amplitude vs. relative distance from the fixed end (3rd mode of vibration), $a_1/W=0.3$, $L_1/L=0.0513$

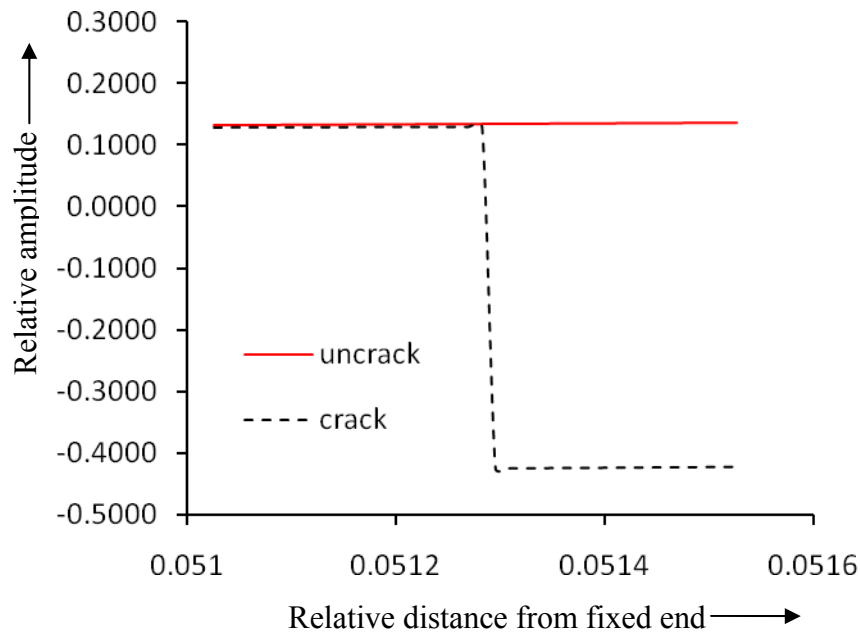


Fig. 3.2.10 (c1) Magnified view of Fig. 3.2.10 (c) at the vicinity of the crack location.

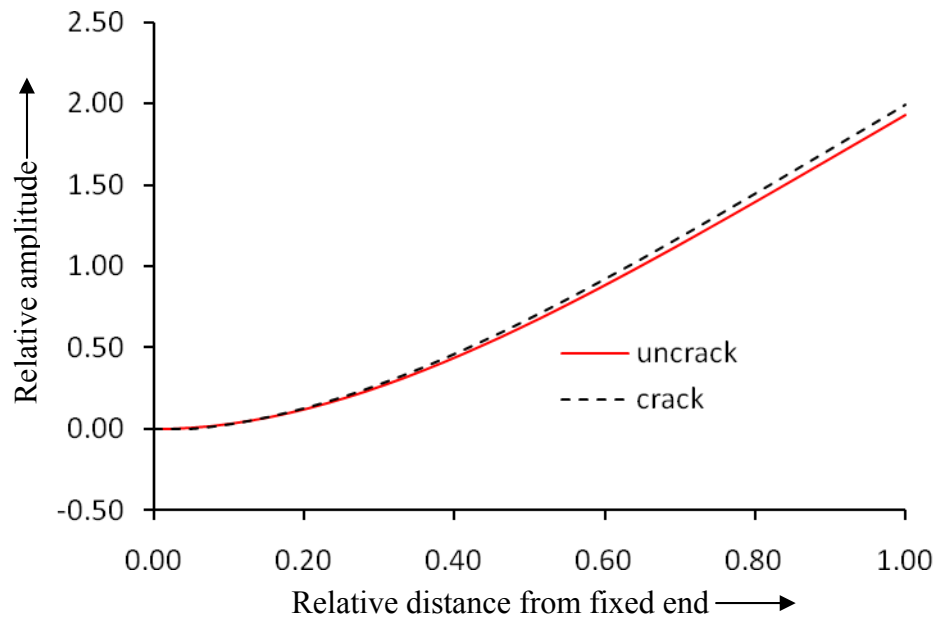


Fig.3.2.11 (a) Relative amplitude vs. relative distance from the fixed end (1st mode of vibration), $a_1/W=0.4$, $L_1/L=0.0513$

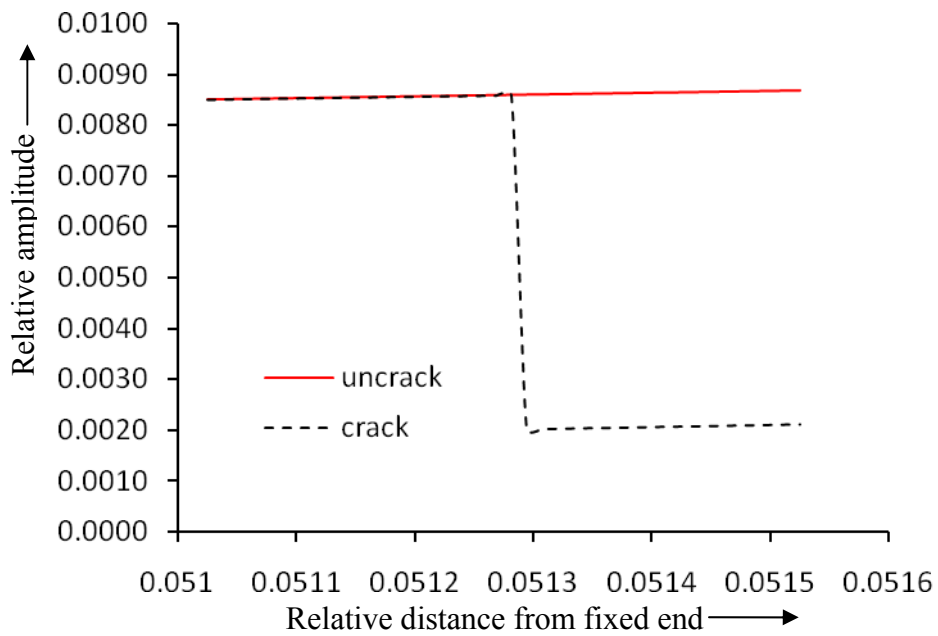


Fig. 3.2.11 (a1) Magnified view of Fig. 3.2.11 (a) at the vicinity of the crack location.

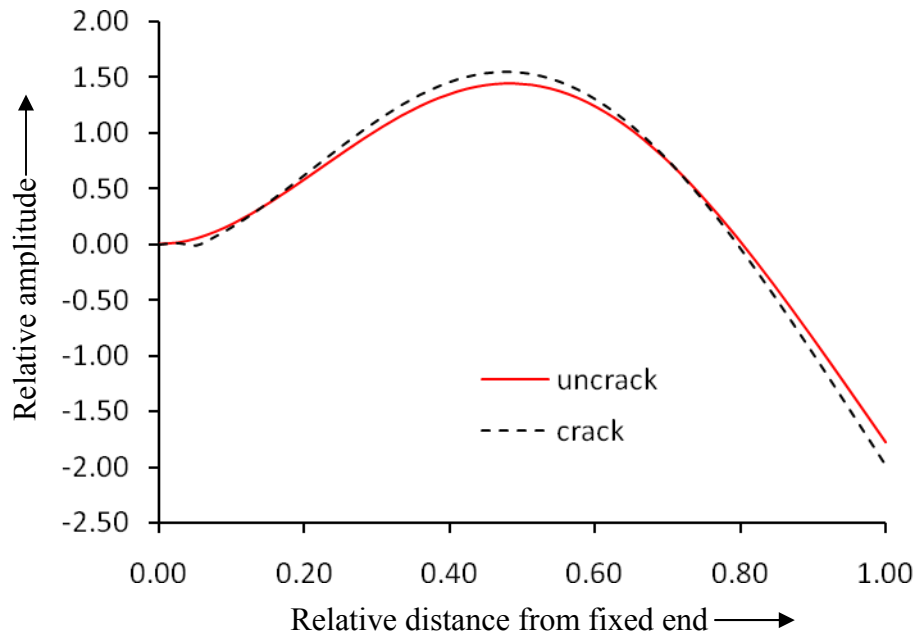


Fig. 3.2.11 (b) Relative amplitude vs. relative distance from the fixed end (2nd mode of vibration), $a_1/W=0.4$, $L_1/L=0.0513$

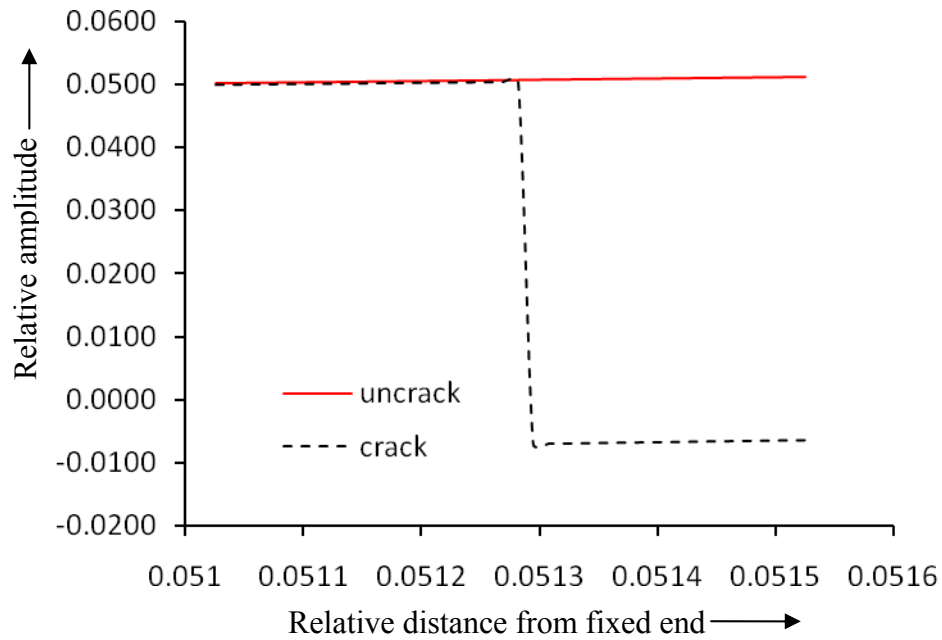


Fig. 3.2.11(b1) Magnified view of Fig. 3.2.11 (b) at the vicinity of the crack location.

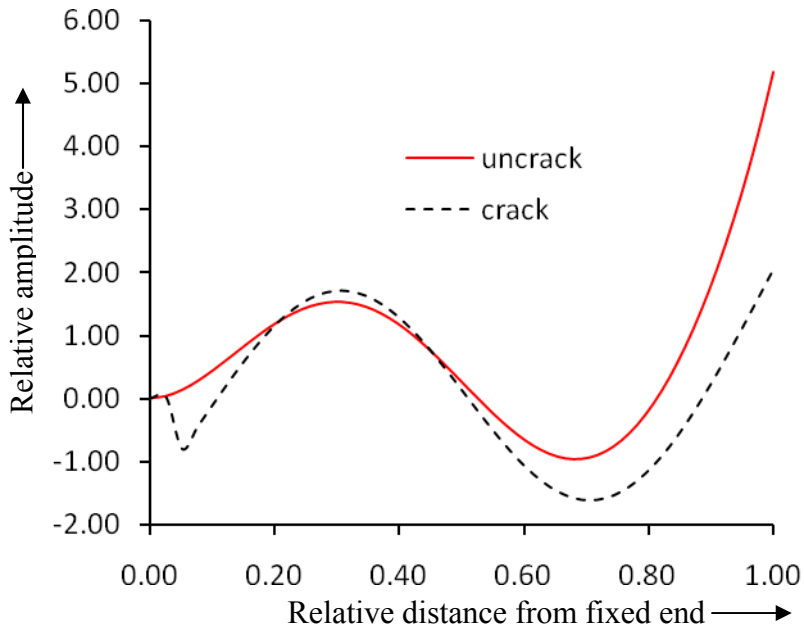


Fig.3.2.11 (c) Relative amplitude vs. relative distance from the fixed end (3rd mode of vibration), $a_1/W=0.4$, $L_1/L=0.0513$

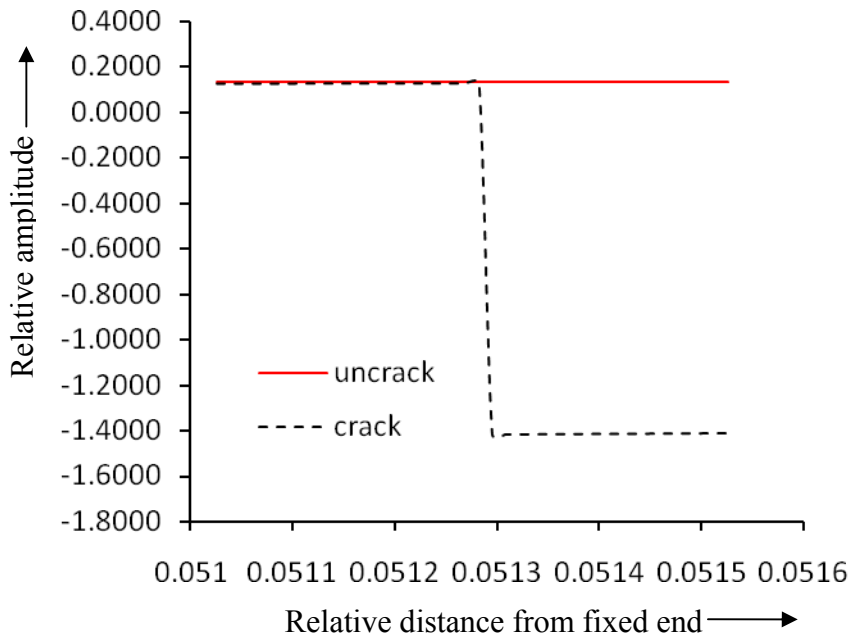


Fig. 3.2.11 (c1) Magnified view of Fig. 3.2.11 (c) at the vicinity of the crack location.

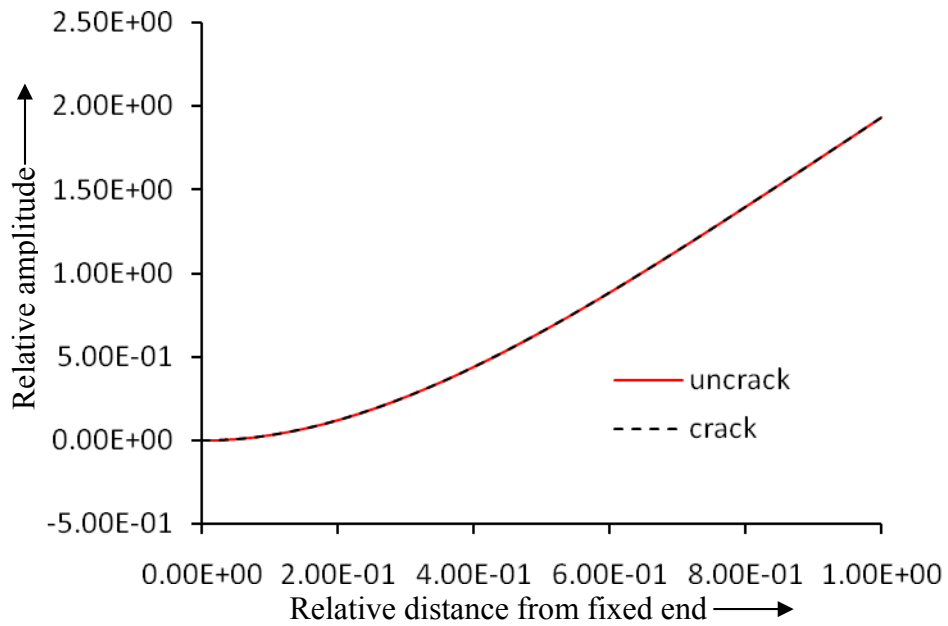


Fig.3.2.12 (a) Relative amplitude vs. relative distance from the fixed end (1st mode of vibration), $a_1/W=0.1$, $L_1/L=0.1795$

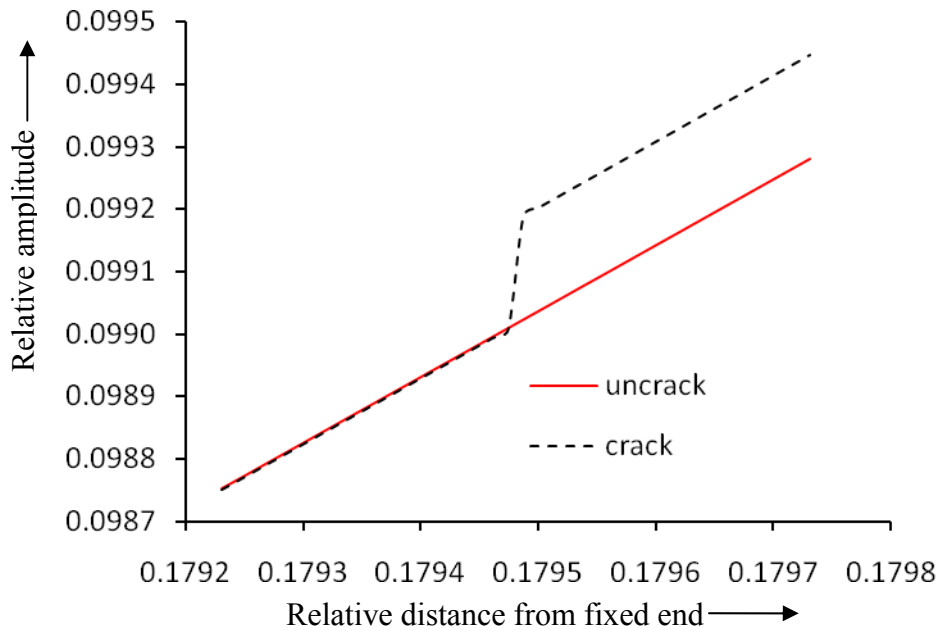


Fig. 3.2.12 (a1) Magnified view of Fig. 3.2.12 (a) at the vicinity of the crack location.

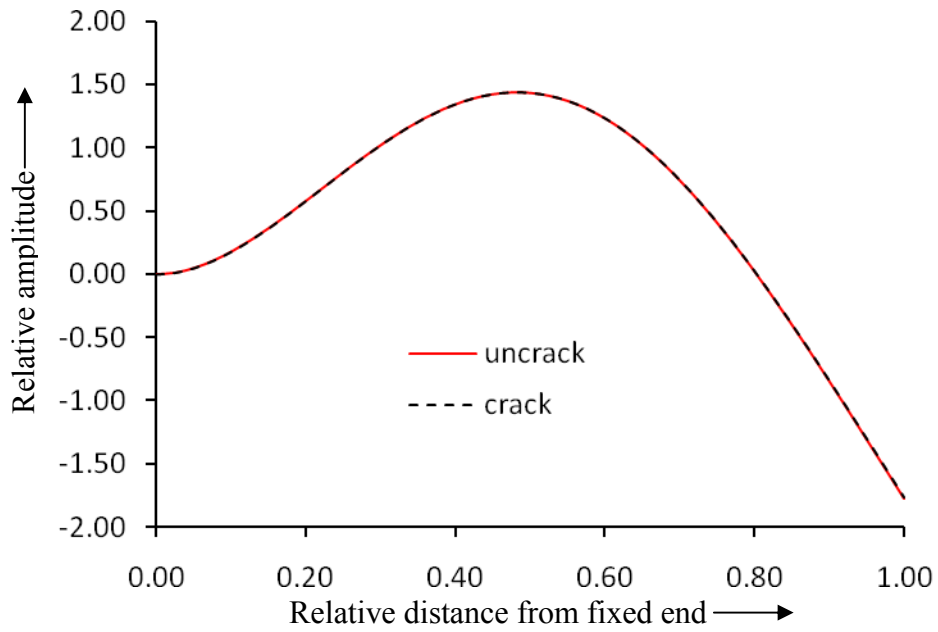


Fig. 3.2.12 (b) Relative amplitude vs. relative distance from the fixed end (2nd mode of vibration), $a_1/W=0.1$, $L_1/L=0.1795$

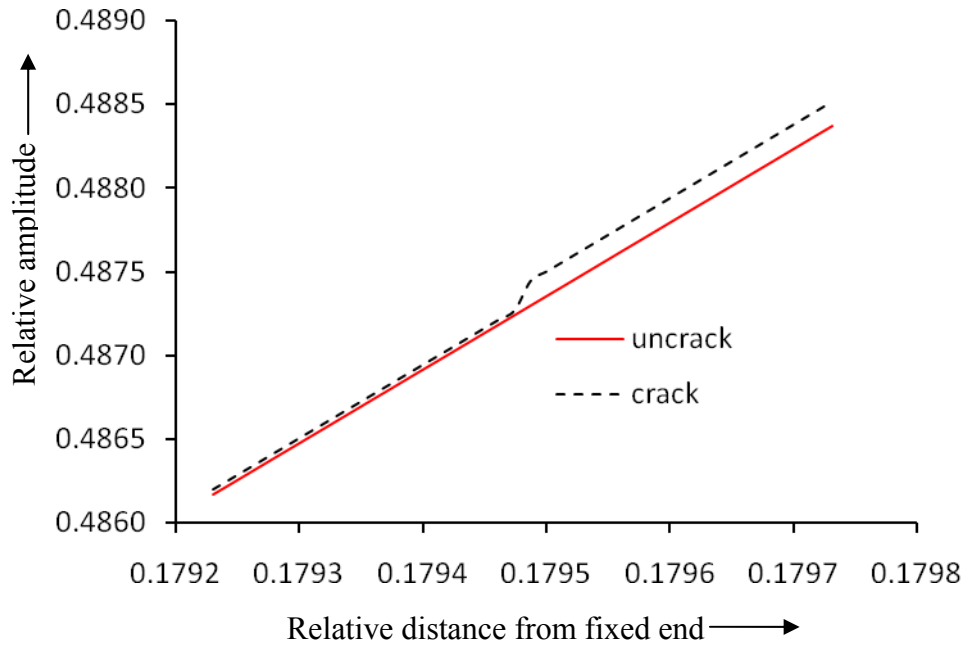


Fig. 3.2.12 (b1) Magnified view of Fig. 3.2.12 (b) at the vicinity of the crack location.

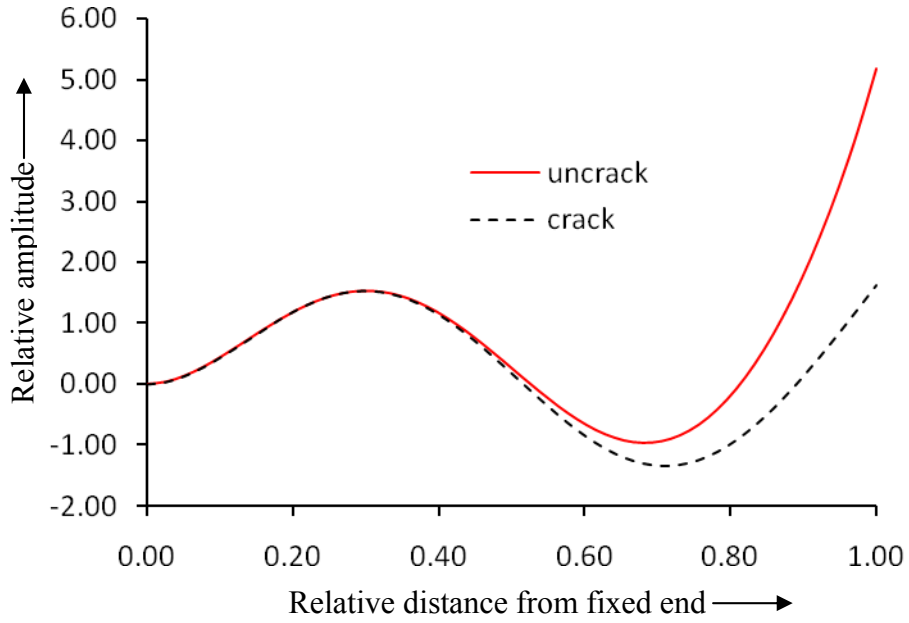


Fig. 3.2.12 (c) Relative amplitude vs. relative distance from the fixed end (3rd mode of vibration), $a_1/W=0.1$, $L_1/L=0.1795$

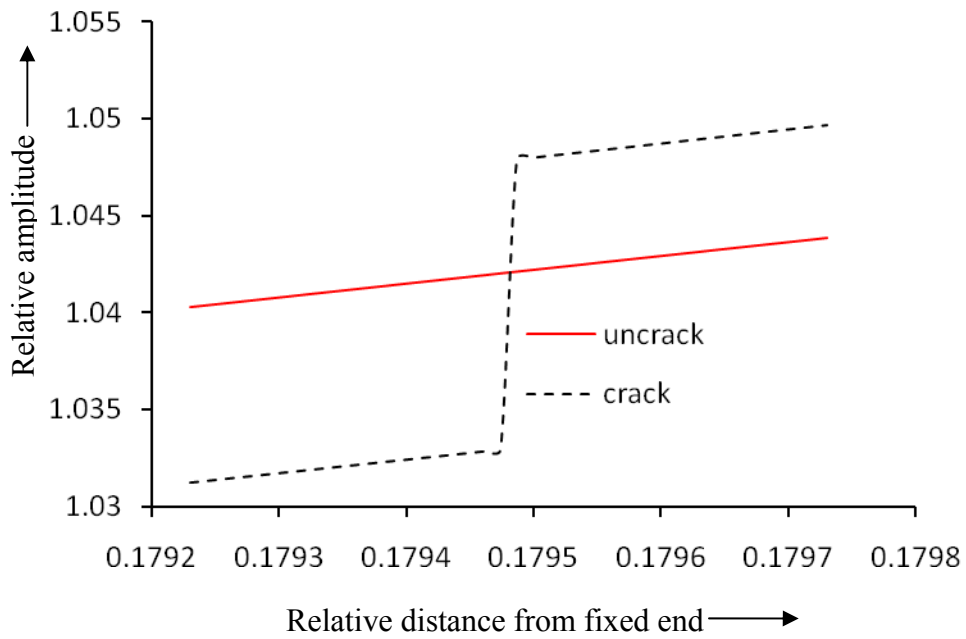


Fig. 3.2.12 (c1) Magnified view of Fig. 3.2.12 (c) at the vicinity of the crack location.

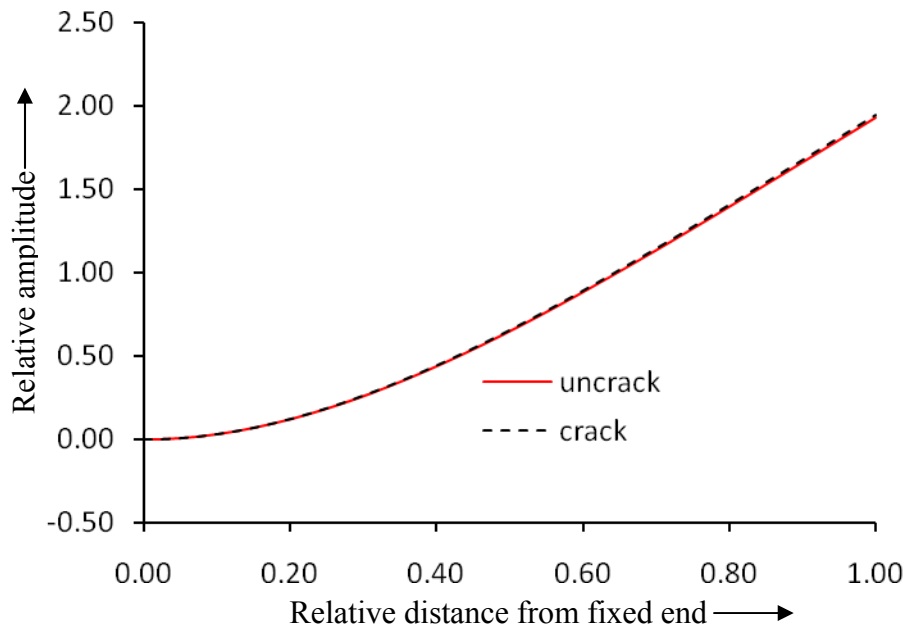


Fig.3.2.13 (a) Relative amplitude vs. relative distance from the fixed end (1st mode of vibration), $a_1/W=0.2$, $L_1/L=0.1795$

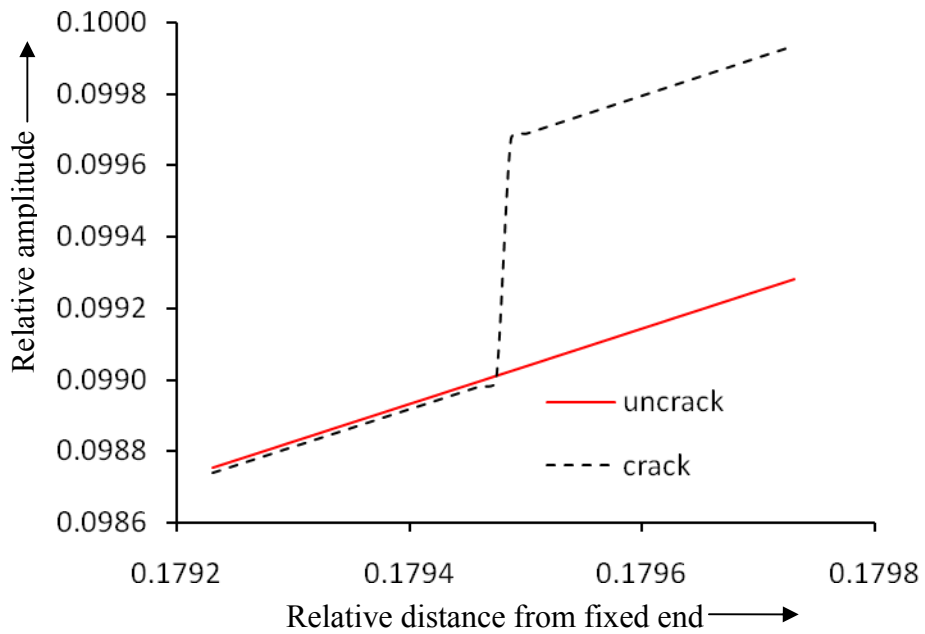


Fig. 3.2.13 (a1) Magnified view of Fig. 3.2.13 (a) at the vicinity of the crack location.

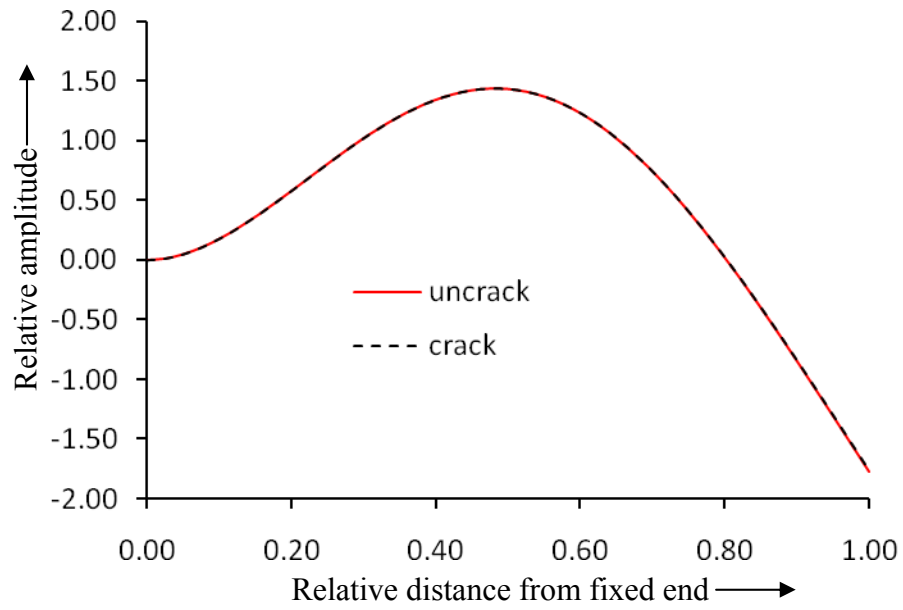


Fig. 3.2.13 (b) Relative amplitude vs. relative distance from the fixed end (2nd mode of vibration), $a_1/W=0.2$, $L_1/L=0.1795$

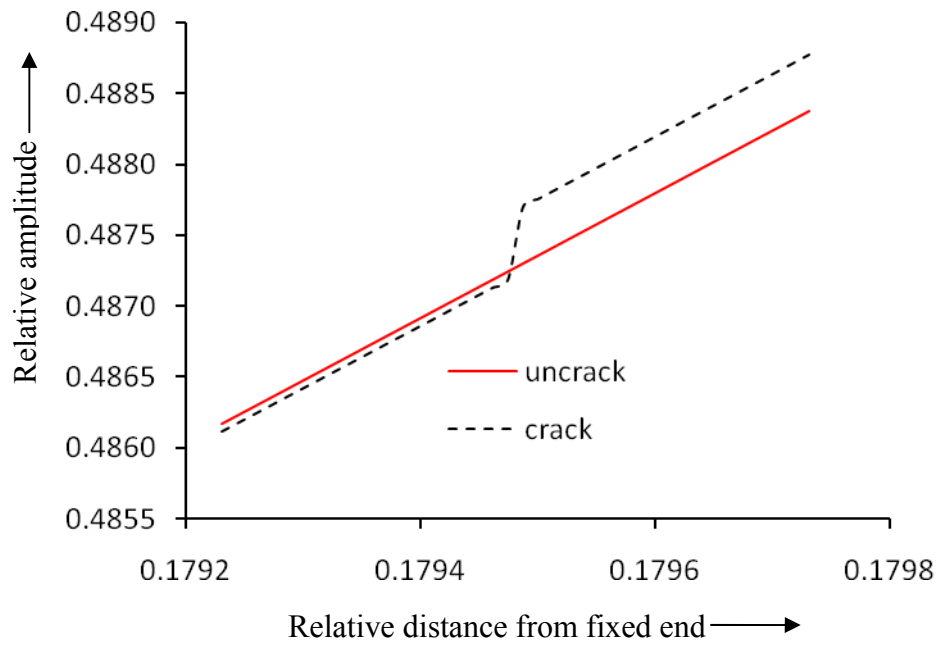


Fig. 3.2.13(b1) Magnified view of Fig. 3.2.13 (b) at the vicinity of the crack location.

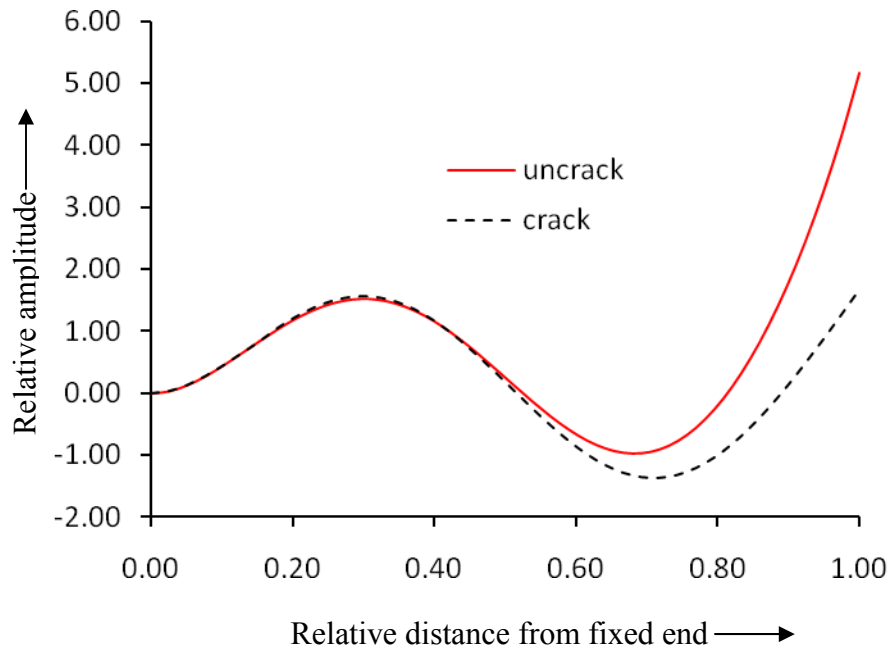


Fig.3.2.13 (c) Relative amplitude vs. relative distance from the fixed end (3rd mode of vibration), $a_1/W=0.2$, $L_1/L=0.1795$

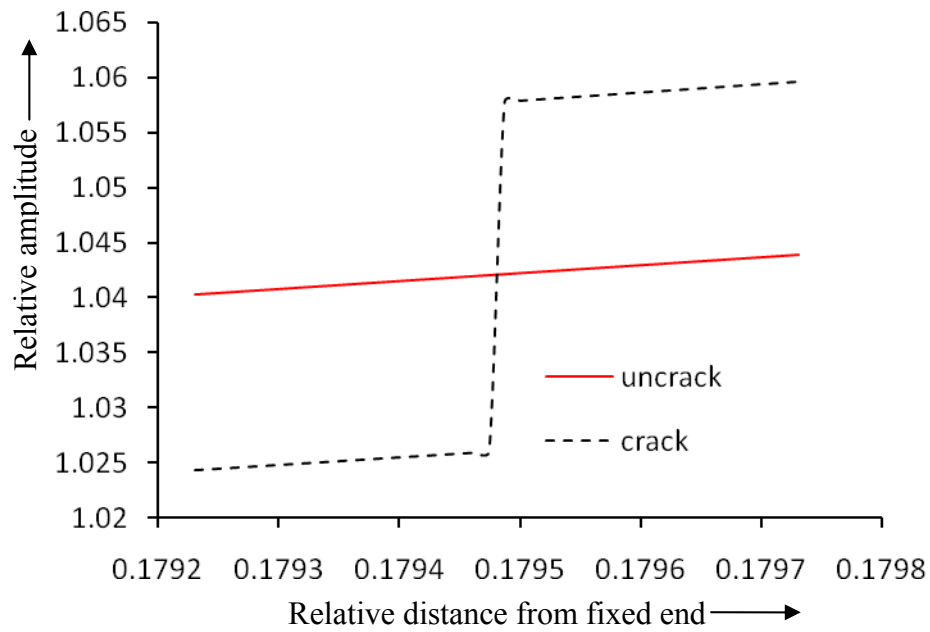


Fig. 3.2.13 (c1) Magnified view of Fig. 3.2.13 (c) at the vicinity of the crack location.

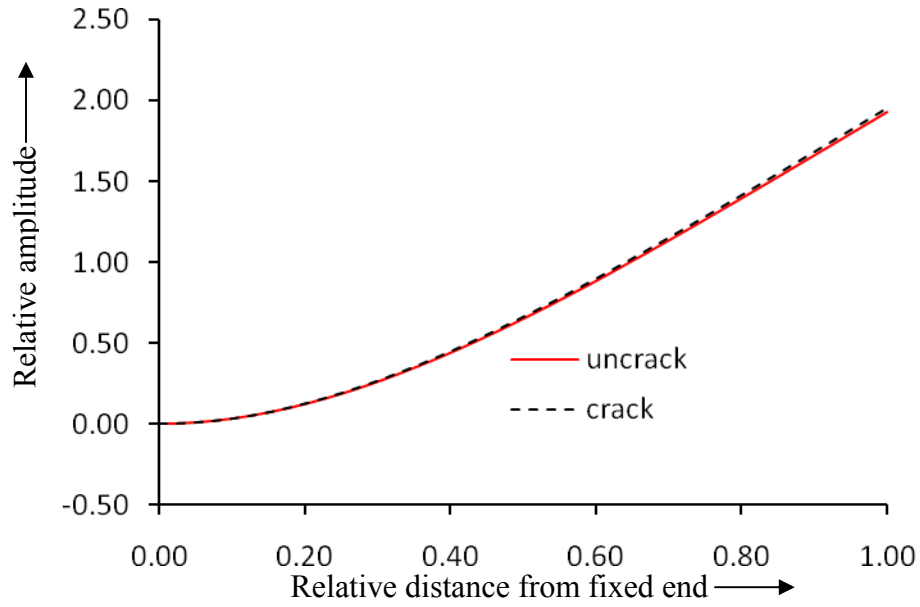


Fig.3.2.14 (a) Relative amplitude vs. relative distance from the fixed end (1st mode of vibration), $a_1/W=0.3$, $L_1/L=0.1795$

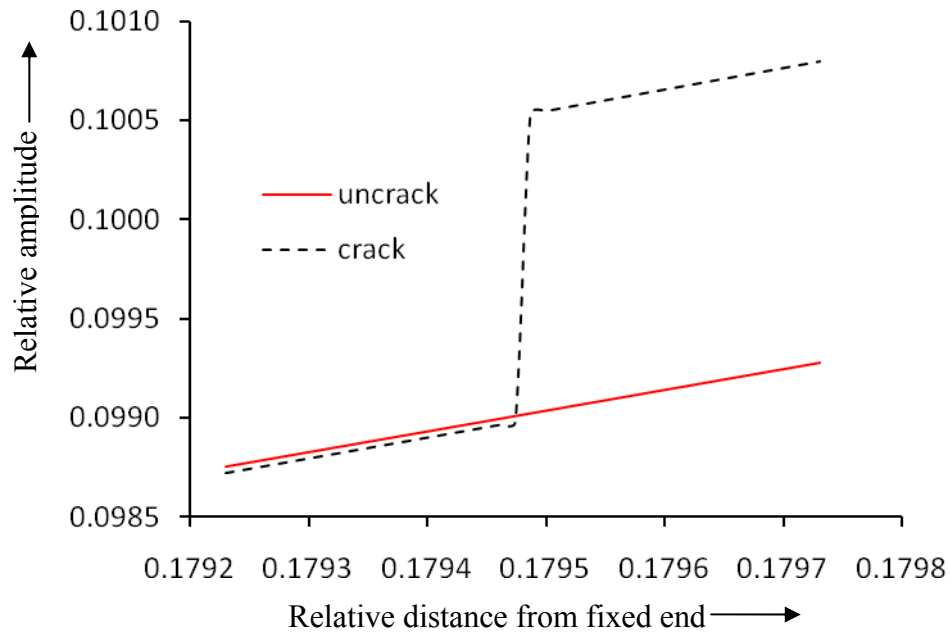


Fig. 3.2.14 (a1) Magnified view of Fig. 3.2.14 (a) at the vicinity of the crack location.

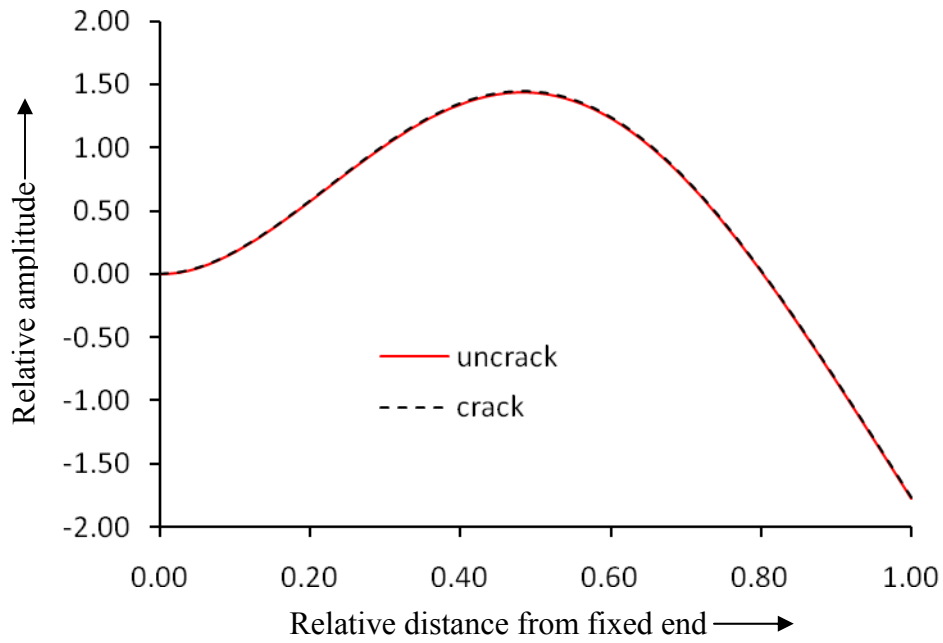


Fig.3.2.14 (b) Relative amplitude vs. relative distance from the fixed end (2nd mode of vibration), $a_1/W=0.3$, $L_1/L=0.1795$

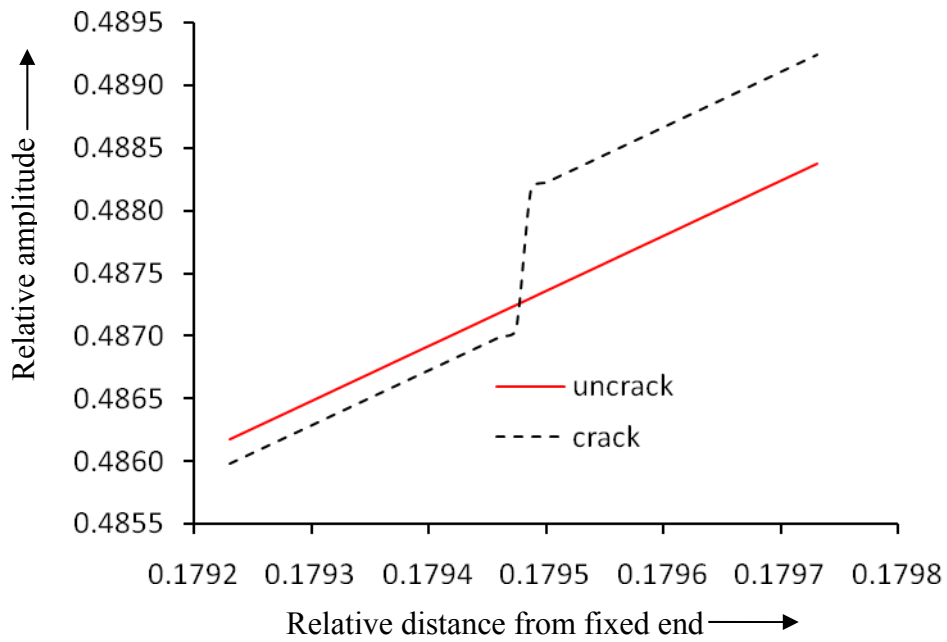


Fig. 3.2.14(b1) Magnified view of Fig. 3.2.14(b) at the vicinity of the crack location.

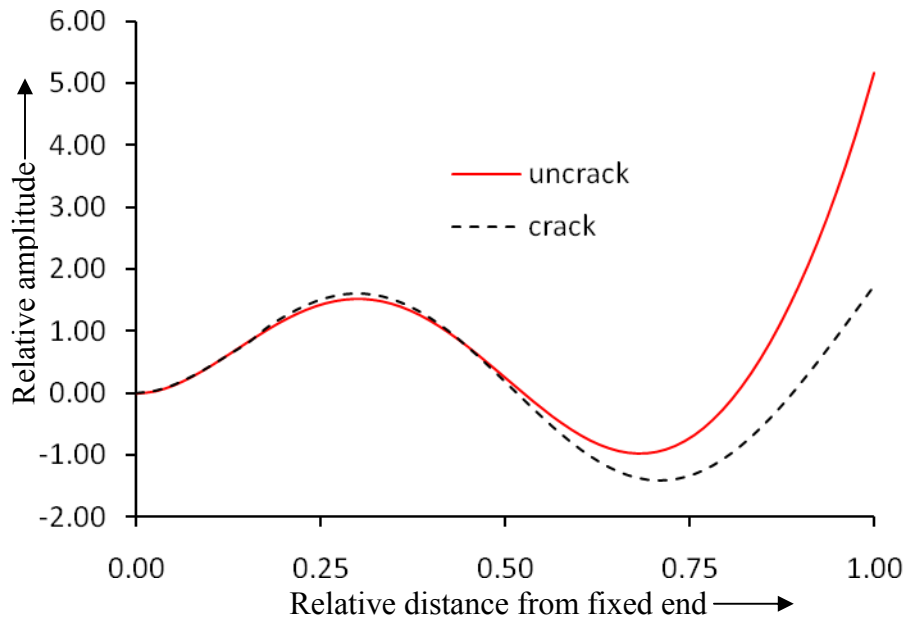


Fig.3.2.14 (c) Relative amplitude vs. relative distance from the fixed end (3rd mode of vibration), $a_1/W=0.3$, $L_1/L=0.1795$

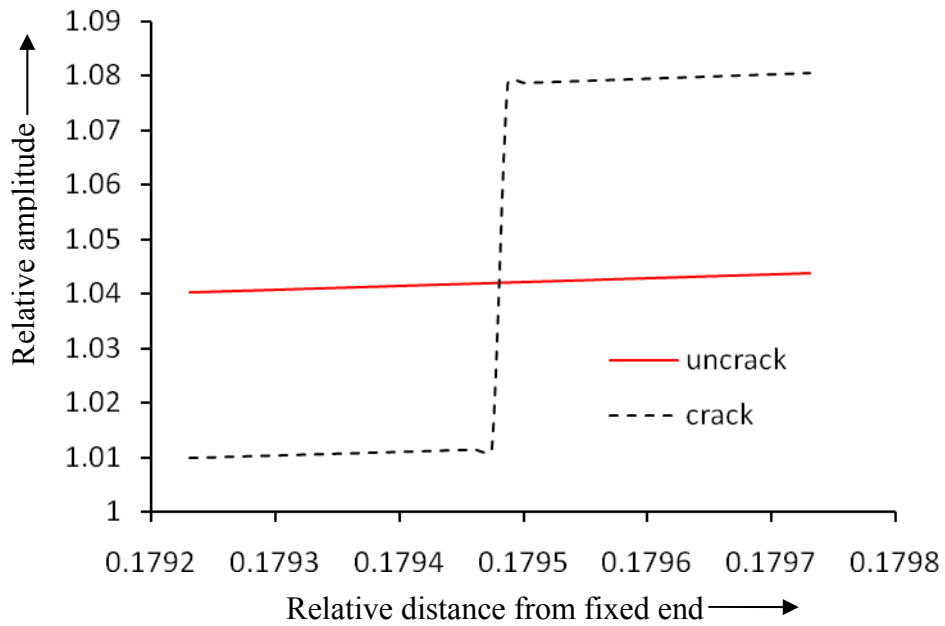


Fig. 3.2.14(c1) Magnified view of Fig. 3.2.14(c) at the vicinity of the crack location.

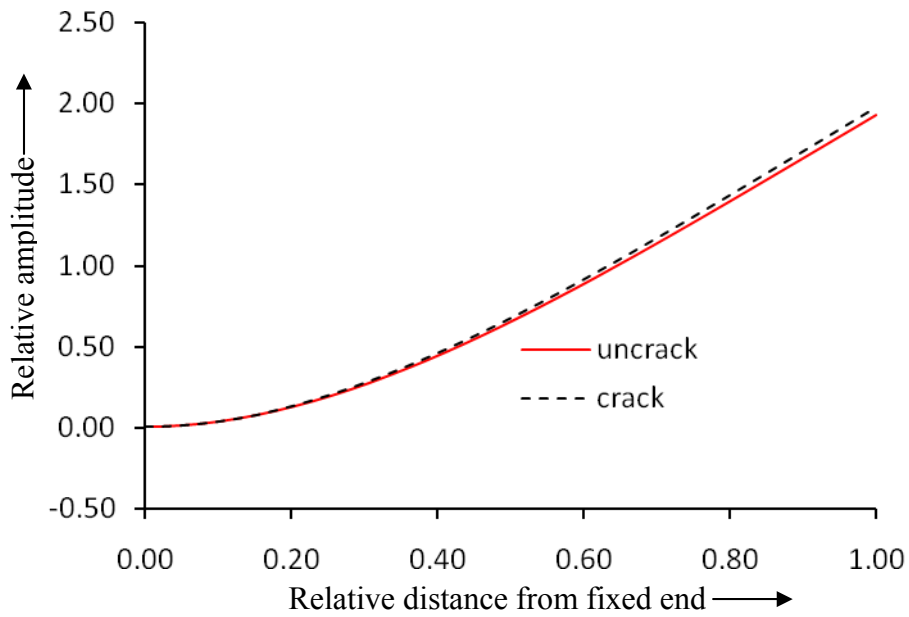


Fig.3.2.15 (a) Relative amplitude vs. relative distance from the fixed end (1st mode of vibration), $a_1/W=0.4$, $L_1/L=0.1795$

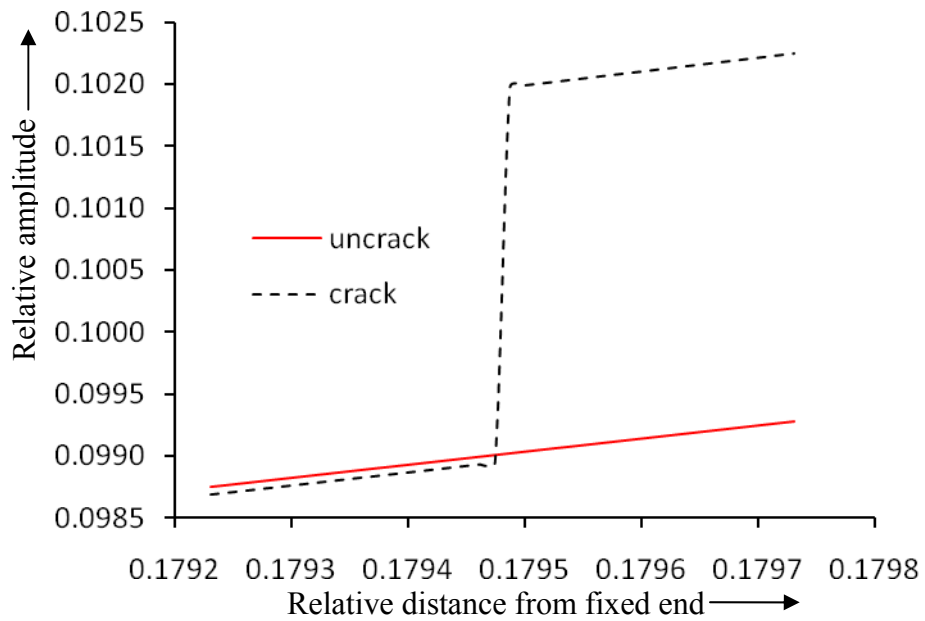


Fig. 3.2.15 (a1) Magnified view of Fig. 3.2.15 (a) at the vicinity of the crack location.

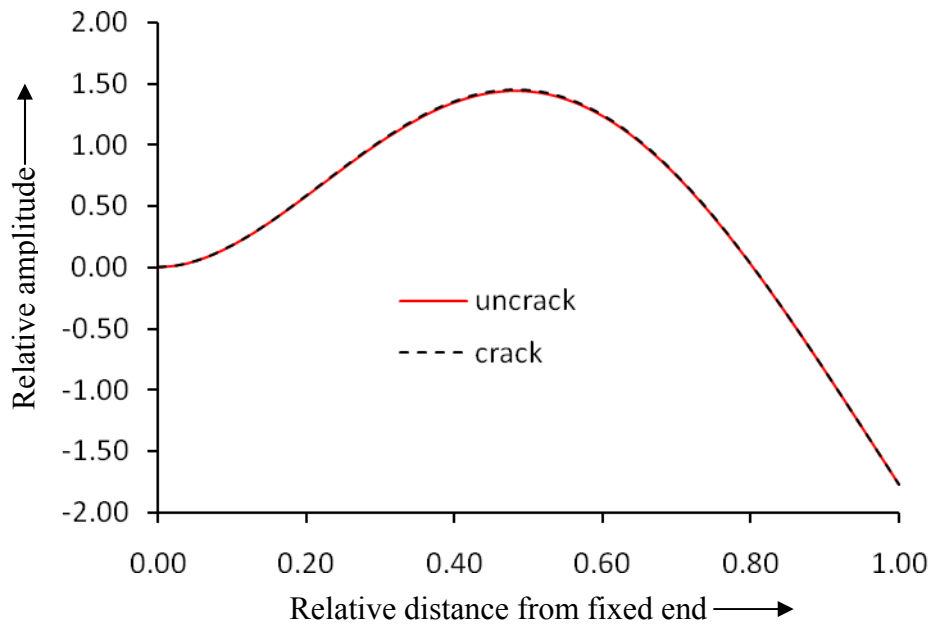


Fig.3.2.15 (b) Relative amplitude vs. relative distance from the fixed end (2nd mode of vibration), $a_1/W=0.4$, $L_1/L=0.1795$

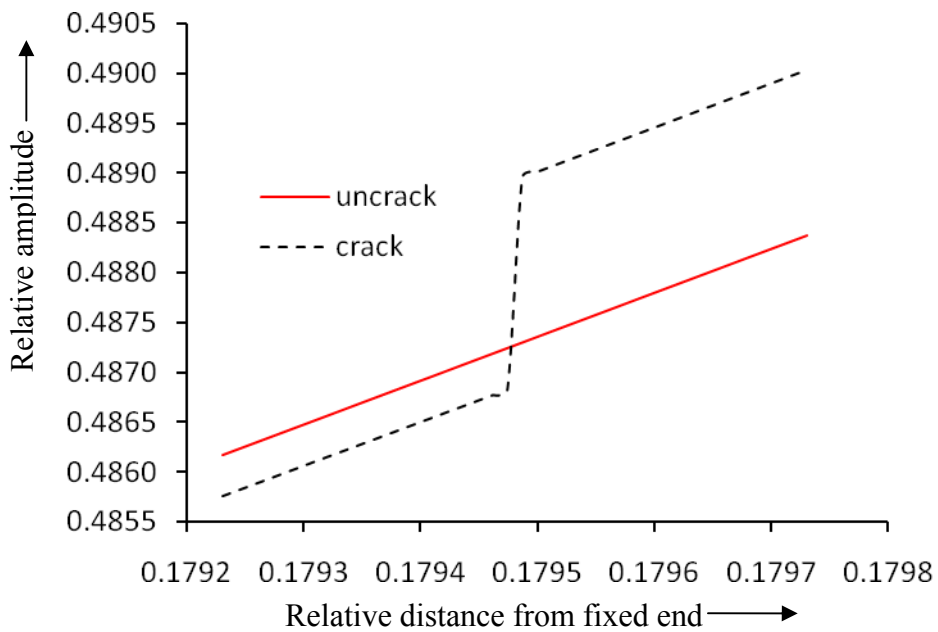


Fig. 3.2.15(b1) Magnified view of Fig. 3.2.15(b) at the vicinity of the crack location.

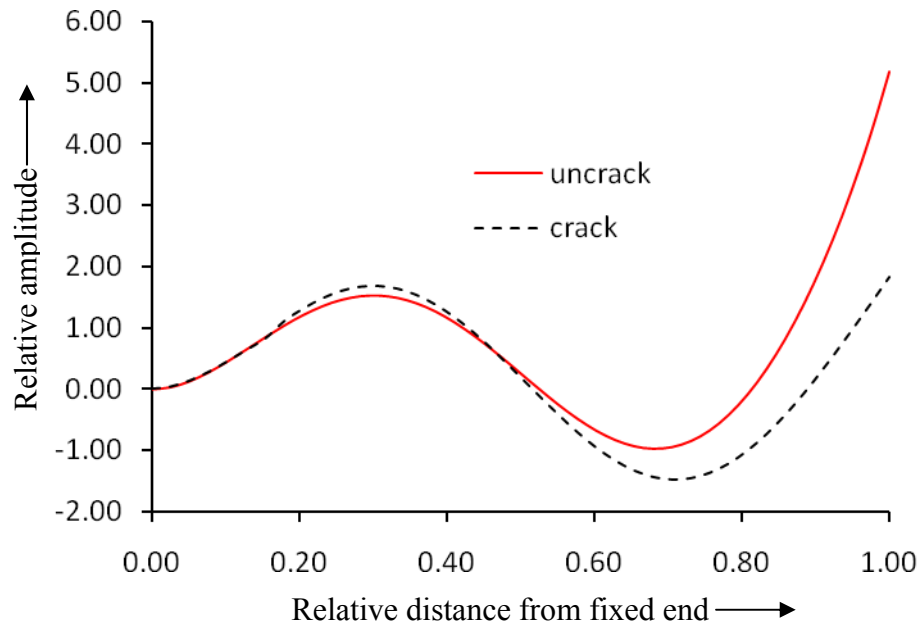


Fig.3.2.15 (c) Relative amplitude vs. relative distance from the fixed end (3rd mode of vibration), $a_1/W=0.4$, $L_1/L=0.1795$

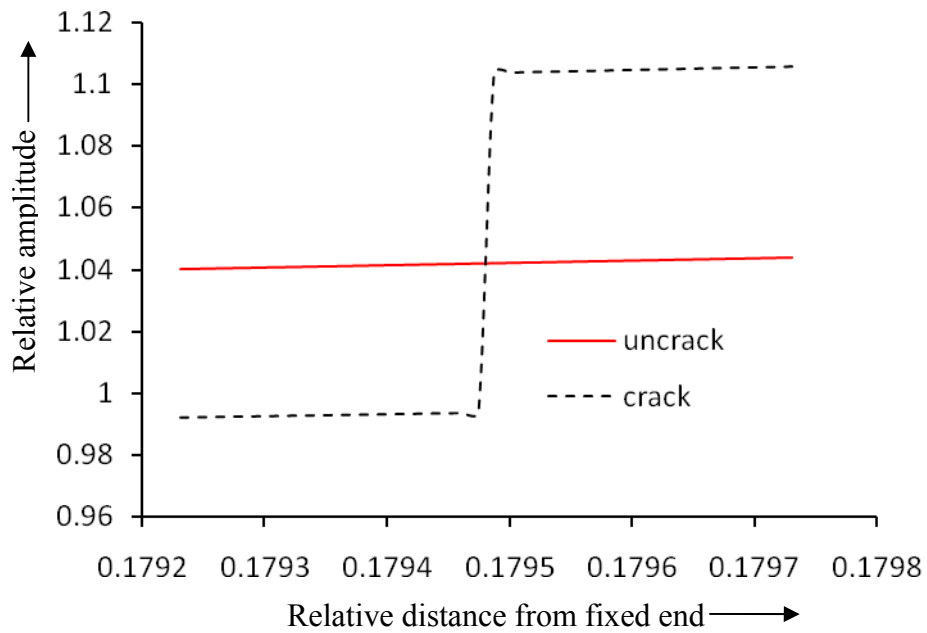


Fig. 3.2.15(c1) Magnified view of Fig. 3.2.15(c) at the vicinity of the crack location.

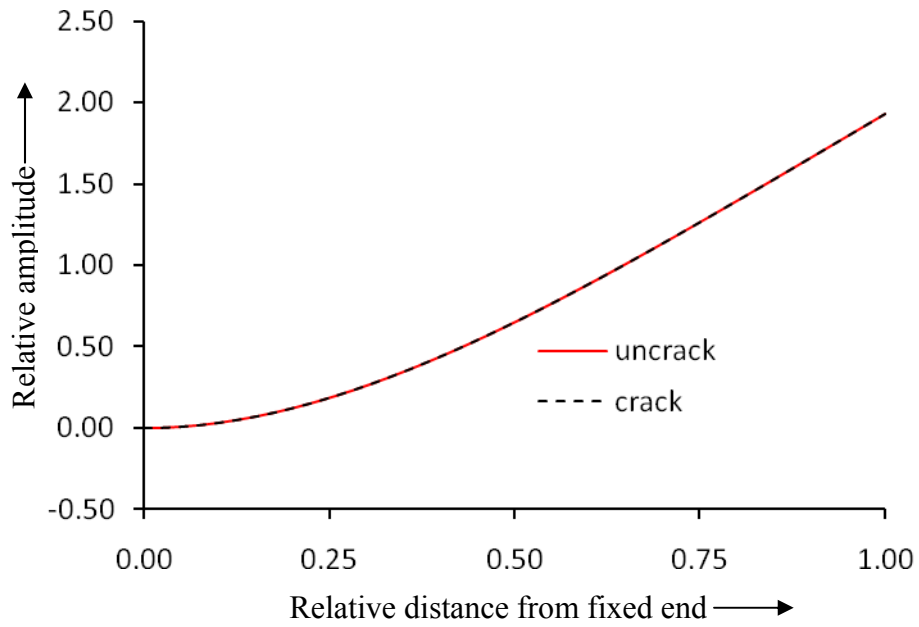


Fig.3.2.16 (a) Relative amplitude vs. relative distance from the fixed end (1st mode of vibration), $a_1/W=0.1$, $L_1/L=0.2564$

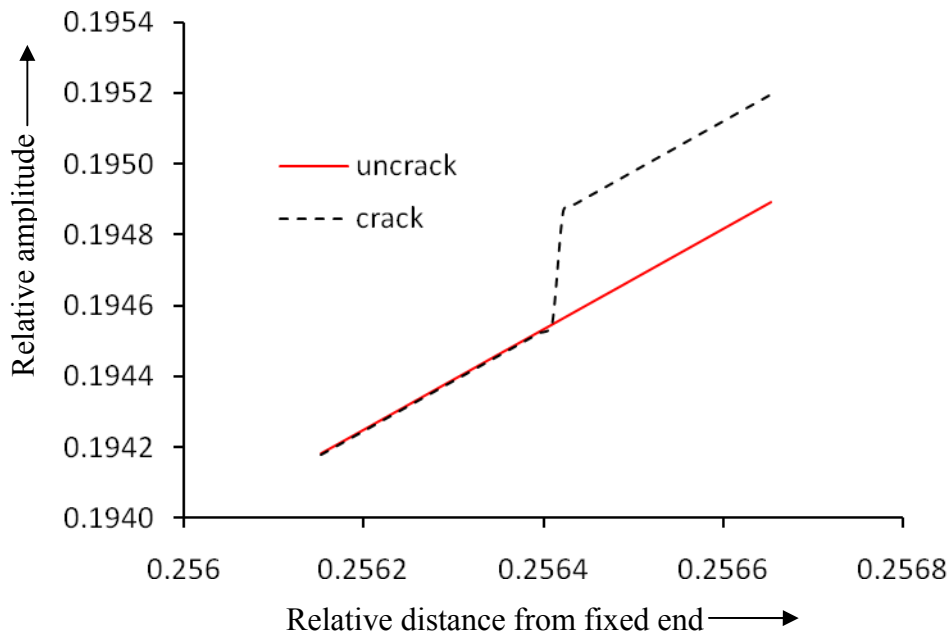


Fig. 3.2.16(a1) Magnified view of Fig. 3.2.16(a) at the vicinity of the crack location.

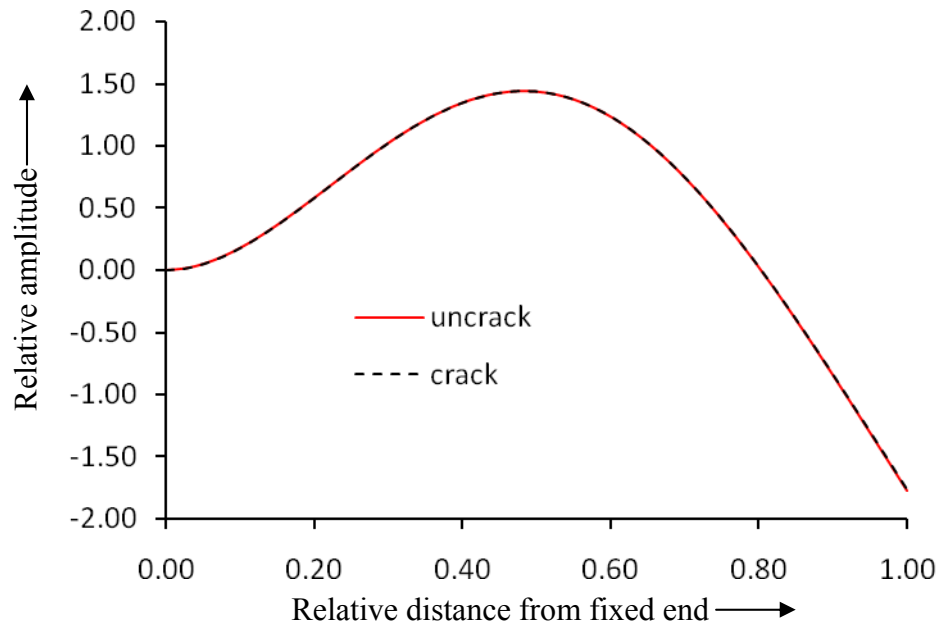


Fig.3.2.16 (b) Relative amplitude vs. relative distance from the fixed end (2nd mode of vibration), $a_1/W=0.1$, $L_1/L=0.2564$

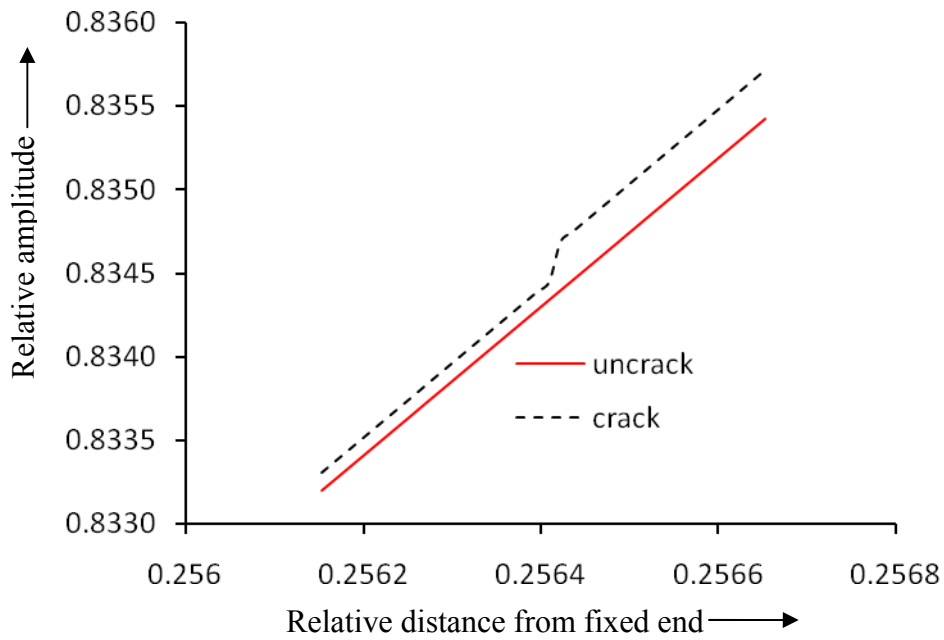


Fig. 3.2.16(b1) Magnified view of Fig. 3.2.16(b) at the vicinity of the crack location.

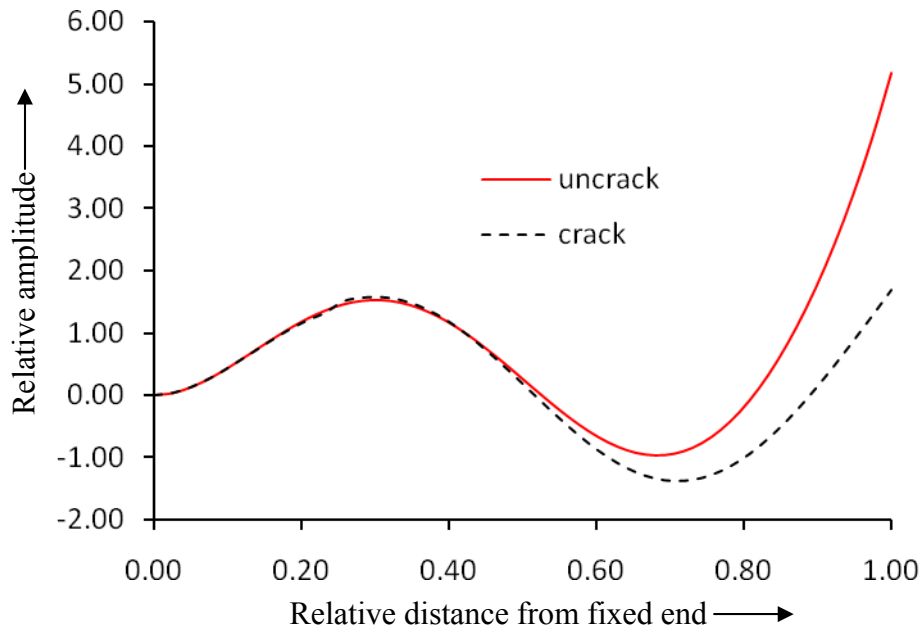


Fig. 3.2.16 (c) Relative amplitude vs. relative distance from the fixed end (3rd mode of vibration), $a_1/W=0.1$, $L_1/L=0.2564$

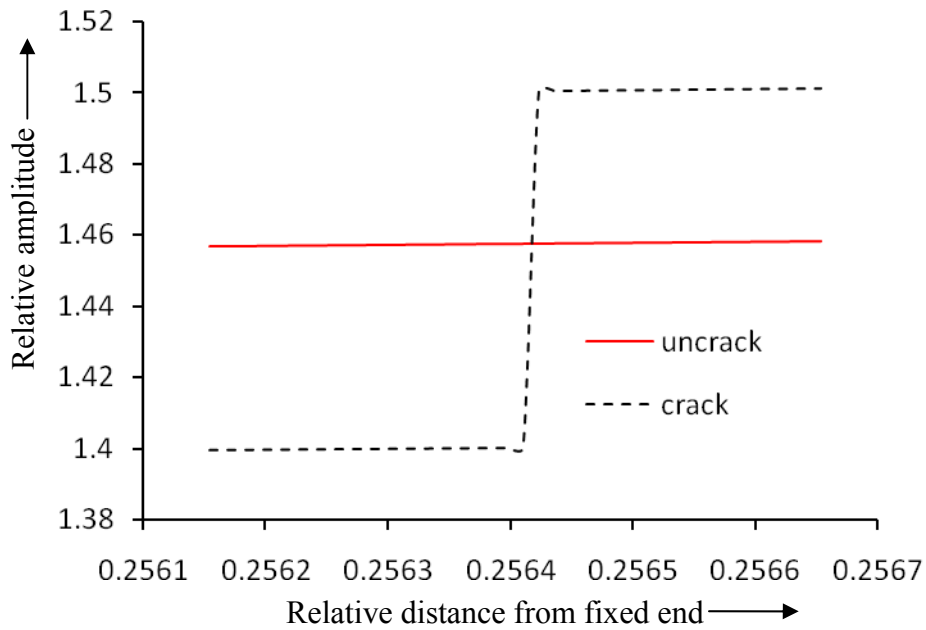


Fig. 3.2.16 (c1) Magnified view of Fig. 3.2.16 (c) at the vicinity of the crack location.

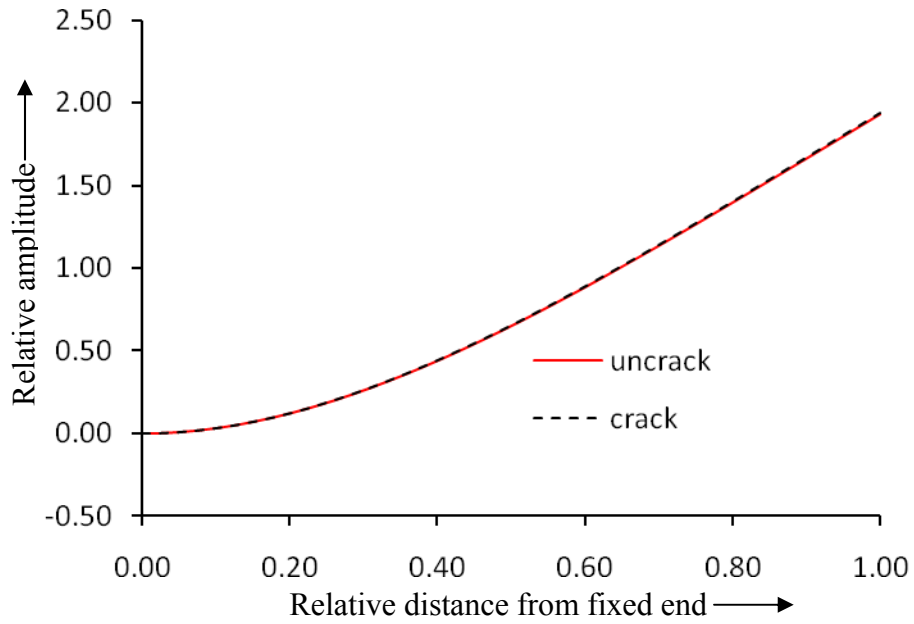


Fig.3.2.17 (a) Relative amplitude vs. relative distance from the fixed end (1st mode of vibration), $a_1/W=0.2$, $L_1/L=0.2564$

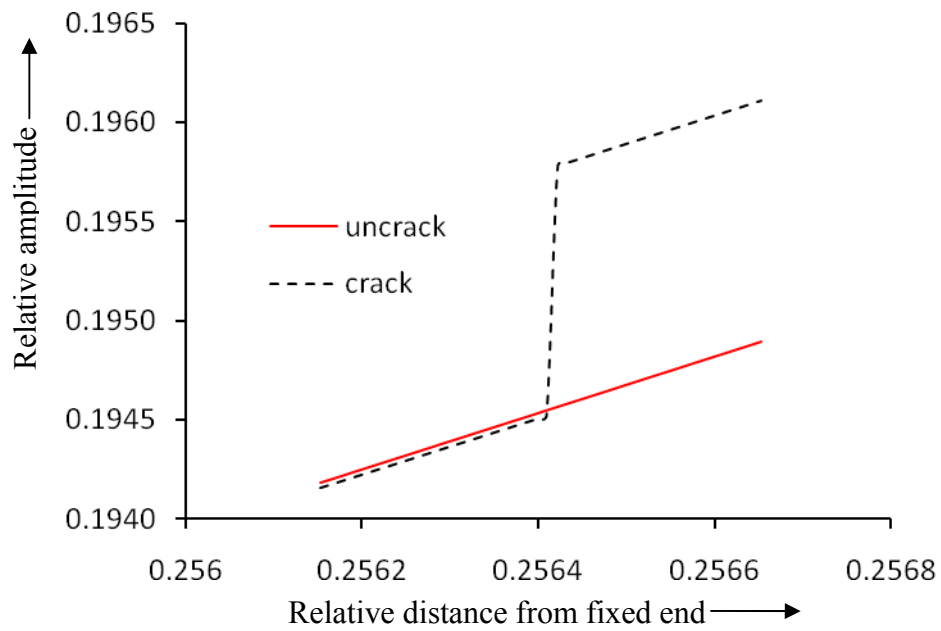


Fig. 3.2.17 (a1) Magnified view of Fig. 3.2.17 (a) at the vicinity of the crack location.

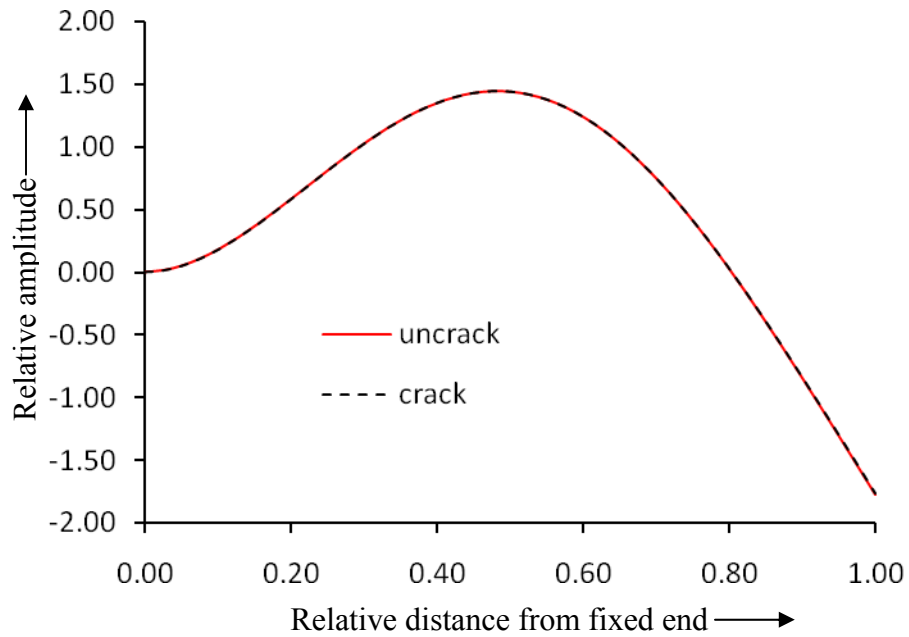


Fig.3.2.17 (b) Relative amplitude vs. relative distance from the fixed end (2nd mode of vibration), $a_1/W=0.2$, $L_1/L=0.2564$

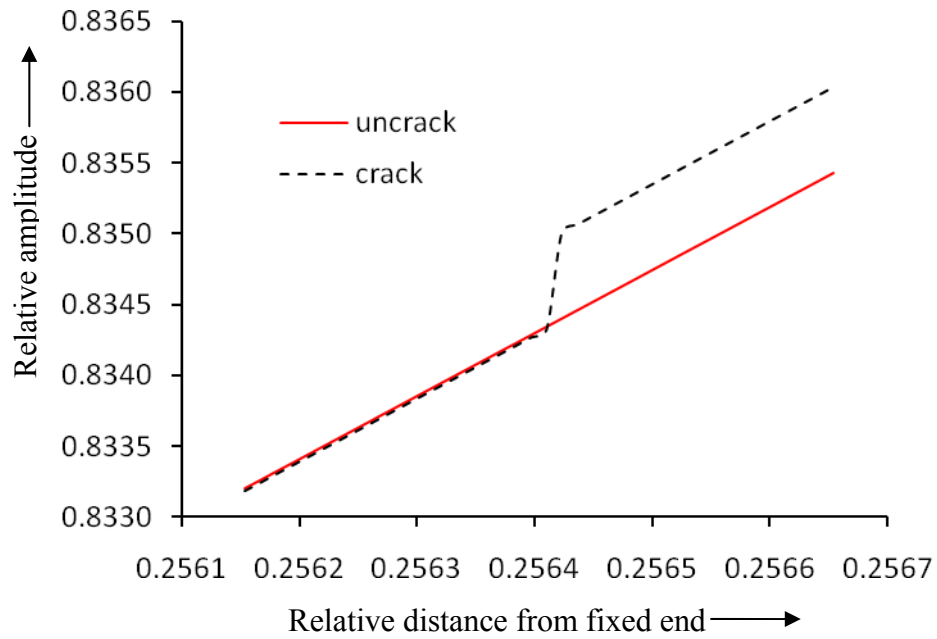


Fig. 3.2.17(b1) Magnified view of Fig. 3.2.17(b) at the vicinity of the crack location.

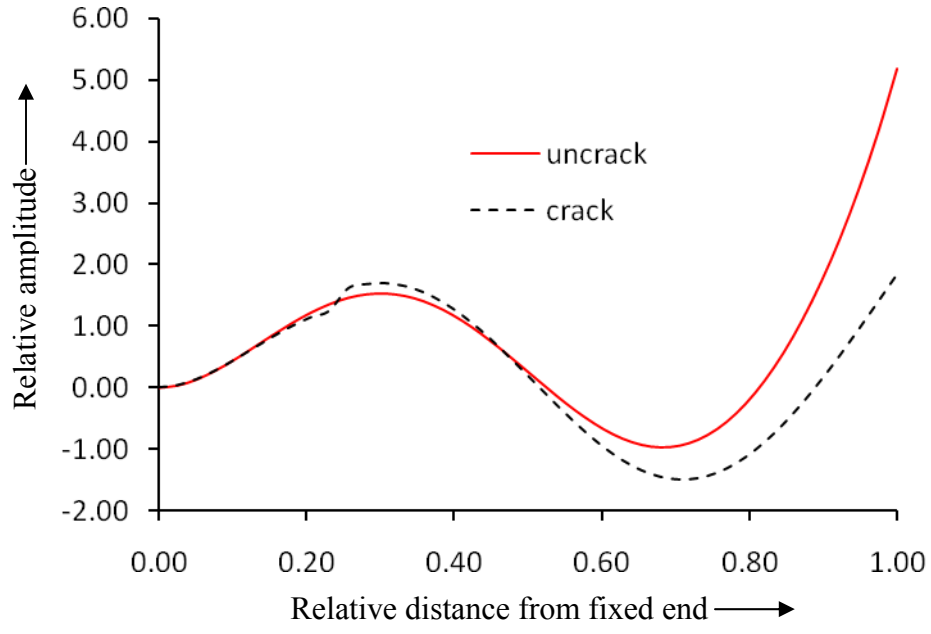


Fig. 3.2.17 (c) Relative amplitude vs. relative distance from the fixed end (3rd mode of vibration), $a_1/W=0.2$, $L_1/L=0.2564$

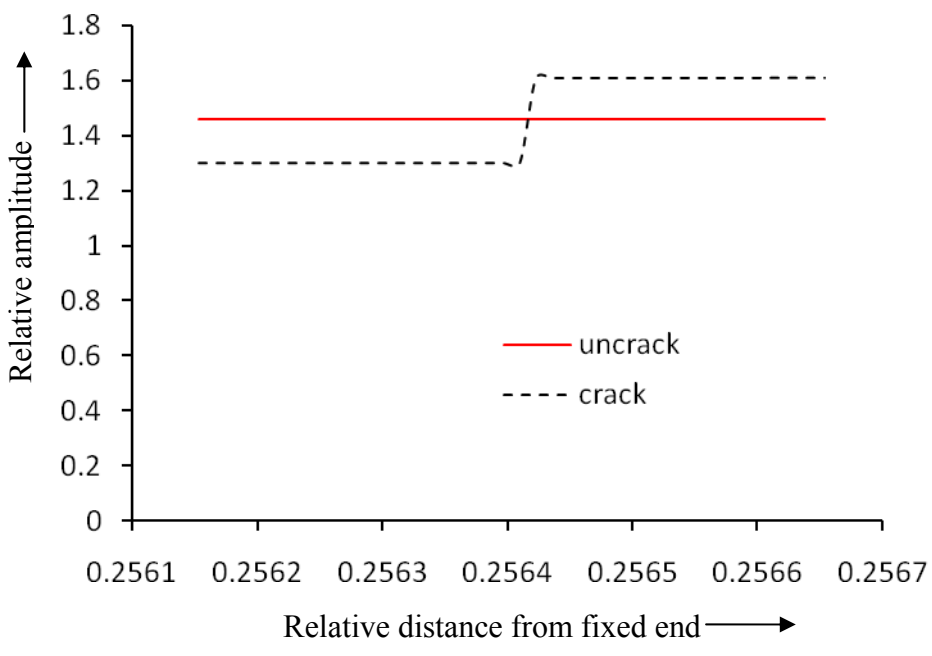


Fig. 3.2.17 (c1) Magnified view of Fig. 3.2.17 (c) at the vicinity of the crack location.

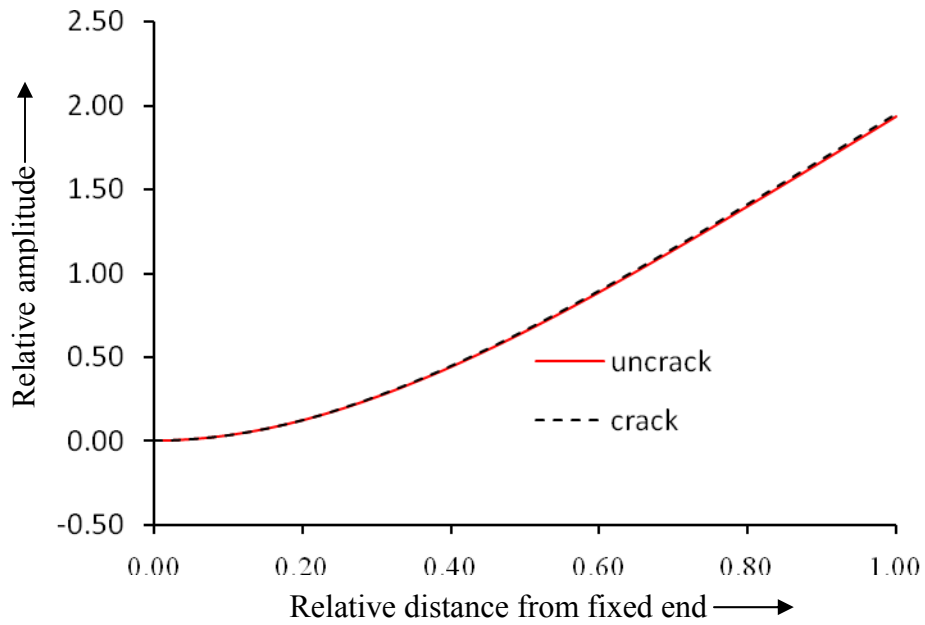


Fig.3.2.18 (a) Relative amplitude vs. relative distance from the fixed end (1st mode of vibration), $a_1/W=0.3$, $L_1/L=0.2564$

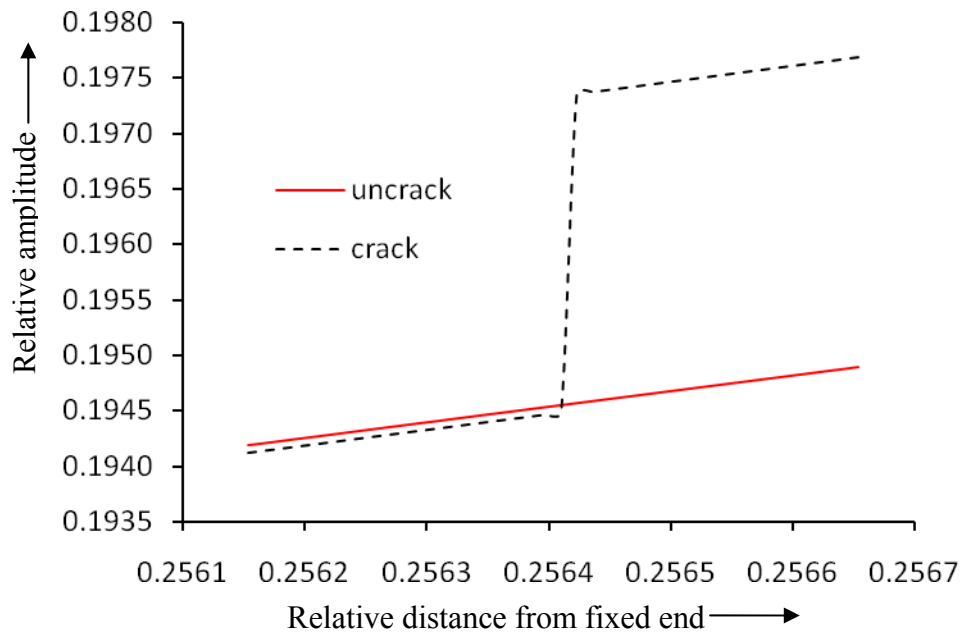


Fig. 3.2.18 (a1) Magnified view of Fig. 3.2.18 (a) at the vicinity of the crack location.

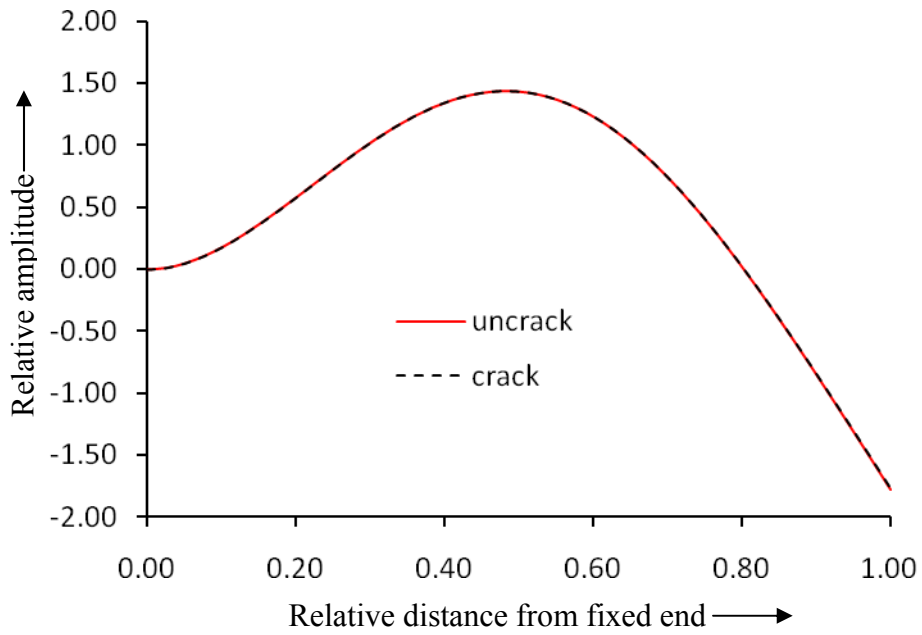


Fig.3.2.18 (b) Relative amplitude vs. relative distance from the fixed end (2nd mode of vibration), $a_1/W=0.3$, $L_1/L=0.2564$

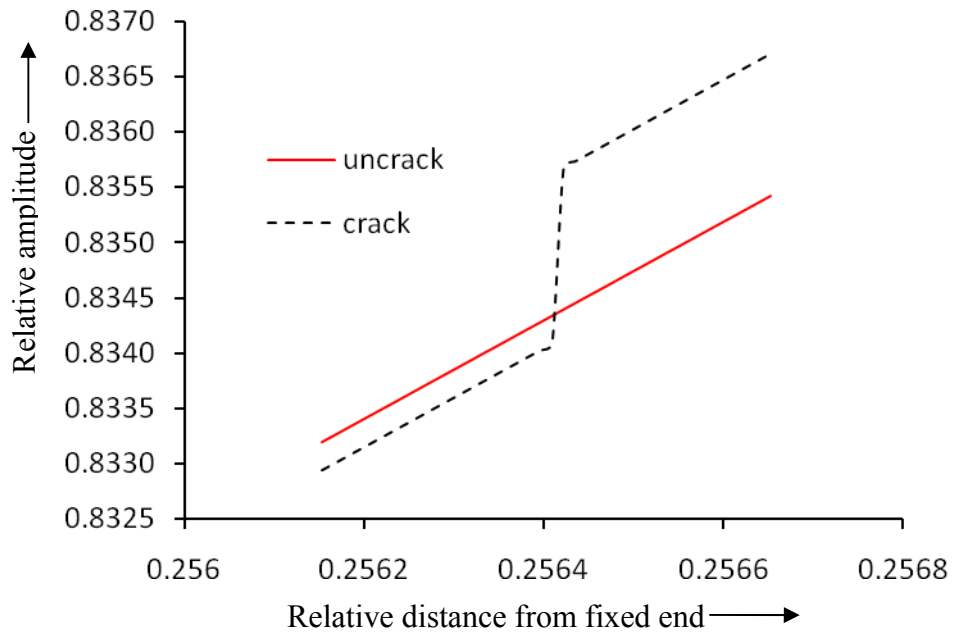


Fig. 3.2.18(b1) Magnified view of Fig. 3.2.18 (b) at the vicinity of the crack location.

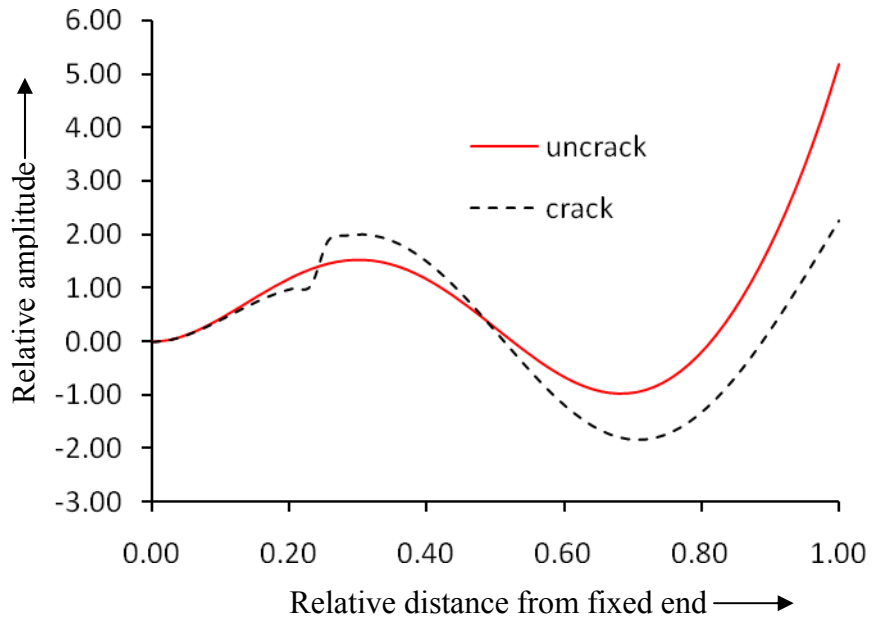


Fig. 3.2.18 (c) Relative amplitude vs. relative distance from the fixed end (3^{rd} mode of vibration), $a_1/W=0.3$, $L_1/L=0.2564$

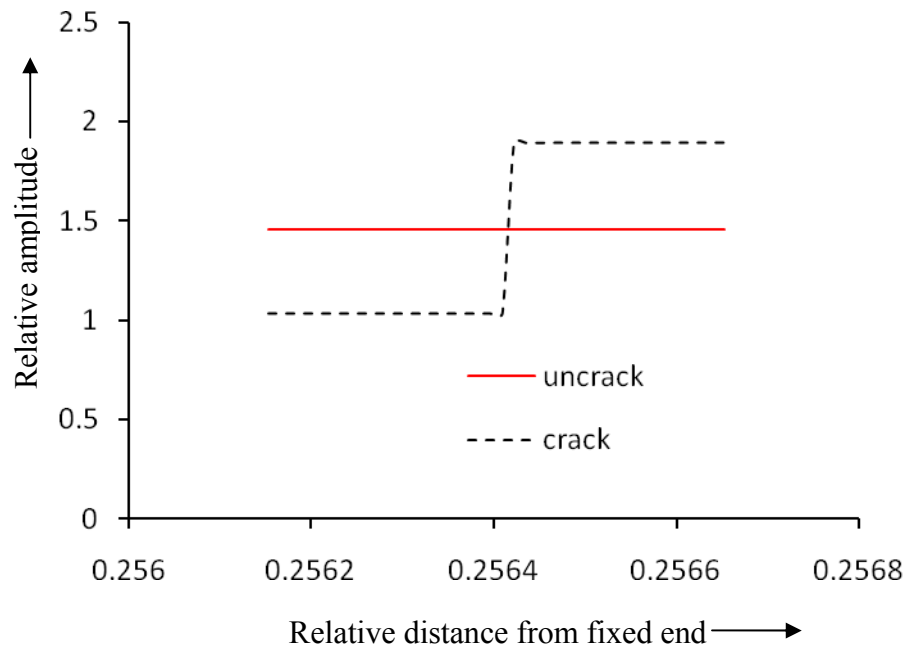


Fig. 3.2.18 (c1) Magnified view of Fig. 3.2.18 (c) at the vicinity of the crack location.

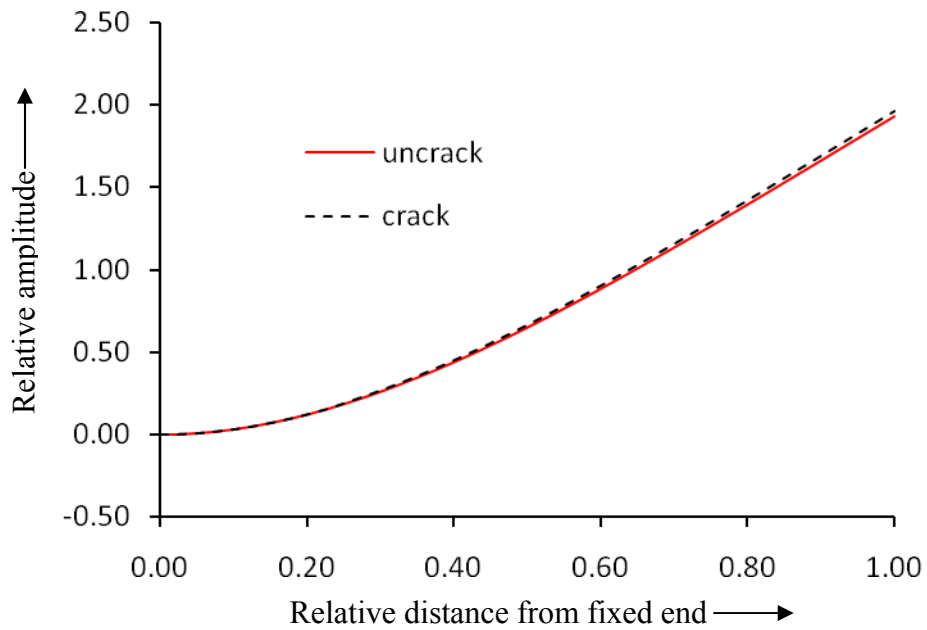


Fig.3.2.19 (a) Relative amplitude vs. relative distance from the fixed end (1st mode of vibration), $a_1/W=0.4$, $L_1/L=0.2564$

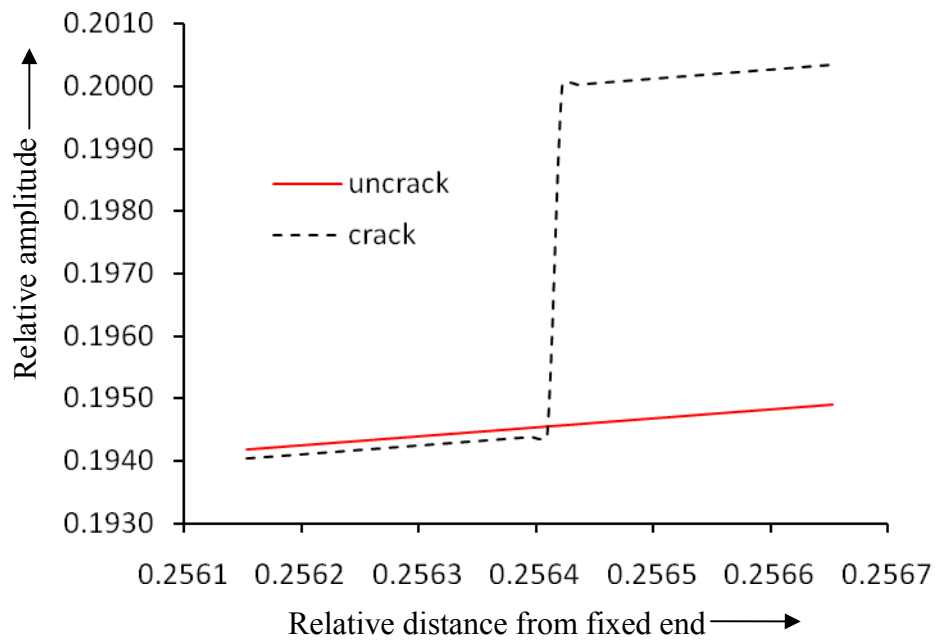


Fig. 3.2.19 (a1) Magnified view of Fig. 3.2.19 (a) at the vicinity of the crack location.

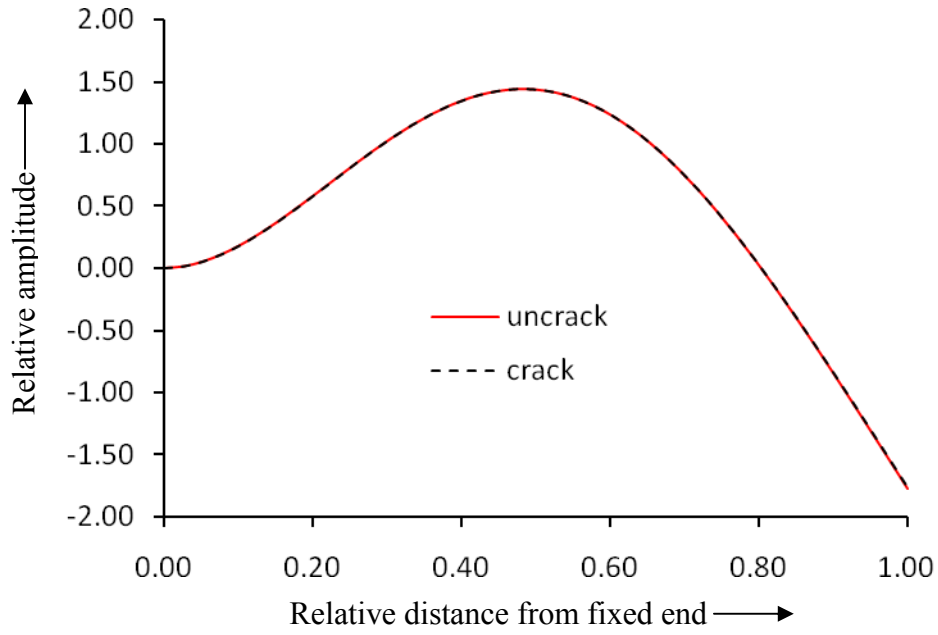


Fig.3.2.19 (b) Relative amplitude vs. relative distance from the fixed end (2nd mode of vibration), $a_1/W=0.4$, $L_1/L=0.2564$

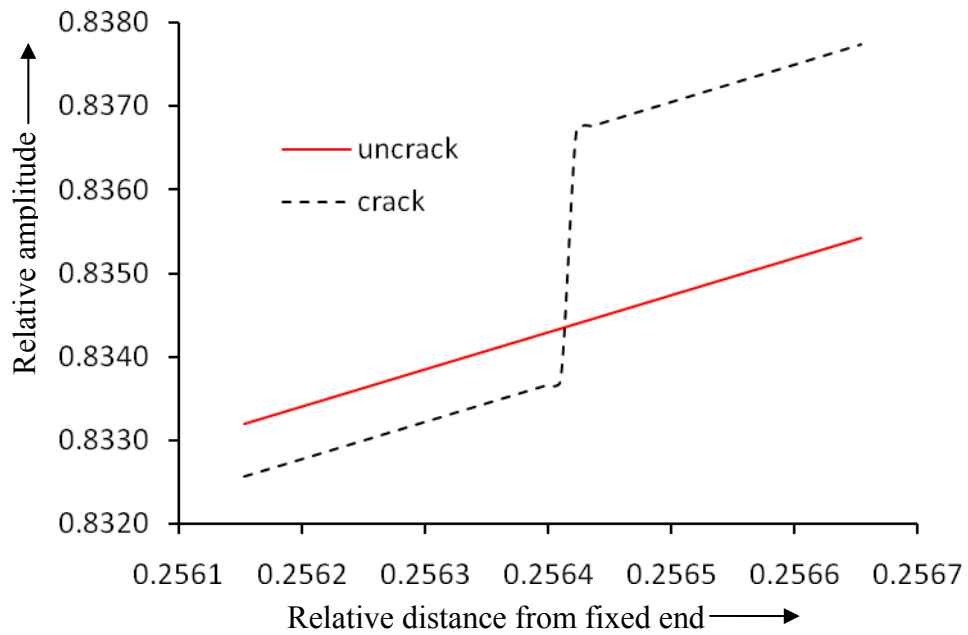


Fig. 3.2.19(b1) Magnified view of Fig. 3.2.19(b) at the vicinity of the crack location.

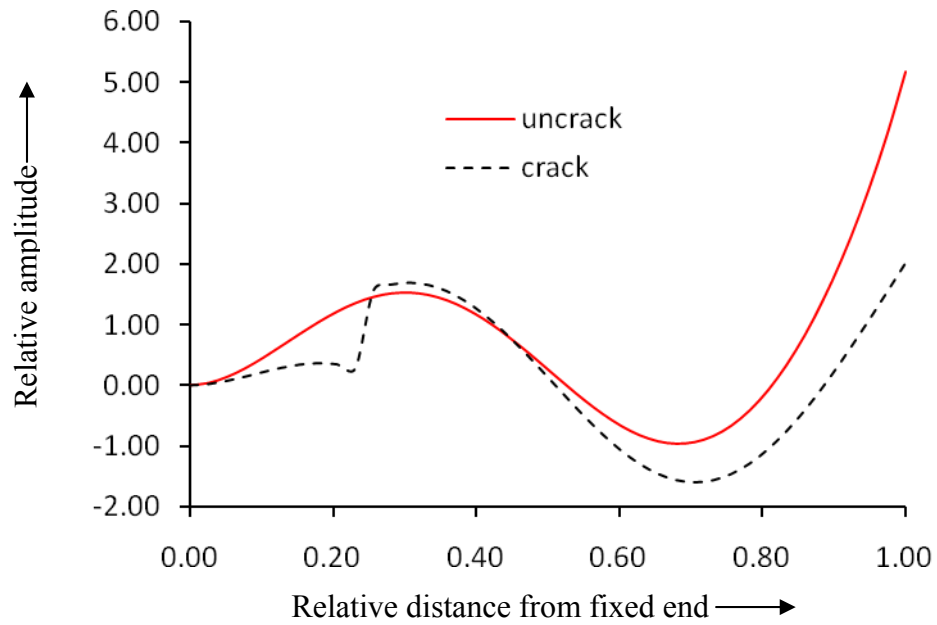


Fig.3.2.19 (c) Relative amplitude vs. relative distance from the fixed end (3rd mode of vibration), $a_1/W=0.4$, $L_1/L=0.2564$

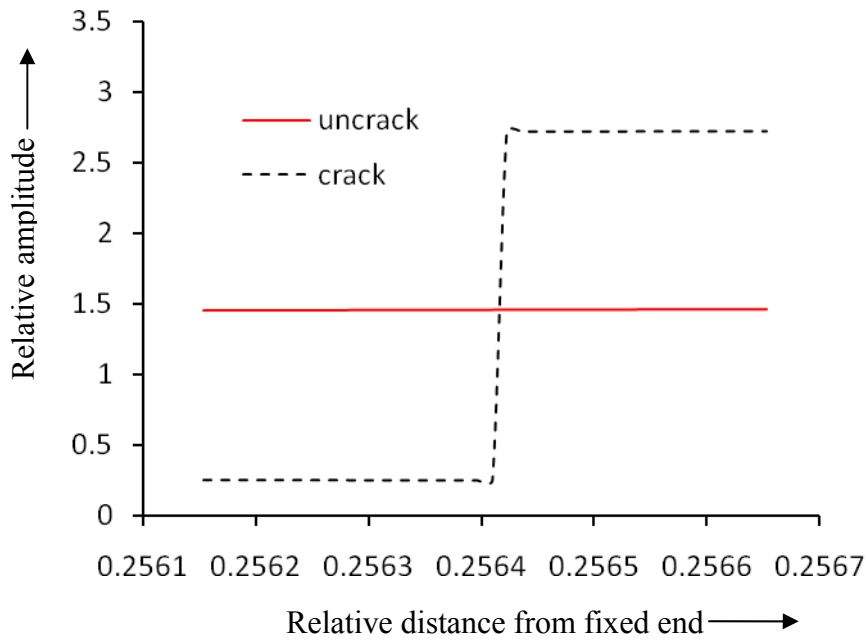


Fig. 3.2.19 (c1) Magnified view of Fig. 3.2.19 (c) at the vicinity of the crack location.

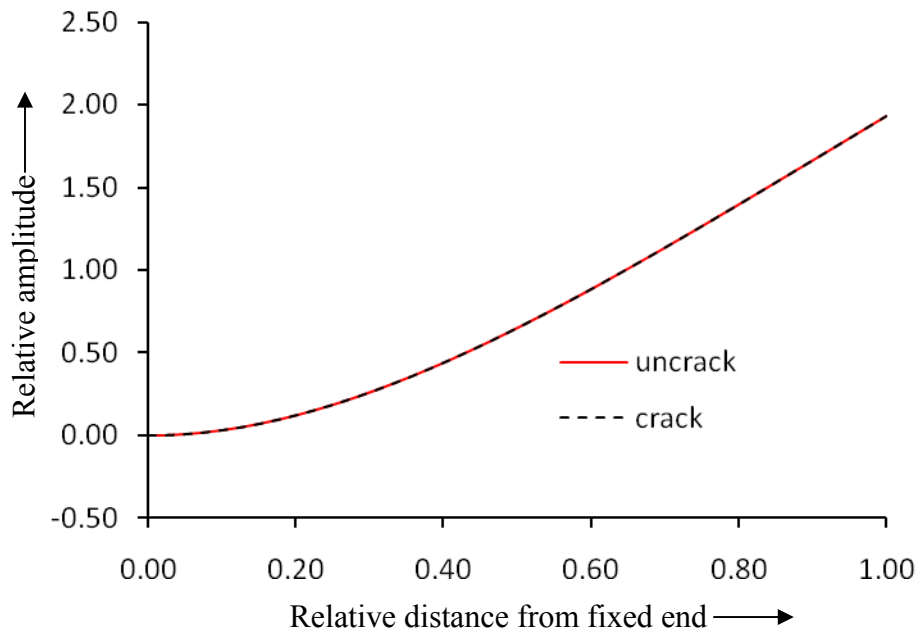


Fig.3.2.20 (a) Relative amplitude vs. relative distance from the fixed end (1st mode of vibration), $a_1/W=0.1$, $L_1/L=0.3846$

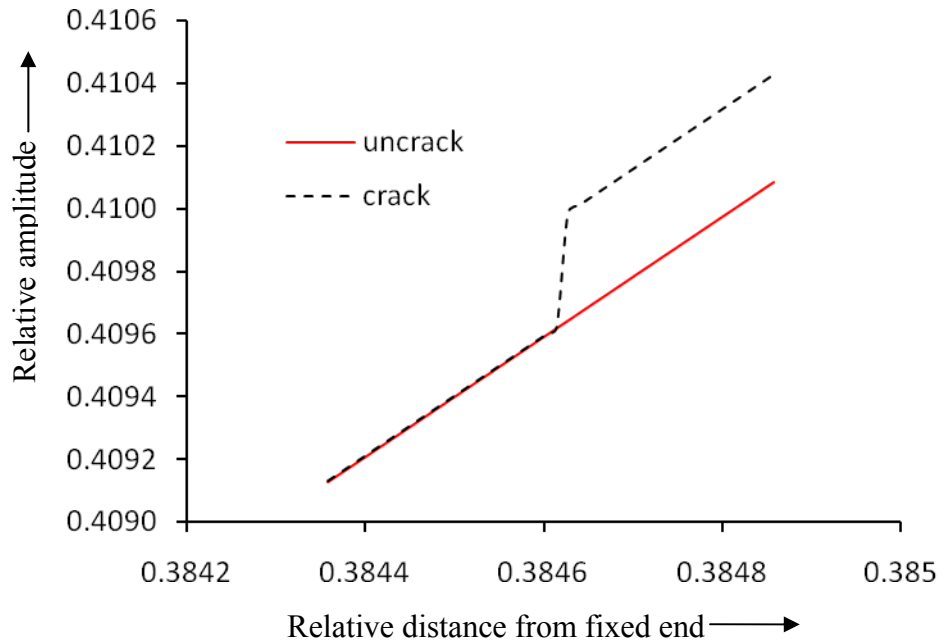


Fig. .3.2.20 (a1) Magnified view of Fig. 3.2.20 (a) at the vicinity of the crack location.

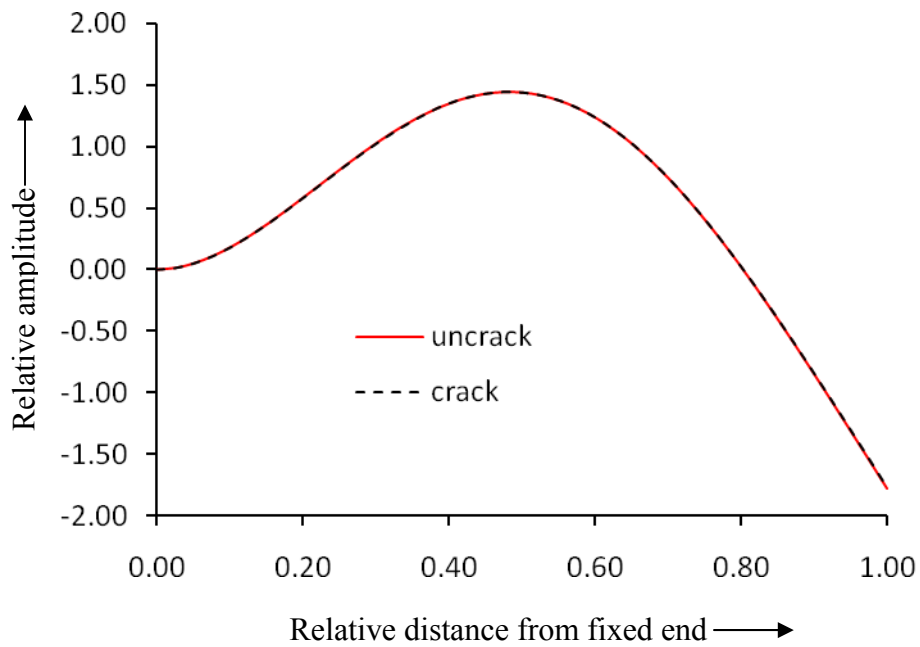


Fig.3.2.20 (b) Relative amplitude vs. relative distance from the fixed end (2nd mode of vibration), $a_1/W=0.1$, $L_1/L=0.3846$

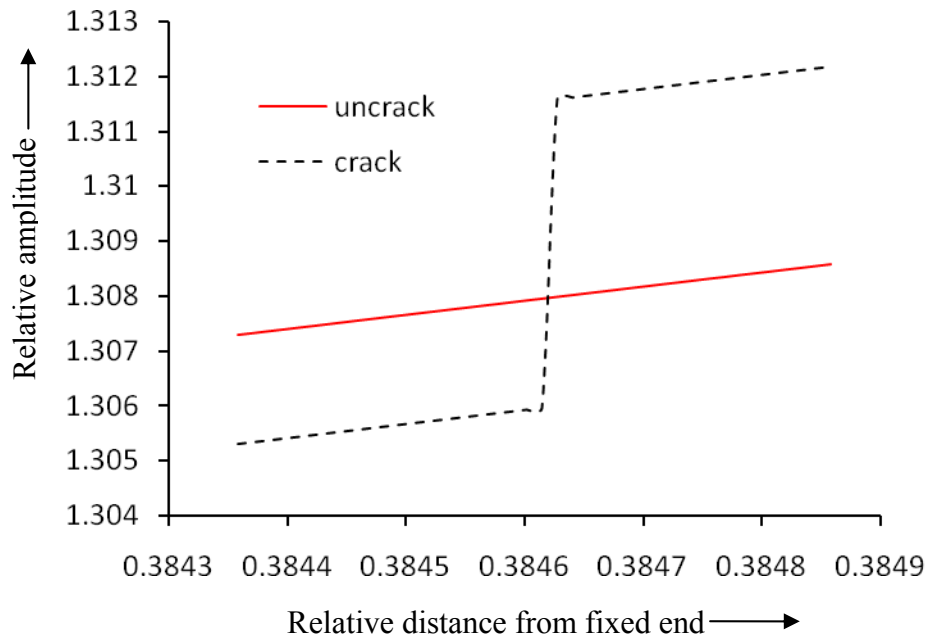


Fig. 3.2.20(b1) Magnified view of Fig. 3.2.20 (b) at the vicinity of the crack location.

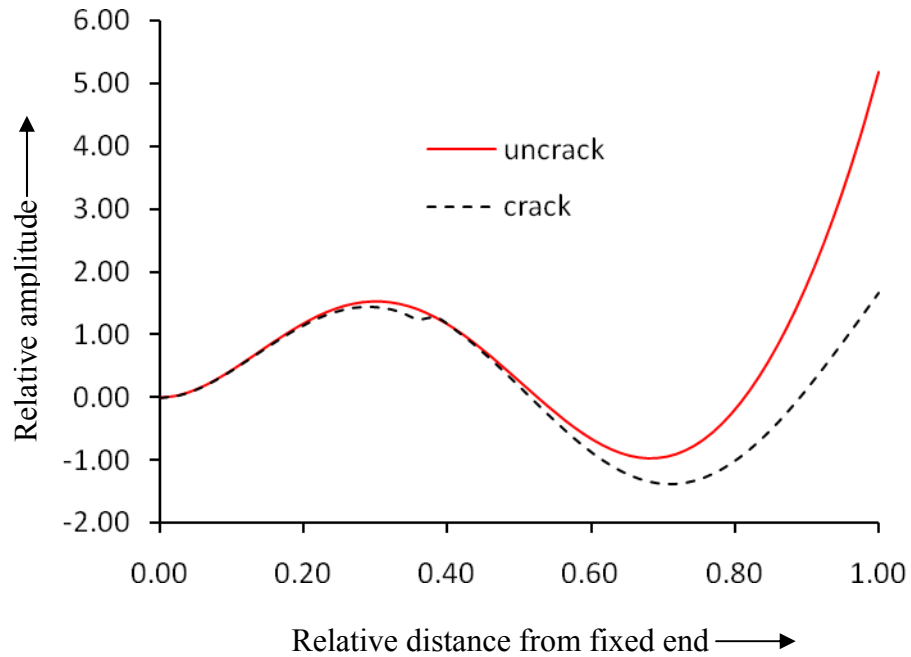


Fig.3.2.20 (c) Relative amplitude vs. relative distance from the fixed end (3rd mode of vibration), $a_1/W=0.1$, $L_1/L=0.3846$

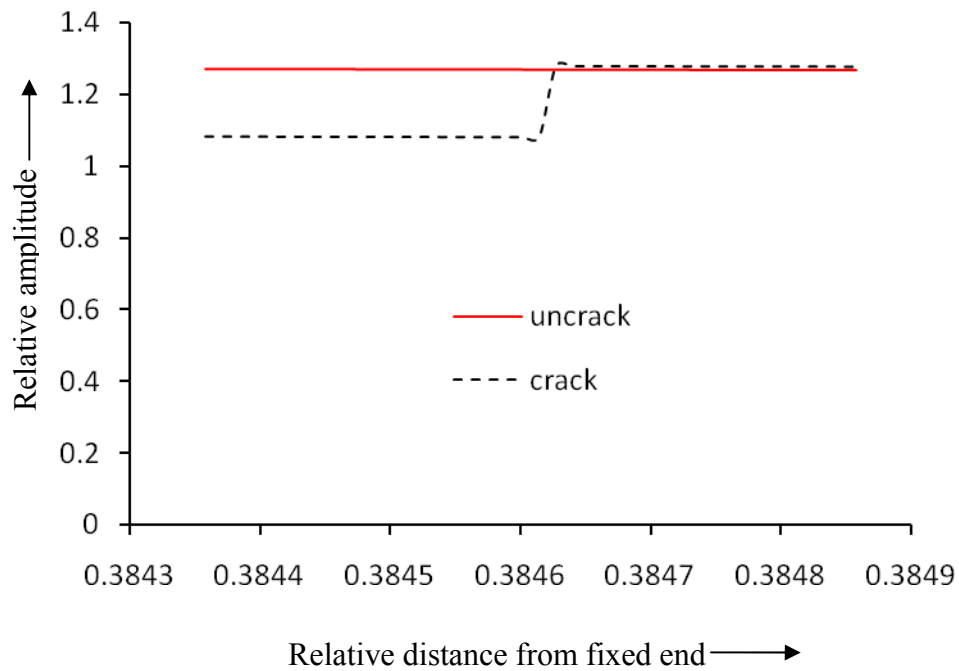


Fig. 3.2.20 (c1) Magnified view of Fig. 3.2.20 (c) at the vicinity of the crack location.

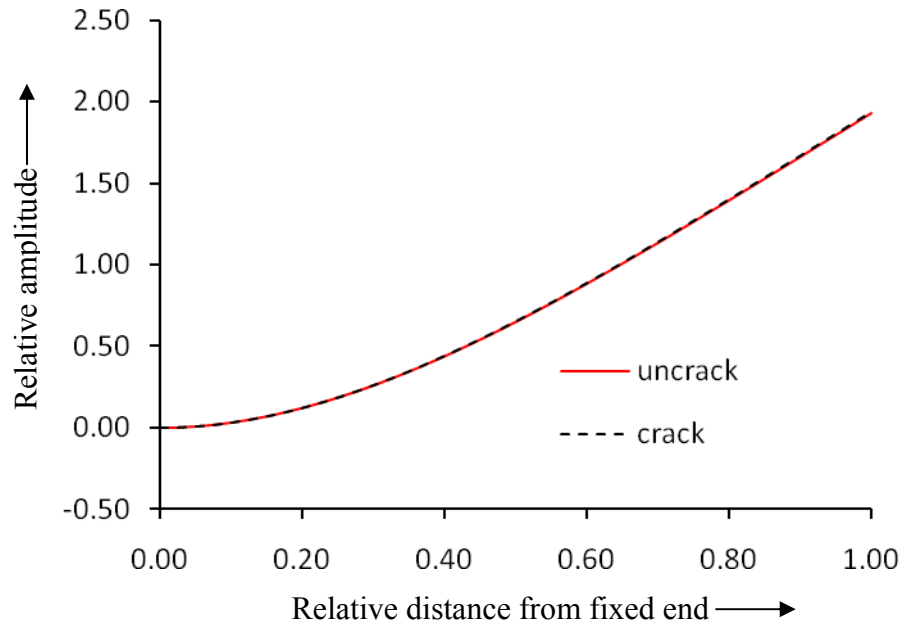


Fig.3.2.21 (a) Relative amplitude vs. relative distance from the fixed end (1st mode of vibration), $a_1/W=0.2$, $L_1/L=0.3846$

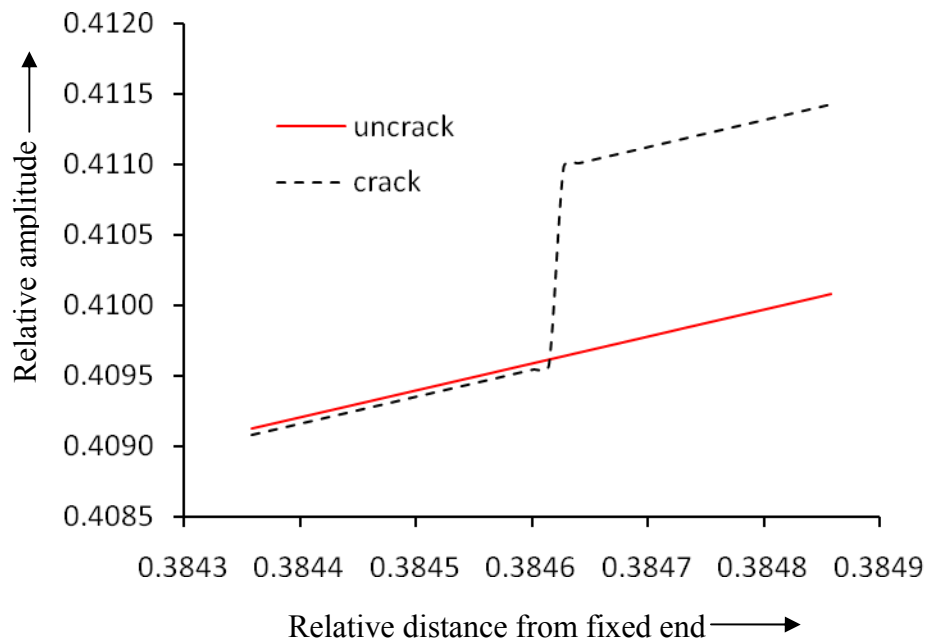


Fig. 3.2.21 (a1) Magnified view of Fig. 3.2.21 (a) at the vicinity of the crack location.

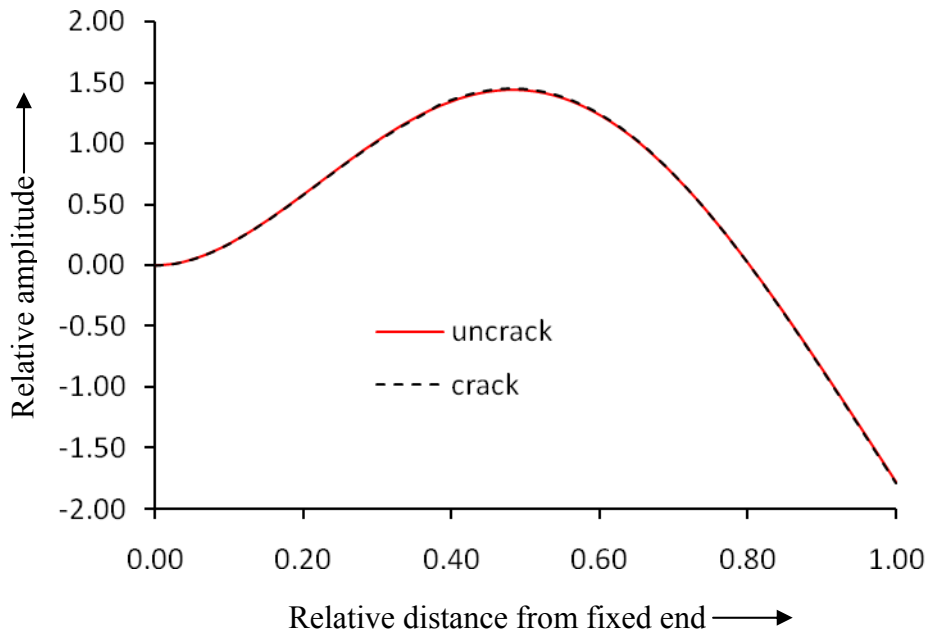


Fig.3.2.21 (b) Relative amplitude vs. relative distance from the fixed end (2nd mode of vibration), $a_1/W=0.2$, $L_1/L=0.3846$

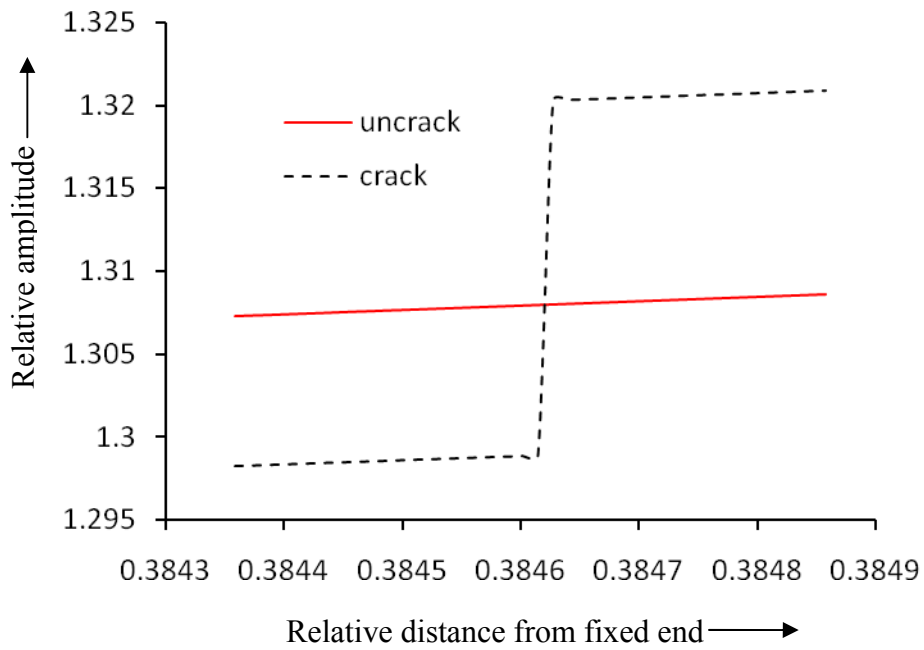


Fig. 3.2.21 (b1) Magnified view of Fig. 3.2.21 (b) at the vicinity of the crack location.

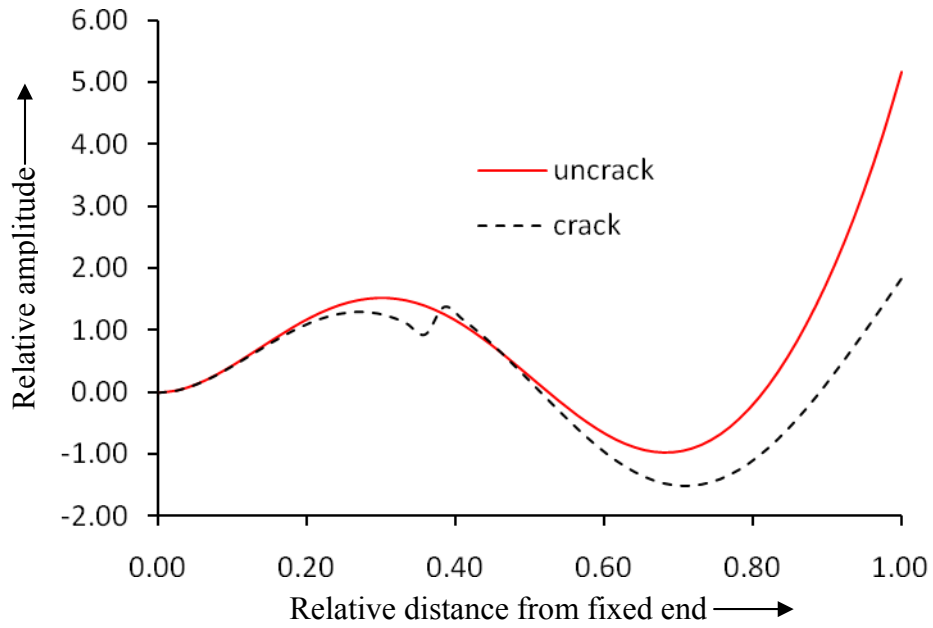


Fig.3.2.21(c) Relative amplitude vs. relative distance from the fixed end (3rd mode of vibration), $a_1/W=0.2$, $L_1/L=0.3846$

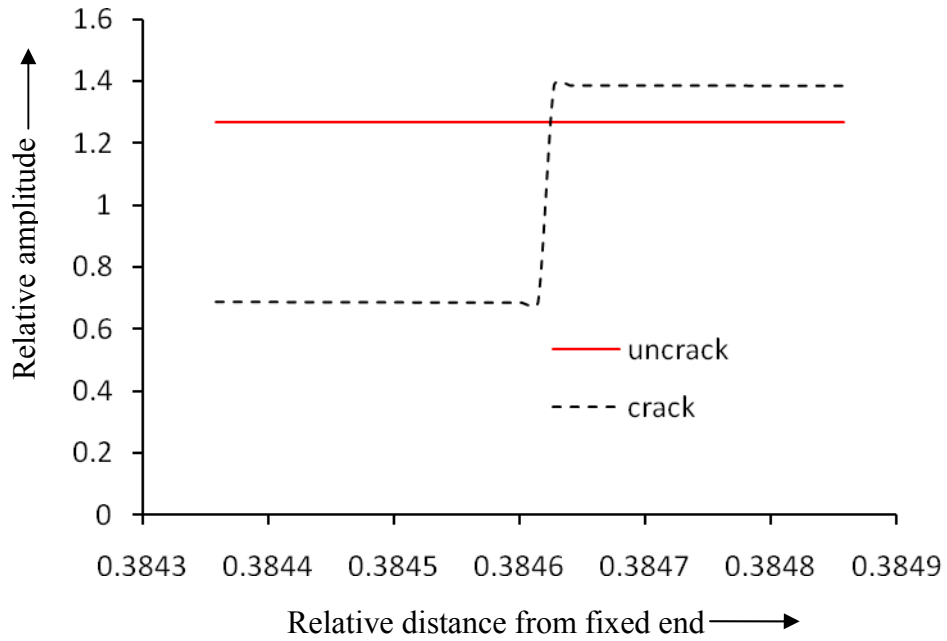


Fig. 3.2.21(c1) Magnified view of Fig. 3.2.21(c) at the vicinity of the crack location.

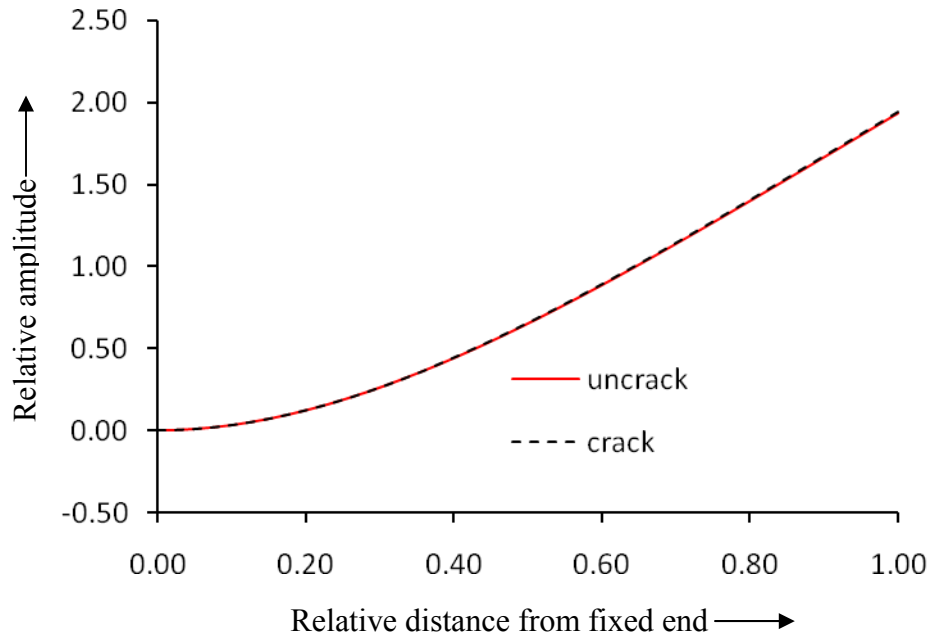


Fig.3.2.22 (a) Relative amplitude vs. relative distance from the fixed end (1st mode of vibration), $a_1/W=0.3$, $L_1/L=0.3846$

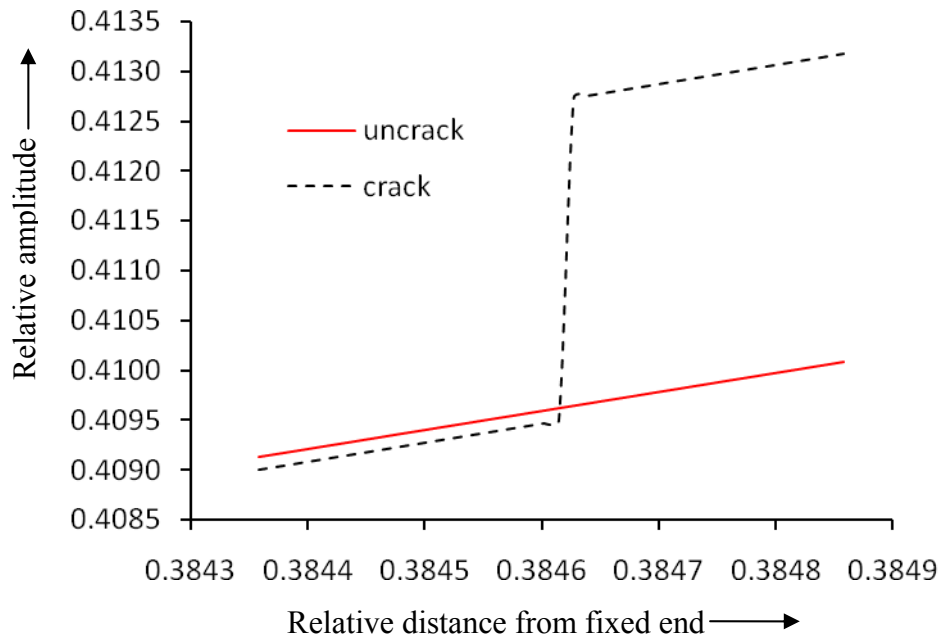


Fig. 3.2.22 (a1) Magnified view of Fig. 3.2.22 (a) at the vicinity of the crack location.

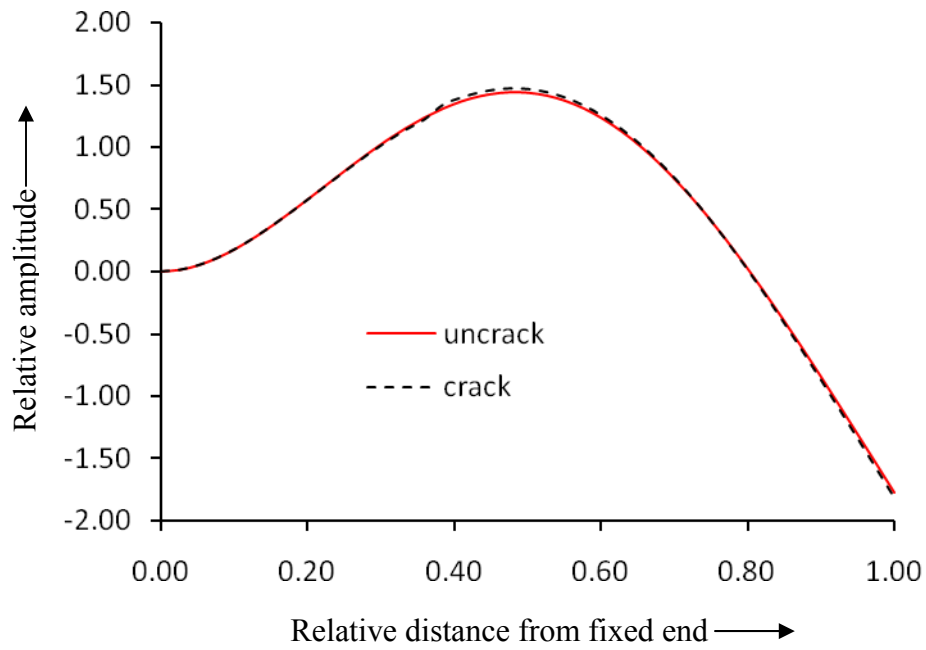


Fig.3.2.22 (b) Relative amplitude vs. relative distance from the fixed end (2nd mode of vibration), $a_1/W=0.3$, $L_1/L=0.3846$

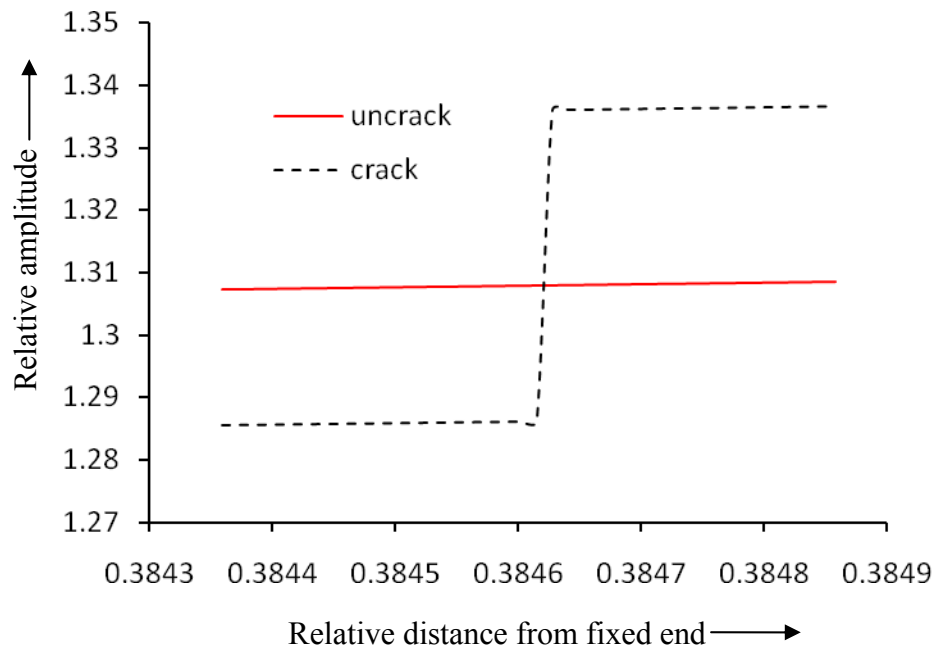


Fig. 3.2.22 (b1) Magnified view of Fig. 3.2.22 (b) at the vicinity of the crack location.

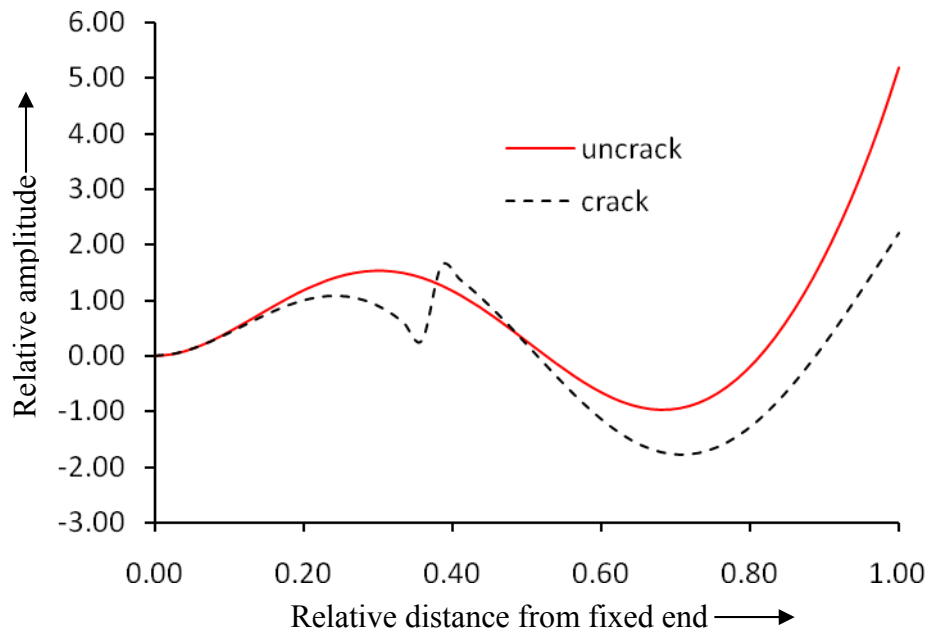


Fig.3.2.22 (c) Relative amplitude vs. relative distance from the fixed end (3rd mode of vibration), $a_1/W=0.3$, $L_1/L=0.3846$

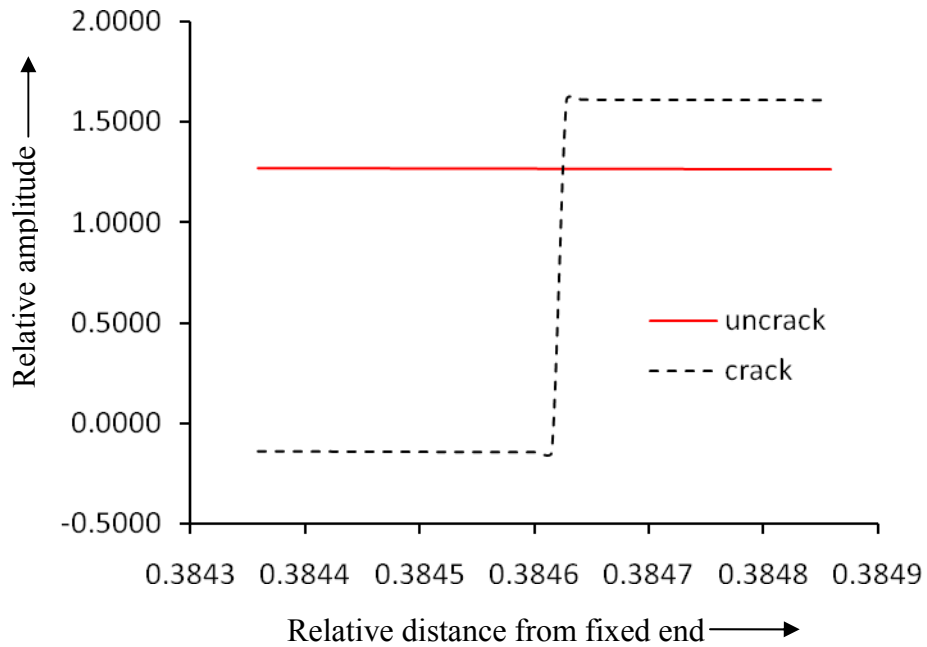


Fig. 3.2.22 (c1) Magnified view of Fig. 3.2.22 (c) at the vicinity of the crack location.

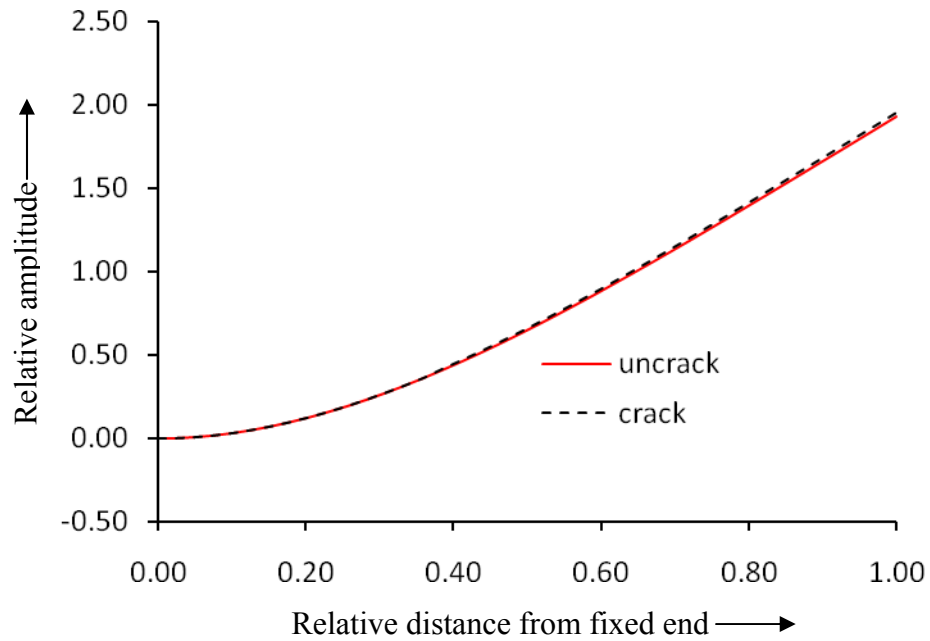


Fig.3.2.23 (a) Relative amplitude vs. relative distance from the fixed end (1st mode of vibration), $a_1/W=0.4$, $L_1/L=0.3846$

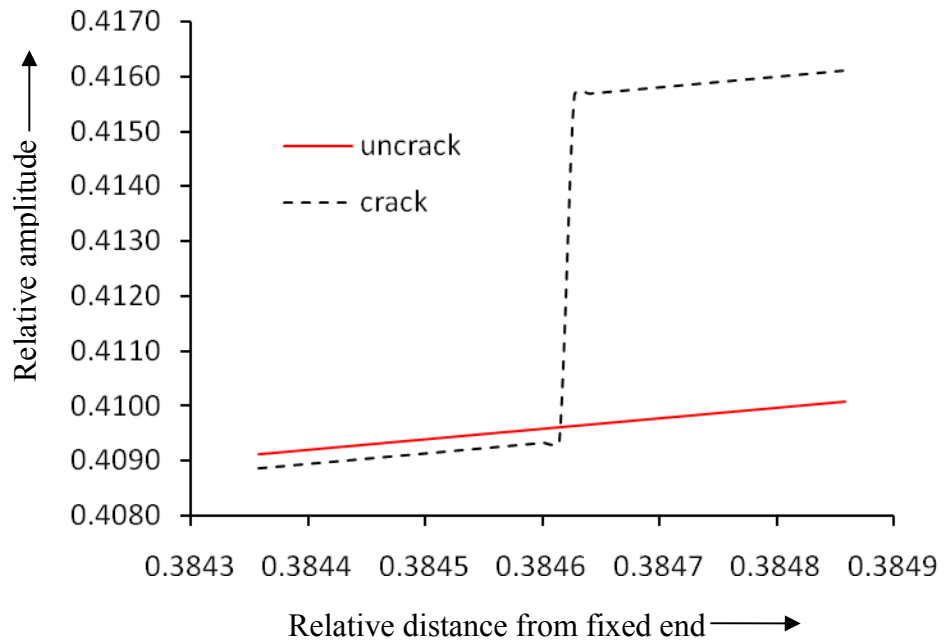


Fig. 3.2.23 (a1) Magnified view of Fig. 3.2.23 (a) at the vicinity of the crack location.

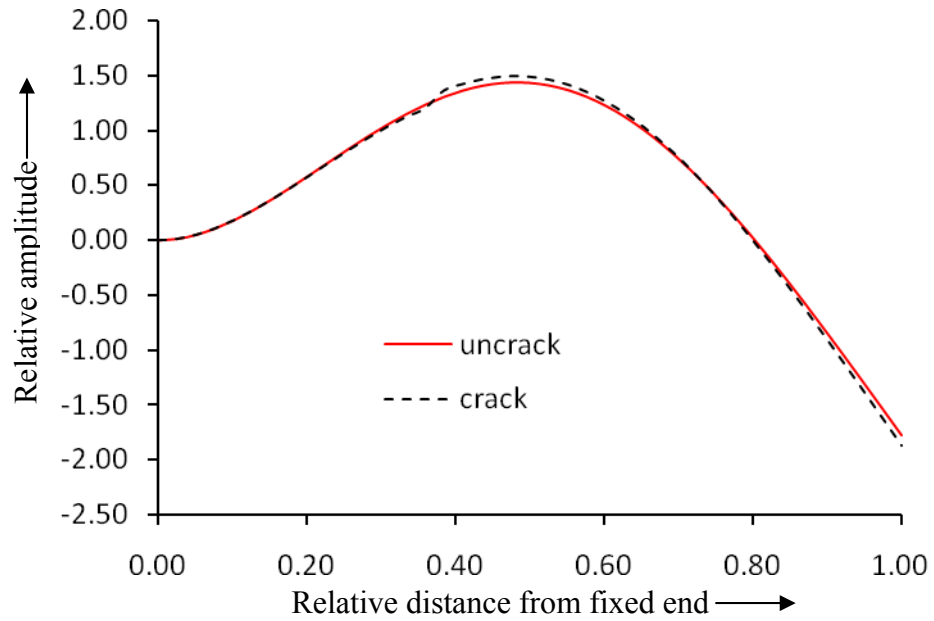


Fig.3.2.23 (b) Relative amplitude vs. relative distance from the fixed end (2nd mode of vibration), $a_1/W=0.4$, $L_1/L=0.3846$

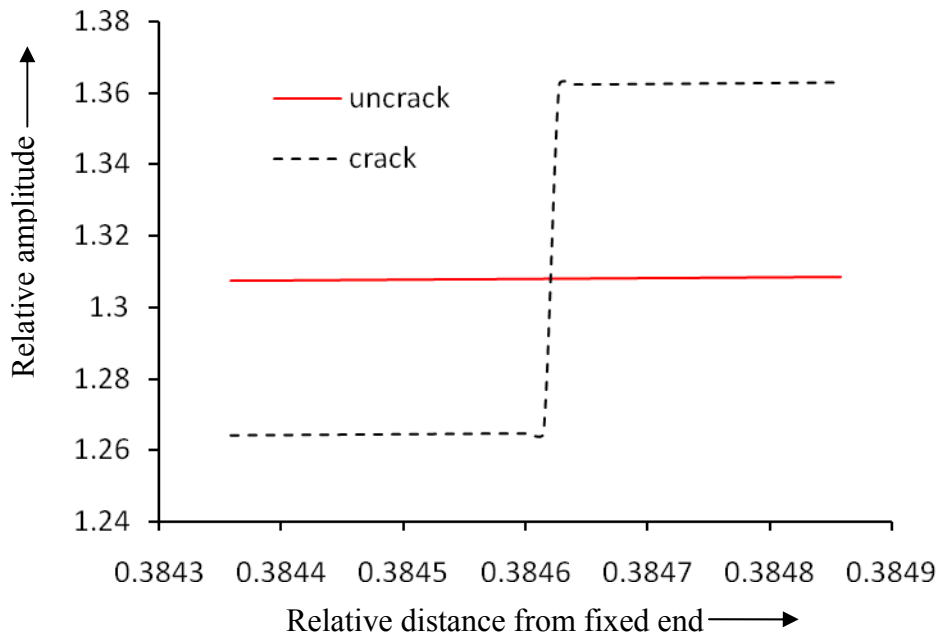


Fig. 3.2.23(b1) Magnified view of Fig. 3.2.23(b) at the vicinity of the crack location.

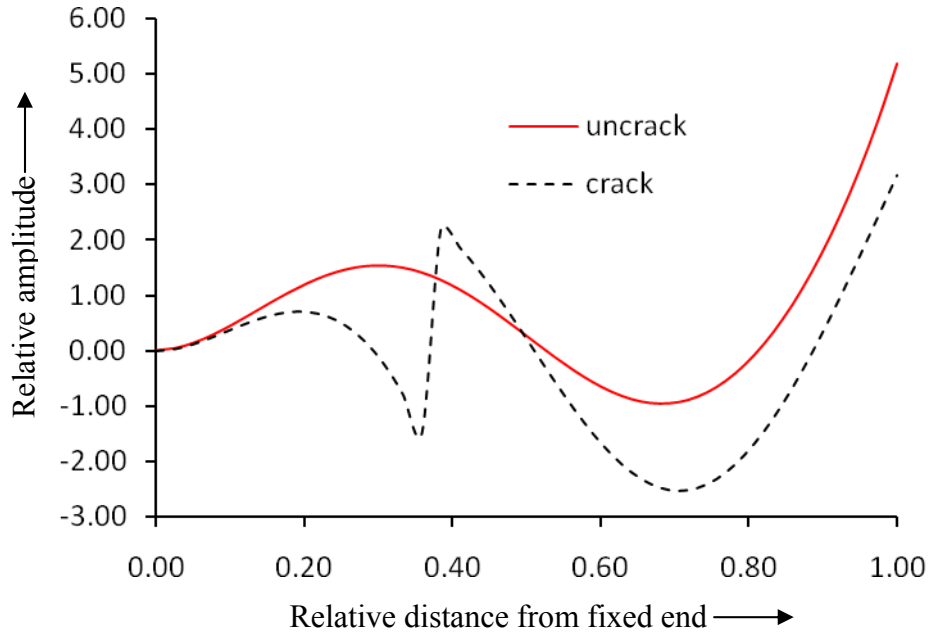


Fig.3.2.23 (c) Relative amplitude vs. relative distance from the fixed end (3rd mode of vibration), $a_1/W=0.4$, $L_1/L=0.3846$

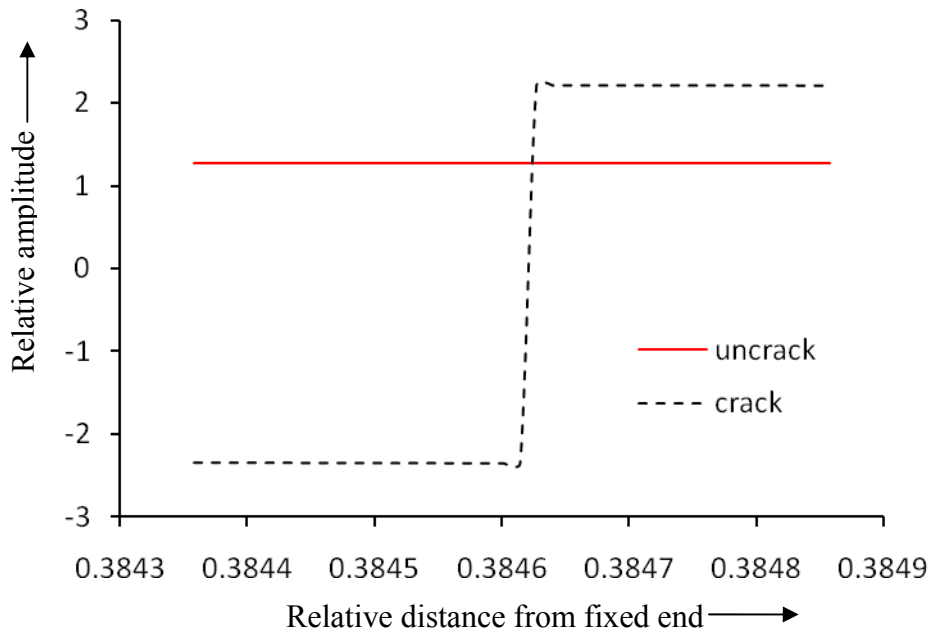


Fig. 3.2.23 (c1) Magnified view of Fig. 3.2.23 (c) at the vicinity of the crack location.

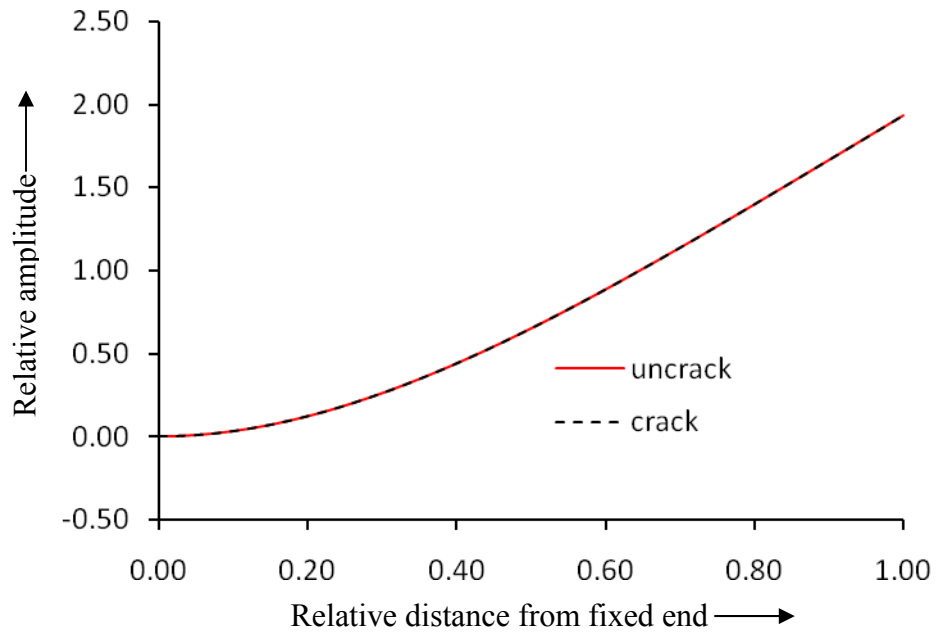


Fig.3.2.24 (a) Relative amplitude vs. relative distance from the fixed end (1st mode of vibration), $a_1/W=0.1$, $L_1/L=0.5128$

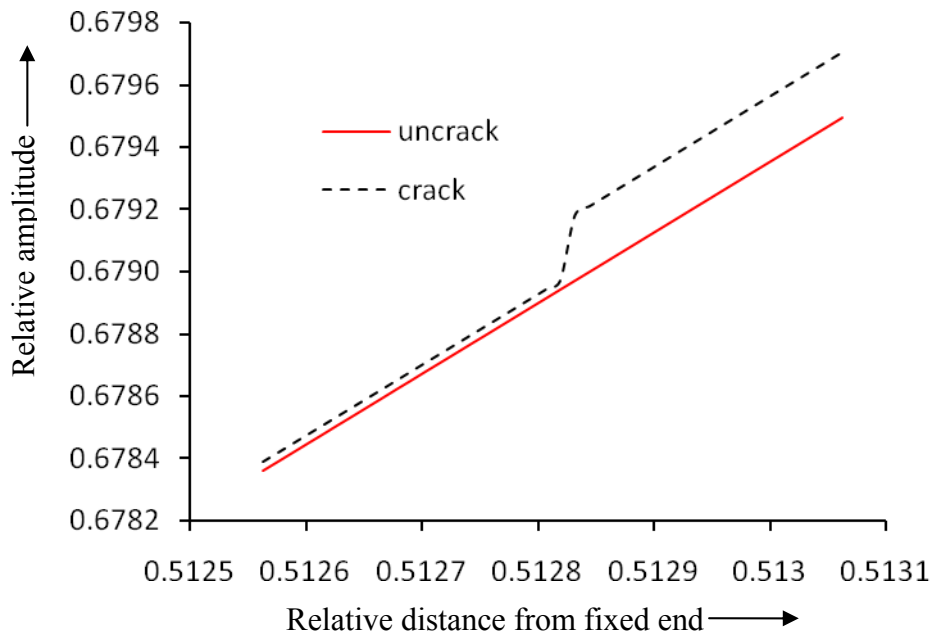


Fig. 3.2.24 (a1) Magnified view of Fig. 3.2.24 (a) at the vicinity of the crack location.

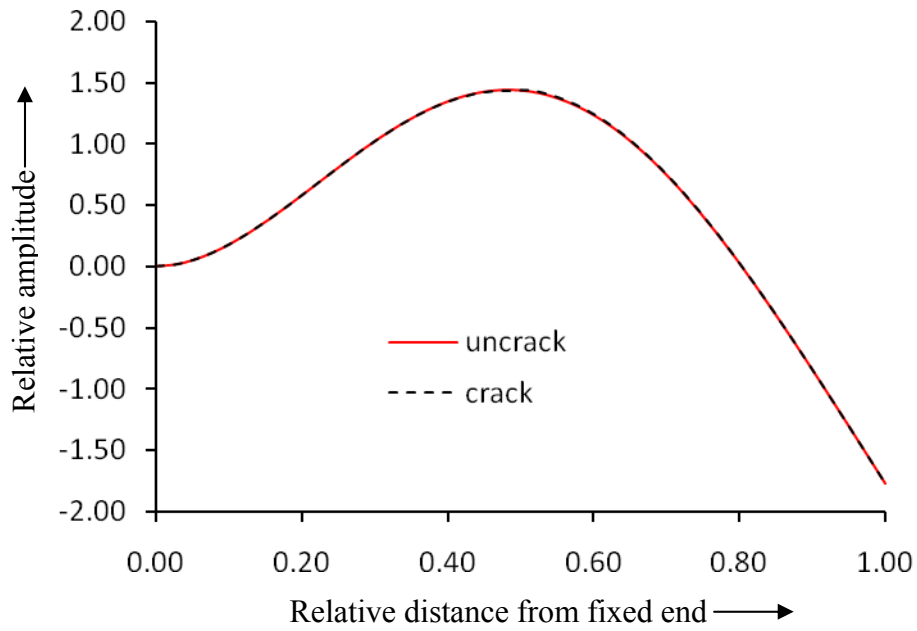


Fig.3.2.24 (b) Relative amplitude vs. relative distance from the fixed end (2nd mode of vibration), $a_1/W=0.1$, $L_1/L=0.5128$

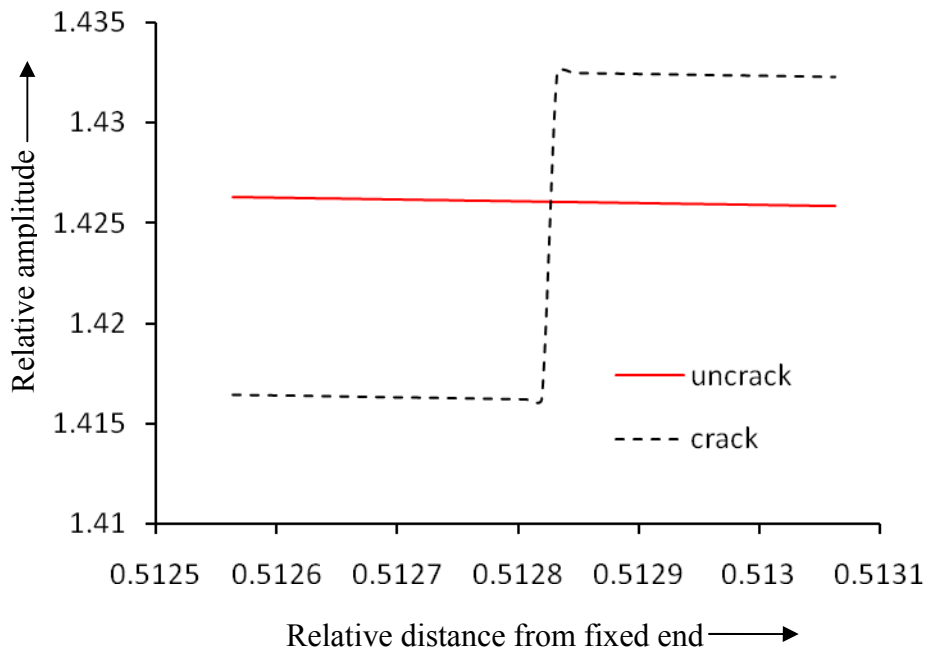


Fig. 3.2.24(b1) Magnified view of Fig. 3.2.24 (b) at the vicinity of the crack location.

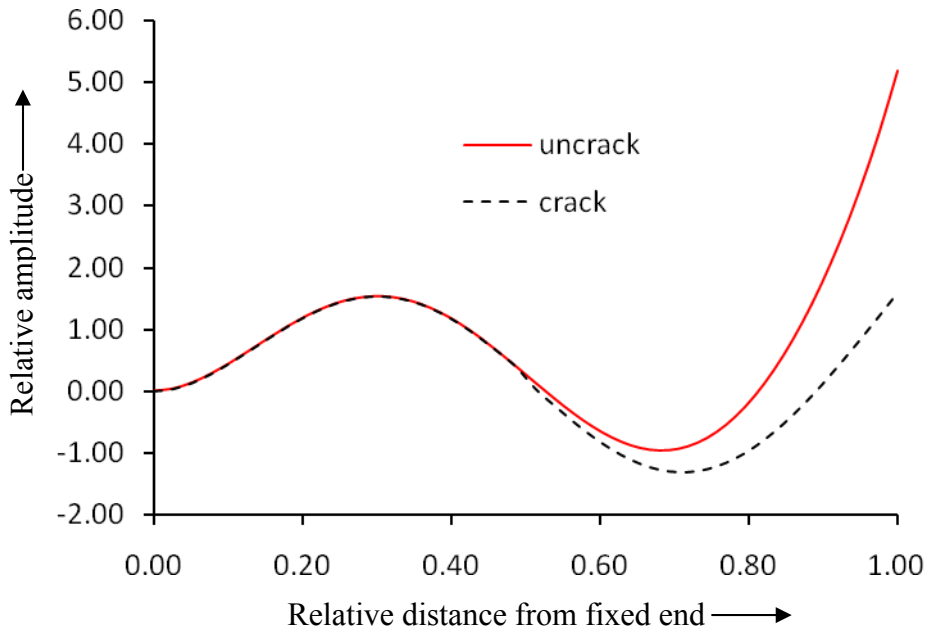


Fig.3.2.24 (c) Relative amplitude vs. relative distance from the fixed end (3rd mode of vibration), $a_1/W=0.1$, $L_1/L=0.5128$

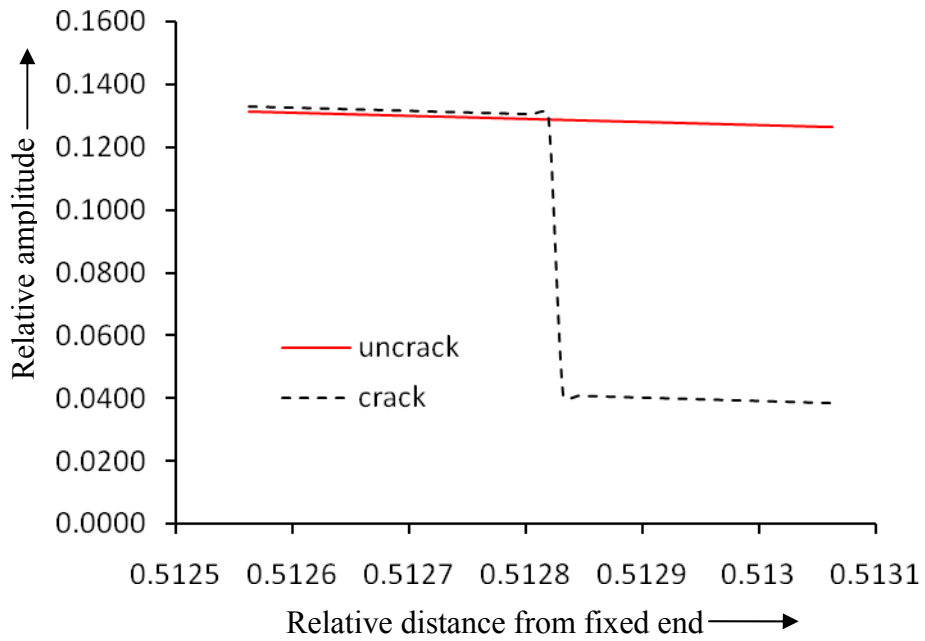


Fig. 3.2.24 (c1) Magnified view of Fig. 3.2.24 (c) at the vicinity of the crack location.

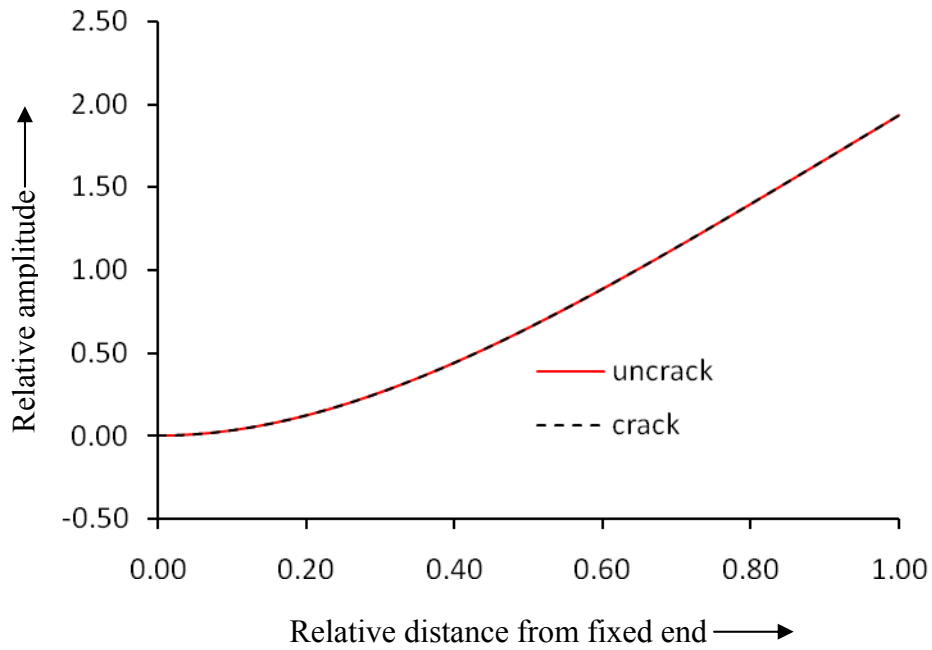


Fig. 3.2.25(a) Relative amplitude vs. relative distance from the fixed end (1st mode of vibration), $a_1/W=0.2$, $L_1/L=0.5128$

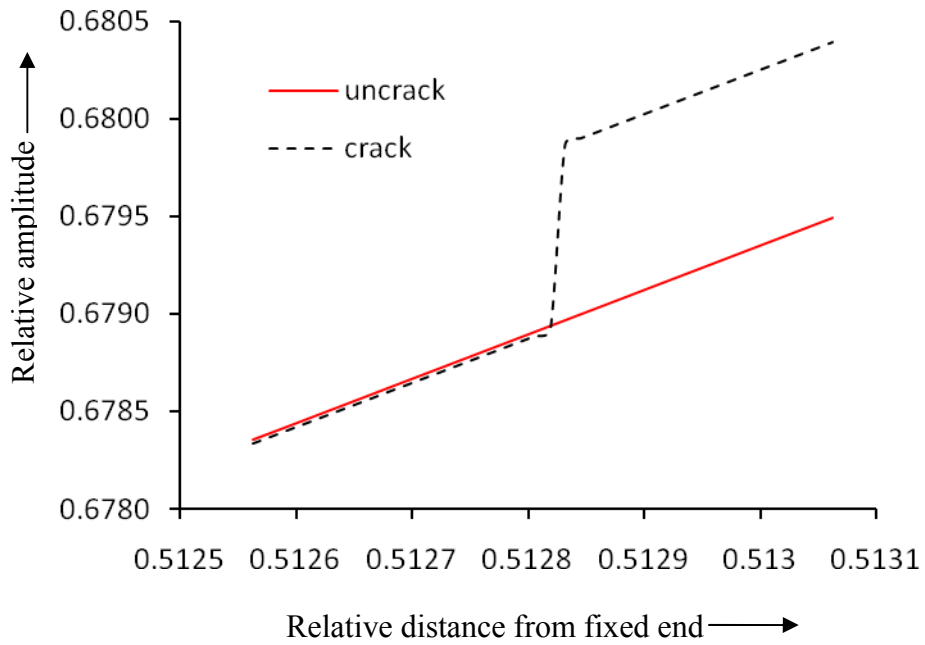


Fig. 3.2.25(a1) Magnified view of Fig. 3.2.25(a) at the vicinity of the crack location.

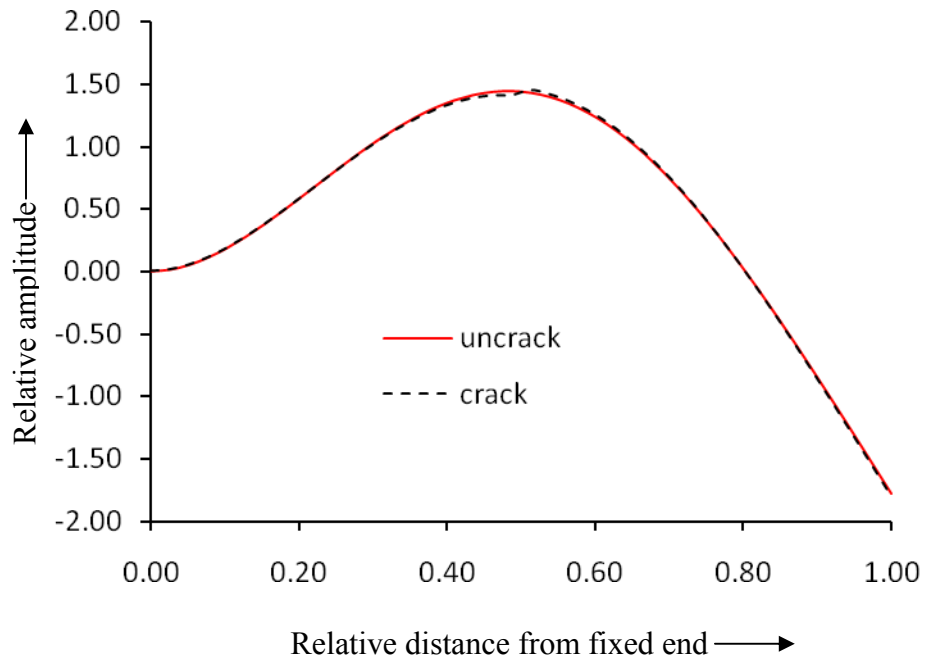


Fig. 3.2.25(b) Relative amplitude vs. relative distance from the fixed end (2nd mode of vibration), $a_1/W=0.2$, $L_1/L=0.5128$

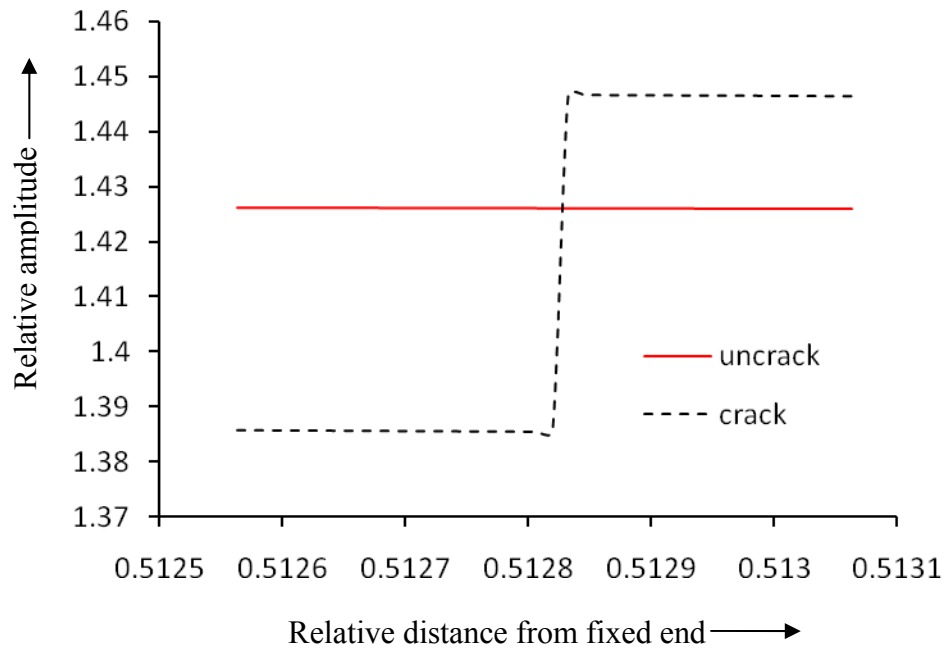


Fig. 3.2.25(b1) Magnified view of Fig.3.2.25 (b) at the vicinity of the crack location.

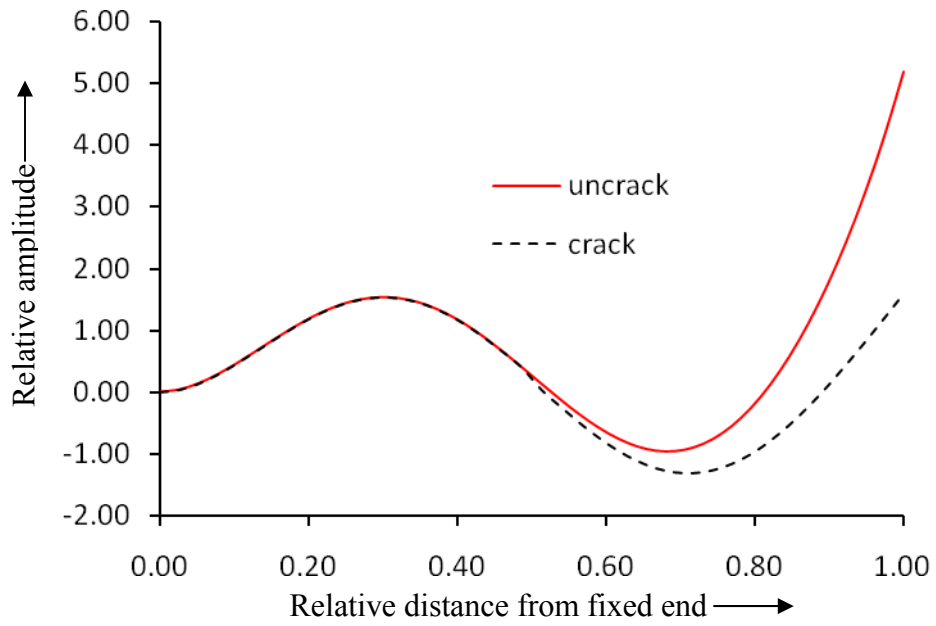


Fig. 3.2.25(c) Relative amplitude vs. relative distance from the fixed end (3rd mode of vibration), $a_1/W=0.2$, $L_1/L=0.5128$

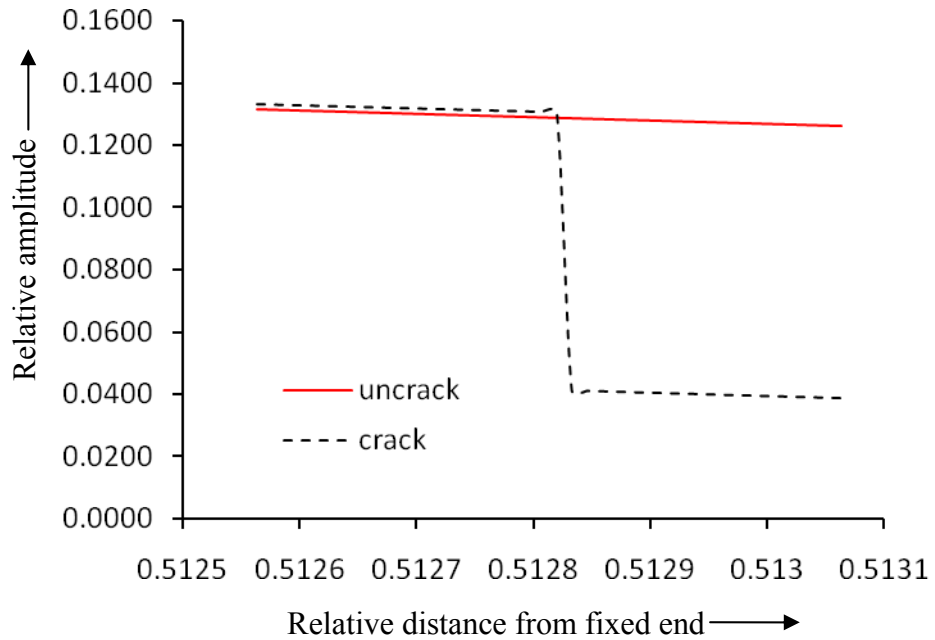


Fig. 3.2.25(c1) Magnified view of Fig. 3.2.25(c) at the vicinity of the crack location.

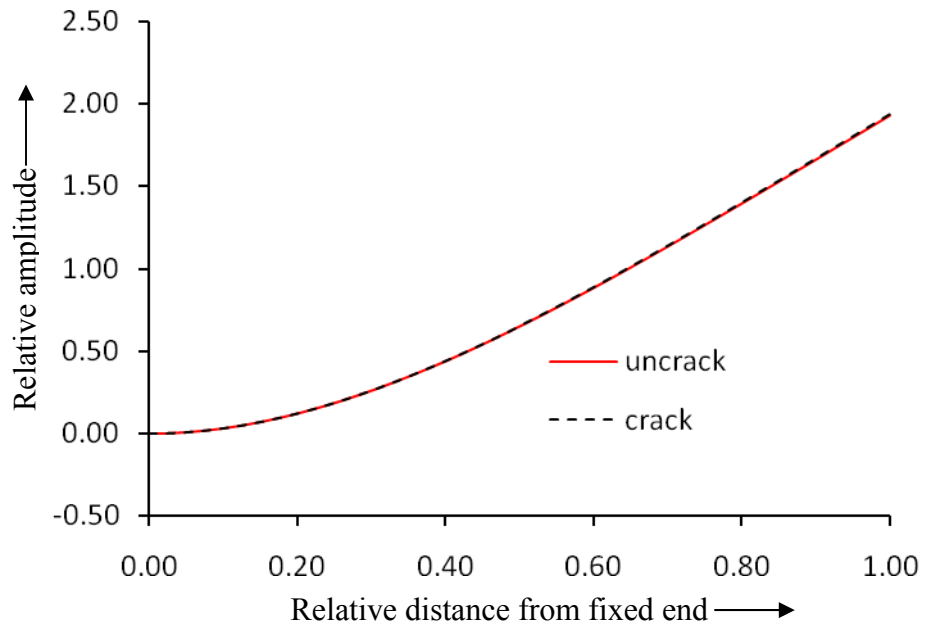


Fig.3.2.26(a) Relative amplitude vs. relative distance from the fixed end (1st mode of vibration), $a_1/W=0.3$, $L_1/L=0.5128$

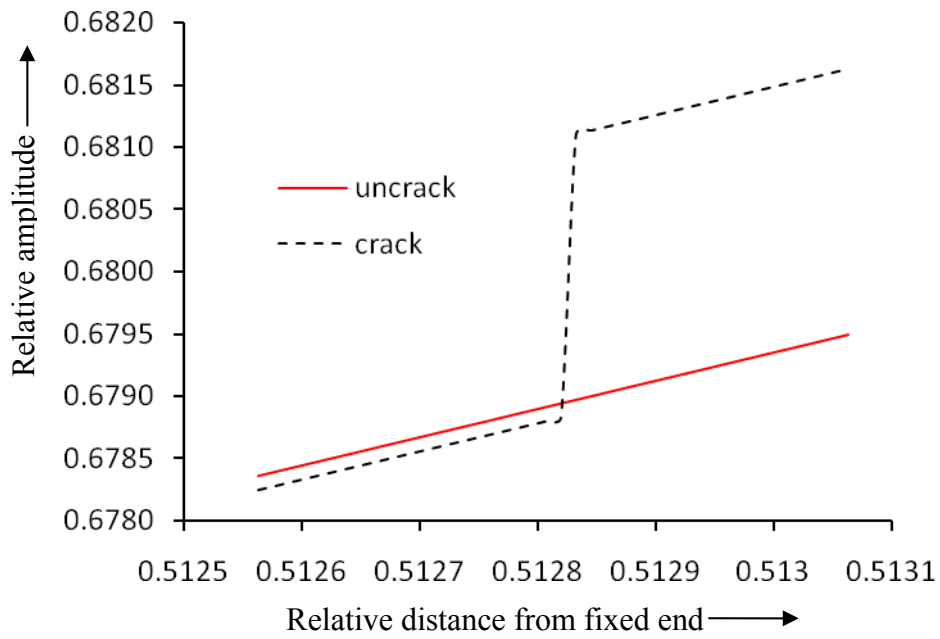


Fig. 3.2.26(a1) Magnified view of Fig. 3.2.26(a) at the vicinity of the crack location.

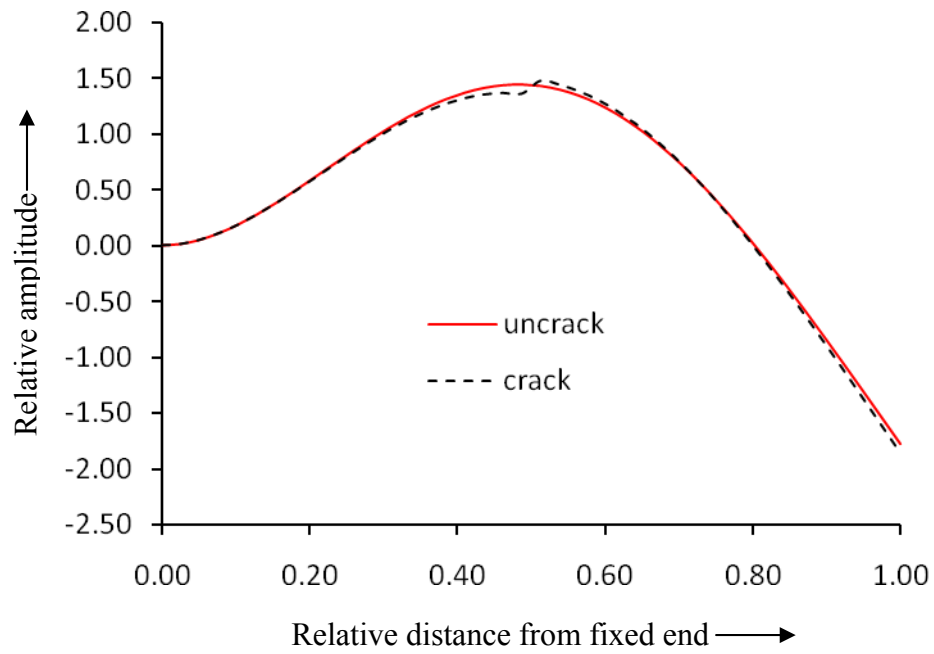


Fig.3.2.26 (b) Relative amplitude vs. relative distance from the fixed end 2nd mode of vibration), $a_1/W=0.3$, $L_1/L=0.5128$

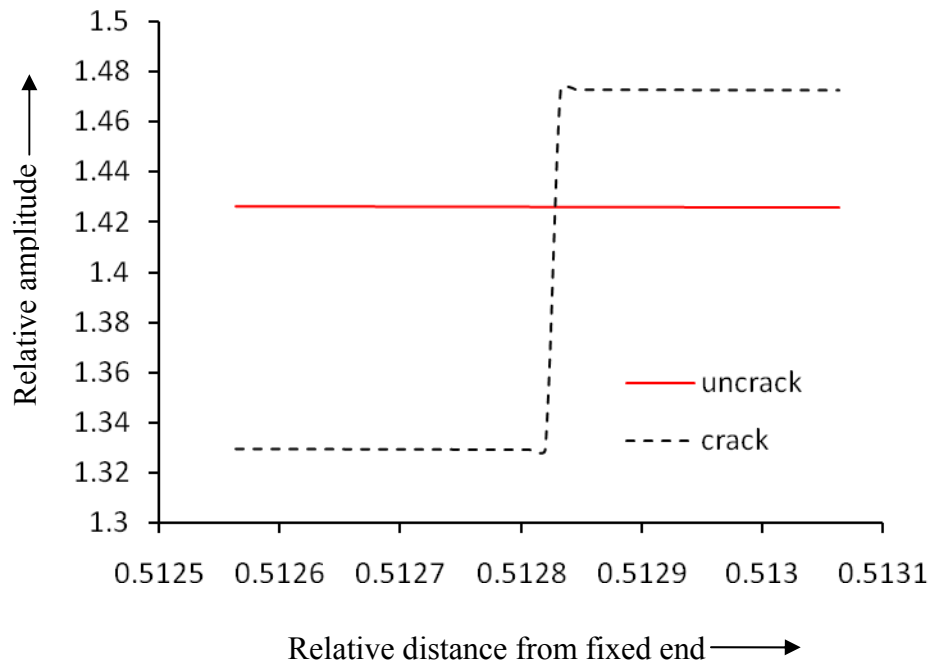


Fig. 3.2.26(b1) Magnified view of Fig. 3.2.26(b) at the vicinity of the crack location.

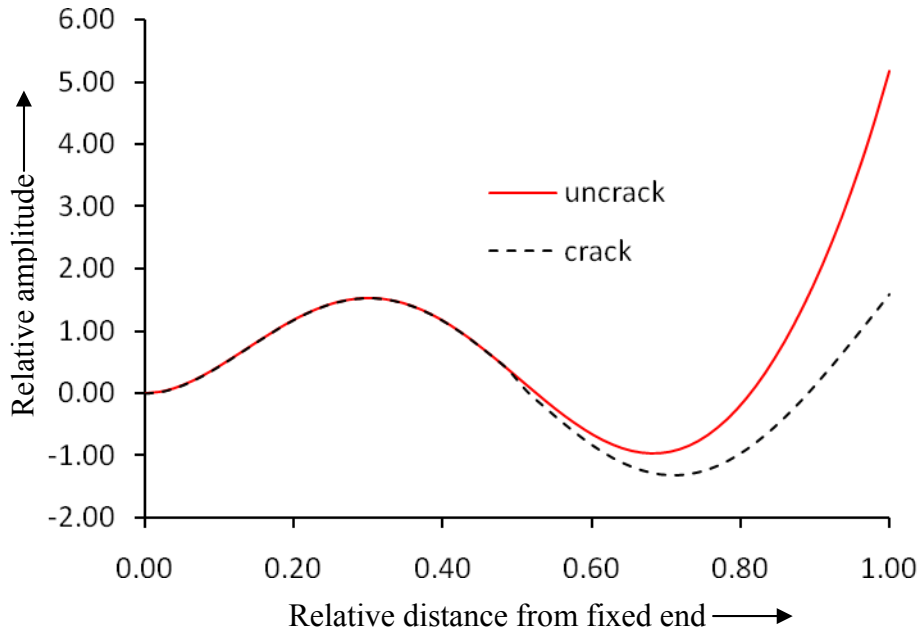


Fig. 3.2.26(c) Relative amplitude vs. relative distance from the fixed end (3rd mode of vibration), $a_1/W=0.3$, $L_1/L=0.5128$

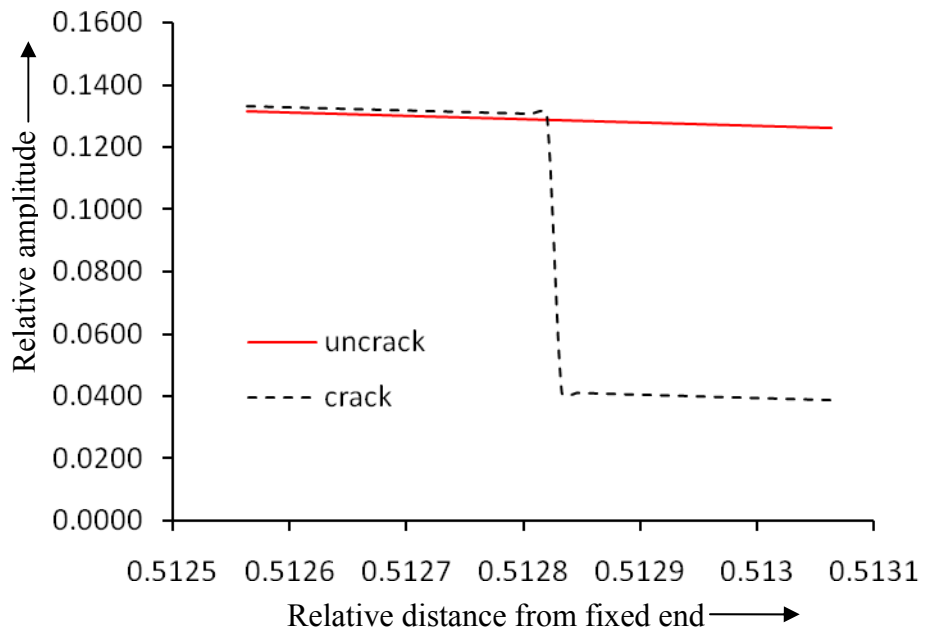


Fig. 3.2.26(c1) Magnified view of Fig. 3.2.26(c) at the vicinity of the crack location.

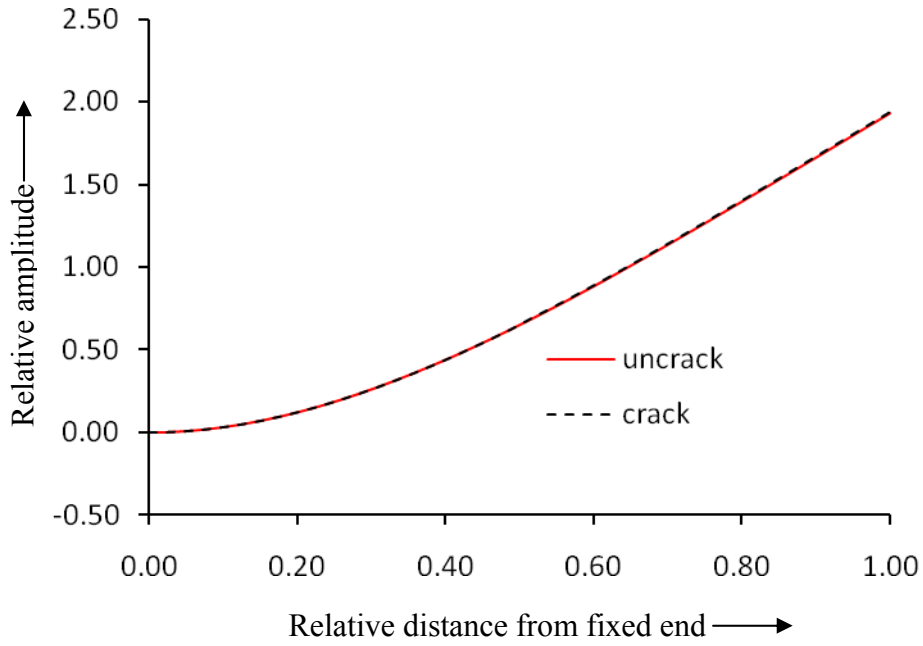


Fig. 3.2.27(a) Relative amplitude vs. relative distance from the fixed end (1st mode of vibration), $a_1/W=0.4$, $L_1/L=0.5128$

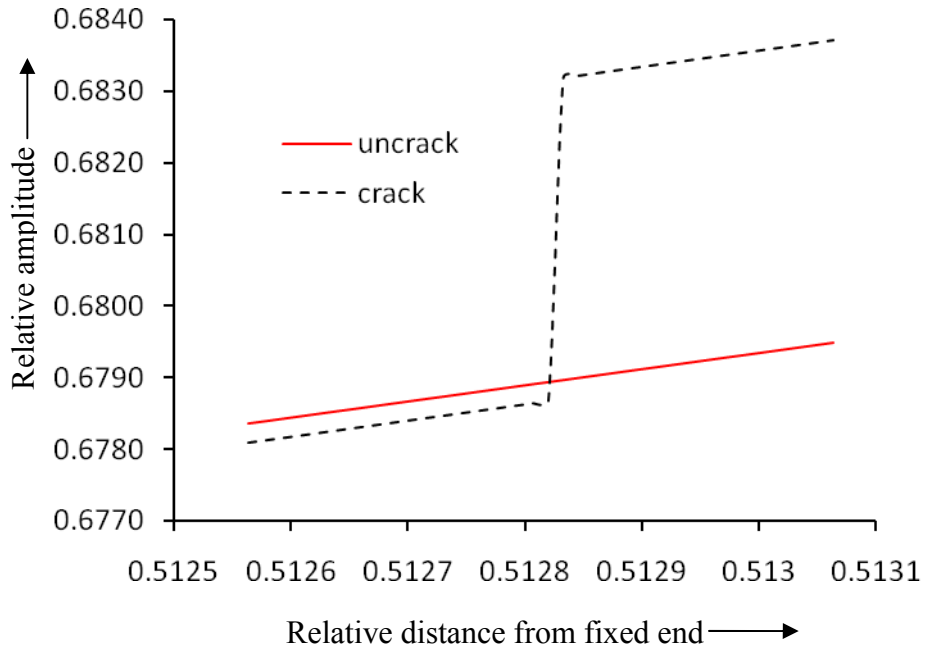


Fig. 3.2.27(a1) Magnified view of Fig. 3.2.27(a1) at the vicinity of the crack location.

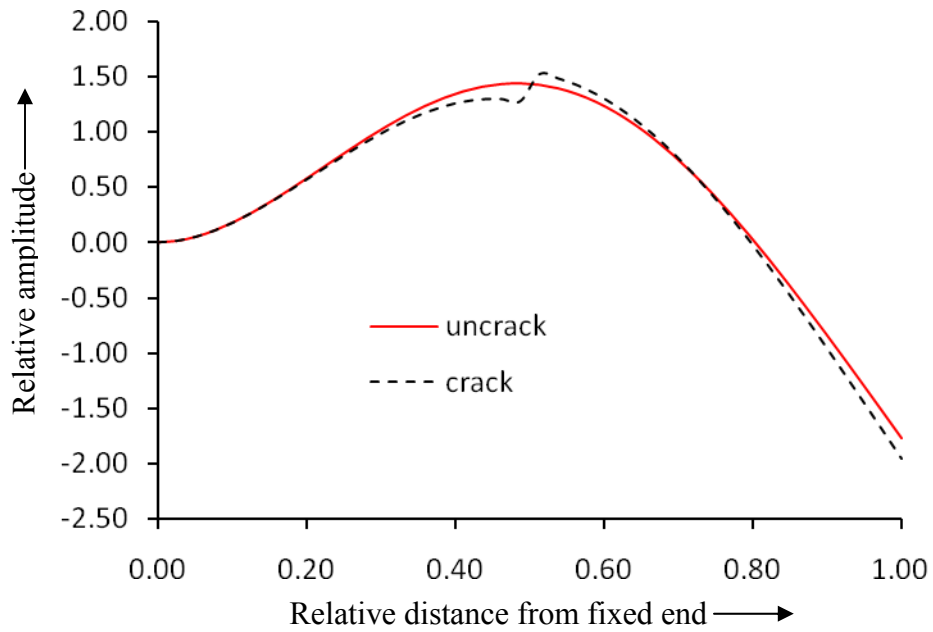


Fig.3.2.27 (b) Relative amplitude vs. relative distance from the fixed end (2nd mode of vibration), $a_1/W=0.4$, $L_1/L=0.5128$

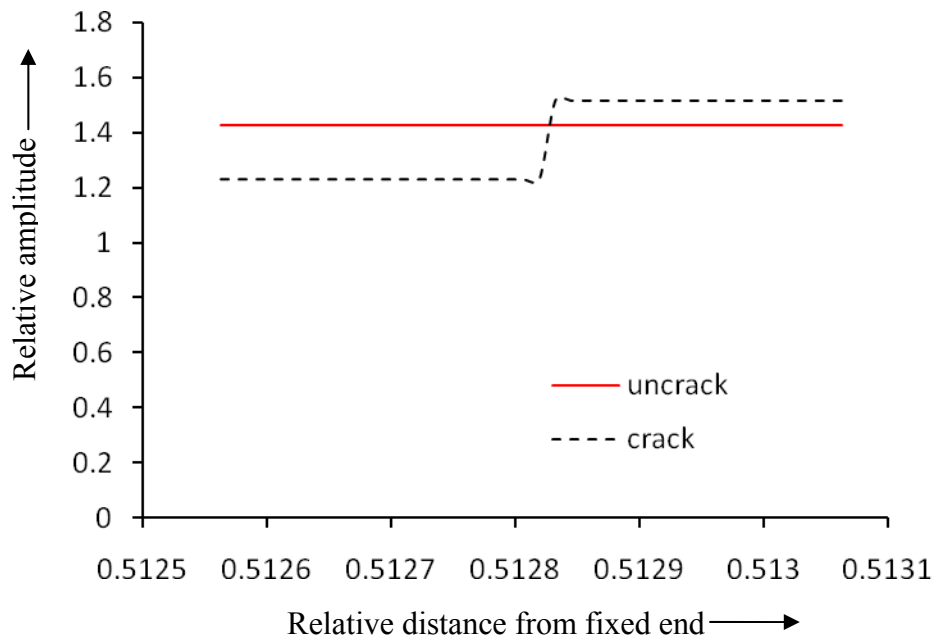


Fig. 3.2.27(b1) Magnified view of Fig. 3.2.27(b) at the vicinity of the crack location.

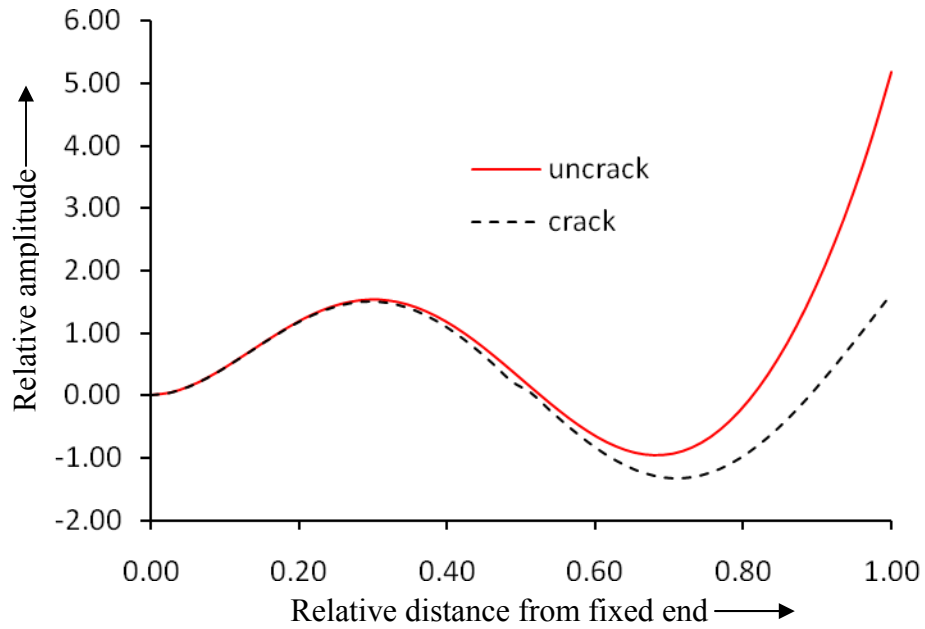


Fig. 3.2.27(c) Relative amplitude vs. relative distance from the fixed end (3rd mode of vibration), $a_1/W=0.4$, $L_1/L=0.5128$

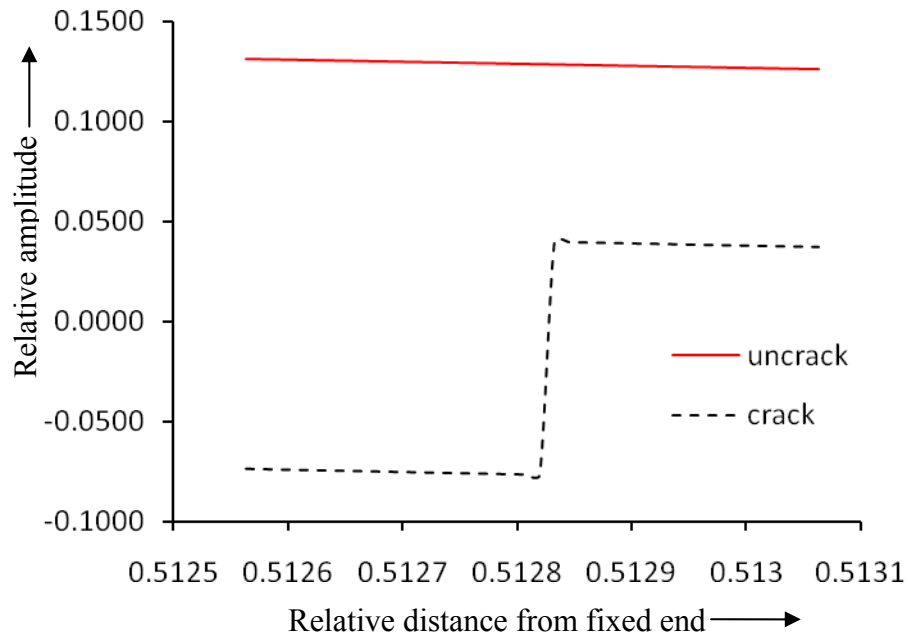


Fig. 3.2.27(c1) Magnified view of fig. Fig. 3.2.27(c) at the vicinity of the crack location.

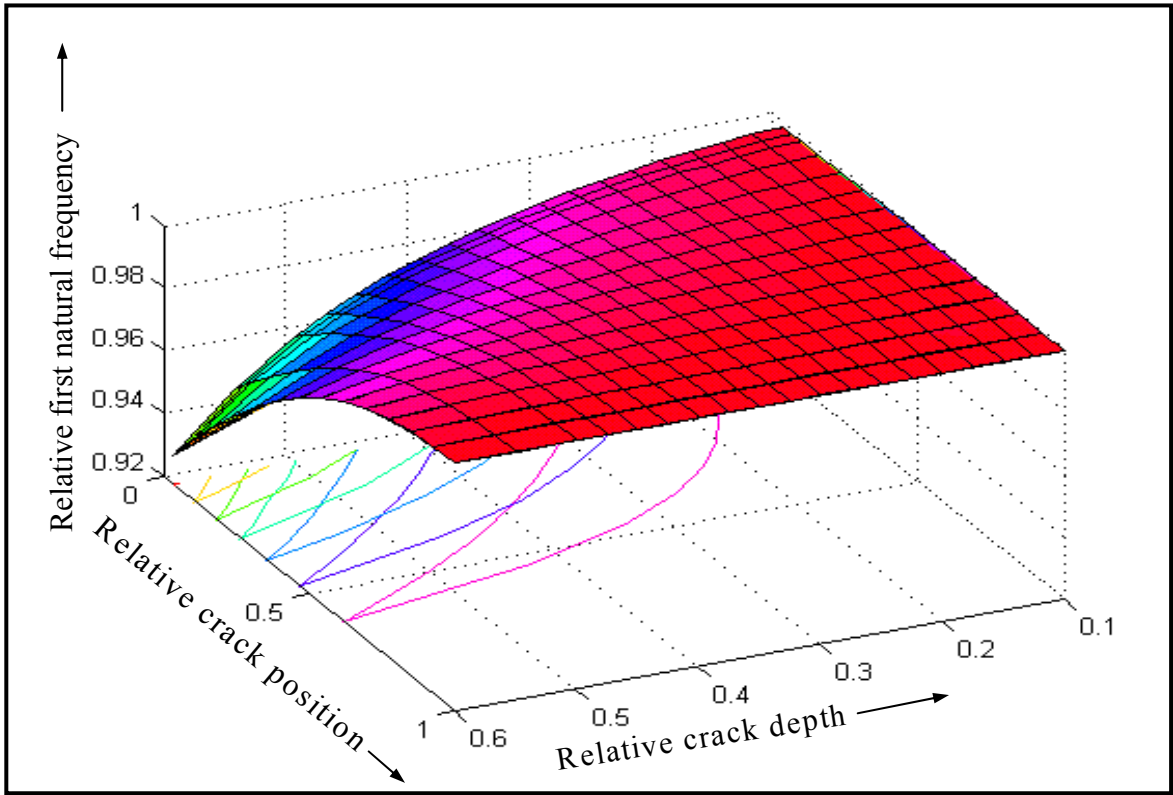


Fig. 3.2.28 (a) Three dimensional cum contour plot for relative first natural frequency

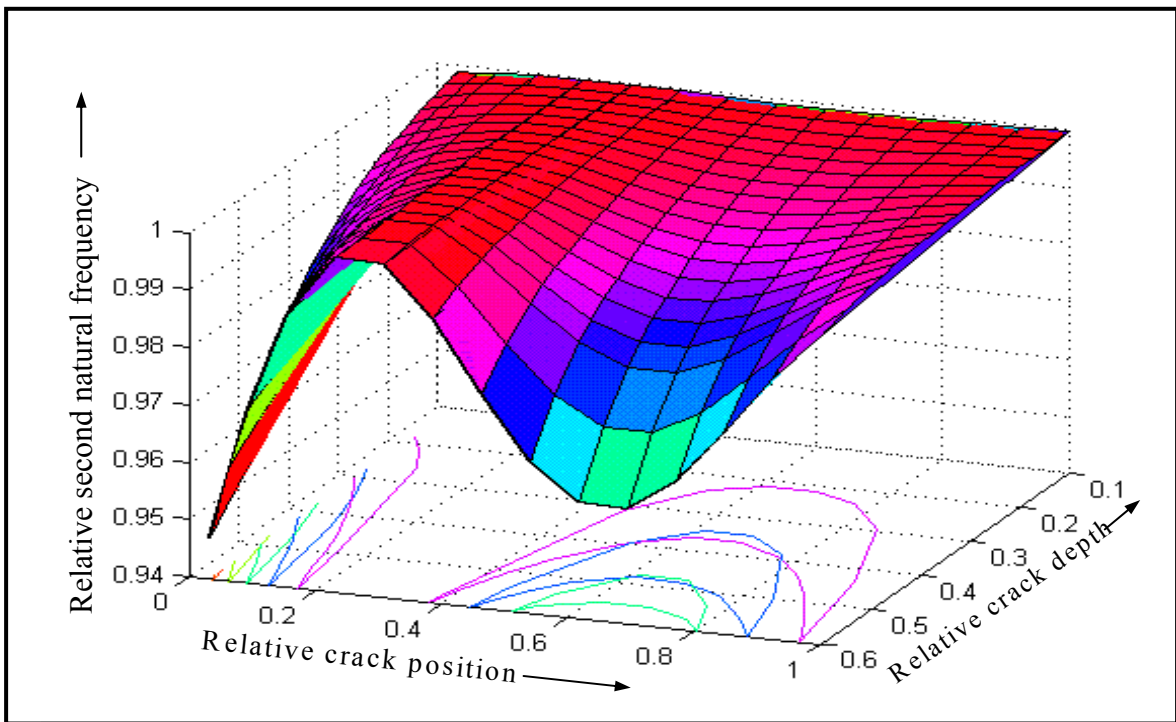


Fig.3.2.28 (b) Three dimensional cum contour plot for relative second natural frequency

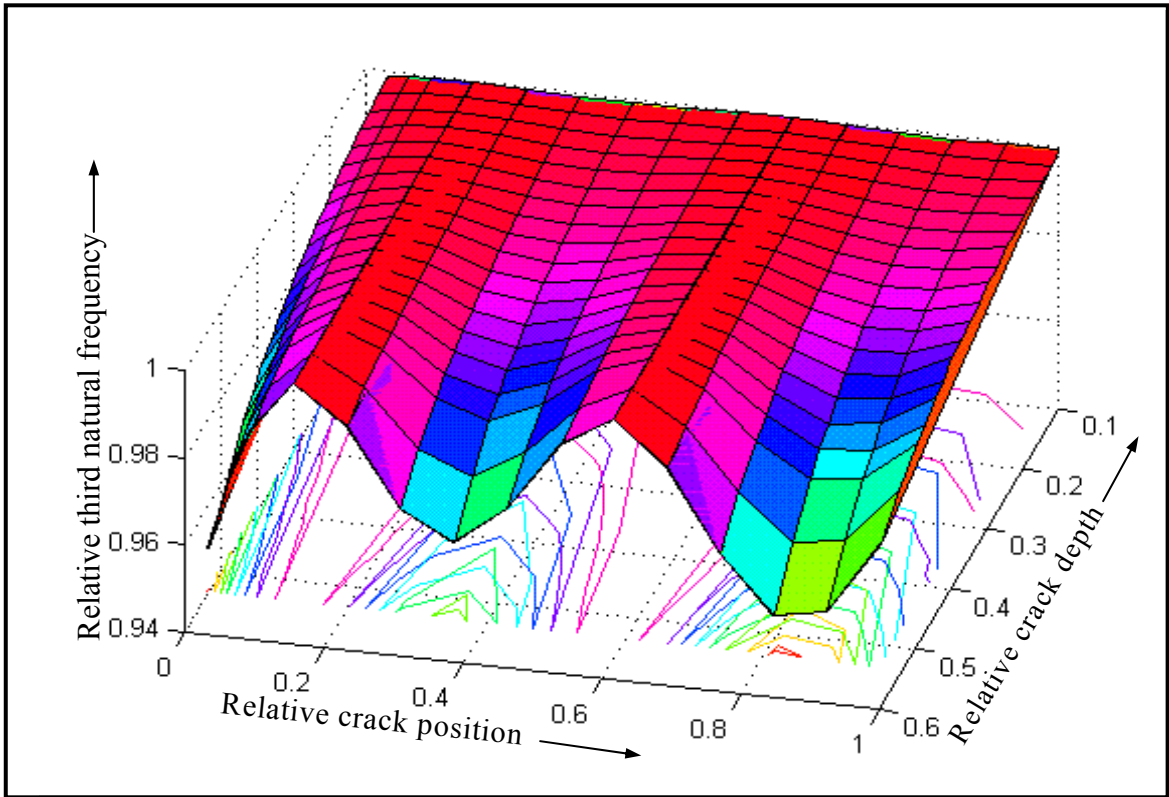


Fig. 3.2.28 (c) Three dimensional cum contour plot for relative third natural frequency

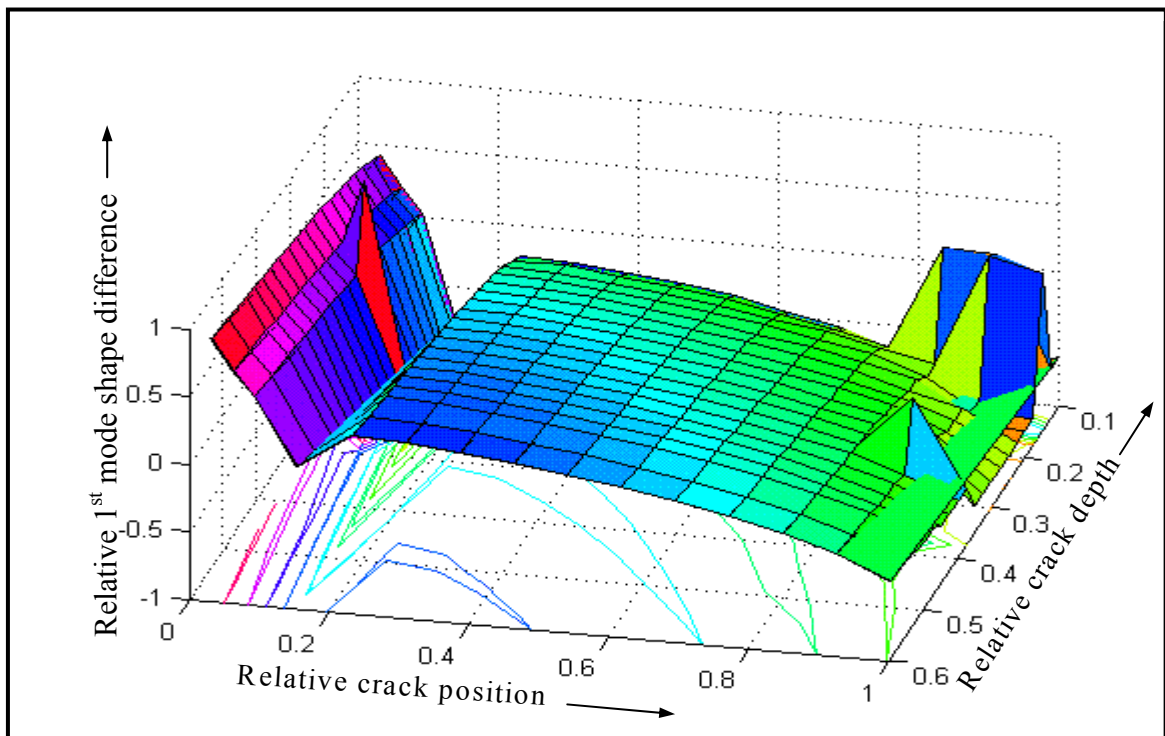


Fig. 3.2.29 (a) Three dimensional cum contour plot for relative 1st mode shape difference

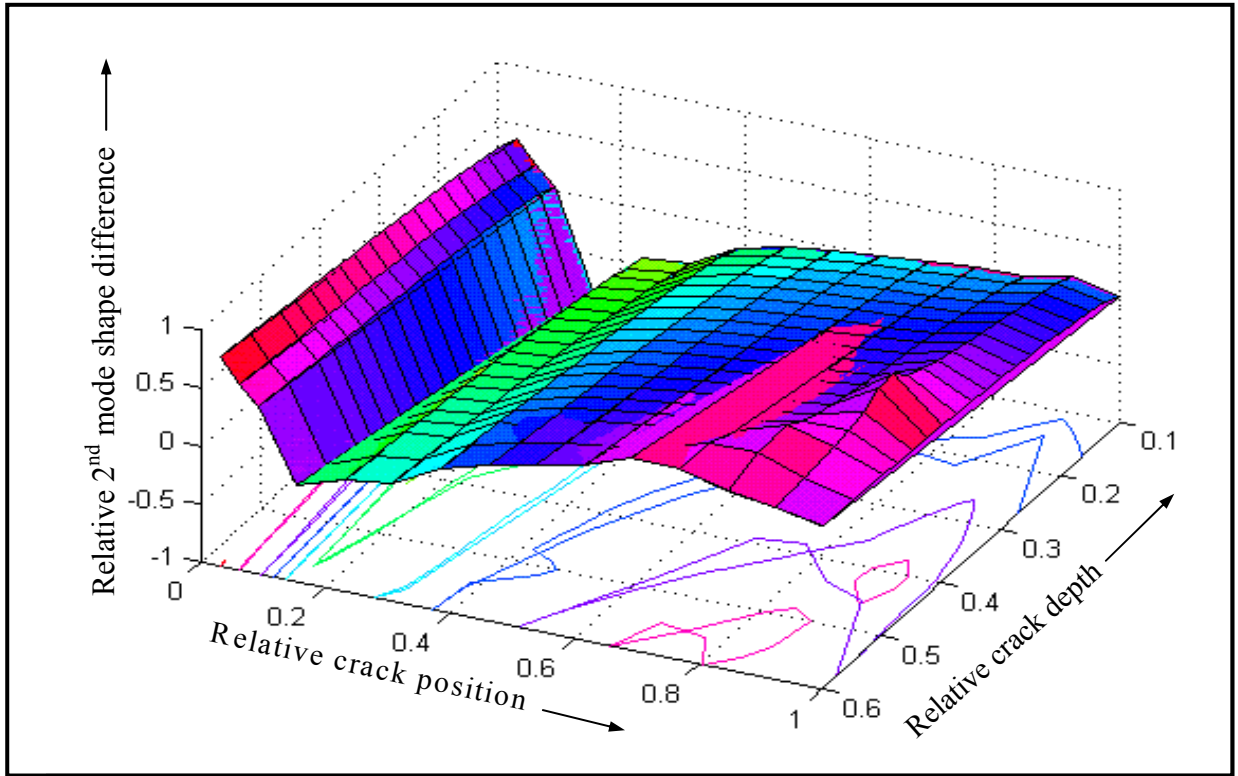


Fig. 3.2.29 (b) Three dimensional cum contour plot for relative 2nd mode shape difference

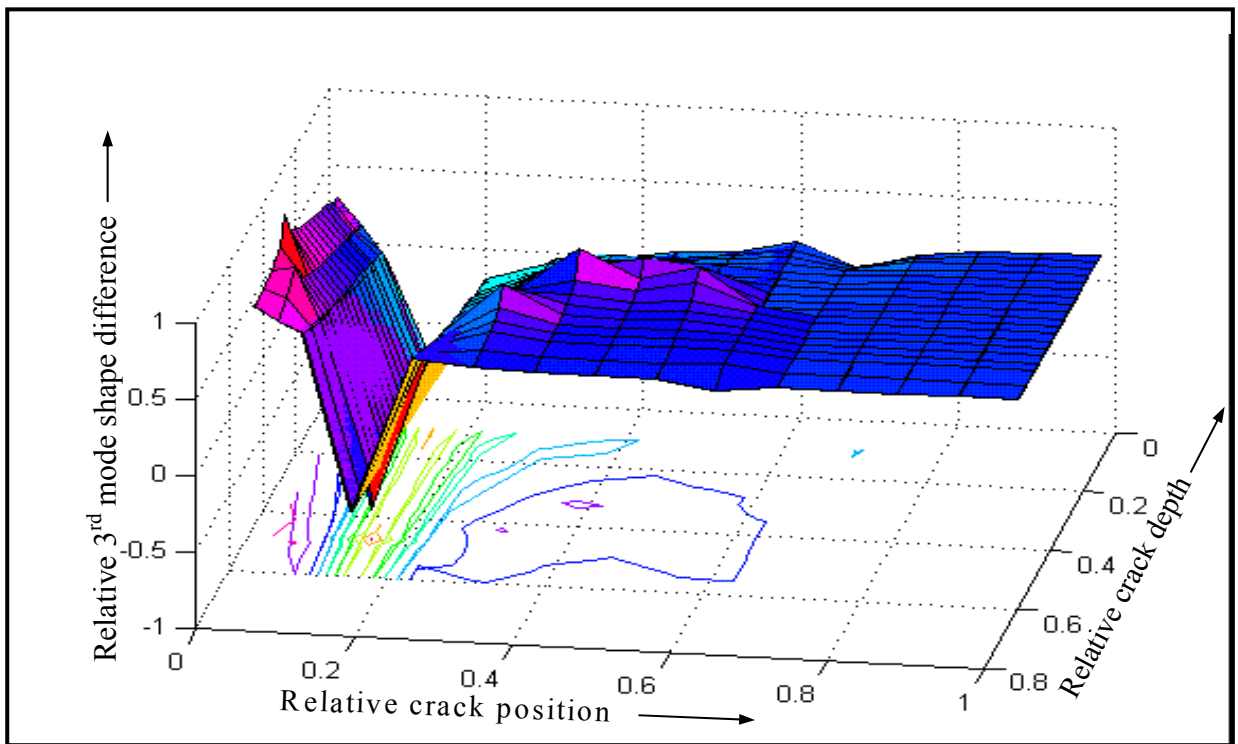
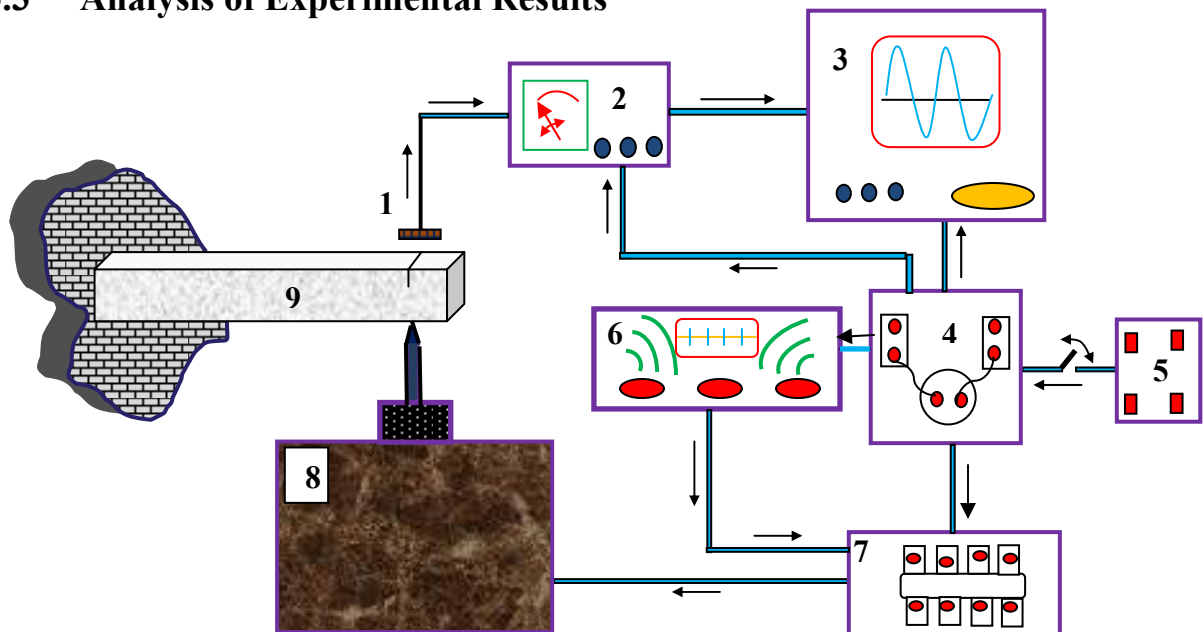


Fig. 3.2.29 (c) Three dimensional cum contour plot for relative 3rd mode shape difference

3.3 Analysis of Experimental Results



- | | | |
|---|-----------------------|--------------------------------|
| 1. Vibration Pick-up
(Accelerometer) | 4. Distribution box | 7. Power amplifier |
| 2. Vibration analyser
(PULSE Lite Type 3560L) | 5. Power supply | 8. Vibration exciter |
| 3. Vibration indicator
with software
(PULSE labshop software) | 6. Function generator | 9. Cantilever beam
specimen |

Fig. 3.3.1 Schematic block diagram of experimental set-up

An experimental set-up is used for carrying out the experiment as shown in the schematic diagram (Fig. 3.3.1). A number of tests are conducted on aluminum beam specimen (800 x 50 x 6 mm) with a transverse crack as shown in Fig. 3.3.1 for determining the amplitude of vibration, natural frequencies and mode shapes. The beam is allowed to vibrate under 1st, 2nd and 3rd modes of vibration.

3.3.1 Experimental Results

The experimental results for relative amplitude at different relative crack location (0.026, 0.05128) and relative crack depths (0.3, 0.4) are depicted in Fig.3.3.2 to Fig. 3.3.4. Corresponding numerical results are also plotted for cracked and un-cracked beam in the same graphs for immediate comparison.

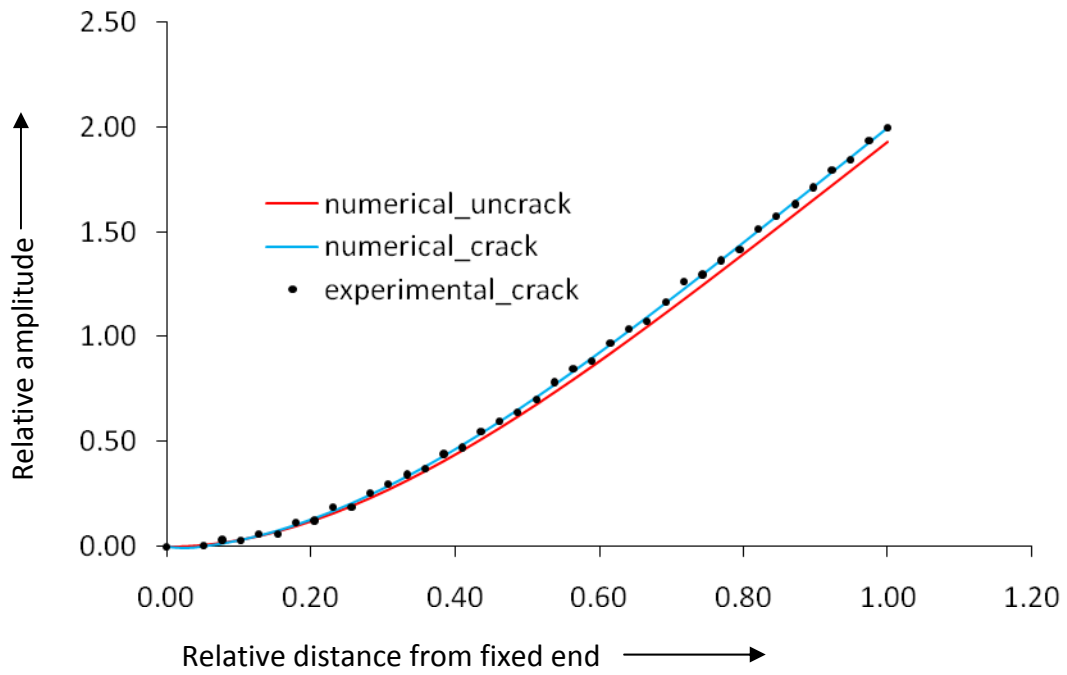


Fig.3.3.2 (a) Relative amplitude vs. relative distance from the fixed end (1st mode of vibration), $a_1/W=0.4$, $L_1/L=0.026$

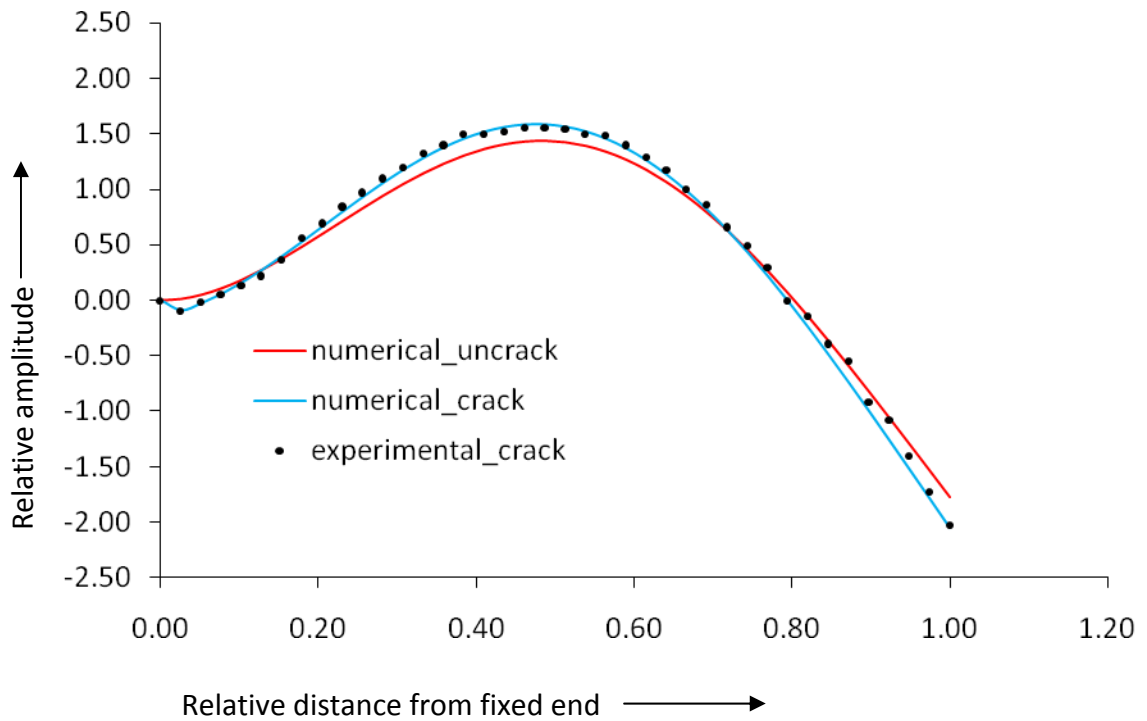


Fig.3.3.2 (b) Relative amplitude vs. relative distance from the fixed end (2nd mode of vibration), $a_1/W=0.4$, $L_1/L=0.026$

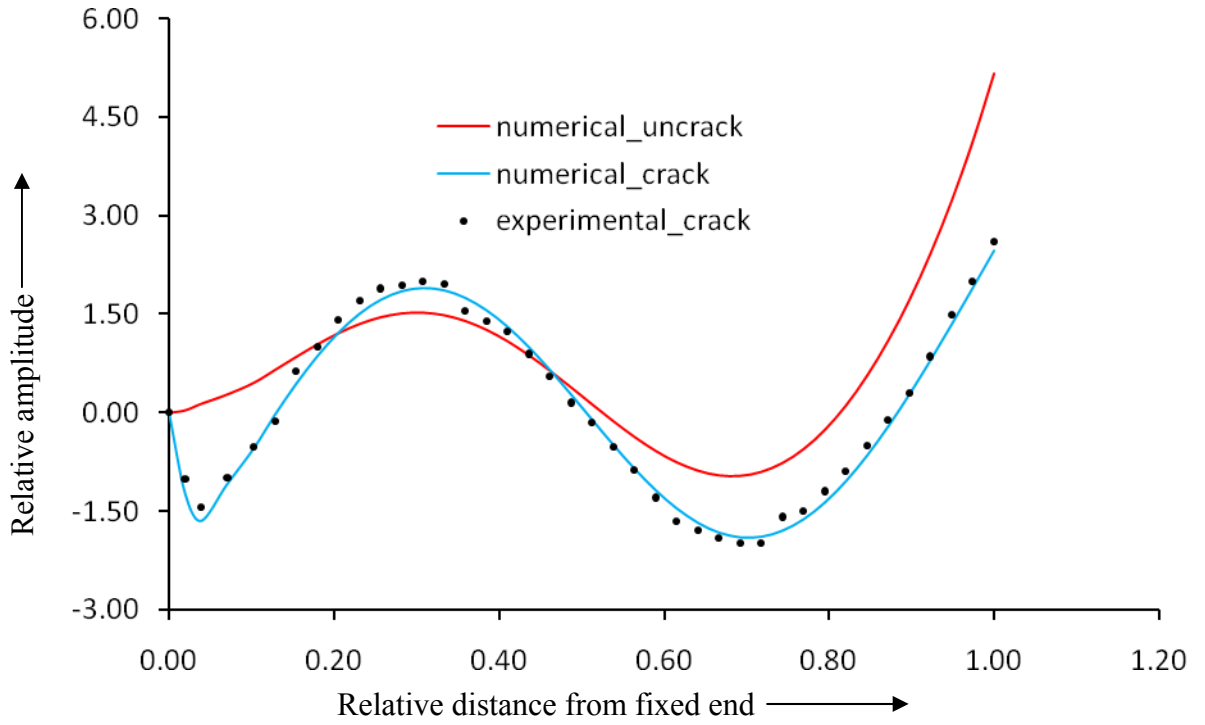


Fig.3.3.2 (c) Relative amplitude vs. relative distance from the fixed end (3rd mode of vibration), $a_1/W=0.4$, $L_1/L=0.026$

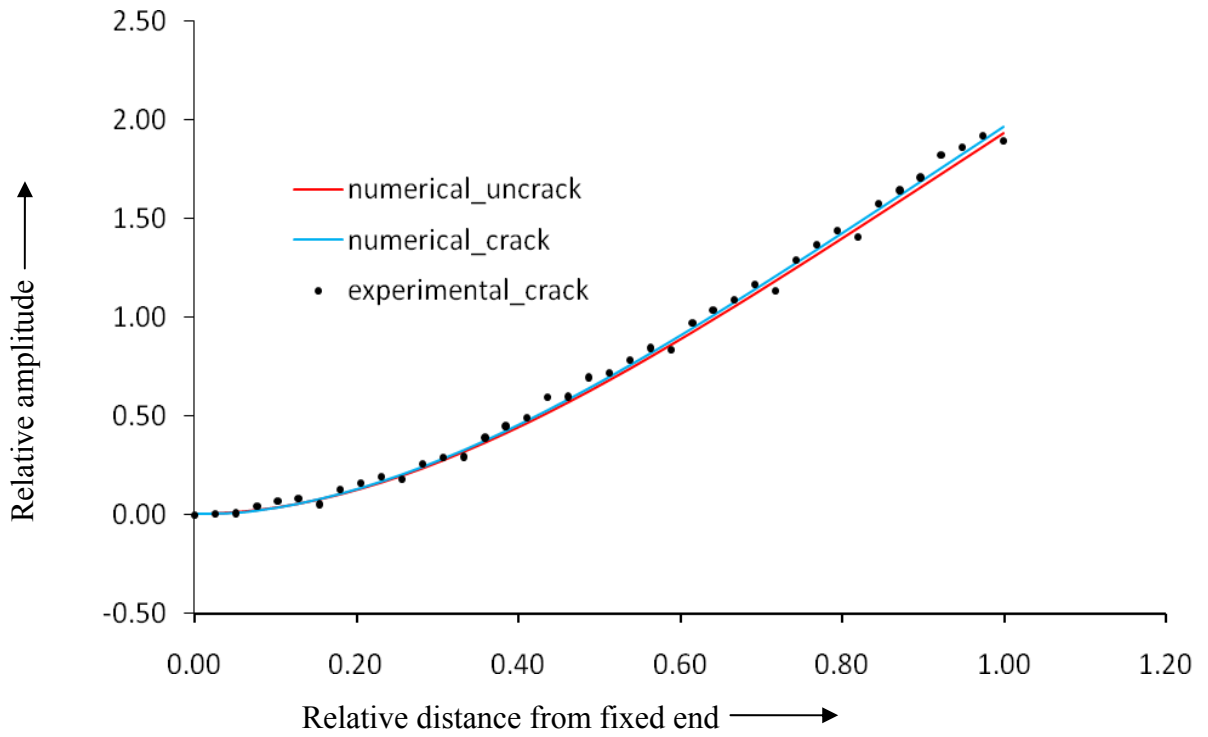


Fig.3.3.3 (a) Relative amplitude vs. relative distance from the fixed end (1st mode of vibration), $a_1/W=0.3$, $L_1/L=0.05128$

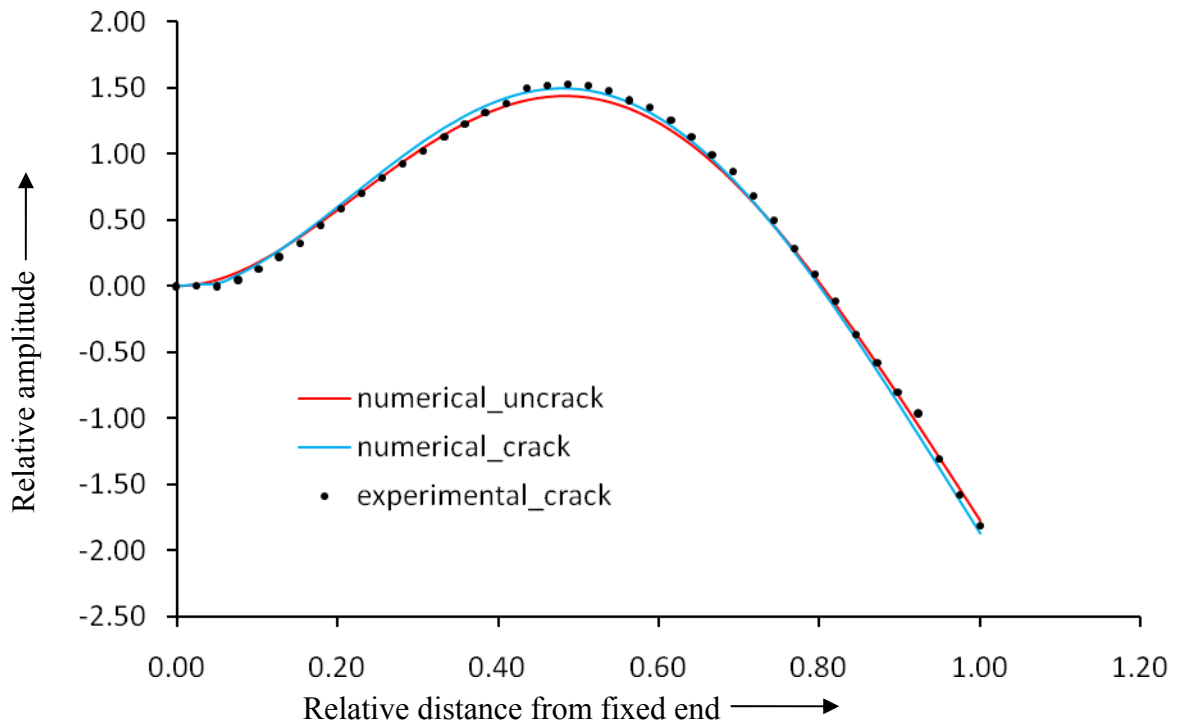


Fig.3.3.3 (b) Relative amplitude vs. relative distance from the fixed end (2nd mode of vibration), $a_1/W = 0.3$, $L_1/L = 0.05128$

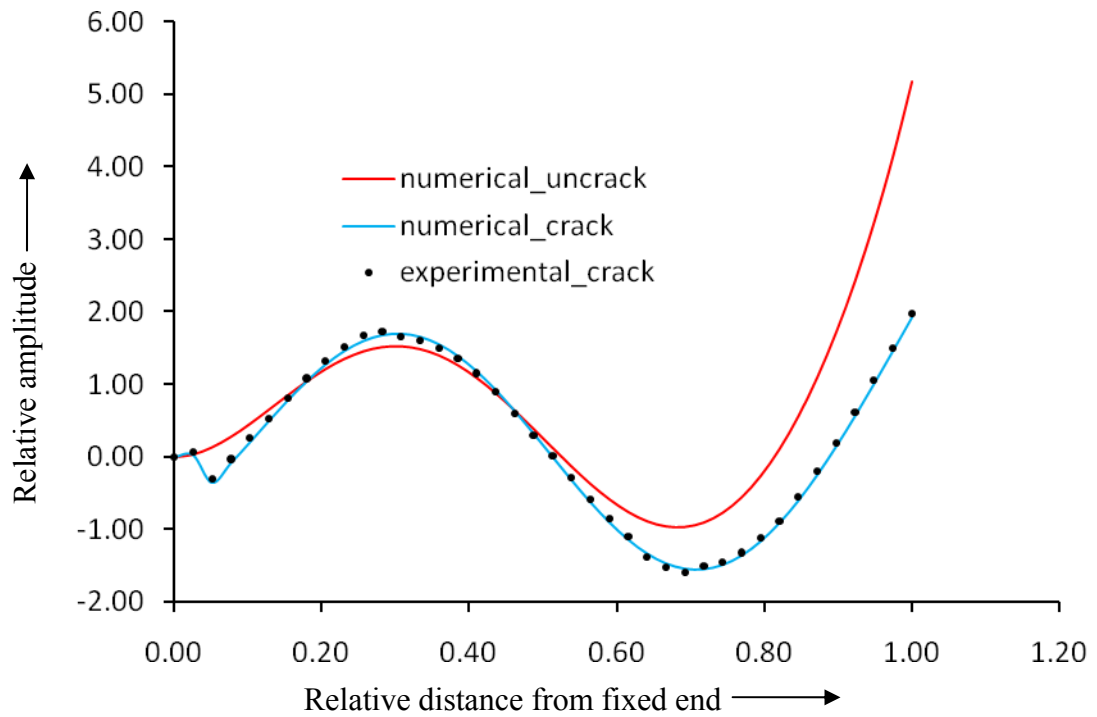


Fig.3.3.3(c) Relative amplitude vs. relative distance from the fixed end (3rd mode of vibration), $a_1/W = 0.3$, $L_1/L = 0.05128$

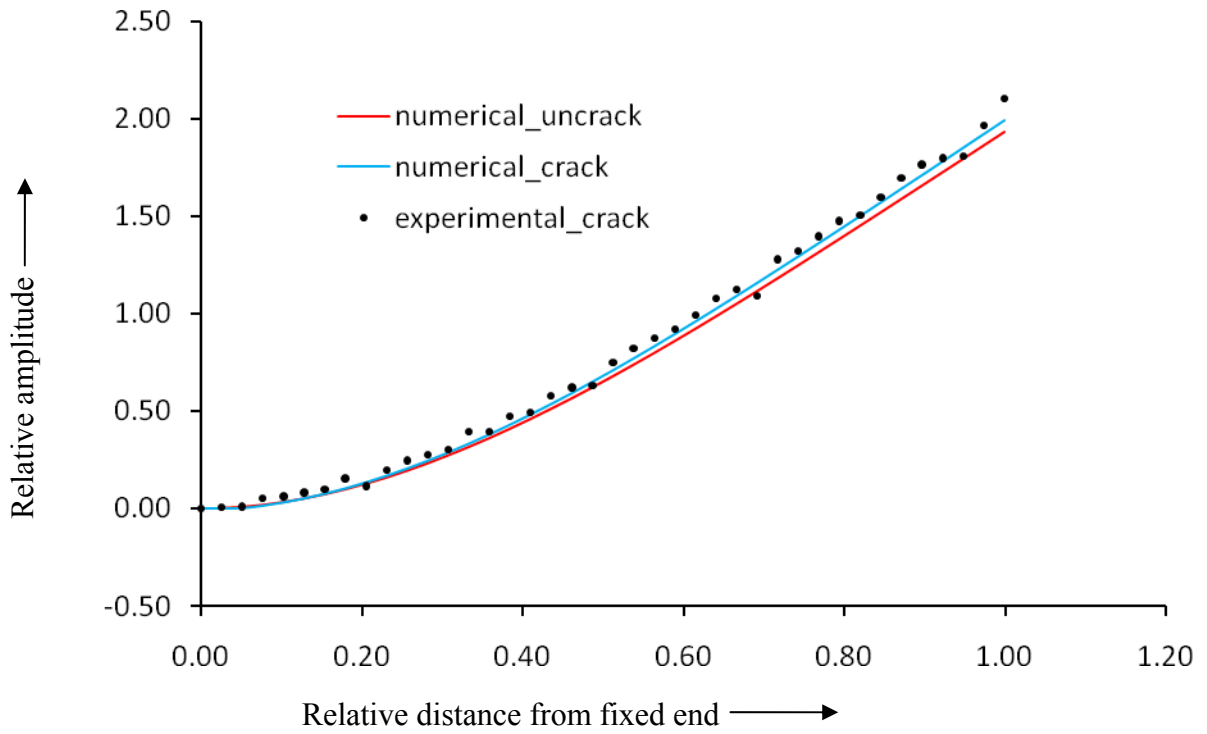


Fig.3.3.4 (a) Relative amplitude vs. relative distance from the fixed end (1st mode of vibration), $a_1/W = 0.4$, $L_1/L = 0.05128$

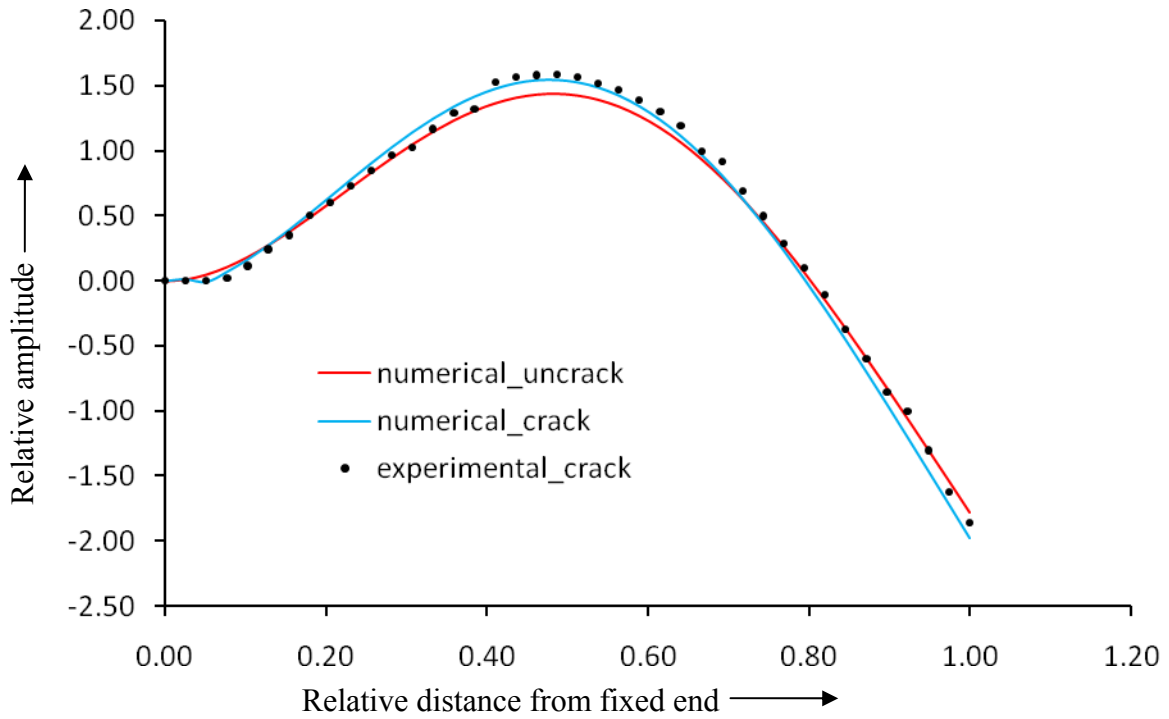


Fig.3.3.4 (b) Relative amplitude vs. relative distance from the fixed end (2nd mode of vibration), $a_1/W = 0.4$, $L_1/L = 0.05128$

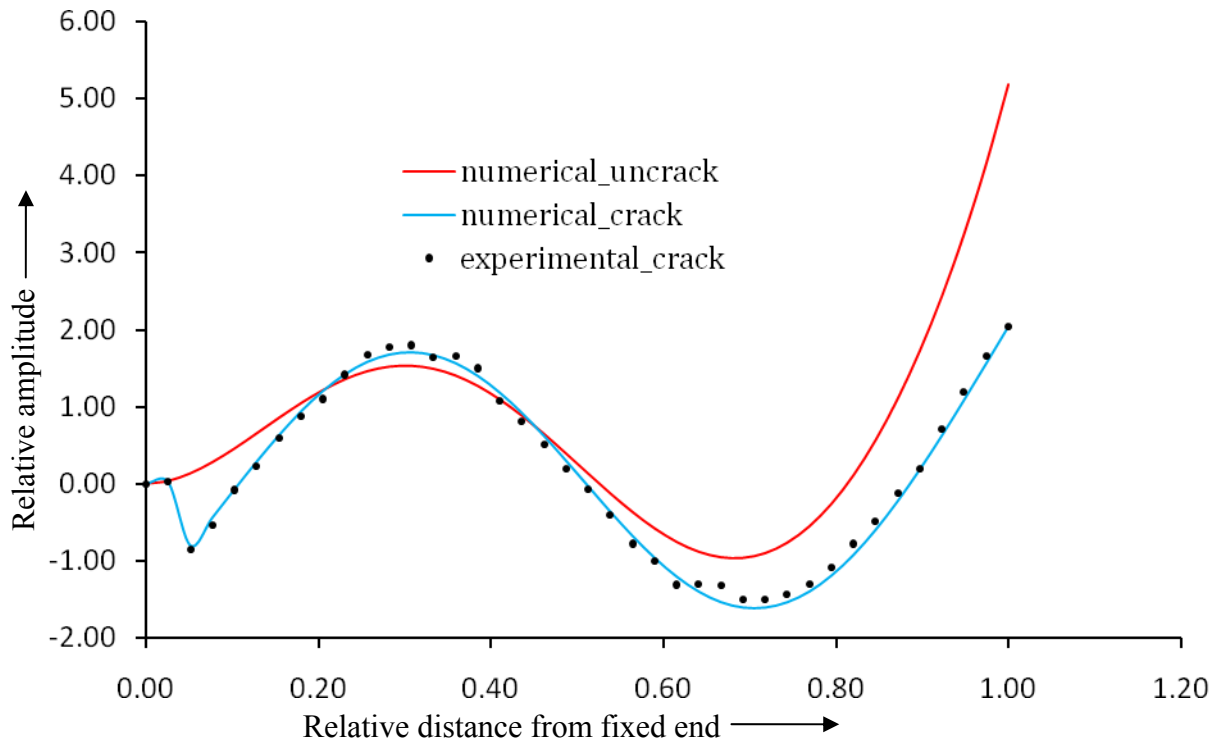


Fig.3.3.4 (c) Relative amplitude vs. relative distance from the fixed end (3rd mode of vibration), $a_1/W = 0.4$, $L_1/L = 0.05128$

3.3.2. Comparison among the Results of Numerical and Experimental Analyses

It is evident from the comparison of experimental and numerical results depicted in the Fig.3.3.2 to Fig. 3.3.4. and Table 3.3.1 that they are in good agreement. Table 3.3.1 delineates the comparison of results between numerical and experimental results. This table depicts ten sets of data out of hundreds of data set recorded to show the comparison between the numerical and experimental results. In Table 3.3.1 column “one” for relative first natural frequency, column “two” for relative second natural frequency, column “three” for relative third natural frequency, column “four” for relative first mode shape difference, column “five” for relative second mode shape difference, column “six” for relative third mode shape difference, column “seven” for relative crack depth and relative crack location of numerical

analysis, column “eight” for relative crack depth and relative crack location of experimental analysis.

Various numerical and experimental results are found out from the above theoretical and experimental analysis. The numerical, experimental results and comparison between the numerical and experimental results are put forward in the graphical and tabular format. The relative natural frequency and relative mode shape difference used in the above analysis can be defined as follows.

$$\text{Relative natural frequency} = \frac{(\text{Natural frequency of cracked beam})}{(\text{Natural frequency of uncracked beam})}$$

$$\text{Relative mode shape difference} = \frac{(\text{Uncrack mode} - \text{Crack mode})}{\text{Uncrack mode}}$$

Relative first natural frequency “fnf”	Relative second natural frequency “snf”	Relative third natural frequency “tnf”	Relative first mode shape difference “fmd”	Relative second mode shape difference “smd”	Relative third mode shape difference “tmd”	Numerical results (relative crack depth “rcd” and location “rcl”)		Experimental results (relative crack depth “rcd” and location “rcl”)	
						rcd	rcl	rcd	rcl
0.9848	0.9958	0.9975	0.2709	0.2372	0.3158	0.202	0.06888	0.205	0.0725
0.9673	0.9874	0.9943	0.3969	0.3247	0.3923	0.427	0.079	0.43	0.08388
0.9623	0.9948	0.9983	0.1814	0.0279	0.0774	0.537	0.15988	0.568	0.1575
0.9756	0.9976	0.9972	0.1383	-0.0823	0.1898	0.394	0.18675	0.391	0.18775
0.9852	0.9984	0.9967	0.01	-0.8678	0.2572	0.231	0.23625	0.23	0.24
0.9723	0.9961	0.9818	0.1947	0.0672	0.4105	0.556	0.2825	0.545	0.28625
0.9823	0.9872	0.9919	0.0726	0.2567	0.3994	0.451	0.40388	0.447	0.40513
0.981	0.9809	0.9931	0.0898	0.3154	0.392	0.497	0.42388	0.495	0.4235
0.986	0.9842	0.9988	-0.032	0.322	0.3965	0.426	0.50125	0.425	0.50375
0.9834	0.9685	0.9974	0.038	0.4558	0.3507	0.542	0.535	0.535	0.53313

Table 3.3.1 Comparison of results between numerical and experimental analyses

3.4 Discussions

From above theoretical, numerical and experimental analysis the following discussions are made. Fig.3.2.1 (a) represents the cracked cantilever beam, Fig.3.2.1 (b) shows the cross sectional view and Fig.3.2.1(c) shows the segment at crack section. Fig. 3.2.2 shows the

variation of dimension-less compliances to that of relative crack depth. It is observed that as the crack depth increases the compliance value increases. Fig.3.2.4 to Fig.3.2.27 show the plots of relative beam distance from fixed end verses relative amplitudes for first, second, third modes of vibration, for different relative crack locations and different relative crack depths. Fig.3.2.28 depicts the variation of relative natural frequencies with respect to relative crack locations and relative crack depth in three dimensional forms, along with the contour plots. Fig.3.2.29 exhibits the variation of relative mode shapes with respect to relative crack locations and relative crack depth in three dimensional forms along with the contour plot. The observations made from the above results are depicted below.

- (1) From Fig.3.2.2 it is observed that as the crack depth increases, the compliances (C_{11} , $C_{12}=C_{21}$, C_{22}) also increase. This is due to decrease in local stiffness at the crack section.
- (2) It is observed from Fig. 3.2.4 to Fig. 3.2.27 that there are remarkable changes in the mode shapes of the beam due to the presence of crack as compared to un-cracked beam.
- (3) It is evident from Fig.3.2.4 that up to the relative crack depth of 0.1 and relative crack location 0.0256, there is no appreciable change in the mode shapes as compared with similar un-cracked beam. However with the magnification of ordinates at the vicinity of crack location as shown in Fig.3.2.4 to Fig.3.2.27, significant variation is noted in mode shapes.
- (4) Similarly for relative crack depth of 0.3 the mode shape variations are more prominent (Fig.3.2.6 to Fig.3.2.27).
- (5) Again with the increase in the relative crack depth up to 0.50, keeping the relative crack location same, it is observed that there is appreciable variation in the 1st and 2nd mode shapes as depicted in Fig.3.26 to Fig.3.2.27. With the magnification of ordinates at the vicinity of crack location (Fig.3.24 to 3.2.27) abrupt changes in mode shape are observed.
- (6) Fig.3.3.2 to Fig.3.3.4 shows the comparison between the experimental and numerical results for the cracked and un-cracked beam.

3.5 Summary

From the above analyses and discussions, the conclusions drawn are depicted as follows. Crack depth and crack location have got effect on mode shapes and natural frequencies of the vibrating structures. At the crack location significant changes in mode shapes are observed in magnified views. These changes will help in depicting the location and intensity of the crack. The mode shapes for the beam with crack obtained theoretically are compared with the experimental results for cross verification. This methodology has been applied for collection of rule and training data set for inverse problem in the subsequent section. The results obtained from various analyses mentioned above shows a very good agreement. The methodology can be utilized for condition monitoring of vibrating structures. Artificial intelligence embedded technique can be developed for smart detection of fault in structures. In the next sections fuzzy inference technique, Neural technique and hybrid technique are applied for predicting crack location and crack depth as an inverse problem for condition monitoring.

Publications

- Das H.C. and Parhi D.R., Modal analysis of vibrating structures impregnated with crack, *International Journal of Applied Mechanics & Engineering*, 13(3), 2008, 639-652.

Chapter 4

ANALYSIS OF FUZZY LOGIC TECHNIQUE FOR CRACK DETECTION

Much research effort has been spent on various structural health monitoring techniques in order to develop a reliable, efficient and economical approach to increase the safety and reduce the maintenance cost of elastic structures. Although improved design methodologies have significantly enhanced the reliability and safety of structures in recent years, it is still not possible to build structures that have zero percent probability of failure. There is an increasing interest in the development of smart structures with built-in fault detection systems that would provide failure warnings. This current research presents methodologies for structural damage detection and assessment using fuzzy logic. The approach for damage detection is based on monitoring various system responses to determine the condition monitoring of a vibrating structure. In this chapter an intelligent controller has been proposed for crack detection algorithm employing fuzzy theory.

4.1 Introduction

It is observed that the human beings do not need precise, numerical information input to make a decision, but they are able to perform highly adaptive control. Humans have a remarkable capability to perform a wide variety of physical and mental tasks without any explicit measurements or computations. Examples of everyday tasks are parking a car, driving in city traffic, playing golf, and summarizing a story. In performing such familiar tasks, humans use perceptions of time, distance, speed, shape, and other attributes of physical and mental objects [152]. Fuzzy logic is a problem-solving control system methodology that lends itself for implementation in systems ranging from simple, small, embedded micro-controllers to large, networked, workstation-based data acquisition and control systems. The theory of fuzzy logic systems is inspired by the remarkable human capability to operate on and reason with perception-based information. The rule-based fuzzy logic provides a scientific formalism for reasoning and decision making with uncertain and imprecise

information. This methodology can be implemented in hardware, software, or a combination of both. Fuzzy logic approach to control problems mimics how a person would make decisions. Fuzzy systems allow for easier understanding as they are expressed in terms of linguistic variables [178]. Damage detection is one of the key aspects in structural engineering both for safety reasons and because of economic benefits that can result. Many non-destructive testing methods for health monitoring have been proposed and investigated. These methods include modal analysis, strain analysis, photo-elastic techniques, ultrasound and acoustic emissions [170]. A fuzzy logic methodology can be presented for structural fault detection based on eigen value, and dynamic responses of vibrating structure.

This chapter proposes an on-line crack detection methodology embedded with a new intelligent fuzzy inference system. In this approach, the fuzzy logic controller is designed and is used to detect the relative crack location and relative crack depth. The designed fuzzy controller has six inputs and two outputs. The inputs to the designed fuzzy controller are relative deviation of first three natural frequencies and relative deviation of first three mode shapes and the outputs are relative crack location and relative crack depth. The fuzzy logic system learns the full dynamics of the cracked beam. The inputs have ten membership functions each and the outputs have forty seven membership functions for relative crack location and nineteen membership functions relative crack depth. Each membership function consists of triangular, trapezoidal and Gaussian membership functions. In this methodology six hundred and ninety two rules have been used to design the fuzzy controllers. This research focuses a fuzzy logic framework to be implemented for on-line crack detection. The results of the proposed fuzzy controller have been compared with the numerical method which shows the effectiveness of the developed method. It is also concluded that the current method can be successfully employed for crack detection. This fuzzy controller designed for crack detection has been authenticated by experimental results.

This chapter organized into five sections following the introduction, the analysis of fuzzy inference system is described in section 4.2. The fuzzy controller design for crack detection and corresponding results are discussed in section 4.3. In section 4.4, the results of the fuzzy controller are compared with experimental and numerical results to demonstrate the superiority of the proposed methodology and finally summary is given in section 4.5.

4.2 Fuzzy Inference System

Fuzzy inference is the process of formulating the mapping from a given input to an output using fuzzy logic. The mapping then provides a basis from which decisions can be made, or patterns discerned. The process of fuzzy inference involves: membership functions, fuzzy logic operators, and if-then rules. Fuzzy inference systems have been successfully applied in fields such as automatic control, fault diagnosis, data classification, decision analysis, expert systems, and computer vision.

In general, there are five parts of the fuzzy inference process.

(i) Input fuzzification: The step is to take the inputs and determine the degree to which they belong to each of the appropriate fuzzy sets via membership functions.

(ii) Antecedent matching: Once the inputs have been fuzzified, the degree to which each part of the antecedent has been satisfied for each rule is known. If the antecedent of a given rule has more than one part, the fuzzy operator is applied to obtain one number that represents the result of the antecedent for that rule. This number will then be applied to the output function.

(iii) Rule fulfillment: A consequent of a rule is a fuzzy set represented by a membership function. In this step, the consequent is reshaped using a function associated with the antecedent.

(iv) Consequent aggregation: Since decisions are based on all the rules in a fuzzy inference system, the rules must be combined in some manner in order to make a decision. Aggregation is the process by which the fuzzy sets that represent the outputs of each rule are combined into a single fuzzy set.

(v) Output defuzzification: Taking fuzzy sets as input, defuzzification outputs a crisp value, which is suitable for analysis and control.

4.2.1 Membership Functions

The membership function of a fuzzy set is a generalization of the indicator function in classical sets. In fuzzy logic, it represents the degree of truth as an extension of valuation. For any set X , a membership function on X is any function from X to the real unit interval $[0, 1]$. Membership functions on X represent fuzzy subsets of X . The membership function which

represents a fuzzy set A is usually denoted by μ_A . For an element x of X , the value $\mu_A(x)$ is called the membership degree of x in the fuzzy set A. The membership degree $\mu_A(x)$ quantifies the grade of membership of the element x to the fuzzy set A. The value 0 means that x is not a member of the fuzzy set; the value 1 means that x is fully a member of the fuzzy set. The values between 0 and 1 characterize fuzzy members, which belong to the fuzzy set only partially.

The **Triangular** membership function with straight lines is defined as

$$\begin{aligned} f(u, \alpha, \beta, \gamma) &= 0 \quad u < \alpha \\ &= (u - \alpha) / (\beta - \alpha) \quad \alpha \leq u \leq \beta \\ &= (\alpha - u) / (\beta - \alpha) \quad \beta \leq u \leq \gamma \\ &= 0 \quad u > \gamma \end{aligned}$$

One typical plot of the triangular membership function is given in Fig. 4.2.1(a).

A **Gaussian** membership function is defined by

$$f(u; m, \sigma) = \exp \left[-\frac{(u-m)^2}{2\sigma^2} \right]$$

Where the parameters m and σ control the center and width of the membership function. A plot of the Gaussian membership function is presented in Fig. 4.2.1(b).

Trapezoidal membership function is defined as

$$\begin{aligned} f(u, a, b, c, d) &= 0 \quad \text{when } u < a \text{ and } u > d \\ &= (u - a) / (b - a) \quad \text{when } a \leq u \leq b \\ &= 1 \quad \text{when } b \leq u \leq c \\ &= (d - u) / (d - c) \quad \text{when } c \leq u \leq d \end{aligned}$$

A plot of the Trapezoidal membership function is furnished in Fig. 4.2.1(c).

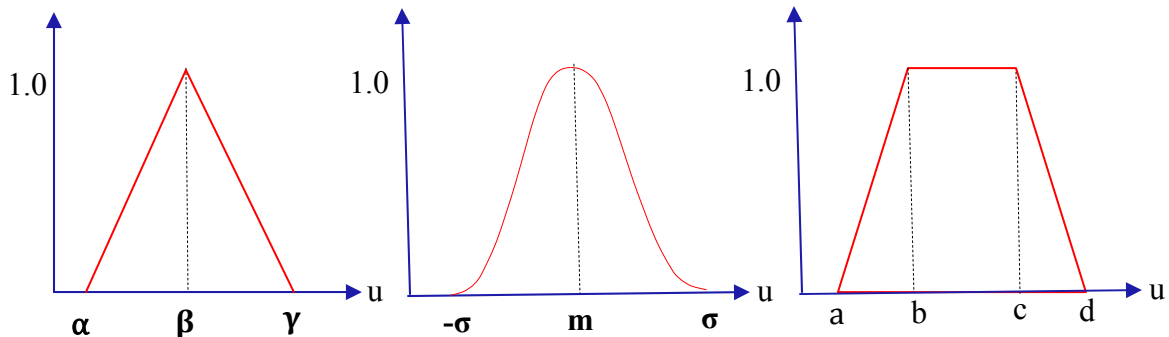


Fig. 4.2.1(a) Triangular membership function

Fig.4.2.1 (b) Gaussian membership function

Fig.4.2.1(c) Trapezoidal membership function

4.2.2 Fuzzy Logic Controllers (FLC) and Fuzzy Reasoning Rules

In a fuzzy logic controller (FLC), the dynamic behavior of a fuzzy system is characterized by a set of linguistic description rules based on expert knowledge. The expert knowledge is usually of the form IF (a set of conditions are satisfied) THEN (a set of consequences can be inferred). Since the antecedents and the consequents of these IF-THEN rules are associated with fuzzy concepts (linguistic terms), they are often called fuzzy conditional statements. In our terminology, a fuzzy control rule is a fuzzy conditional statement in which the antecedent is a condition in its application domain and the consequent is a control action for the system under control. Basically, fuzzy control rules provide a convenient way for expressing control policy and domain knowledge.

Furthermore, several linguistic variables might be involved in the antecedents and the conclusions of these rules. When this is the case, the system will be referred to as a multi-input- multi-output (MIMO) fuzzy system. For example, in the case of two-input-single-output (MISO) fuzzy systems, fuzzy control rules have the form

Rule-1: if x is A_1 and y is B_1 then z is C_1

also

Rule-2: if x is A_2 and y is B_2 then z is C_2

also

•

also

Rule- n : if x is A_n and y is B_n then z is C_n

where x and y are the process state variables, z is the control variable, A_i , B_i , and C_i are linguistic values of the linguistic variables x , y and z .

The inputs to the fuzzy logic controller for crack detection comprises of

Relative first natural frequency = “fnf”; Relative second natural frequency = “snf”;

Relative third natural frequency = “tnf”; Relative first mode shape difference = “fmd”;

Relative second mode shape difference = “smd”;

Relative third mode shape difference = “tmd”.

The linguistic term used for the outputs are as follows;

Relative crack location = “rcl” and Relative crack depth = “rcd”

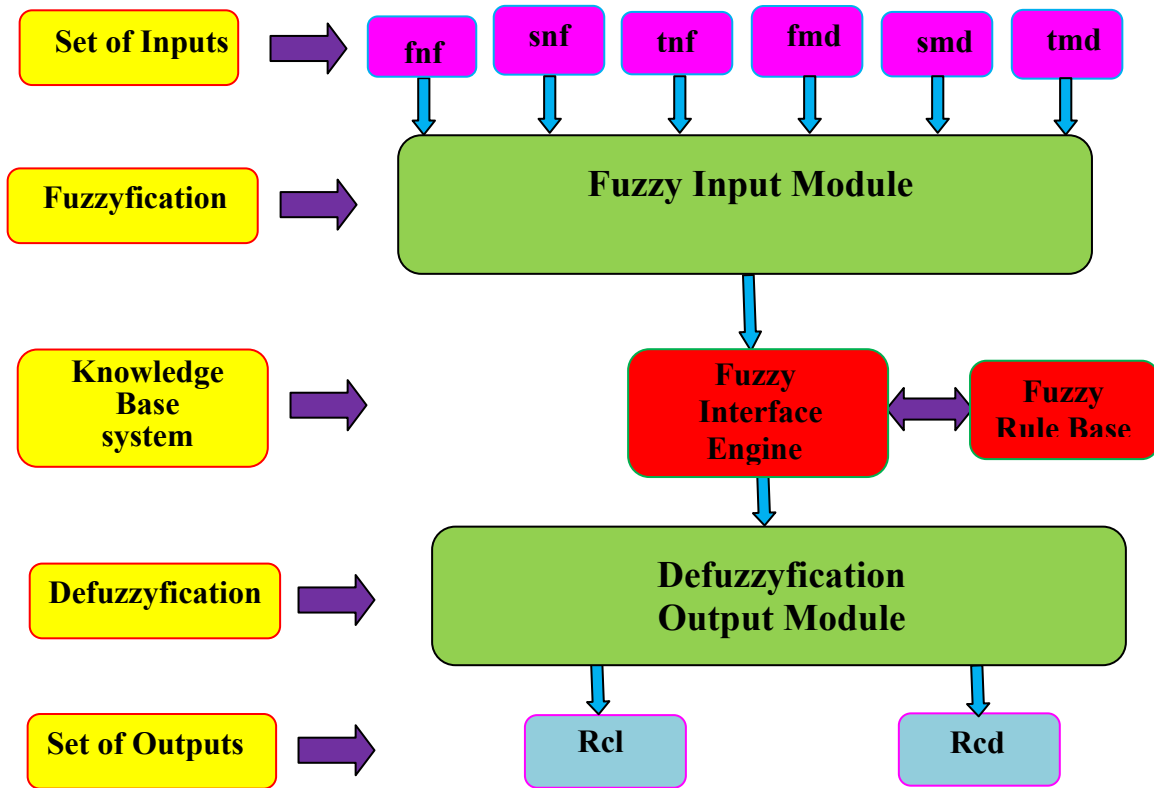


Fig. 4.2.2 Schematic diagram of the fuzzy logic controller for crack detection

4.2.3 Defuzzification

The output of the inference process so far is a fuzzy set, specifying a possibility distribution of control action. In the on-line control, a nonfuzzy (crisp) control action is usually required. Consequently, one must defuzzify the fuzzy control action (output) inferred from the fuzzy control algorithm, namely:

$$z_0 = \text{defuzzifier}(C);$$

where z_0 is the nonfuzzy control output and defuzzifier is the defuzzification operator.

Defuzzification is a process to select a representative element from the fuzzy output C inferred from the fuzzy control algorithm. The widely used defuzzification operators are:

- (a) Centroid of area method
- (b) Mean of maxima method

4.3 Analysis of the Fuzzy Controller used for Crack Detection

fuzzy controllers (Fig. 4.3.1(a), 4.3.2(a), 4.3.3(a)) developed for crack detection has got six input parameters and two output parameters.

The linguistic term used for the inputs are as follows;

Relative first natural frequency = “fnf”; Relative second natural frequency = “snf”;

Relative third natural frequency = “tnf”; Relative first mode shape difference = “fmd”;

Relative second mode shape difference = “smd”;

Relative third mode shape difference = “tmd”.

The linguistic term used for the outputs are as follows;

Relative crack location = “rcl” and Relative crack depth = “rcd”

In the current section the fuzzy controllers are developed with triangular, Gaussian and trapezoidal membership functions. The linguistic terms used in the fuzzy inference system for the membership functions are described in the Table 4.3.1. For each input parameter ten membership functions are taken. For the output parameter “relative crack location (rcl)” forty six membership functions are taken and for the output parameter “relative crack depth (rcd)” nineteen membership functions are taken.

4.3.1 Fuzzy Mechanism for Crack Detection

For the fuzzy subsets, the fuzzy control rules are defined in a general form as follows:

$$\begin{aligned} &\text{If (fnf is fnf}_i \text{ and snf is snf}_j \text{ and tnf is tnf}_k \text{ and fmd is fmd}_l \text{ and smd is smd}_m \\ &\text{and tmd is tmd}_n \text{) then rcl is rcl}_{ijklmn} \text{ and rcd is rcd}_{ijklmn} \end{aligned} \quad (4.3.1)$$

where $i=1$ to 10, $j=1$ to 10, $k = 1$ to 10, $l= 1$ to 10, $m= 1$ to 10, $n= 1$ to 10

Because “fnf”, “snf”, “tnf”, “fmd”, “smd”, “tmd” have ten membership functions each. From expression (4.3.1), two set of rules can be written

$$\left. \begin{aligned} &\text{If (fnf is fnf}_i \text{ and snf is snf}_j \text{ and tnf is tnf}_k \text{ and fmd is fmd}_l \text{ and smd is smd}_m \\ &\text{and tmd is tmd}_n \text{) then rcd is rcd}_{ijklmn} \\ &\text{If (fnf is fnf}_i \text{ and snf is snf}_j \text{ and tnf is tnf}_k \text{ and fmd is fmd}_l \text{ and smd is smd}_m \\ &\text{and tmd is tmd}_n \text{) then rcl is rcl}_{ijklmn} \end{aligned} \right\} (4.3.2)$$

According to the usual fuzzy logic control method [165], a factor W is defined for the rules as follows:

$$W_{ijklmn} = \mu_{\text{fnf}_i}(\text{freq}_i) \wedge \mu_{\text{snf}_j}(\text{freq}_j) \wedge \mu_{\text{tnf}_k}(\text{freq}_k) \wedge \mu_{\text{fmd}_1}(\text{moddif}_1) \wedge \mu_{\text{smd}_m}(\text{moddif}_m) \wedge \mu_{\text{tmd}_n}(\text{moddif}_n)$$

Where freq_i , freq_j and freq_k are the first, second and third relative natural frequencies of the cantilever beam with crack respectively; moddif_1 , moddif_m and moddif_n are the first, second and third mode relative differences of the cantilever beam with crack respectively. By applying the composition rule of inference [165] the membership values of the relative crack location and relative crack depth, $(\text{location})_{\text{rcl}}$ and $(\text{depth})_{\text{rcd}}$ can be computed as;

$$\left. \begin{aligned} \mu_{\text{rcl}_{ijklmn}}(\text{location}) &= W_{ijklmn} \wedge \mu_{\text{rcl}_{ijklmn}}(\text{location}) & \forall \text{length} \in \text{rcl} \\ \mu_{\text{rcd}_{ijklmn}}(\text{depth}) &= W_{ijklmn} \wedge \mu_{\text{rcd}_{ijklmn}}(\text{depth}) & \forall \text{depth} \in \text{rcd} \end{aligned} \right\} \quad (4.3.3)$$

The overall conclusion by combining the outputs of all the fuzzy rules can be written as follows:

$$\left. \begin{aligned} \mu_{\text{rcl}}(\text{location}) &= \mu_{\text{rcl}_{111111}}(\text{location}) \vee \dots \vee \mu_{\text{rcl}_{ijklmn}}(\text{location}) \vee \dots \vee \mu_{\text{rcl}_{10\ 10\ 10\ 10\ 10\ 10}}(\text{location}) \\ \mu_{\text{rcd}}(\text{depth}) &= \mu_{\text{rcd}_{111111}}(\text{depth}) \vee \dots \vee \mu_{\text{rcd}_{ijklmn}}(\text{depth}) \vee \dots \vee \mu_{\text{rcd}_{10\ 10\ 10\ 10\ 10\ 10}}(\text{depth}) \end{aligned} \right\} \quad (4.3.4)$$

The crisp values of relative crack location and relative crack depth are computed using the centroid of area method [165] as:

$$\left. \begin{aligned} \text{relative crack location} = \text{rcl} &= \frac{\int (\text{location}) \cdot \mu_{\text{rcl}}(\text{location}) \cdot d(\text{location})}{\int \mu_{\text{rcl}}(\text{location}) \cdot d(\text{location})} \\ \text{relativecrackdepth} = \text{rcd} &= \frac{\int (\text{depth}) \cdot \mu_{\text{rcd}}(\text{depth}) \cdot d(\text{depth})}{\int \mu_{\text{rcd}}(\text{depth}) \cdot d(\text{depth})} \end{aligned} \right\} \quad (4.3.5)$$

4.3.2 Fuzzy Controller for Finding out Crack Depth and Crack Location

The inputs to the fuzzy controller are relative deviation of first natural frequency; relative deviation of second natural frequency; relative deviation of third natural frequency; relative

first mode shape difference; relative second mode shape difference and relative third mode shape difference. The outputs from the fuzzy controller are relative crack depth and relative crack location. Several hundred fuzzy rules are outlined to train the fuzzy controller. Twenty numbers of the fuzzy rules out of several hundred fuzzy rules are being listed in Table 4.3.2.

4.3.3 Results of Fuzzy Controller

In the current research the fuzzy controller is designed with three types of membership functions i.e triangular (Fig. 4.3.1), gaussian (Fig. 4.3.2) and trapezoidal (Fig. 4.3.3). Fig.4.3.4 shows the defuzzyfication of triangular membership function fuzzy controller results when the rule-1 and rule-19 are activated from Table 4.3.2. Fig.4.3.5 shows the defuzzyfication of Gaussian membership function fuzzy controller results when the rule-1 and rule-19 are activated from Table 4.3.2. Fig. 4.3.6 shows the defuzzyfication of trapezoidal membership function fuzzy controller results when the rule-1 and rule-19 are activated from Table 4.3.2. Table 4.3.3 presents the comparison of results between triangular, Gaussian and trapezoidal fuzzy controller, numerical analysis and experimental analysis. In this table ten sets of inputs out of several hundred sets are taken. Corresponding ten set of outputs through the fuzzy controller, numerical analysis and experimental analysis are depicted in the same table. In the Table 4.3.3 the first column represents the relative first natural frequency (fnf), the second column represents the relative of second natural frequency (snf), the third column represents the relative of third natural frequency (tnf), the fourth column represents the relative first mode shape difference (fmd), the fifth column represents the relative second mode shape difference (smd), the sixth column represents the relative third mode shape difference (tmd) as inputs ,the seventh column presents the outputs relative crack location(rcl), relative crack depth(rcd) from the triangular membership function fuzzy controller, the eighth column presents the outputs, relative crack location(rcl), relative crack depth(rcd) from the gaussian membership function fuzzy controller ,the ninth column presents the outputs, relative crack location(rcl), relative crack depth(rcd) from the trapezoidal membership function fuzzy controller, the tenth column presents the outputs, relative crack location(rcl), relative crack depth(rcd) from the numerical analysis and the

eleventh column presents the outputs, relative crack location(rcl), relative crack depth(rcd) from the experimental analysis.

4.4 Discussions

In this chapter fuzzy controller has been addressed for prediction of crack location and crack depth. Three types of membership functions such as triangular function (Fig. 4.2.1(a)), gaussian function (Fig. 4.2.1(b)) and trapezoidal function (Fig. 4.2.1(c)) have been used for designing the fuzzy controllers. The working principle for the fuzzy controller has been depicted in Fig. 4.2.2. The complete architecture of triangular, Gaussian and trapezoidal fuzzy controller are presented in Fig. 4.3.1, Fig. 4.3.2 and Fig. 4.3.3 respectively. The linguistic terms of the fuzzy membership function have been given in Table 4.3.1. Table 4.3.2 gives twenty sets of the fuzzy rules sets being used for the fuzzy controller. Fig. 4.3.4 to Fig. 4.3.6 exhibits the fuzzy results after defuzzification when rule 1 and 19 of the Table 4.3.2 are activated for triangular, gaussian, trapezoidal membership functions respectively. Table 4.3.3 gives the comparison of the results obtained from numerical, experimental, fuzzy controller with triangular membership function, fuzzy controller with gaussian membership function and fuzzy controller with trapezoidal membership function. During comparison a good agreement is seen between the results. It is evident from the Table 4.3.3 that the average percentage deviation of the results of the triangular membership function fuzzy controller is 2.9%, for gaussian membership function fuzzy controller is 0.9% and for trapezoidal membership function fuzzy controller is 1.5%.

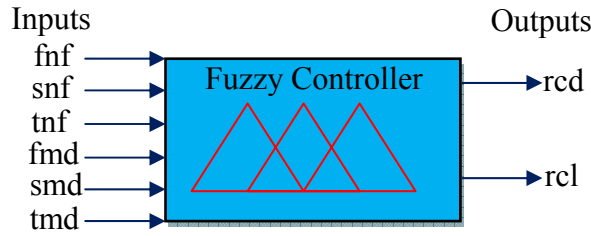


Fig. 4.3.1(a) Triangular fuzzy controller

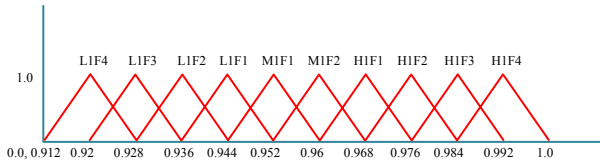


Fig. 4.3.1(b1) Triangular membership functions for relative natural frequency for first mode of vibration

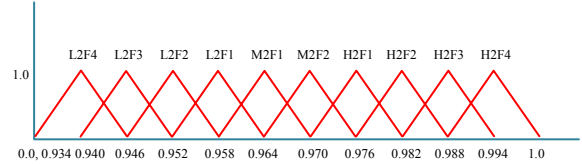


Fig. 4.3.1(b2) Triangular membership functions for relative natural frequency for second mode of vibration

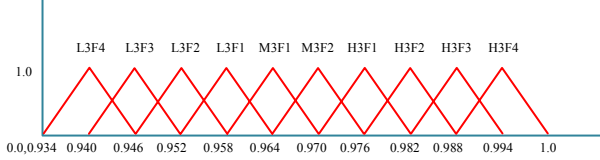


Fig. 4.3.1(b3) Triangular membership functions for relative natural frequency for third mode of vibration

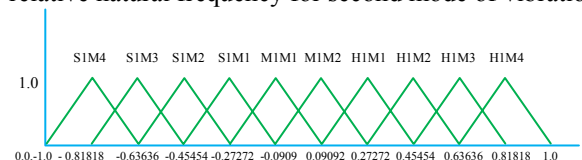


Fig. 4.3.1(b4) Triangular membership functions for relative mode shape difference for first mode of vibration

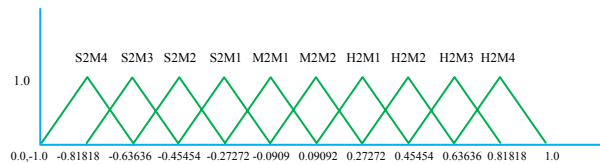


Fig. 4.3.1(b5) Triangular membership functions for relative mode shape difference for second mode of vibration

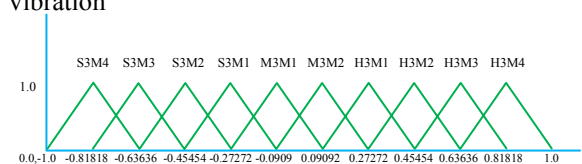


Fig. 4.3.1(b6) Triangular membership functions for relative mode shape difference for third mode of vibration

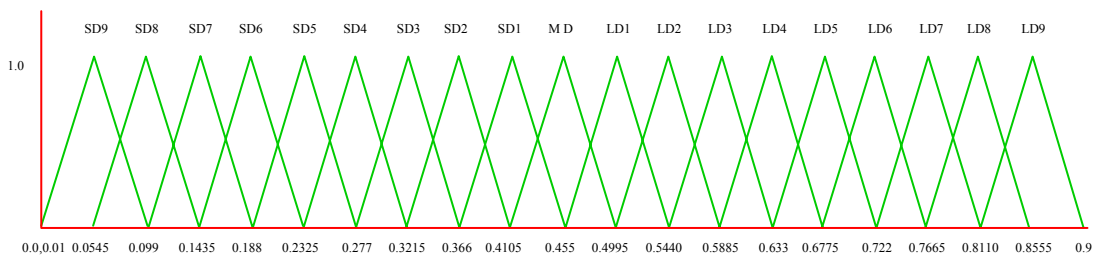


Fig. 4.3.1(b7) Triangular membership functions for relative crack depth

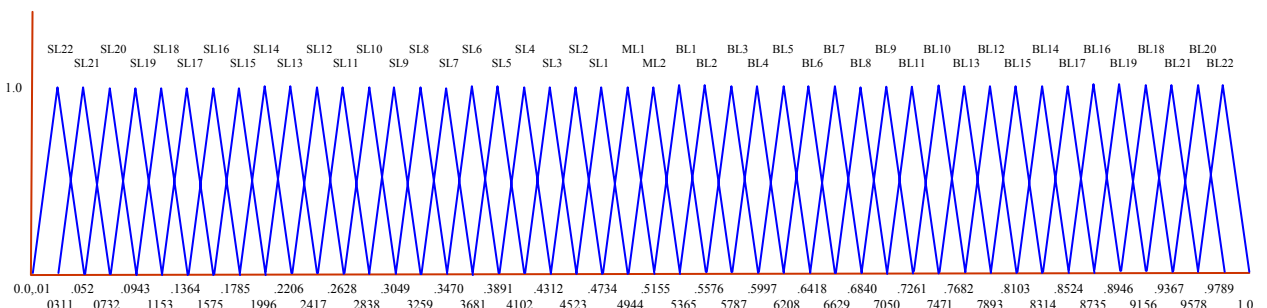


Fig. 4.3.1(b8) Triangular membership functions for relative crack location

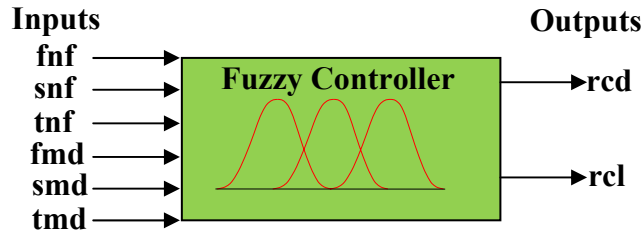


Fig. 4.3.2(a) Gaussian fuzzy controller

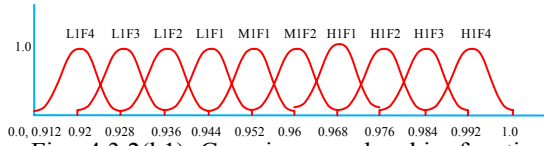


Fig. 4.3.2(b1) Gaussian membership functions for relative natural frequency for first mode of vibration

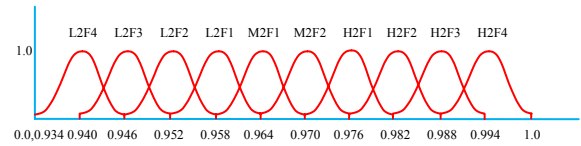


Fig. 4.3.2(b2) Gaussian membership functions for relative natural frequency for second mode of vibration

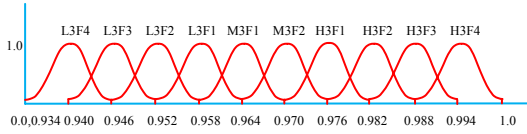


Fig. 4.3.2(b3) Gaussian membership functions for relative natural frequency for third mode of vibration

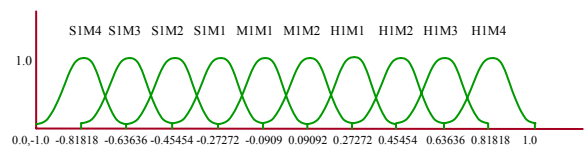


Fig. 4.3.2(b4) Gaussian membership functions for relative mode shape difference for first mode of vibration

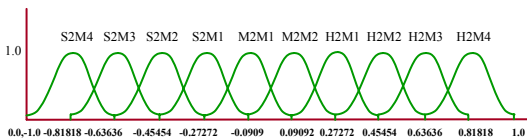


Fig. 4.3.2(b5) Gaussian membership functions for relative mode shape difference for second mode of vibration

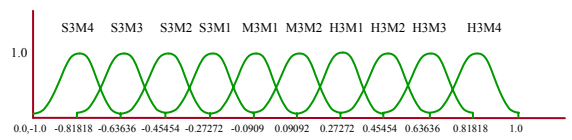


Fig. 4.3.2(b6). Gaussian membership functions for relative mode shape difference for third mode of vibration

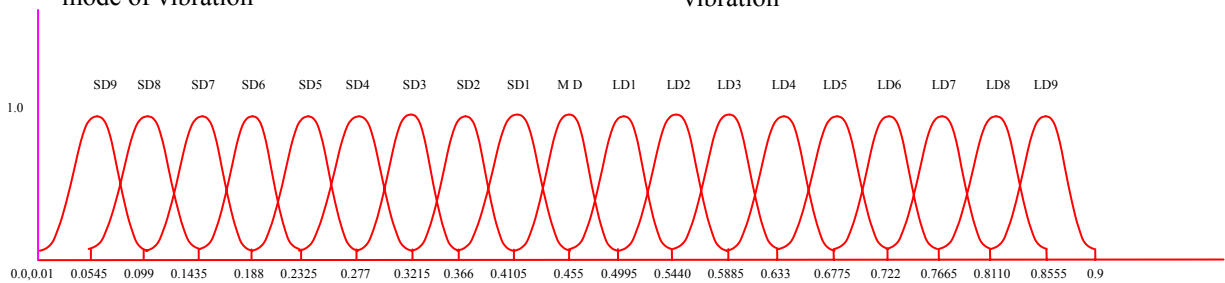


Fig. 4.3.2(b7) Gaussian membership functions for relative crack depth

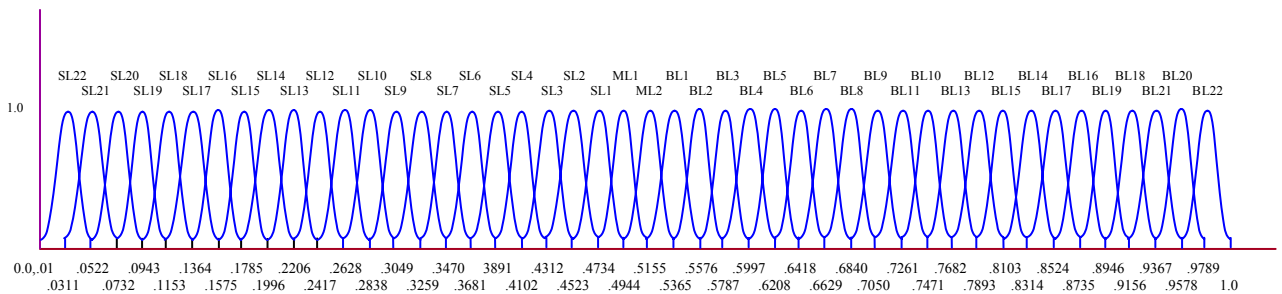


Fig. 4.3.2(b8.) Gaussian membership functions for relative crack location

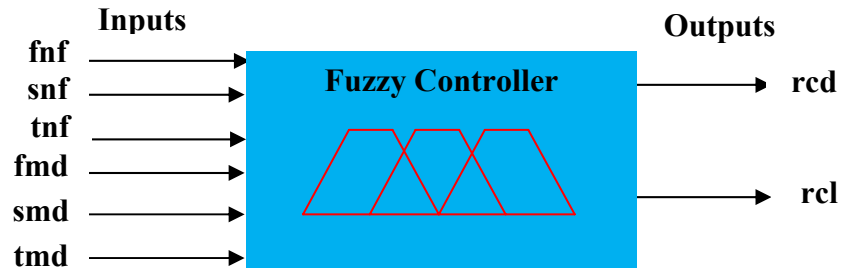


Fig. 4.3.3(a) Trapezoidal fuzzy controller.

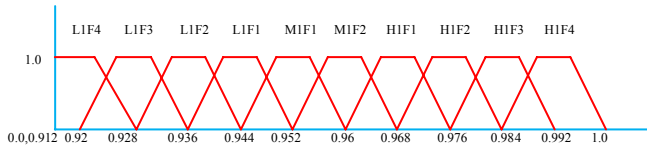


Fig. 4.3.3(b1) Trapezoidal membership functions for relative natural frequency for first mode of vibration.

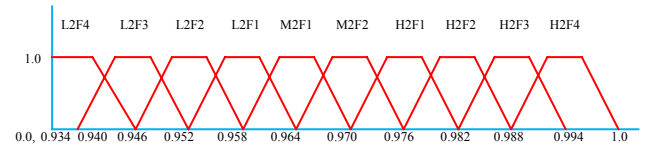


Fig. 4.3.3 (b2) Trapezoidal Membership functions for relative natural frequency for second mode of vibration.

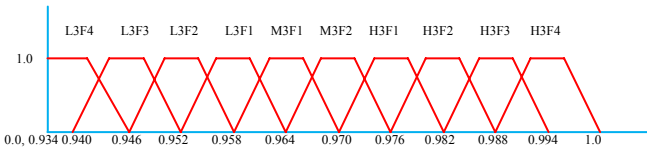


Fig. 4.3.3 (b3) Trapezoidal membership functions for relative natural frequency for third mode of vibration.

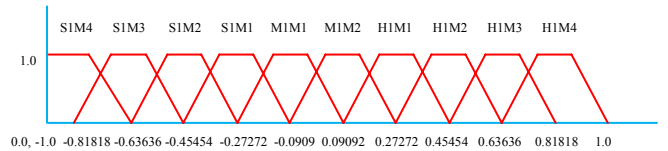


Fig. 4.3.3 (b4) Trapezoidal membership functions for relative mode shape difference for first mode of vibration.

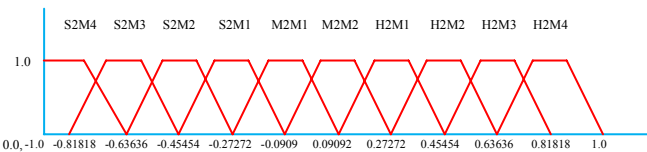


Fig. 4.3.3 (b5) Trapezoidal membership functions for relative mode shape difference for second mode of vibration.

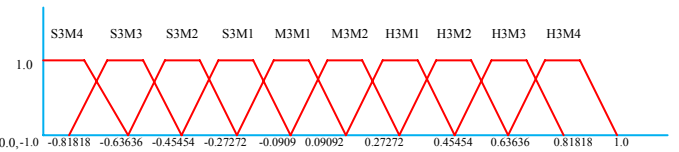


Fig. 4.3.3 (b6) Trapezoidal membership functions for relative mode shape difference for third mode of vibration.

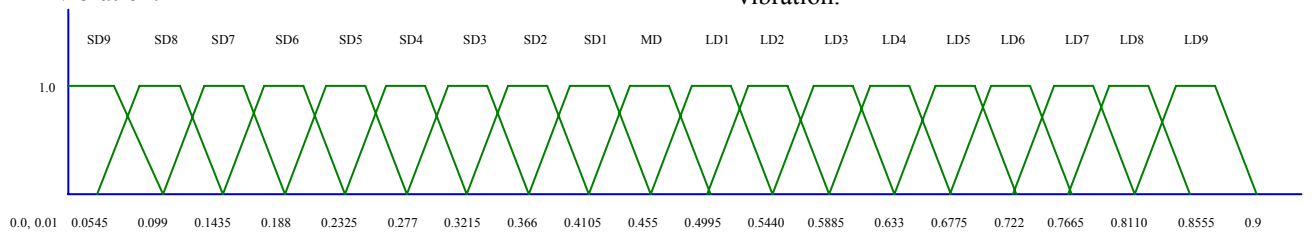


Fig. 4.3.3 (b7) Trapezoidal membership functions for relative crack depth.

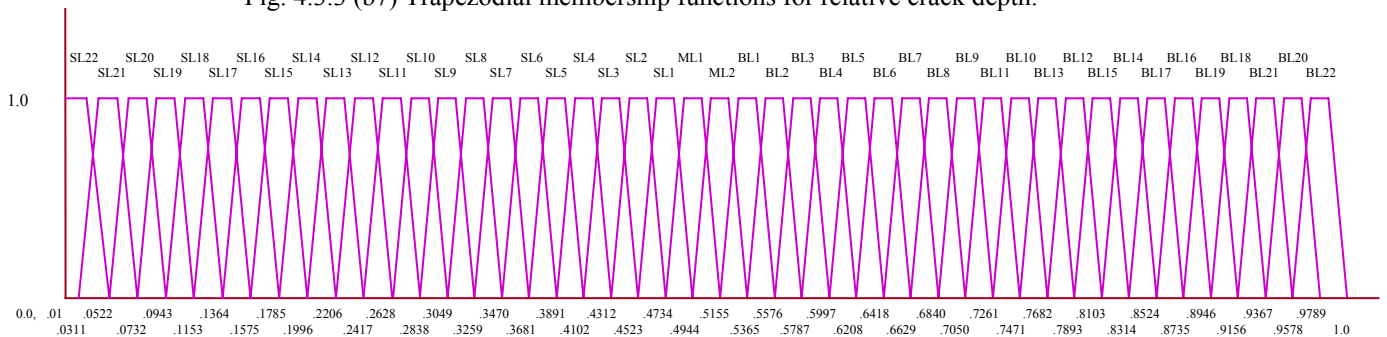


Fig. 4.3.3 (b8) Trapezoidal membership functions for relative crack location.

Memberships Function Name	Linguistic Terms	Description and range of the Linguistic terms
L1F1,L1F2,L1F3,L1F4	fnf _{1 to 4}	Low ranges of relative natural frequency for first mode of vibration in descending order respectively
M1F1,M1F2	fnf _{5,6}	Medium ranges of relative natural frequency for first mode of vibration in ascending order respectively
H1F1,H1F2,H1F3,H1F4	fnf _{7 to 10}	Higher ranges of relative natural frequency for first mode of vibration in ascending order respectively
L2F1,L2F2,L2F3,L2F4	snf _{1 to 4}	Low ranges of relative natural frequency for second mode of vibration in descending order respectively
M2F1,M2F2	snf _{5,6}	Medium ranges of relative natural frequency for second mode of vibration in ascending order respectively
H2F1,H2F2,H2F3,H2F4	snf _{7 to 10}	Higher ranges of relative natural frequencies for second mode of vibration in ascending order respectively
L3F1,L3F2,L3F3,L3F4	tnf _{1 to 4}	Low ranges of relative natural frequencies for third mode of vibration in descending order respectively
M3F1,M3F2	tnf _{5,6}	Medium ranges of relative natural frequencies for third mode of vibration in ascending order respectively
H3F1,H3F2,H3F3,H3F4	tnf _{7 to 10}	Higher ranges of relative natural frequencies for third mode of vibration in ascending order respectively
S1M1,S1M2,S1M3,S1M4	fmd _{1 to 4}	Small ranges of first relative mode shape difference in descending order respectively
M1M1,M1M2	fmd _{5,6}	medium ranges of first relative mode shape difference in ascending order respectively
H1M1,H1M2,H1M3,H1M4	fmd _{7 to 10}	Higher ranges of first relative mode shape difference in ascending order respectively
S2M1,S2M2,S2M3,S2M4	smd _{1 to 4}	Small ranges of second relative mode shape difference in descending order respectively
M2M1,M2M2	smd _{5,6}	medium ranges of second relative mode shape difference in ascending order respectively
H2M1,H2M2,H2M3,H2M4	smd _{7 to 10}	Higher ranges of second relative mode shape difference in ascending order respectively
S3M1,S3M2,S3M3,S3M4	tmd _{1 to 4}	Small ranges of third relative mode shape difference in descending order respectively
M3M1,M3M2	tmd _{5,6}	medium ranges of third relative mode shape difference in ascending order respectively
H3M1,H3M2,H3M3,H3M4	tmd _{7 to 10}	Higher ranges of third relative mode shape difference in ascending order respectively
SL1,SL2.....SL22	rcl _{1 to 22}	Small ranges of relative crack location in descending order respectively
ML1,ML2	rcl _{23,24}	Medium ranges of relative crack location in ascending order respectively
BL1,BL2.....BL22	rcl _{25 to 46}	Bigger ranges of relative crack location in ascending order respectively
SD1,SD2.....SD9	rcd _{1 to 9}	Small ranges of relative crack depth in descending order respectively
MD	rcd ₁₀	Medium relative crack depth
LD1,LD2.....LD9	rcd _{11 to 19}	Larger ranges of relative crack depth in ascending order respectively

Table 4.3.1 Description of fuzzy linguistic terms

Sl.No.	Examples of some rules used in the fuzzy controller
1	If fnf is H1F3,snf is H2F4,tnf is H3F1,fmd is H1M3,smd is H2M3,tmd is H3M3, then rcd is SD8,and rcl is SL22
2	If fnf is H1F3,snf is H2F3,tnf is H3F1,fmd is H1M3,smd is H2M3,tmd is H3M3, then rcd is SD8,and rcl is SL22
3	If fnf is H1F1,snf is M2F1,tnf is L3F2,fmd is H1M4,smd is H2M4,tmd is H3M4, then rcd is MD,and rcl is SL22
4	If fnf is M1F1,snf is L2F2,tnf is L3F2,fmd is H1M4,smd is H2M4,tmd is H3M4, then rcd is LD5,and rcl is SL22
5	If fnf is H1F1,snf is M2F1,tnf is L3F1,fmd is H1M3,smd is H2M3,tmd is H3M3, then rcd is LD1,and rcl is SL21
6	If fnf is M1F1,snf is L2F1,tnf is L3F2,fmd is H1M4,smd is H2M3,tmd is H3M4, then rcd is LD6,and rcl is SL21
7	If fnf is H1F2,snf is M2F2,tnf is M3F2,fmd is H1M3,smd is H2M3,tmd is H3M9, then rcd is SD1,and rcl is SL20
8	If fnf is H1F3,snf is H2F4,tnf is H3F2,fmd is H1M2,smd is H2M1,tmd is H3M2, then rcd is SD7,and rcl is SL19
9	If fnf is H1F1,snf is M2F2,tnf is H3F2,fmd is H1M2,smd is H2M2,tmd is H3M2, then rcd is LD2,and rcl is SL18
10	If fnf is H1F3,snf is H2F4,tnf is H3F3,fmd is S1M1,smd is S2M1,tmd is S3M1, then rcd is SD3,and rcl is SL17
11	If fnf is H1F1,snf is H2F3,tnf is H3F2,fmd is H1M2,smd is H2M1,tmd is H3M1, then rcd is LD2,and rcl is SL16
12	If fnf is H1F2,snf is H2F4,tnf is H3F2,fmd is H1M2,smd is M2M2,tmd is H3M2, then rcd is LD1,and rcl is SL15
13	If fnf is H1F2,snf is H2F4,tnf is H3F1,fmd is H1M2,smd is M2M2,tmd is H3M2, then rcd is MD,and rcl is SL14
14	If fnf is H1F1,snf is H2F4,tnf is M3F1,fmd is H1M2,smd is M2M2,tmd is H3M3, then rcd is LD4,and rcl is SL13
15	If fnf is H1F2,snf is H2F4,tnf is L3F1,fmd is H1M2,smd is M2M1,tmd is H3M3, then rcd is LD3,and rcl is SL12
16	If fnf is H1F3,snf is H2F4,tnf is M3F1,fmd is H1M2,smd is H2M1,tmd is H3M3, then rcd is SD2,and rcl is SL10
17	If fnf is M1F1,snf is M2F2,tnf is L3F3,fmd is H1M2,smd is H2M2,tmd is H3M3, then rcd is LD9,and rcl is SL9
18	If fnf is M1F2,snf is M2F1,tnf is L3F3,fmd is H1M2,smd is H2M2,tmd is H3M3, then rcd is LD9,and rcl is SL7
19	If fnf is H1F4,snf is H2F4,tnf is H3F1,fmd is H1M3,smd is H2M3,tmd is H3M3, then rcd is SD9,and rcl is SL21
20	If fnf is H1F4,snf is H2F3,tnf is M3F2,fmd is M1M1,smd is H2M2,tmd is H3M3, then rcd is SD4,and rcl is BL7

Table 4.3.2 Examples of twenty fuzzy rules being used in fuzzy controller

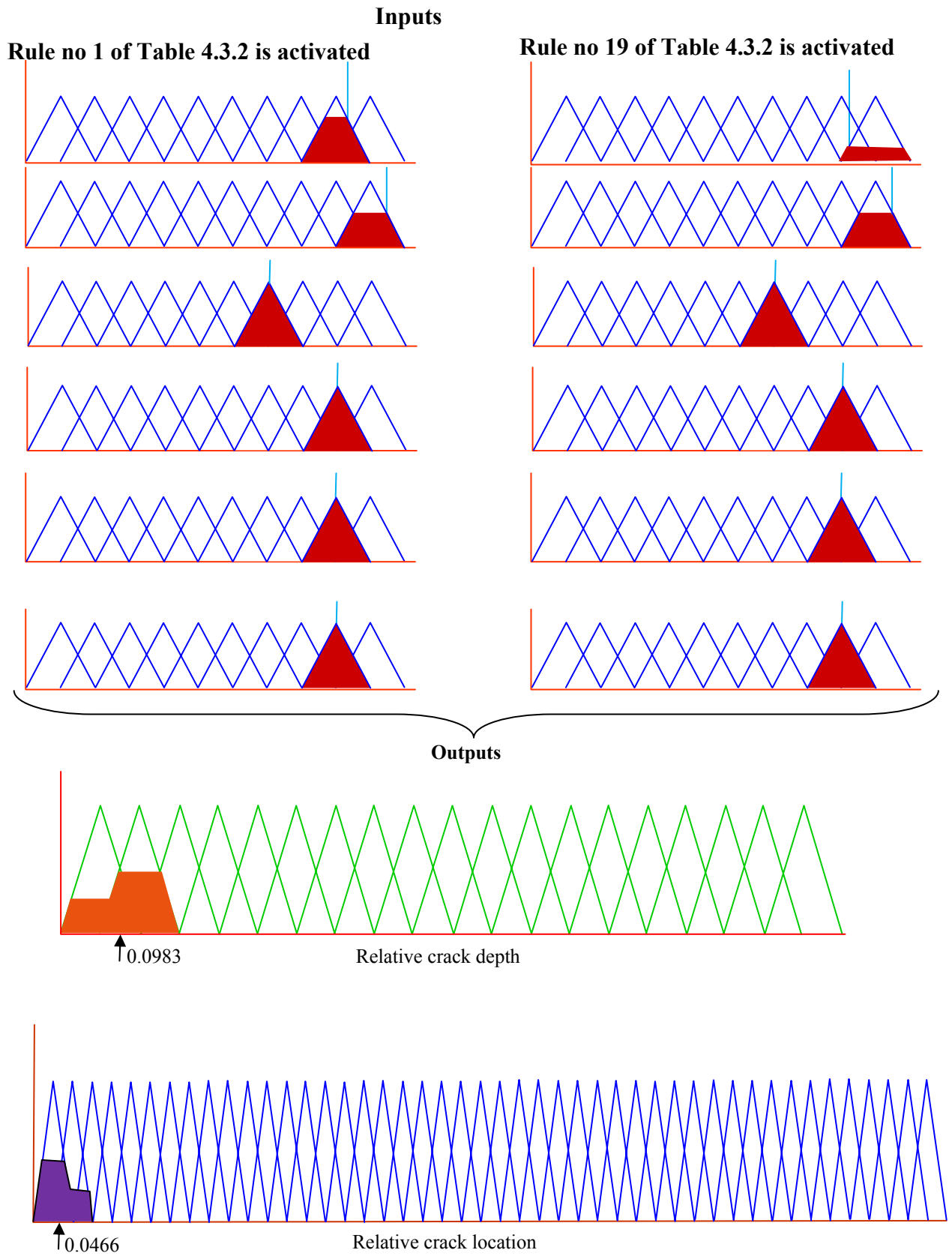


Fig.4.3.4 Resultant values of relative crack depth and relative crack location from triangular fuzzy controller when Rules 1 and 19 of Table 4.3.2 are activated

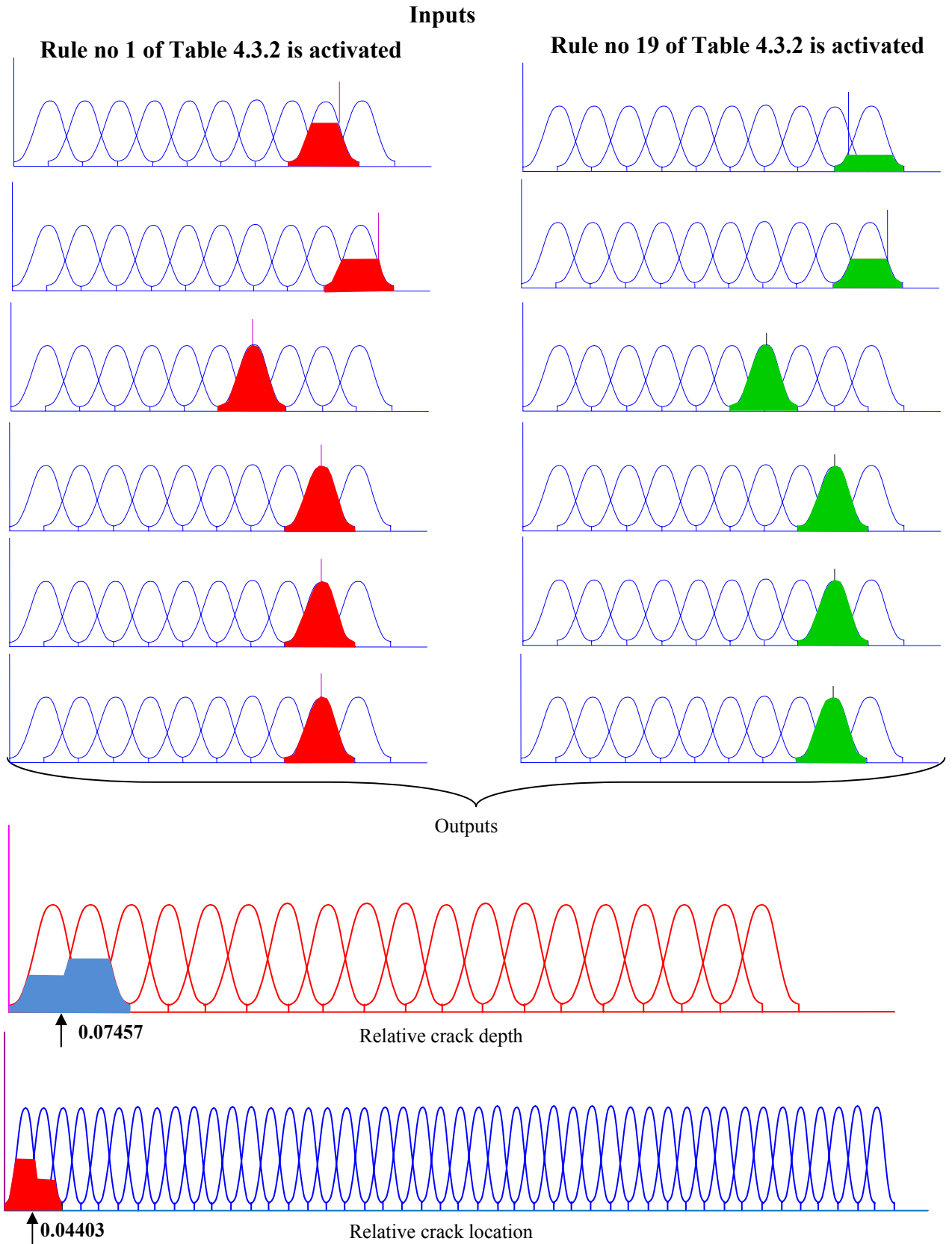


Fig. 4.3.5 Resultant values of relative crack depth and relative crack location from gaussian fuzzy controller when Rules 1 and 19 of Table 4.3.2 are activated

Inputs

Rule no 1 of Table 4.3.2 is activated

Rule no 19 of Table 4.3.2 is activated

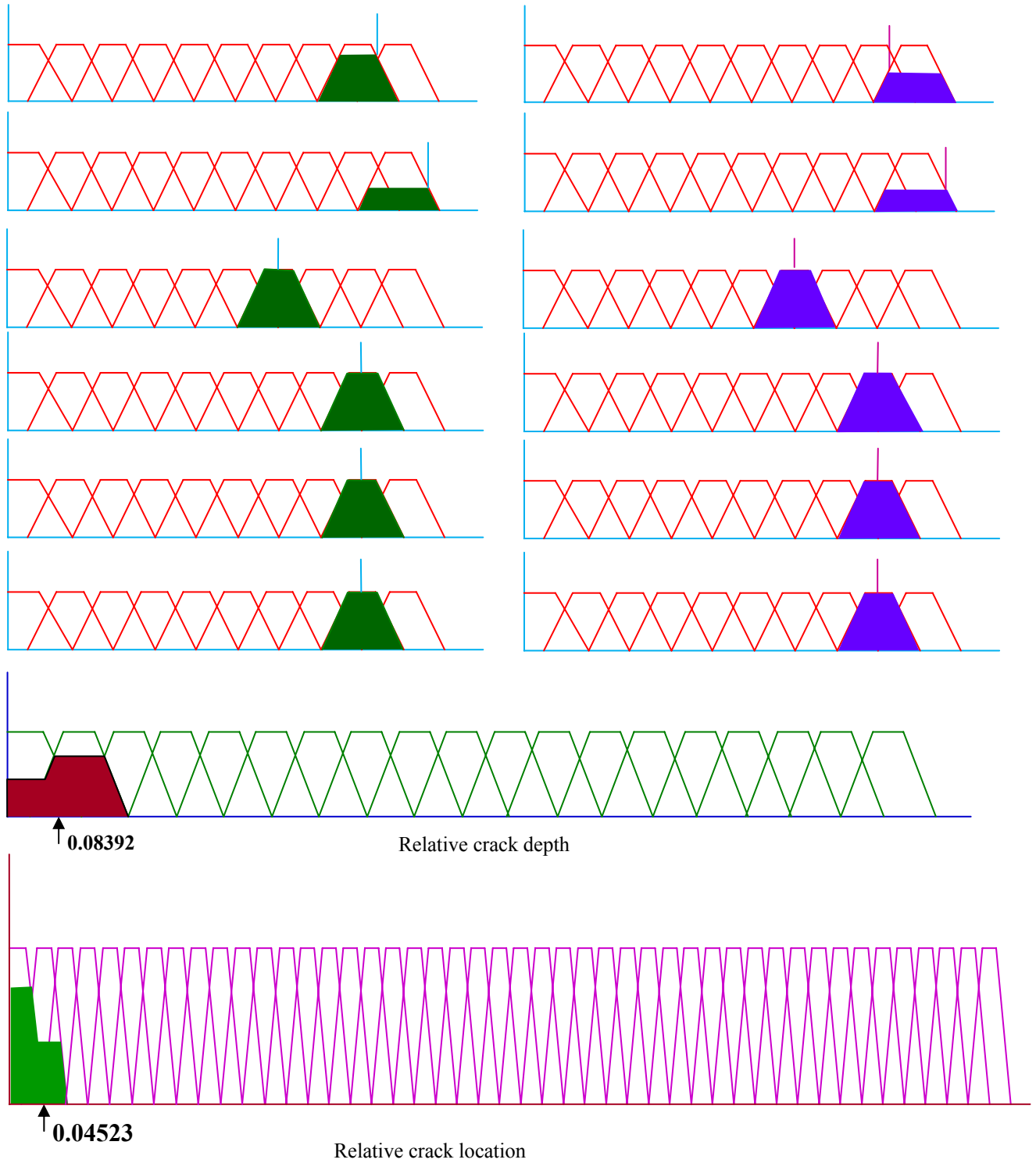


Fig. 4.3.6 Resultant values of relative crack depth and relative crack location from trapezoidal fuzzy controller when Rules 1 and 19 of Table 4.3.2 are activated.

Relative first natural frequency “fnf”	Relative second natural frequency “snf”	Relative third natural frequency “tnf”	Relative first mode shape difference “fmd”	Relative second mode shape difference “smd”	Relative third mode shape difference “tmd”	Triangular Fuzzy Controller (relative crack depth “rcd” and location “rel”)		Gaussian Fuzzy Controller (relative crack depth “rcd” and location “rel”)		Trapezoidal Fuzzy Controller (relative crack depth “rcd” and location “rel”)		Numerical (relative crack depth “rcd” and location “rel”)		Experimental (relative crack depth “rcd” and location “rel”)	
						rcd	rel	rcd	rel	rcd	rel	rcd	rel	rcd	rel
0.9848	0.9958	0.9975	0.2709	0.2372	0.3158	0.202	0.07163	0.203	0.07138	0.202	0.07163	0.202	0.06888	0.205	0.07250
0.9673	0.9874	0.9943	0.3969	0.3247	0.3923	0.441	0.08238	0.431	0.08138	0.441	0.08238	0.427	0.07900	0.43	0.08388
0.9623	0.9948	0.9983	0.1814	0.0279	0.0774	0.557	0.15825	0.548	0.15913	0.557	0.15825	0.537	0.15988	0.568	0.15750
0.9756	0.9976	0.9972	0.1383	-0.0823	0.1898	0.382	0.18475	0.389	0.18725	0.382	0.18475	0.394	0.18675	0.391	0.18775
0.9852	0.9984	0.9967	0.01	-0.8678	0.2572	0.229	0.23613	0.227	0.23688	0.229	0.23613	0.231	0.23625	0.23	0.24000
0.9723	0.9961	0.9818	0.1947	0.0672	0.4105	0.545	0.27625	0.552	0.28375	0.545	0.27625	0.556	0.28250	0.545	0.28625
0.9823	0.9872	0.9919	0.0726	0.2567	0.3994	0.446	0.40338	0.449	0.40438	0.446	0.40338	0.451	0.40388	0.447	0.40513
0.981	0.9809	0.9931	0.0898	0.3154	0.392	0.498	0.42263	0.495	0.42363	0.498	0.42263	0.497	0.42388	0.495	0.42350
0.986	0.9842	0.9988	-0.032	0.322	0.3965	0.428	0.50363	0.425	0.50188	0.428	0.50363	0.426	0.50125	0.425	0.50375
0.9834	0.9685	0.9974	0.038	0.4558	0.3507	0.534	0.53538	0.537	0.53313	0.534	0.53538	0.542	0.53500	0.535	0.53313

Table 4.3.3 Comparison of results between triangular, gaussian and trapezoidal fuzzy controller, numerical analysis and experimental analysis

4.5 Summary

From the above analyses and discussions, the conclusions drawn are depicted as follows. Crack depth and crack location have got effect on mode shapes and natural frequencies of the vibrating structures. The fuzzy controllers developed here take natural frequencies and mode shape differences for prediction of crack location and crack depth. The predicted results from fuzzy controllers for crack location and crack depth are compared with the theoretical and experimental results for cross verification. They show a very good agreement. The result of gaussian membership function fuzzy controller is more accurate in comparison to other two controllers. The developed fuzzy controller along with the methodology can be used as a robust tool for fault detection in cracked structures.

Publications

- Das H.C. and Parhi D.R., Damage Analysis of Cracked Structure Using Fuzzy Control Technique, *International Journal of Acoustics and Vibration*, 13(2) , 2008 , 3-14.
- Parhi D.R. and Das H.C., Structural damage detection by fuzzy- gaussian technique, *International Journal of Applied Mathematics and Mechanics*, 4(2), 2008, 39-59.
- Das H.C. and Parhi D.R., Identification of Crack Location and Intensity in a Cracked Beam by Fuzzy Reasoning, *International Journal of Intelligent Systems Technologies and Applications* (In Press).
- Das H.C. and Parhi D.R., Online fuzzy logic crack detection of a cantilever beam, *International Journal of Knowledge-Based and Intelligent Engineering Systems*, 12(2), 2008, 157-171.
- Parhi D.R. and Das H.C. Smart crack detection of a beam using fuzzy logic controller, *International Journal of Computational Intelligence: Theory and Practice*, 3(1), 2008, 9-21.
- Das H.C. and Parhi D.R., Detection of crack in cantilever structures using fuzzy-gaussian interface technique, *American Institute of Aeronautics and astronautics journal*, 47(1), 2009, 105-115.

Chapter 5

ANALYSIS OF ARTIFICIAL NEURAL NETWORK FOR CRACK DETECTION

Engineering structures used in wide range of civil, mechanical and aeronautical fields are prone to damage such as crack formation and deterioration during their service period. An effective and reliable structural crack detection methodology can be a useful tool for timely determination of damage and deterioration in structural members. Crack detection methodologies attempt to determine whether structural damage has occurred, as well as the location and extent of any such damage. The information obtained by crack detection methodology can play a vital role in the development of economical repair and retrofit programmes. Crack can be detected and quantified by on-line crack detection techniques using vibration-based analysis data in the service life of a structure. The effects of crack on a structure changes the natural frequencies and mode shapes. Hence, crack can be detected using artificial intelligence technique from dynamic analysis using natural frequencies and mode shapes. This chapter presents on-line diagnostic technology for crack detection in terms of crack location and its intensity in elastic structures using artificial neural network technique. An intelligent controller has been proposed in this chapter using feed forward multilayer neural network trained by back-propagation algorithm for crack diagnosis. The results of the developed neural controller are compared with experimental results, which are satisfactory and show a very good agreement.

5.1 Introduction

Artificial Neural Networks (ANN) [184,189] are relatively crude electronic models based on the neural structure of the brain. The field goes by many names, such as connectionism, parallel distributed processing, neurocomputing, natural intelligent systems, machine learning algorithms, and artificial neural networks. According to [189] “A neural network is a massively parallel distributed processor made up of simple processing units, called neurons, which have a natural tendency for storing experiential knowledge and making it available for

use". This knowledge is acquired from the environment through a learning process and is stored in connections between the neurons, known as synaptic weights.

Generalization ability: Generalization [189] refers to the neural network producing reasonable outputs for inputs not encountered during training (learning). This information-processing capability makes it possible for neural networks to solve complex (large-scale) problems that are currently intractable.

Non-linearity: Artificial neural networks can be used even for non-linear problems [175,180] as the interconnected neurons can be either linear or non-linear. This feature is extremely important in the field of structural health monitoring as the signals from complex structures under variable loading may be non-linear.

Input-Output mapping: This is the most powerful feature of the neural network which involves supervised learning. The network tries to correlate a unique input signal with a desired response. It modifies the synaptic weights by a learning process in order to achieve the desired response. Training the network involves feeding the network with a set of input signals and the corresponding desired response.

Adaptivity: Neural networks adapt easily to changes in the environment, by adjusting the synaptic weight accordingly on retraining the system. Real-time networks which are capable of changing its synaptic weights automatically can be designed for non-stationary environmental conditions.

Evidential response: For pattern classification purposes, networks can be designed to provide information about the pattern to be selected, as well as the confidence of the decision made. This helps in rejecting indistinct patterns, thereby improving the classification performance of the network.

Contextual information: Related information is dealt naturally by the network as the knowledge is represented by the very structure and activation state of the network.

Fault tolerance: Neural networks are inherently fault tolerant. If the neural networks are implemented in hardware form, and if a neuron or a connecting link is damaged, then only the output quality deteriorates [189] rather than the system failing completely.

Over the past few years researchers around the globe have been focusing their attention towards the development of real-time structural health monitoring systems. This field is of paramount importance especially with the structures that are prone to in-service defects. This necessitates the need for an online structural health monitoring system, which is capable of determining the presence of the damage such as crack (in the incipient stage itself), determining the location of the damage and the size of the damage. Various non-destructive techniques which are capable of achieving the goal have been discovered. For complex situations (variable loading, variable damage level, and variable type of damage) using complex structures the response signal obtained from the sensors (damage signature vector) will be complicated. This makes it difficult to decode the signal to determine the damage location and damage. Moreover, it is also difficult or impossible to create accurate mathematical models for complex structures due to both geometric and material property non-linearity. This is where the role of Artificial Neural Networks is of utmost importance.

The following features of neural networks make it an effective tool in structural health monitoring. Scores of researchers have documented the use of artificial neural networks in tandem with existing non-destructive testing techniques for the purpose of structural health monitoring. Fang et al. [208] in their research have explored the structural damage detection using frequency response functions (FRFs) as input data to the back-propagation neural network (BPNN). Their analysis results on a cantilevered beam show that, in damage cases the neural network can assess damage conditions with very good accuracy. Rajakarunakaran et al. [210] in their paper have presented the development of artificial neural network-based model for the fault detection of centrifugal pumping system. The fault detection model is developed by using two different artificial neural network approaches, namely feed forward network with back propagation algorithm and binary adaptive resonance network (ART1). They have tested the performance of the developed back propagation and ART1 model for a total of seven categories of faults in the centrifugal pumping system.

In this chapter an on-line crack detection methodology has been proposed using feed forward multilayer neural network trained by back-propagation algorithm. The artificial neural network controller is designed and is used to detect the relative crack location and relative crack depth. The developed neural network controller has six inputs and two outputs. The inputs to the designed neural network controller are relative first three natural frequencies and relative first three mode shape differences and the out puts are relative crack location and relative crack depth. This chapter describes the application of neural network technique for on-line crack detection. The results of the developed neural network controller have been compared with the results of fuzzy controller and numerical method and found to be most accurate. Hence it is concluded that the developed method can be more accurately applied for crack detection. The developed neural network controller has been authenticated by experiments.

This chapter is outlined into six sections following the introduction; the neural network technology and its importance in the field of structural health monitoring along with multi-layer perceptron architecture trained by back-propagation algorithm is described in section 5.2. The chapter 5.3 presents the analysis of neural network controller design for crack detection and corresponding results are discussed. In section 5.4, the results of the neural network controller are compared with the results of fuzzy controller, experimental and numerical analysis to demonstrate the superiority of the proposed methodology and finally the discussions and summary are described in section 5.5 and 5.6.

5.2 Neural Network Technique

The field of neural network technique can be thought of as being related to artificial intelligence, machine learning, fault detection, parallel processing, statistics, and other fields. The attraction of neural networks is that they are best suited to solve the problems that are the most difficult to solve by traditional computational methods.

5.2.1 Design of Neural Network

A neural network is a massively parallel distributed processor that has a natural propensity for storing experimental knowledge and making it available for further use. It resembles the brain in two respects:

1. Knowledge is acquired by the network through a learning process.
2. Interneuron connection strengths known as synaptic weights and are used to store the knowledge.

The procedure used to perform the learning process is called a learning algorithm, the function of which is to modify the synaptic weights of the network in an orderly fashion so as to attain a desired design objective. In neural network a neuron is an information processing unit. Fig.5.2.1 shows the model of a neuron. A neuron model can be identified by three basic elements, which is described below.

- i) A set of synapses or connecting links, each of which is characterized by a weight or strength of its own. Specifically, a signal x_j at the input of synapse j connected to neuron k is multiplied by the synaptic weight w_{kj} . In the synaptic weight w_{kj} the subscript refers to the neuron in question and the second subscript refers to the input end of the synapse to which the weight refers.
- ii). An adder for summing the input signals, weighted by the respective synapses of the neuron.
- iii). An activation function for limiting the amplitude of the output of a neuron. Generally the normalised amplitude range of the output of a neuron is given as the closed unit interval $[0,1]$ or alternatively $[-1,1]$.

In mathematical terms, we can describe a neuron k by writing the following pair of equations:

$$u_k = \sum_{j=1}^p w_{kj} x_j \quad (5.2.1)$$

$$y_k = f(u_k) \quad (5.2.2)$$

Where x_1, x_2, \dots, x_p are the input signals; $w_{k1}, w_{k2}, \dots, w_{kp}$ are the synaptic weights of neuron k ; u_k is the linear combiner output; $f(\cdot)$ is the activation function; and y_k is the output signal of the neuron.

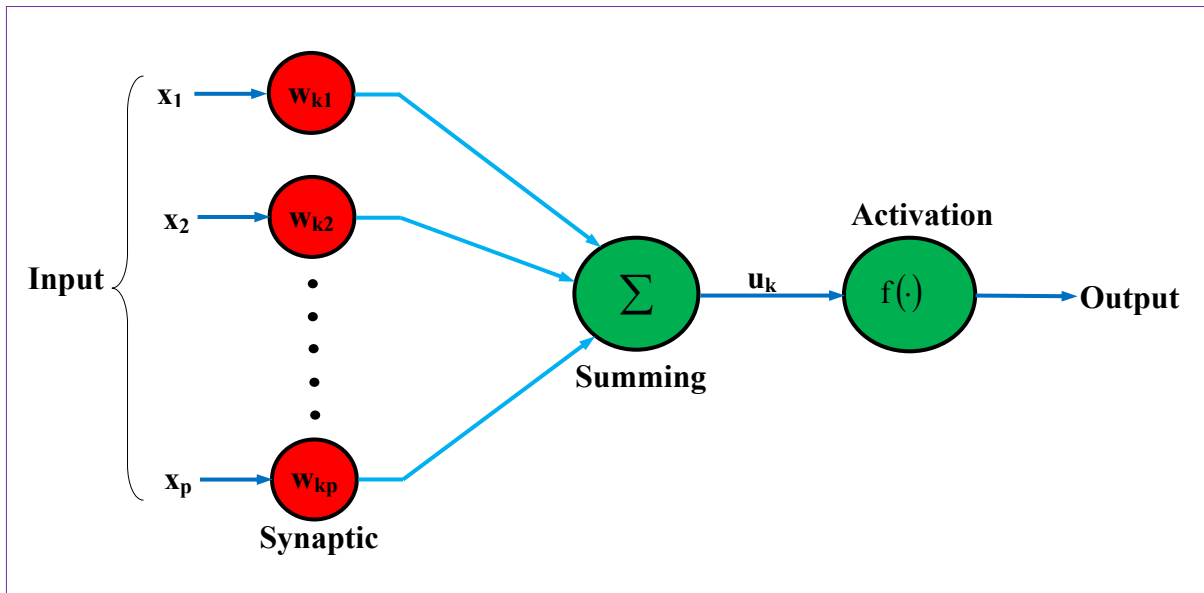


Fig. 5.2.1 Model of a neuron

The use of neural networks in various fields offers the following useful properties due to which it can be applied to many fields.

- In a neural network modification of the synaptic weights can be done by a set of training samples (i.e. supervised learning). For this, a training set will be presented to the neural network for training and the synaptic weights of the network are modified so as to minimise the difference between the desired response and the actual response.
- Neural networks have a built-in capability to adapt their synaptic weights in the surrounding environment. In particular, a neural network trained to operate in a specific environment can deal with minor changes in the operating environmental conditions.
- A neural network implemented has the potential to be inherently fault tolerant in the sense that its performance is degraded gracefully under adverse operating conditions.

5.2.2 Activation Function

The activation function, denoted by $f(\cdot)$, defines the output of a neuron in terms of the activity level at its input. Generally three types of activation functions are used (e.g.

Threshold Activation Function, Ramping Activation Function, Hyperbolic tangent Activation function).

5.2.2.1 Threshold Activation Function

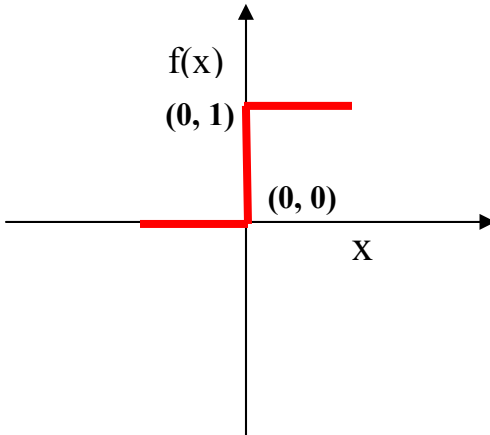


Fig.5.2.2 Threshold activation function

The Threshold Activation Function is shown in Fig.5.2.2. This function limits the output of the neuron to either 0, if the net input argument x is less than zero; or 1, if x is greater than or equal to zero.

Mathematically the Threshold Activation Function can be described as:

$$f(x) = \begin{cases} 1 & \text{if } x \geq 0 \\ 0 & \text{if } x < 0 \end{cases} \quad (5.2.3)$$

5.2.2.2 Ramping Activation Function

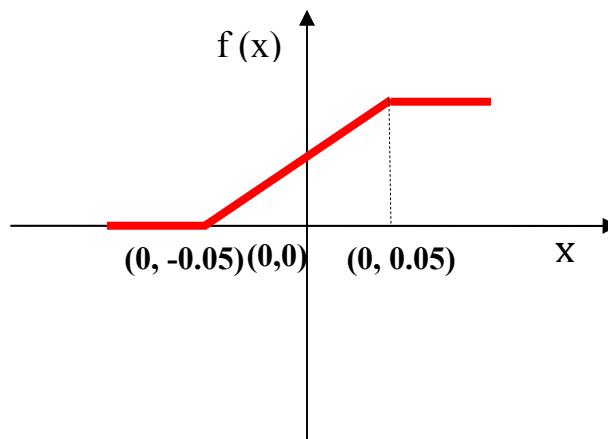


Fig.5.2.3 Ramping activation function

The Ramping Activation Function is shown in Fig.5.2.3.

Mathematically the Ramping Activation Function can be described as:

$$f(x) = \begin{cases} 1 & \text{if } x \geq \frac{1}{2} \\ x & \text{if } \frac{1}{2} > x > -\frac{1}{2} \\ 0 & \text{if } x \leq -\frac{1}{2} \end{cases} \quad (5.2.4)$$

5.2.2.3 Hyperbolic Tangent Activation Function

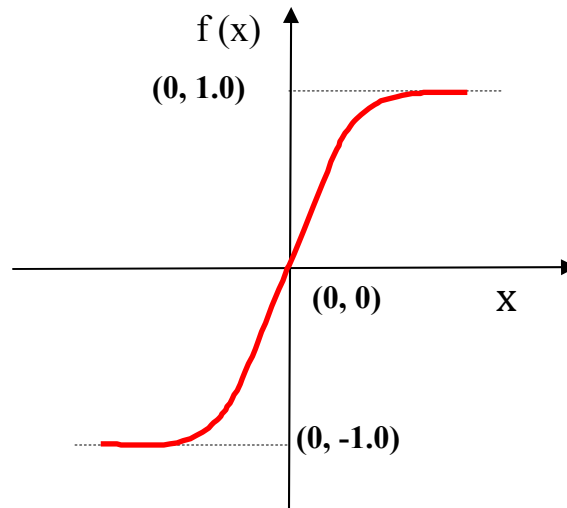


Fig.5.2.4 Hyperbolic tangent activation function

The *hyperbolic tangent* activation function is shown in Fig.5.2.4.

Mathematically the Ramping Activation Function can be described as:

$$f(x) = \frac{e^x - e^{-x}}{e^x + e^{-x}} \quad (5.2.5)$$

5.2.3 Modeling of Back Propagation Neural Network

The back propagation paradigm trains a neural network using a gradient descent algorithm in which the mean square error between the network's output and the desired output is minimized. This creates a global cost function that is minimized iteratively by 'back propagating' the error from the output nodes to the input nodes. Once the network's error has decreased to less than or equal to the specified threshold, the network has converged and is

considered to be trained. A simpler version of back propagation, the simple delta rule or the perceptron convergence procedure, which are applicable only in networks with only one modifiable connection layer can be proven to find a solution for all input-output mappings which are realizable in that simpler architecture. The error surface in such networks has only one minimum, and the system moves on this error surface towards this minimum (and stays there after it has reached it). This is not true for back propagation in a network with more than one modifiable connection layers. That is, although in practice one can almost always find a network architecture (even with only two layers of modifiable connections) that can realize a particular input-output mapping, this is not guaranteed. This is because in a network with hidden layer(s) of nodes, i.e. nodes that are neither in the input nor in the output layer – the error surface has, in addition to the global, “lowest”, minimum also local minima, and the system can get stuck in such local error minima. The Fig. 5.2.5 shows a typical architecture for networks with back propagation as the learning rule.

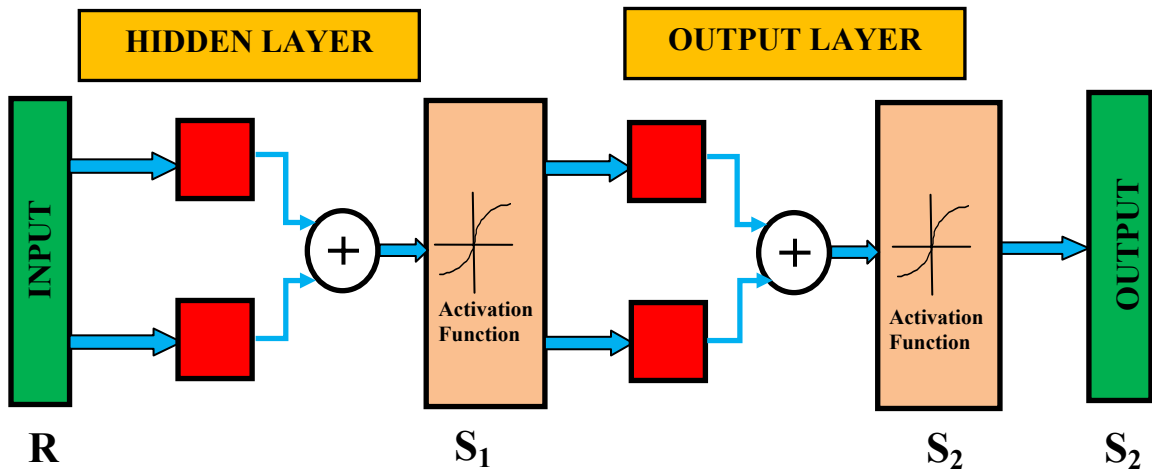


Fig. 5.2.5 Architecture of feed forward multilayer neural network trained by back- propagation algorithm

5.3 Analysis of Neural Network Controller used for Crack Detection

A feed forward multilayer neural network controller trained by back-propagation algorithm has been developed for detection of the relative crack location and relative crack depth (Fig.5.3.1) for the cracked cantilever beam. The neural network controller has got six input parameters and two output parameters.

The inputs to the neural network controller are as follows;

Relative first natural frequency = “fnf”; Relative second natural frequency = “snf”;

Relative third natural frequency = “tnf”; Relative first mode shape difference = “fmd”;

Relative second mode shape difference = “smd” and

Relative third mode shape difference = “tmd”.

The outputs from the neural network are as follows;

Relative crack location = “rcl” and Relative crack depth = “rcd”

The back propagation neural network has got ten layers (i.e. input layer, output layer and eight hidden layers). The neurons associated with the input and output layers are six and two respectively. The neurons associated in the eight hidden layers are twelve, thirty-six, fifty, one hundred fifty, three hundred, one hundred fifty, fifty and eight respectively. The input layer neurons represent relative deviation of first three natural frequencies and first three relative mode shape difference. The output layer neurons represent relative crack location and relative crack depth. The neurons are taken in order to give the neural network a diamond shape (Fig.5.3.2).

5.3.1 Neural Controller Mechanism for Crack Detection

The neural network used is a ten-layer perceptron [189]. The chosen number of layers was found empirically to facilitate training. The input layer has six neurons, three for first three relative natural frequencies and other three for first three relative mode shape difference. The output layer has two neurons, which represent relative crack location and relative crack depth. The first hidden layer has 12 neurons, the second hidden layer has 36 neurons, the third hidden layer has 50 neurons, the fourth hidden layer has 150 neurons, the fifth hidden layer has 300 neurons, the sixth hidden layer has 150 neurons, the seventh hidden layer has 50 neurons and the eighth hidden layer has 8 neurons. These numbers of hidden neurons are also found empirically. Fig. 5.3.2 depicts the neural network with its input and output signals.

The neural network is trained with 800 patterns representing typical scenarios, some of which are depicted in Table5.3.1. For example, from Table5.3.1, when the first three relative natural frequencies and first three mode shape differences are 0.9839, 0.9903, 0.9938, 0.0127,

0.8437, and 0.2639 respectively then the relative crack location and relative crack depth are 0.225 and 0.25 respectively. The neural network is trained to give outputs such as relative crack depth and relative crack location.

During training and during normal operation, the input patterns fed to the neural network comprise the following components:

$$y_1^{\{1\}} = \text{relative deviation of first natural frequency} \quad (5.3.1(a))$$

$$y_2^{\{1\}} = \text{relative deviation of second natural frequency} \quad (5.3.1(b))$$

$$y_3^{\{1\}} = \text{relative deviation of third natural frequency} \quad (5.3.1(c))$$

$$y_4^{\{1\}} = \text{relative deviation of first mode shape} \quad (5.3.1(d))$$

$$y_5^{\{1\}} = \text{relative deviation of second mode shape} \quad (5.3.1(e))$$

$$y_6^{\{1\}} = \text{relative deviation of third mode shape} \quad (5.3.1(f))$$

These input values are distributed to the hidden neurons which generate outputs given by [189]:

$$y_j^{\{\text{lay}\}} = f(V_j^{\{\text{lay}\}}) \quad (5.3.2)$$

where

$$V_j^{\{\text{lay}\}} = \sum_i W_{ji}^{\{\text{lay}\}} \cdot y_i^{\{\text{lay}-1\}} \quad (5.3.3)$$

lay = layer number

j = label for j^{th} neuron in hidden layer 'lay'

i = label for i^{th} neuron in hidden layer ‘lay-1’

$W_{ji}^{\{\text{lay}\}}$ = weight of the connection from neuron i in layer ‘lay-1’

to neuron j in layer ‘lay’

$f(\cdot)$ = activation function, chosen in this work as the hyperbolic tangent function:

$$f(x) = \frac{e^x - e^{-x}}{e^x + e^{-x}} \quad (5.3.4)$$

During training, the network output $\theta_{\text{actual}, n}$ may differ from the desired output $\theta_{\text{desired}, n}$ as specified in the training pattern presented to the network. A measure of the performance of the network is the instantaneous sum-squared difference between $\theta_{\text{desired}, n}$ and $\theta_{\text{actual}, n}$ for the set of presented training patterns:

$$\text{Err} = \frac{1}{2} \sum_{\text{all training patterns}} (\theta_{\text{desired}, n} - \theta_{\text{actual}, n})^2 \quad (5.3.5)$$

Where $\theta_{\text{actual}, n}$ ($n=1$) represents Relative crack location (“rcl”)

$\theta_{\text{actual}, n}$ ($n=2$) represents Relative crack depth (“rcd”)

The error back propagation method is employed to train the network [189]. This method requires the computation of local error gradients in order to determine appropriate weight corrections to reduce Err. For the output layer, the error gradient $\delta^{\{10\}}$ is:

$$\delta^{\{10\}} = f'(V_1^{\{10\}}) (\theta_{\text{desired}, n} - \theta_{\text{actual}, n}) \quad (5.3.6)$$

The local gradient for neurons in hidden layer $\{\text{lay}\}$ is given by:

$$\delta_j^{\{lay\}} = f'(V_j^{\{lay\}}) \left(\sum_k \delta_k^{\{lay+1\}} W_{kj}^{\{lay+1\}} \right) \quad (5.3.7)$$

The synaptic weights are updated according to the following expressions:

$$W_{ji}(t+1) = W_{ji}(t) + \Delta W_{ji}(t+1) \quad (5.3.8)$$

$$\text{and } \Delta W_{ji}(t+1) = \alpha \Delta W_{ji}(t) + \eta \delta_j^{\{lay\}} y_i^{\{lay-1\}} \quad (5.3.9)$$

where

α = momentum coefficient (chosen empirically as 0.2 in this work)

η = learning rate (chosen empirically as 0.35 in this work)

t = iteration number, each iteration consisting of the presentation of a training pattern and correction of the weights.

The final output from the neural network is:

$$\theta_{\text{actual},n} = f(V_n^{\{10\}}) \quad (5.3.10)$$

where

$$V_n^{\{10\}} = \sum_i W_{ni}^{\{10\}} y_i^{\{9\}} \quad (5.3.11)$$

Sl. no	Input to the Neural Network Controller						Desired output from the Neural Network Controller	
	Relative first natural frequency “fnf”	Relative second natural frequency “snf”	Relative third natural frequency “tnf”	Relative first mode shape difference “fmd”	Relative second mode shape difference “smd”	Relative third mode shape difference “tmd”	Relative crack Location “rcl”	Relative crack depth “rcd”
1	0.9592	0.9616	0.9801	0.4013	0.8437	0.4071	0.15	0.525
2	0.9632	0.9886	0.9927	0.2852	0.4466	0.3642	0.1	0.425
3	0.9715	0.9903	0.9931	0.2016	0.3248	0.4127	0.175	0.4
4	0.9728	0.9905	0.9938	0.1917	0.3186	0.4103	0.075	0.2
5	0.9789	0.9931	0.9939	0.1418	0.2983	0.3937	0.275	0.55
6	0.9831	0.9936	0.9947	0.092	0.2611	0.3872	0.225	0.25
7	0.9839	0.9954	0.9968	0.0702	0.2439	0.3207	0.4	0.525
8	0.9863	0.9961	0.9969	0.0364	0.0917	0.2639	0.425	0.5
9	0.9902	0.9968	0.9982	0.0294	0.0598	0.1823	0.525	0.55
10	0.9941	0.9990	0.9991	0.0127	0.0263	0.0698	0.5	0.45

Table 5.3.1 Examples of the training patterns for training of the neural network controller

5.3.2 Neural Controller for finding out Crack Depth and Crack Location

The inputs to the neural controller are relative first natural frequency; relative second natural frequency; relative third natural frequency; relative first mode shape difference; relative second mode shape difference and relative third mode shape difference. The outputs from the fuzzy controller are relative crack depth and relative crack location. The neural network controller is trained with 800 patterns representing typical scenarios, out of which ten rules are depicted in Table 5.3.1.

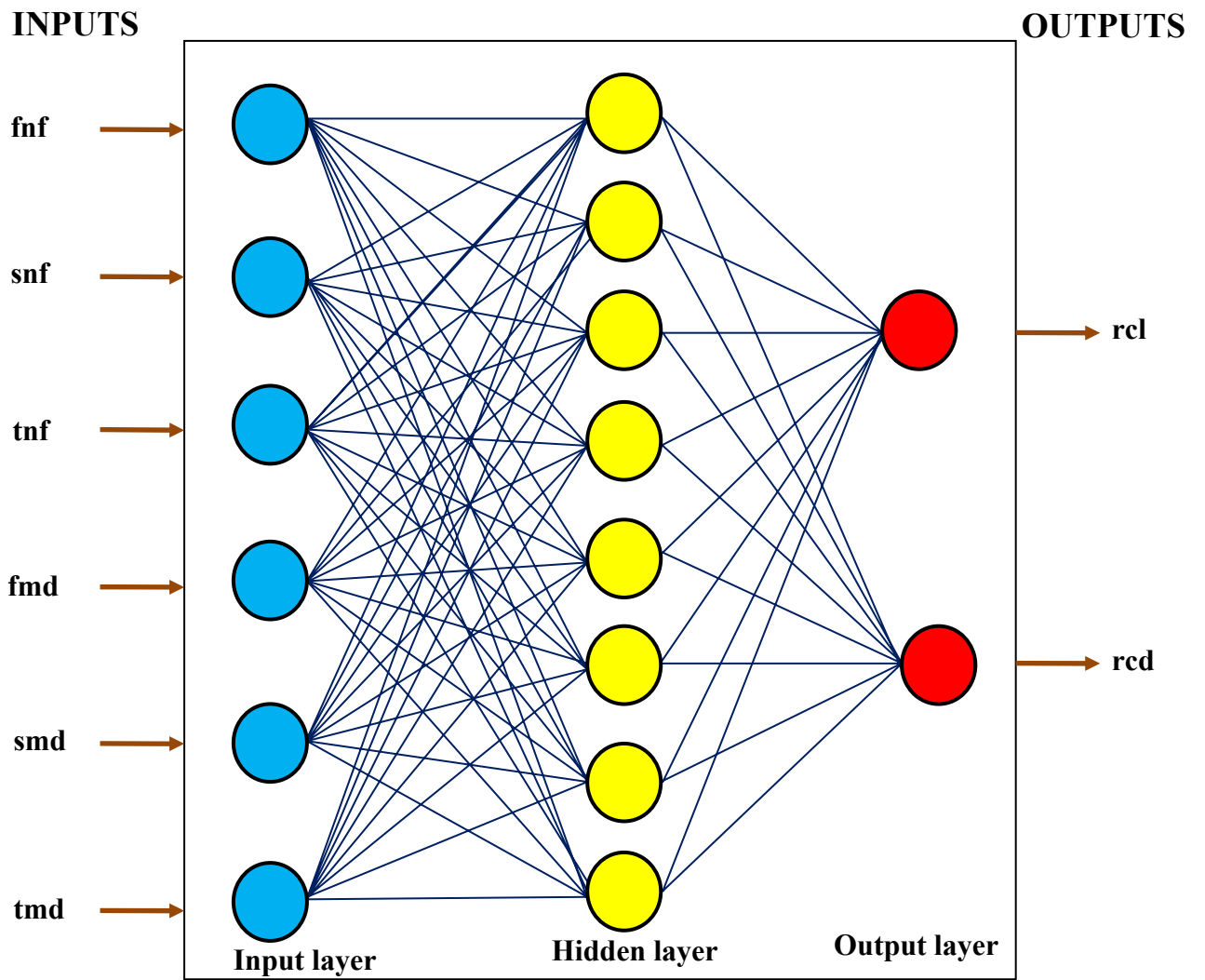


Fig. 5.3.1 Multi layer neural network controller

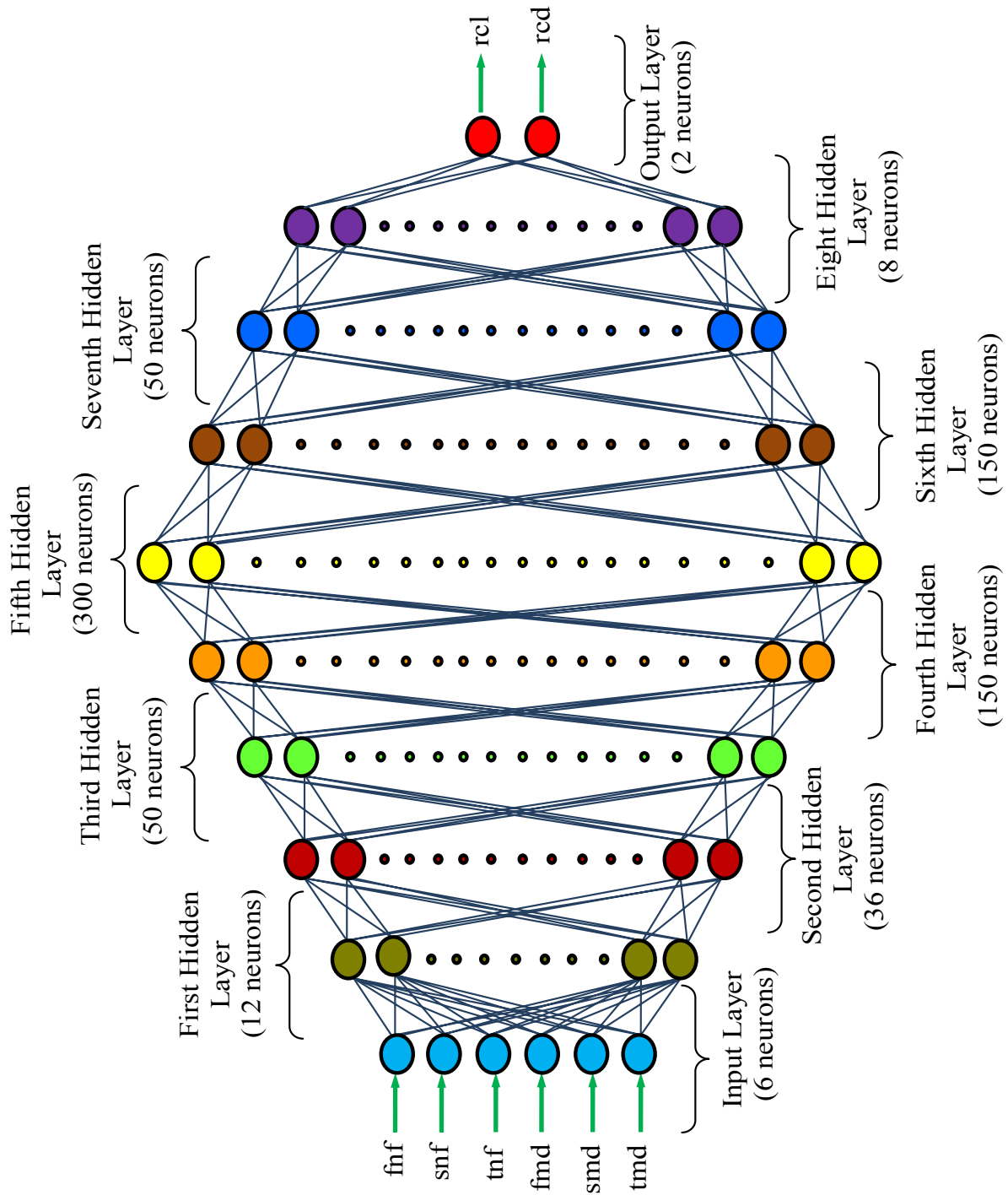


Fig. 5.3.2 Ten-layer neural network controller for crack detection

Relative first natural frequency “fnf”	Relative second natural frequency “snf”	Relative third natural frequency “tnf”	Relative first mode shape difference “fmd”	Relative second mode shape difference “smd”	Relative third mode shape difference “tmd”	Neural Network Controller (relative crack depth “rcd” and location “rcl”)		Triangular Fuzzy Controller (relative crack depth “rcd” and location “rcl”)		Gaussian Fuzzy Controller (relative crack depth “rcd” and location “rcl”)		Trapezoidal Fuzzy Controller (relative crack depth “rcd” and location “rcl”)		Numerical (relative crack depth “rcd” and location “rcl”)		Experimental (relative crack depth “rcd” and location “rcl”)	
						rcd	rel	rcd	rel	rcd	rel	rcd	rel	rcd	rel	rcd	rel
0.9848	0.9958	0.9975	0.2709	0.2372	0.3158	0.203	0.072	0.202	0.07163	0.203	0.07138	0.202	0.07163	0.202	0.06888	0.205	0.07250
0.9673	0.9874	0.9943	0.3969	0.3247	0.3923	0.431	0.081	0.441	0.08238	0.431	0.08138	0.441	0.08238	0.427	0.07900	0.43	0.08388
0.9623	0.9948	0.9983	0.1814	0.0279	0.0774	0.548	0.159	0.557	0.15825	0.548	0.15913	0.557	0.15825	0.537	0.15988	0.568	0.15750
0.9756	0.9976	0.9972	0.1383	-0.0823	0.1898	0.389	0.187	0.382	0.18475	0.389	0.18725	0.382	0.18475	0.394	0.18675	0.391	0.18775
0.9852	0.9984	0.9967	0.01	-0.8678	0.2572	0.227	0.238	0.229	0.23613	0.227	0.23688	0.229	0.23613	0.231	0.23625	0.23	0.24000
0.9723	0.9961	0.9818	0.1947	0.0672	0.4105	0.552	0.286	0.545	0.27625	0.552	0.28375	0.545	0.27625	0.556	0.28250	0.545	0.28625
0.9823	0.9872	0.9919	0.0726	0.2567	0.3994	0.449	0.405	0.446	0.40338	0.449	0.40438	0.446	0.40338	0.451	0.40388	0.447	0.40513
0.981	0.9809	0.9931	0.0898	0.3154	0.392	0.495	0.424	0.498	0.42263	0.495	0.42363	0.498	0.42263	0.497	0.42388	0.495	0.42350
0.986	0.9842	0.9988	-0.032	0.322	0.3965	0.425	0.503	0.428	0.50363	0.425	0.50188	0.428	0.50363	0.426	0.50125	0.425	0.50375
0.9834	0.9685	0.9974	0.038	0.4558	0.3507	0.537	0.534	0.534	0.53538	0.537	0.53313	0.534	0.53538	0.542	0.53500	0.535	0.53313

Table 5.3.2 Comparison of results between neural controller, fuzzy controller, numerical analysis and experimental analysis.

5.4 Results of Neural Controller

The feed forward neural network controller developed in the current research is a ten-layer perceptron. The artificial neural network controller is designed and is used to detect the relative crack location and relative crack depth. The results of the developed neural controller are compared (Table 5.3.2) with the fuzzy controller results of chapter-4, experimental and numerical results of chapter-3. In the Table 5.3.2, ten sets of inputs out of several hundred sets are taken. The inputs to different analyses made above are relative first three natural frequencies and relative first three mode shape differences and the out puts are relative crack location and relative crack depth. Corresponding ten set of outputs from the developed neural network controller, fuzzy controller, numerical analysis and experimental analysis are depicted in the Table 5.3.2. In the Table 5.3.2, the first column represents the relative 1st natural frequency (fnf), the second column represents the relative of 2nd natural frequency (snf), the third column represents the relative of 3rd natural frequency (tnf), the fourth column represents the relative 1st mode shape difference (fmd), the fifth column represents the relative 2nd mode shape difference (smd), the sixth column represents the relative 3rd mode shape difference (tmd) as inputs and the rest coloumns represents the outputs as relative crack location and relative crack depth obtained from different analyses.

5.5 Discussions

This section describes the application of artificial neural network controller for prediction of crack size and severity. The working principles of neural network technique (Fig.5.2.1) and activation function (Fig.5.2.2) have been depicted in section 5.2. The feed forward multi layer neural network trained by back propagation algorithm (Fig.5.2.5) has been used for designing the neural network controller. The ten layer feed forward controller and a schematic diagram of multi layer neural network controller for crack diagnosis are depicted in Fig.5.3.2 and Fig.5.3.1 respectively. These two figures express the complete architecture of the neural controller for crack detection. Few of the examples of training patterns out of several hundreds training patterns for neural network controller are given in the Table 5.3.1.

The Fig.5.3.2 represents a multi layer controller with ten set of rules for training with 1st three relative natural frequencies and 1st three relative mode shape differences as inputs and relative crack location and relative crack depth as outputs. The comparison of the results from neural controller, fuzzy controllers, numerical analysis and experimental analysis are expressed in Table 5.3.2. It is evident from the Table 5.3.2 that the average percentage deviation of the results of neural network controller is 1%.

5.6 Summary

From the analysis mentioned above and discussions, the summaries drawn are depicted below. The neural network controller trained with eight hundred training patterns consist of different crack location and crack depth. The neural network gives out puts such as relative crack depth and relative crack location, very close to the experimental results. The ten layer perceptron neural network has different number of neurons in the ten layers for processing the input data like relative natural frequencies and mode shapes. It is observed that the error in the output of the controller is considerably reduced from the desired output by employing back propagation method. The developed controller predicts the crack location and its intensity very closely to the actual results. The result from the controller is compared with the output from numerical, fuzzy and experimental analysis for checking the robustness of the developed system. The data collected from the controller is used for training the hybrid technique such as fuzzy- neuro and MANFIS methods in next chapters for on line condition monitoring of dynamically vibrating structures with higher accuracy and less computational time.

Publications

- Das H.C. and Parhi D.R., Application of Neural network for fault diagnosis of cracked cantilever beam, *IEEE International Symposium on Biologically Inspired Computing and Applications (BICA-2009)*, Bhubaneswar, India, December 21-22, 2009, 353-358.

Chapter 6

ANALYSIS OF HYBRID FUZZY-NEURO SYSTEM FOR CRACK DETECTION

Research on hybrid systems is one of the key issues of developing intelligent systems. It can be applied by hybridising artificial neural networks, fuzzy logic, knowledge-based systems, genetic algorithms and evolutionary computation. Neural network technology and fuzzy inference system are becoming well recognized tools of designing an identifier/controller capable of perceiving the operating environment and imitating a human operator with high performance. The motivation behind the use of fuzzy neuro approaches is based on the complexity of real life systems. In this respect, fuzzy neuro design approaches combine architectural and philosophical aspects of an expert resulting in an artificial brain which can be used as a controller. It is known that the fuzzy inference systems and neural networks are universal approximators. In the following section fuzzy inference technique and neural network hybridized together to produce fuzzy-neuro controller for fault diagnosis.

6.1 Introduction

Hybrid intelligent systems being the product of fuzzy logic and neural networks are computational machines with unique capabilities for dealing with both numerical data and linguistic knowledge (fuzzy) information. As the hybrid system refers to combinations of artificial neural networks and fuzzy logic it incorporates the capability of both fuzzy logic and neural network technique. This hybrid method can give better results than the independent techniques. Fuzzy systems make use of knowledge expressed in the form of linguistic rules, thus they offer the possibility of implementing expert human knowledge and experience. Neural network learning techniques automate this process, significantly reducing development time, and resulting in better performance. Fuzzy neuro hybridization results in a hybrid intelligent system that synergizes these two techniques by combining the human-like reasoning style of fuzzy systems with the learning and connectionist structure of neural networks. Hence, this methodology can be effectively utilized for prediction of crack location and crack depth in engineering structures with the vibration signatures as in put parameters.

This current research addresses the fault detection of a cracked cantilever beam using hybrid fuzzy neuro intelligence technique. The fuzzy-neuro controller has two parts. The first part comprises of fuzzy controller and the second part addresses the neural controller. The input parameters to the fuzzy controller are first three relative natural frequencies and first three mode shape differences. The output parameters of the fuzzy controller are initial relative crack depth and initial relative crack location. The input parameters to the neural segment of fuzzy-neuro controller are first three relative natural frequencies and first three mode shape differences along with the interim outputs of fuzzy controller. The output parameters of the fuzzy-neuro controller are final relative crack depth and final relative crack location. For deriving the fuzzy rules and training patterns of natural frequencies, mode shapes, crack depths and crack locations, theoretical expressions have been developed. Several fuzzy rules and training patterns for the fuzzy segment and neural segment of fuzzy-neuro controller are derived respectively. Experiments have been conducted for verifying the robustness of the developed fuzzy-neuro controller. The results of the developed fuzzy-neuro controller and experimental method are in very good agreement.

This chapter is divided into six sections. The section 6.1 briefs the hybrid intelligent system and its importance in advance computing. The analysis of the fuzzy-neuro controller, the mechanism of fuzzy controller and neural controller for crack detection are depicted in section 6.2. In section 6.3 the results of the hybrid intelligent controller are compared with the results of neural controller (chapter 5), fuzzy controller (chapter 4), experimental and numerical analysis (chapter 3) to demonstrate the effectiveness of the proposed methodology. Finally the discussions and summary are described in section 6.4 and 6.5 respectively.

6.2 Analysis of Fuzzy-Neuro Controller

In the current investigation damage analysis of dynamic structures has been addressed using inverse approach i.e. hybrid computational fuzzy neuro technique. This hybrid technique comprises of two parts; i.e. fuzzy controller and neural controller. The fuzzy controller has six input parameters and two output parameters. The input parameters to the fuzzy controller are first three relative natural frequencies and first three mode shape differences. The output parameters of the fuzzy controller are initial relative crack depth and relative crack location.

The input parameters to the neural segment of fuzzy-neuro controller are first three relative natural frequencies and first three mode shape differences. The output parameters of the fuzzy-neuro controller are final relative crack depth and relative crack location. Three types of membership functions i.e Triangular, Gaussian and Trapezoidal are used in the fuzzy-neuro controller and accordingly three fuzzy-neuro controllers such as triangular membership function fuzzy-neuro controller (Fig.6.2.1), gaussian membership function fuzzy-neuro controller (Fig.6.2.2) and trapezoidal membership function fuzzy-neuro controller (Fig.6.2.3) are designed for prediction of crack location and crack depth.

6.2.1 Analysis of the Fuzzy Segment of Fuzzy-Neuro Controller

The fuzzy part of the developed fuzzy-neuro controller has got six input parameters and two output parameters. The linguistic terms used for the inputs in the fuzzy system of the fuzzy-neuro controller are as follows;

Relative first natural frequency = “fnf”

Relative second natural frequency = “snf”;

Relative third natural frequency = “tnf”

Relative first mode shape difference = “fmd”

Relative second mode shape difference = “smd”

Relative third mode shape difference = “tmd”.

The linguistic term used for the outputs are as follows;

Initial relative crack location = “rcl_{initial}” and Initial relative crack depth = “rcd_{initial}”

The membership functions used in the fuzzy segment of fuzzy-neuro controller are shown pictorially in Fig. 4.3.1, Fig. 4.3.2 and Fig. 4.3.3. The linguistic terms of membership functions used in the fuzzy segment of fuzzy-neuro controller are described in the Table 4.3.1. The fuzzy controller mechanism for crack detection has been given in section 4.3.1 and 4.3.2 of chapter 4.

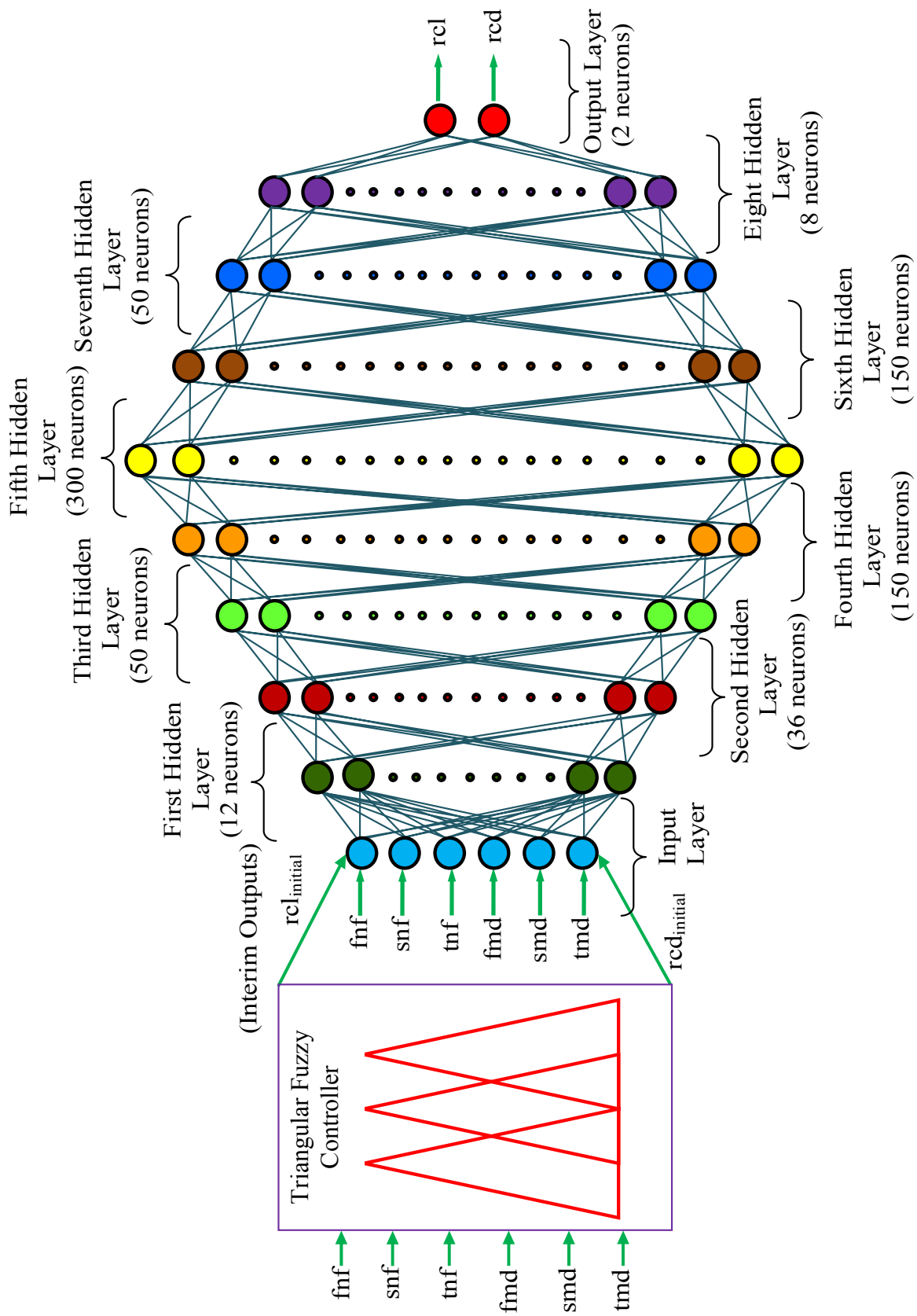


Fig.6.2.1 Triangular fuzzy-neuro controller for crack detection

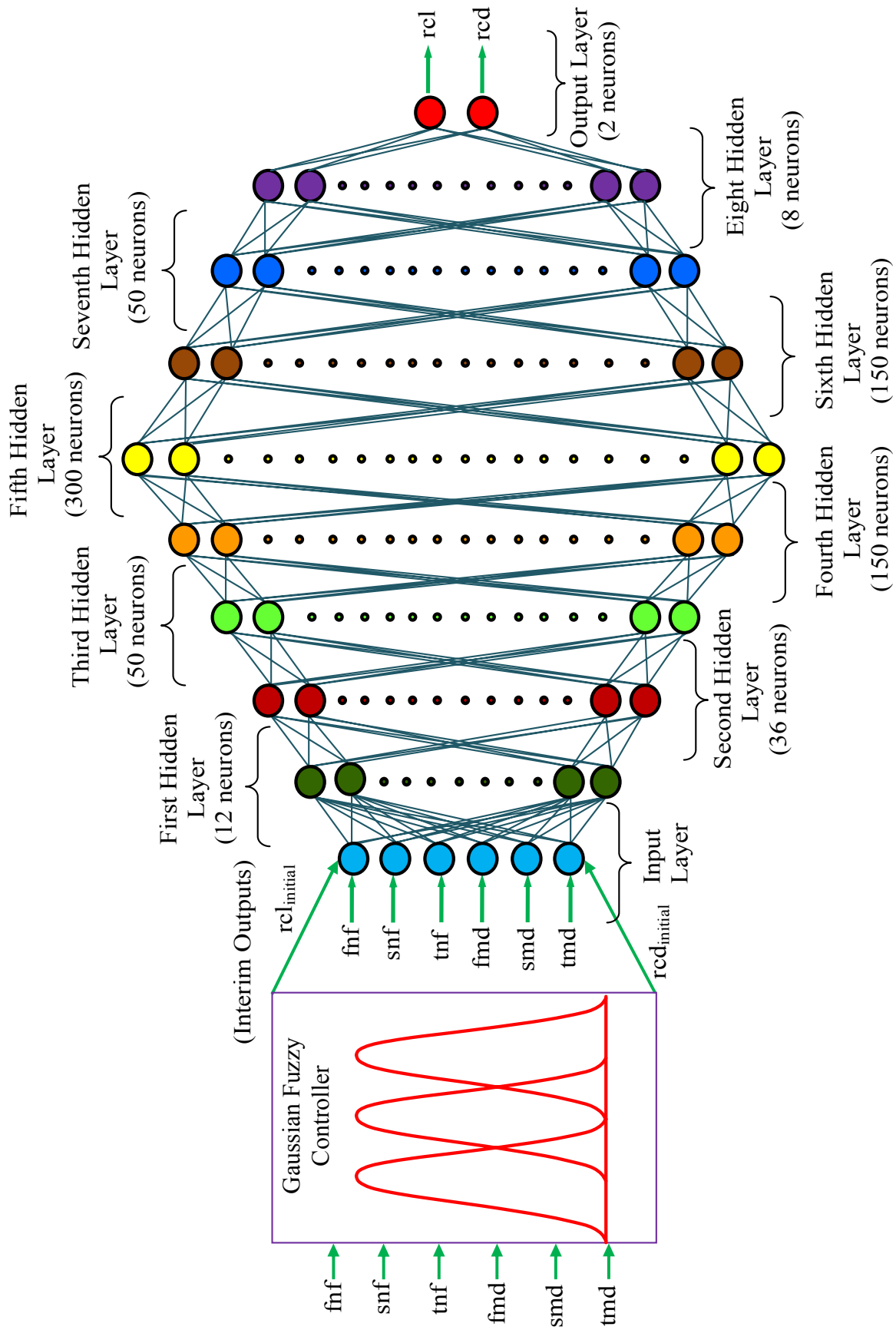


Fig.6.2.2 Gaussian fuzzy-neuro controller for crack detection

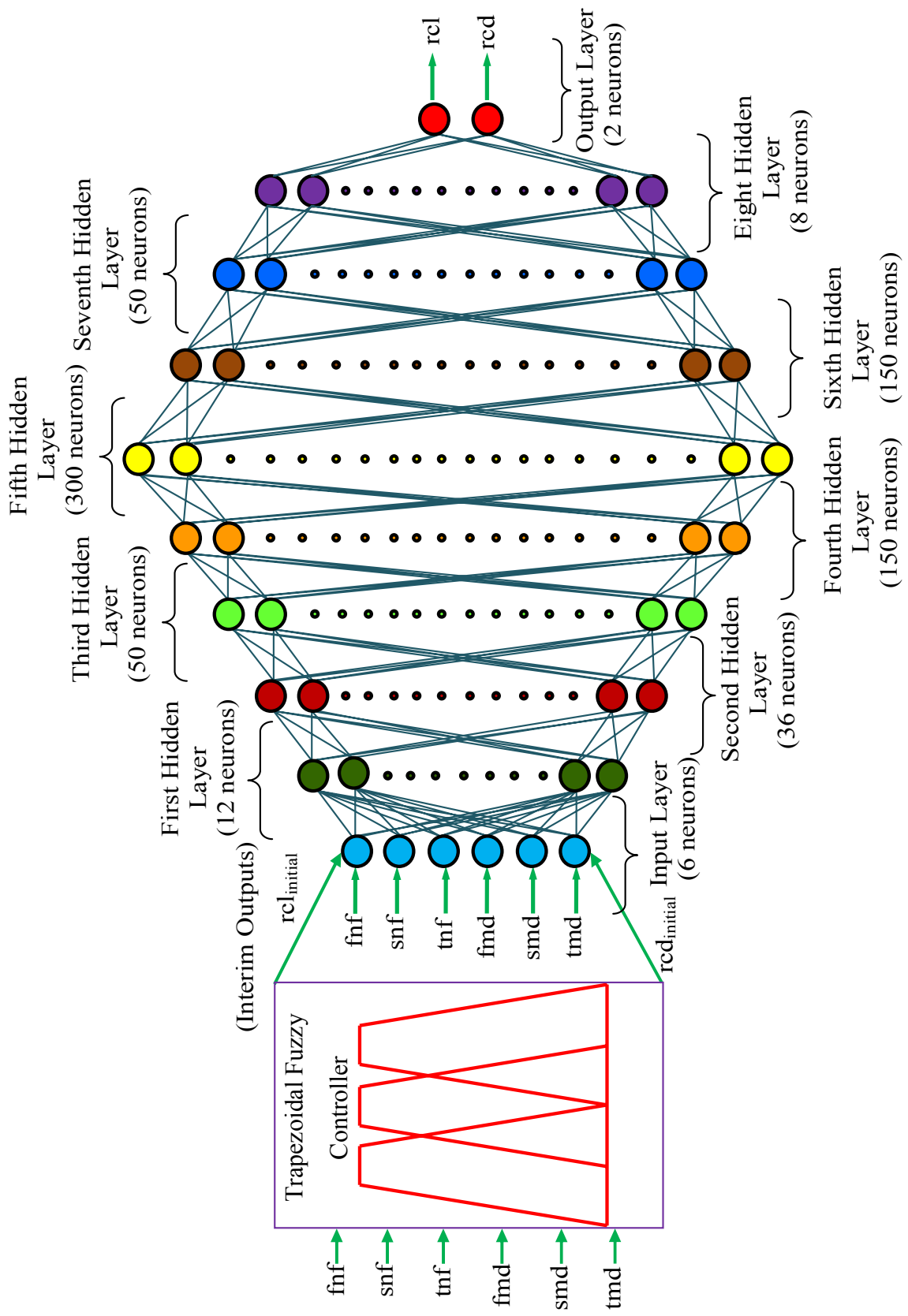


Fig.6.2.3 Trapezoidal fuzzy-neuro controller for crack detection

6.2.2 Analysis of the Neural Segment of Fuzzy-Neuro Controller

In the fuzzy-neuro controller, the fuzzy segment will be inherited from chapter four, section 4.2.2. The fuzzy segment in the fuzzy-neuro controller will give the intermittent result for relative crack depth and relative crack location. The neural segment of the fuzzy-neuro controller has eight inputs such as intermittent relative crack depth and relative crack location obtained from the fuzzy segment along with first three relative natural frequencies and first three relative mode shape difference. The output from the fuzzy-neuro controller is the refined result for relative crack depth and relative crack location. The analysis of the neural network used in the fuzzy-neuro controller is given below.

The neural segment of the fuzzy-neuro controller is a ten layer feed forward neural network trained by back propagation algorithm. The fuzzy-neuro controller has been developed for detection of the relative crack location and relative crack depth. The neural network has got eight input parameters and two output parameters.

The inputs to the neural segment of the fuzzy-neuro controller are as follows;

Relative first natural frequency = “fnf”; Relative second natural frequency = “snf”;

Relative third natural frequency = “tnf”; Relative first mode shape difference = “fmd”;

Relative second mode shape difference = “smd” and

Relative third mode shape difference = “tmd”.

Initial relative crack depth(output of the fuzzy segment)= “rcd_{initial}”

Initial relative crack location (output of the fuzzy segment)= “rcl_{initial}”

The final outputs from the fuzzy-neuro controller are;

Final relative crack location = “rcl_{final}” and Final Relative crack depth = “rcd_{final}”

The back propagation neural network used in fuzzy-neuro controller has got ten layers (i.e. input layer, output layer and eight hidden layers). The neurons associated with the input and output layers are eight and two respectively. The neurons associated in the eight hidden layers are twelve, thirty-six, fifty, one hundred fifty, three hundred, one hundred fifty, fifty and eight respectively. The input layer neurons represent first three relative natural frequencies and first three relative mode shape difference along with the two interim outputs from the the fuzzy segment. The output layer neurons represent final relative crack location

and final relative crack depth. The neurons are taken in order to give the neural network a diamond shape. The neural controller mechanism for crack detection may be referred from section 5.3.1 and 5.3.2 of chapter 5.

6.2.3 Results of Fuzzy-Neuro Controller

The results obtained after analyzing the fuzzy segment and neural segment of fuzzy-neuro controller are given in Tables 6.2.1 and 6.2.2. A comparison of results between the triangular membership fuzzy-neuro controller, gaussian membership fuzzy-neuro controller, trapezoidal membership fuzzy-neuro controller, numerical analysis and experimental analysis is depicted in Table 6.2.1. Again the comparison of results between the three fuzzy-neuro controllers, neural network controller, triangular, gaussian and trapezoidal fuzzy controller is presented in Table 6.2.2. Ten sets of random inputs out of several hundred sets are taken in all the above tables for comparison of accuracy of the results. The inputs to different analyses made above are first three relative natural frequencies and first three relative mode shape differences and the out puts are relative crack location and relative crack depth. Corresponding ten set of outputs from the developed fuzzy-neuro controllers, neural network controller, fuzzy controllers, numerical analysis and experimental analysis are presented in the Table 6.2.1 and Table 6.2.2. In the Tables 6.2.1 and 6.2.2 the first column represents the relative 1st natural frequency (fnf), the second column represents the relative 2nd natural frequency (snf), the third column represents the relative 3rd natural frequency (tnf), the fourth column represents the relative 1st mode shape difference (fmd), the fifth column represents the relative 2nd mode shape difference (smd), the sixth column represents the relative 3rd mode shape difference (tmd) as inputs and the rest columns represents the outputs (i.e. relative crack location and relative crack depth). It is observed from the Tables 6.2.1 and 6.2.2 that the average percentage deviation of the results of gaussian membership fuzzy-neuro controller is 0.55%. For the triangular membership fuzzy-neuro controller and trapezoidal membership fuzzy-neuro controller the average percentage deviation of the results are 0.95% and 0.85% respectively.

Relative first natural frequency “fnf”	Relative second natural frequency “snf”	Relative third natural frequency “tnf”	Relative first mode shape difference “fmd”	Relative second mode shape difference “smd”	Relative third mode shape difference “tmd”	Triangular Fuzzy Neuro Controller (relative crack depth “rcd” and location “rcl”)		Gaussian Fuzzy Neuro Controller (relative crack depth “rcd” and location “rcl”)		Trapezoidal Fuzzy Neuro Controller (relative crack depth “rcd” and location “rcl”)		Numerical (relative crack depth “rcd” and location “rcl”)		Experimental (relative crack depth “rcd” and location “rcl”)	
						rcd	rcl	rcd	rcl	rcd	rcl	rcd	rcl	rcd	rcl
0.9848	0.9958	0.9975	0.2709	0.2372	0.3158	0.204	0.071	0.203	0.069	0.202	0.07163	0.202	0.069	0.205	0.073
0.9673	0.9874	0.9943	0.3969	0.3247	0.3923	0.429	0.082	0.431	0.079	0.431	0.08038	0.427	0.079	0.43	0.084
0.9623	0.9948	0.9983	0.1814	0.0279	0.0774	0.552	0.158	0.548	0.16	0.542	0.15825	0.537	0.160	0.568	0.158
0.9756	0.9976	0.9972	0.1383	-0.0823	0.1898	0.393	0.188	0.389	0.18725	0.385	0.18475	0.394	0.187	0.391	0.188
0.9852	0.9984	0.9967	0.01	-0.8678	0.2572	0.229	0.239	0.227	0.2364	0.23	0.23613	0.231	0.236	0.23	0.240
0.9723	0.9961	0.9818	0.1947	0.0672	0.4105	0.551	0.285	0.552	0.283	0.545	0.28325	0.556	0.283	0.545	0.286
0.9823	0.9872	0.9919	0.0726	0.2567	0.3994	0.449	0.404	0.449	0.404	0.446	0.40338	0.451	0.404	0.447	0.405
0.981	0.9809	0.9931	0.0898	0.3154	0.392	0.496	0.424	0.495	0.424	0.497	0.42363	0.497	0.424	0.495	0.424
0.986	0.9842	0.9988	-0.032	0.322	0.3965	0.425	0.503	0.425	0.50188	0.426	0.50163	0.426	0.501	0.425	0.504
0.9834	0.9685	0.9974	0.038	0.4558	0.3507	0.538	0.534	0.537	0.53313	0.534	0.53538	0.542	0.535	0.535	0.533

Table 6.2.1 Comparison of the results of the fuzzy-neuro controllers with the results of numerical and experimental analyses

6.3 Discussion

Results obtained from the analysis of the developed fuzzy-neuro controller and their comparison with neural controller, fuzzy controllers, numerical and experimental analyses, following discussions are made.

Fig. 6.2.1, Fig. 6.2.2 and Fig. 6.2.3 represent the architecture of developed fuzzy-neural controllers with triangular, gaussian and trapezoidal membership functions respectively. These three controllers are used for prediction of crack location and crack depth. Table 6.2.1 and Table 6.2.2 show the comparison of the results of triangular, Gaussian and trapezoidal fuzzy-neuro controllers with the numerical, experimental, neural controller and triangular, gaussian and trapezoidal fuzzy controller results.

6.4 Summary

The results and discussions made above, show that the crack location and its size can be predicted by the help of a fuzzy-neuro controller developed. The fuzzy-neuro controller is based on the natural frequencies and mode shape differences of the structures with crack. The predicted values of crack location and its size are compared with the numerical, experimental, neural and fuzzy controllers results and are found to be in well agreement. This fuzzy-neuro controller can be used as an effective tool for fault diagnosis of the vibrating structures.

Publications

- Das H.C. and Parhi D.R., Fuzzy-Neuro Controller for Smart Fault Detection of A Beam, *International Journal of Acoustics and Vibration*, 13(2), 2009, 55-66.

Chapter 7

ANALYSIS OF MANFIS FOR CRACK DETECTION

It has been established that dynamic behavior of a structure changes due to the presence of crack in the structure. The effect of crack on the vibration signatures of the structure depends mainly on the location and depth of the crack. To identify the location and depth of a crack in a structure, a new method is presented in this chapter which uses multiple adaptive neuro-fuzzy-evolutionary technique (MANFIS). With this MANFIS, it is possible to formulate the inverse problem. MANFIS is used to obtain the outputs (the relative crack location and relative crack depth) from the inputs (the first three natural frequencies and first three mode shapes). This new method has been applied to diagnose fault on a cracked cantilever beam and the results are promising.

In the MANFIS controller after the input layer there are five layers out of which three layers are fixed layers and two layers are adaptive layers. The adaptive neuro-fuzzy hybrid system combines the advantages of fuzzy logic system, which deal with explicit knowledge that can be explained and understood, and neural networks, which deal with implicit knowledge, which can be acquired by learning. The merger of neural networks and fuzzy logic led to the creation of neuro-fuzzy controllers which are currently one of the most popular research fields. The inputs to MANFIS are relative deviation of first three natural frequencies and relative values of percentage deviation for first three mode shapes and outputs are relative crack depth and relative crack location. A learning algorithm based on neural network technique has been developed to tune the parameters of fuzzy membership functions. The experimental results agree well with the MANFIS results, proves the authenticity of the theory developed.

7.1 Introduction

Recently sophisticated vibration monitoring techniques have been available for monitoring and diagnosis of faulty vibrating structures. Among them, the artificial intelligence techniques such as neural networks, fuzzy logic, expert systems and so on are at the priority. One of the hybrid artificial intelligence techniques i.e. multiple adaptive neuro-fuzzy-evolutionary technique have woken up a lot among the researchers in the recent years. The MANFIS approach is becoming one of the major areas of interest because it gets the benefits of neural networks as well as of fuzzy logic systems and it removes the individual disadvantages by combining them on the common features.

In this chapter for diagnosis of the crack in the structure multiple adaptive neuro-fuzzy inference system methodology has been applied. The adaptive neuro-fuzzy controller has got input layer, hidden layers and out put layer. The input layer is the fuzzy layer. The other layers are neural layers. The inputs to the fuzzy layer are relative deviation of first three natural frequencies and relative values of percentage deviation for first three mode shapes. The final outputs of the MANFIS controller are relative crack depth and relative crack location. Several hundreds fuzzy rules and neural network training patterns are derived using natural frequencies, mode shapes, crack depths and crack locations. Real results have been obtained using the experimental setup. Comparison between the simulation and experimental results, exhibits a good agreement between them. This methodology can be effectively used for condition monitoring of dynamic structures.

This chapter is organised into five sections following the introduction; the entire analysis of MANFIS architecture has been discussed in section 7.2. The analysis of MANFIS used for crack detection has been discussed in section 7.3. The results of MANFIS controller are presented in section 7.4 and comparisons of results of MANFIS with other methods discussed previously are analyzed in section 7.5. Finally, the discussions and summary are given in section 7.6 and 7.7 respectively.

7.2 Analysis of Multiple Adaptive Neuro-Fuzzy Inference System for Crack Detection

The multiple adaptive neuro fuzzy inference system is an integrated system of artificial neural network (ANN) and fuzzy inference system (FIS). The ANFIS controller used is a first order Takagi Sugeno Fuzzy Model [258]. In the current analysis, there are six inputs and two outputs. They are as follows:

Relative first natural frequency (x1) = “fnf”; Relative second natural frequency (x2) = “snf”;
 Relative third natural frequency (x3) = “tnf”; Relative first mode shape difference (x4) = “fmd”;
 Relative second mode shape difference (x5) = “smd”
 Relative third mode shape difference (x6) = “tmd”.

The outputs are as follows;

Relative crack location = “rcl” and Relative crack depth = “rcd”

As in the current investigation there are two outputs, multiple ANFIS (MANFIS) architecture has been used (Fig. 7.2.1).

The “if then” rules for the MANFIS architecture is defined as follows;

$$\left. \begin{array}{l} \text{IF } x_1 \text{ is } A_j, x_2 \text{ is } B_k, x_3 \text{ is } C_m, x_4 \text{ is } D_n, x_5 \text{ is } E_o, x_6 \text{ is } F_p \\ \text{THEN} \\ f_{e,i} = p_{e,i} x_1 + r_{e,i} x_2 + s_{e,i} x_3 + t_{e,i} x_4 + u_{e,i} x_5 + v_{e,i} x_6 + z_{e,i} \end{array} \right\} \quad (7.2.1)$$

Where;

$$\left. \begin{array}{l} f_{1,i} = rcl_i = p_{1,i} x_1 + r_{1,i} x_2 + s_{1,i} x_3 + t_{1,i} x_4 + u_{1,i} x_5 + v_{1,i} x_6 + z_{1,i} ; \\ \text{for relative crack length.} \\ f_{2,i} = rcd_i = p_{2,i} x_1 + r_{2,i} x_2 + s_{2,i} x_3 + t_{2,i} x_4 + u_{2,i} x_5 + v_{2,i} x_6 + z_{2,i} ; \\ \text{for relative crack depth.} \end{array} \right\} \quad (7.2.2)$$

$e = 1, 2 ; j = 1 \text{ to } q_1 ; k = 1 \text{ to } q_2 ; m = 1 \text{ to } q_3 ; n = 1 \text{ to } q_4 ; o = 1 \text{ to } q_5 \text{ and } p = 1 \text{ to } q_6 \text{ and}$
 $i = 1 \text{ to } q_1, q_2, q_3, q_4, q_5, q_6$

A, B, C, D, E and F are the fuzzy membership sets defined for the input variables x_1 (fnf), x_2 (snf), x_3 (tnf), x_4 (fmd), x_5 (smd) and x_6 (tmd). q_1, q_2, q_3, q_4, q_5 and q_6 are the number of member ship functions for the fuzzy systems of the inputs x_1, x_2, x_3, x_4, x_5 and x_6 respectively.

“rc1” and “rcd” are the linear consequent functions defined in terms of the inputs (x_1, x_2, x_3, x_4, x_5 and x_6). $p_{1,i}, r_{1,i}, s_{1,i}, t_{1,i}, u_{1,i}, v_{1,i}, z_{1,i}, p_{2,i}, r_{2,i}, s_{2,i}, t_{2,i}, u_{2,i}, v_{2,i}$ and $z_{2,i}$ are the consequent parameters of the ANFIS fuzzy model. In the ANFIS model nodes of the same layer have similar functions. The output signals from the nodes of the previous layer are the input signals for the current layer. The output obtained with the help of the node function will be the input signals for the subsequent layer.

Layer 1: Every node in this layer is an adaptive node (square node) with a particular fuzzy membership function (node function) specifying the degrees to which the inputs satisfy the quantifier. For six inputs the outputs from nodes are given as follows;

$$\begin{aligned}
 O_{1,g,e} &= \mu_{Ag}(x) \quad \text{for } g = 1, \dots, q_1 && \text{(for input } x_1) \\
 O_{1,g,e} &= \mu_{Bg}(x) \quad \text{for } g = q_1+1, \dots, q_1+q_2 && \text{(for input } x_2) \\
 O_{1,g,e} &= \mu_{Cg}(x) \quad \text{for } g = q_1+q_2+1, \dots, q_1+q_2+q_3 && \text{(for input } x_3) \\
 O_{1,g,e} &= \mu_{Dg}(x) \quad \text{for } g = q_1+q_2+q_3+1, \dots, q_1+q_2+q_3+q_4 && \text{(for input } x_4) \\
 O_{1,g,e} &= \mu_{Eg}(x) \quad \text{for } g = q_1+q_2+q_3+q_4+1, \dots, q_1+q_2+q_3+q_4+q_5 && \text{(for input } x_5) \\
 O_{1,g,e} &= \mu_{Fg}(x) \quad \text{for } g = q_1+q_2+q_3+q_4+q_5+1, \dots, q_1+q_2+q_3+q_4+q_5+q_6 && \text{(for input } x_6)
 \end{aligned} \tag{7.2.3}$$

Here the membership functions for A, B, C, D, E and F considered are the bell shaped function.

The membership function for A,B,C,D,E and F considered in “layer 1” are the bell shaped function (Fig. 7.2.1) and are defined as follows;

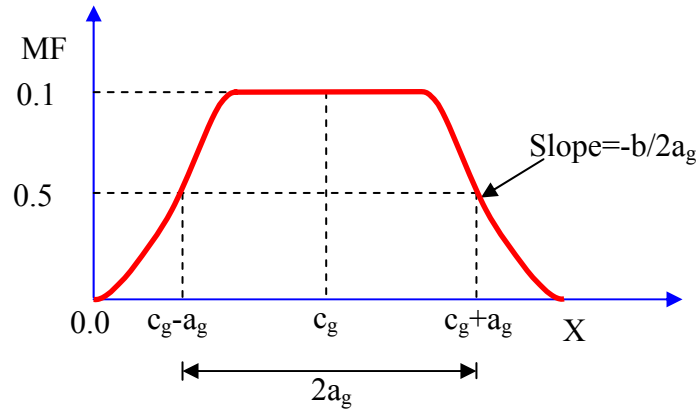


Fig. 7.2.1 Bell-shaped membership function

$$\mu_{A_g}(x) = \frac{1}{1 + \left\{ \left(\frac{x - c_g}{a_g} \right)^2 \right\}^{b_g}} ; \quad g = 1, \dots, q_1 \quad (7.2.4 \text{ (i)})$$

$$\mu_{B_g}(x) = \frac{1}{1 + \left\{ \left(\frac{x - c_g}{a_g} \right)^2 \right\}^{b_g}} ; \quad g = q_1 + 1, \dots, q_1 + q_2 \quad (7.2.4 \text{ (ii)})$$

$$\mu_{C_g}(x) = \frac{1}{1 + \left\{ \left(\frac{x - c_g}{a_g} \right)^2 \right\}^{b_g}} ; \quad g = q_1 + q_2 + 1, \dots, q_1 + q_2 + q_3 \quad (7.2.4 \text{ (iii)})$$

$$\mu_{D_g}(x) = \frac{1}{1 + \left\{ \left(\frac{x - c_g}{a_g} \right)^2 \right\}^{b_g}} ; \quad g = q_1 + q_2 + q_3 + 1, \dots, q_1 + q_2 + q_3 + q_4 \quad (7.2.4 \text{ (iv)})$$

$$\mu_{Eg}(x) = \frac{1}{1 + \left\{ \left(\frac{x - c_g}{a_g} \right)^2 \right\}^{b_g}} ; \quad g = q_1 + q_2 + q_3 + q_4 + 1, \dots, q_1 + q_2 + q_3 + q_4 + q_5 \quad (7.2.4 \text{ (v)})$$

$$\mu_{Fg}(x) = \frac{1}{1 + \left\{ \left(\frac{x - c_g}{a_g} \right)^2 \right\}^{b_g}} ; \quad g = q_1 + q_2 + q_3 + q_4 + q_5 + 1, \dots, q_1 + q_2 + q_3 + q_4 + q_5 + q_6 \quad (7.2.4 \text{ (vi)})$$

Where a_g, b_g and c_g are the parameters for the fuzzy membership function. The ball-shaped function changes its pattern as per the change of the parameters. This change will give the various contour of bell shaped function as needed in accord with the data set for the problem considered.

Layer 2: Every node in this layer is a fixed node (circular) labeled as “Π”. The output denoted by $O_{2,i,e}$. The output is the product of all incoming signal.

$$O_{2,i,e} = w_{i,e} = \mu_{Ag}(x) \mu_{Bg}(x) \mu_{Cg}(x) \mu_{Dg}(x) \mu_{Eg}(x) \mu_{Fg}(x) ; \quad (7.2.5)$$

for $i = 1, \dots, q_1, q_2, q_3, q_4, q_5, q_6$ and $g = 1, \dots, q_1 + q_2 + q_3 + q_4 + q_5 + q_6$

The output of each node of the second layer represents the firing strength (degree of fulfillment) of the associated rule. The T-nom operator algebraic product $\{ T_{ap}(a,b) = ab \}$, has been used to obtain the firing strength ($w_{i,e}$).

Layer 3: Every node in this layer is a fixed node (circular) labeled as “N”. The output of the i th. node is calculated by taking the ratio of firing strength of i th. rule ($w_{i,e}$) to the sum of all rules’ firing strength.

$$O_{3,i,e} = \bar{w}_{i,e} = \frac{w_{i,e}}{\sum_{r=1}^{r=q1.q2.q3.q4.q5.q6} w_{r,e}} \quad (7.2.6)$$

This output gives a normalized firing strength.

Layer 4: Every node in this layer is an adaptive node (square node) with a node function.

$$O_{4,i,e} = \bar{w}_{i,e} f_{e,i} = \bar{w}_{i,e} (p_{e,i} x1 + r_{e,i} x2 + s_{e,i} x3 + t_{e,i} x4 + u_{e,i} x5 + v_{e,i} x6 + z_{e,i}) \quad (7.2.7)$$

Where $\bar{w}_{i,e}$ is a normalized firing strength form (output) from layer 3 and $\{p_{e,i}, r_{e,i}, s_{e,i}, t_{e,i}, u_{e,i}, v_{e,i}, z_{e,i}\}$ is the parameter set for relative crack location($e=1$) and relative crack depth ($e=2$). Parameters in this layer are referred to as consequent parameters.

Layer 5: The single node in this layer is a fixed node (circular) labeled as “ Σ ”, which computes the overall output as the summation of all incoming signals.

$$O_{5,1,e} = \sum_{i=1}^{i=q1.q2.q3.q4.q5.q6} \bar{w}_{i,e} f_{e,i} = \frac{\sum_{i=1}^{i=q1.q2.q3.q4.q5.q6} w_{i,e} f_{e,i}}{\sum_{i=1}^{i=q1.q2.q3.q4.q5.q6} w_{i,e}} \quad (7.2.8)$$

In the current developed ANFIS structure there are six dimensional space partition and has “ $q_1 \times q_2 \times q_3 \times q_4 \times q_5 \times q_6$ ” regions. Each region is governed by a fuzzy if then rule. The first layer (consists of premise or antecedent parameters) of the ANFIS is dedicated to fuzzy sub space. The parameters of the fourth layer are referred as consequent parameters and are used to optimize the network. During the forward pass of the hybrid learning algorithm node outputs go forward until layer four and the consequent parameters are identified by least square method. In the backward pass, error signals propagate backwards and the premise parameters are updated by a gradient descent method.

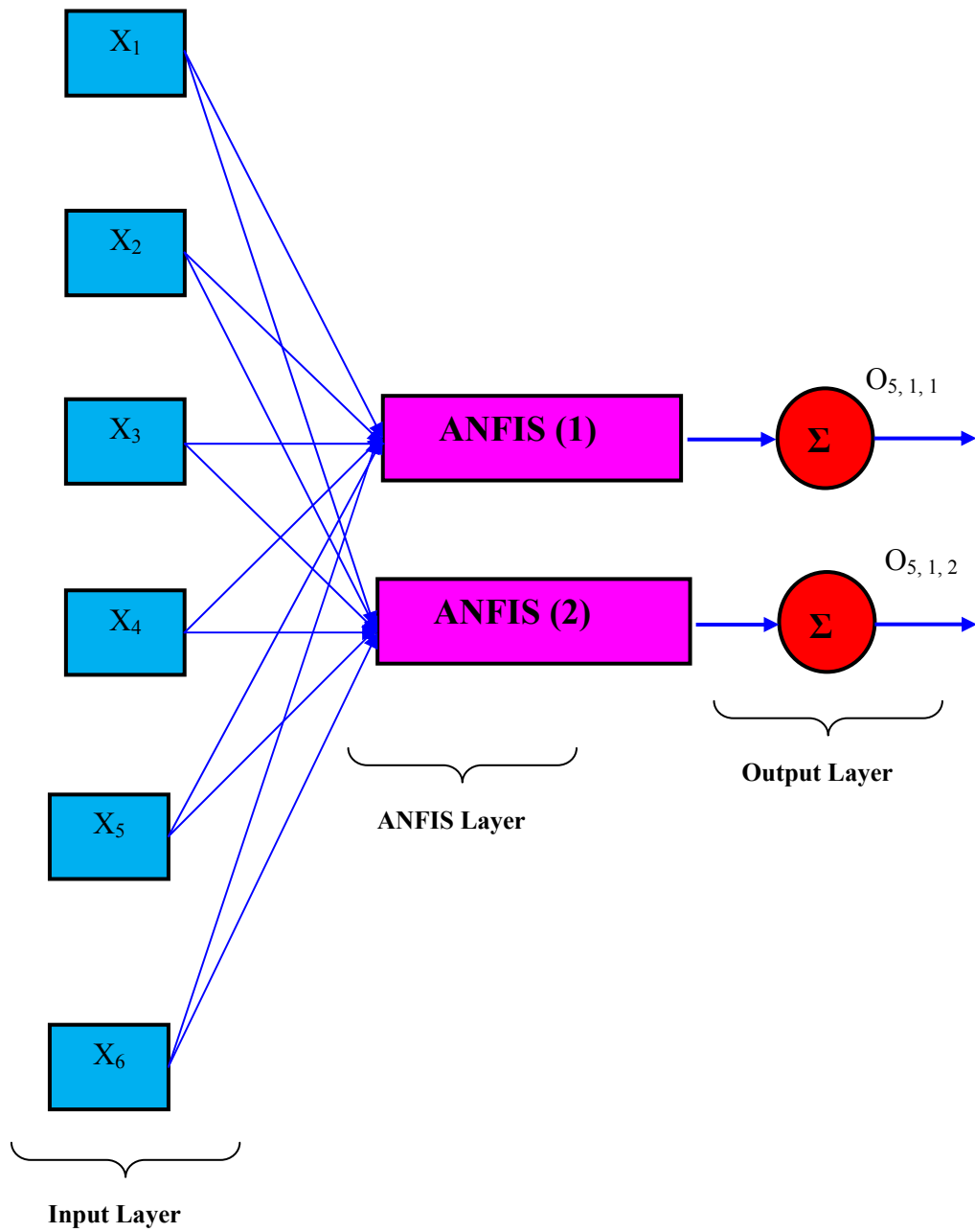


Fig. 7.2.2 Multiple ANFIS (MANFIS) controller for crack detection

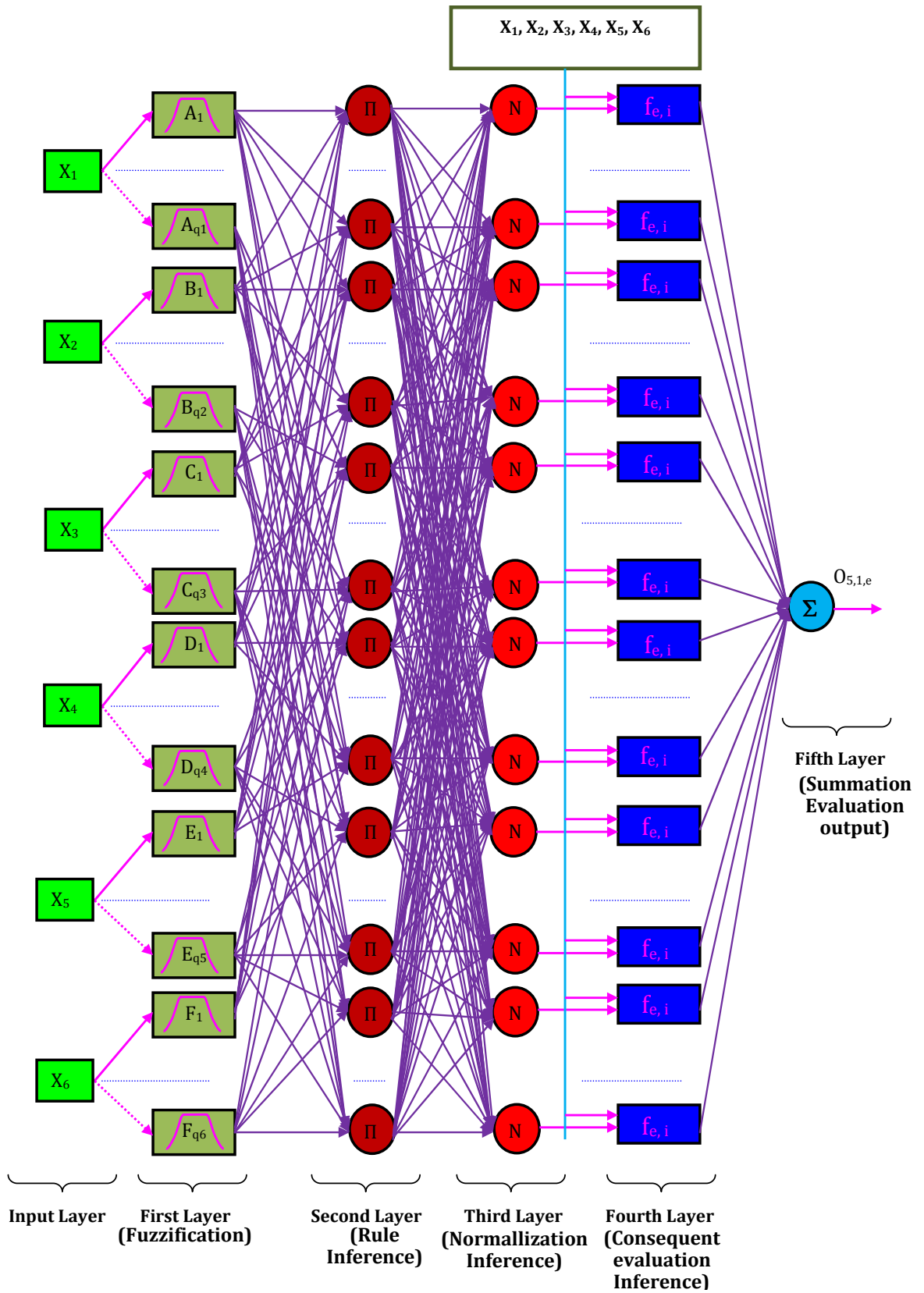


Fig. 7.2.3 Adaptive Neuro Fuzzy Inference System (ANFIS) for crack detection

7.3 Results of MANFIS Controller

The multiple adaptive neuro-fuzzy inference system is designed and developed to predict the relative crack location and relative crack depth. A comparison of results between the developed MANFIS, numerical analysis and experimental analysis is presented in Table 7.3.1. Finally the comparisons of results between the developed MANFIS, triangular fuzzy-neuro controller, gaussian fuzzy-neuro controller, trapezoidal fuzzy-neuro controller of chapter-6, neural controller of chapter-5 and triangular fuzzy controller, gaussian fuzzy controller and trapezoidal fuzzy controller of chapter-4 are presented in Table 7.3.2. In the Tables 7.3.1 and 7.3.2 ten sets of random inputs out of several hundred sets of inputs are taken. The inputs to different analyses described above, are relative first three natural frequencies and relative first three mode shape differences and the out puts are relative crack location and relative crack depth. Corresponding ten set of output results from the developed MANFIS controller, triangular fuzzy-neuro controller, gaussian fuzzy-neuro controller, trapezoidal fuzzy-neuro controller, neural controller, triangular fuzzy controller, gaussian fuzzy controller , trapezoidal fuzzy controller, numerical analysis and experimental analysis are given in the Table 7.3.1 and Table 7.3.2. In the Tables 7.3.1 and 7.3.2 the first column represents the relative 1st natural frequency (fnf), the second column represents the relative 2nd natural frequency (snf), the third column represents the relative 3rd natural frequency (tnf), the fourth column represents the relative 1st mode shape difference (fmd), the fifth column represents the relative 2nd mode shape difference (smd), the sixth column represents the relative 3rd mode shape difference (tmd) as inputs and the rest coloumns represents the outputs of relative crack location and relative crack depth.

Relative first natural frequency	Relative second natural frequency	Relative third natural frequency	Relative first mode shape difference	Relative second mode shape difference	Relative third mode shape difference	MANFIS Controller (relative crack depth “rcl” and location “rcl”)		Numerical (relative crack depth “rcl” and location “rcl”)		Experimental (relative crack depth “rcl” and location “rcl”)	
						rcl	rcl	rcl	rcl	rcl	rcl
“fnf”	“snf”	“tnf”	“fmd”	“smd”	“tmd”	rcl	rcl	rcl	rcl	rcl	rcl
0.9848	0.9958	0.9975	0.2709	0.2372	0.3158	0.202	0.0712	0.202	0.06888	0.205	0.0725
0.9673	0.9874	0.9943	0.3969	0.3247	0.3923	0.43	0.08	0.427	0.079	0.43	0.08388
0.9623	0.9948	0.9983	0.1814	0.0279	0.0774	0.543	0.159	0.537	0.15988	0.568	0.1575
0.9756	0.9976	0.9972	0.1383	-0.0823	0.1898	0.392	0.1865	0.394	0.18675	0.391	0.18775
0.9852	0.9984	0.9967	0.01	-0.8678	0.2572	0.231	0.2362	0.231	0.23625	0.23	0.24
0.9723	0.9961	0.9818	0.1947	0.0672	0.4105	0.555	0.2842	0.556	0.2825	0.545	0.28625
0.9823	0.9872	0.9919	0.0726	0.2567	0.3994	0.449	0.404	0.451	0.40388	0.447	0.40513
0.981	0.9809	0.9931	0.0898	0.3154	0.392	0.497	0.424	0.497	0.42388	0.495	0.4235
0.986	0.9842	0.9988	-0.032	0.322	0.3965	0.425	0.503	0.426	0.50125	0.425	0.50375
0.9834	0.9685	0.9974	0.038	0.4558	0.3507	0.538	0.5349	0.542	0.535	0.535	0.53313

Table 7.3.1 Comparison of the results of the MANFIS with the results of numerical and experimental analysis

Relative first natural frequency	Relative second natural frequency	Relative third natural frequency	Relative first mode shape difference	Relative second mode shape difference	Relative third mode shape difference	MANFIS Controller (relative crack depth "rcd" and location "rcf")		Triangular Fuzzy Neuro Controller (relative crack depth "rcd" and location "rcf")		Gaussian Fuzzy Neuro Controller (relative crack depth "rcd" and location "rcf")		Trapezoidal Fuzzy Neuro Controller (relative crack depth "rcd" and location "rcf")		Neural Network Controller (relative crack depth "rcd" and location "rcf")		Triangular Fuzzy Controller (relative crack depth "rcd" and location "rcf")		Gaussian Fuzzy Controller (relative crack depth "rcd" and location "rcf")		Trapezoidal Fuzzy Controller (relative crack depth "rcd" and location "rcf")	
						red	rcf	red	rcf	red	rcf	red	rcf	red	rcf	red	rcf	red	rcf	red	rcf
0.9848	0.9958	0.9975	0.2709	0.2372	0.3158	0.202	0.0712	0.204	0.071	0.203	0.069	0.202	0.07163	0.203	0.072	0.202	0.07163	0.203	0.07138	0.202	0.07163
0.9673	0.9874	0.9943	0.3969	0.3247	0.3923	0.43	0.08	0.429	0.082	0.431	0.079	0.431	0.08038	0.431	0.081	0.441	0.08238	0.431	0.08138	0.441	0.08238
0.9623	0.9948	0.9983	0.1814	0.0279	0.0774	0.543	0.159	0.552	0.158	0.548	0.16	0.542	0.15825	0.548	0.159	0.557	0.15825	0.548	0.15913	0.557	0.15825
0.9756	0.9976	0.9972	0.1383	-0.0823	0.1898	0.392	0.1865	0.393	0.188	0.389	0.1872	0.385	0.18475	0.389	0.187	0.382	0.18475	0.389	0.18725	0.382	0.18475
0.9852	0.9984	0.9967	0.01	-0.8678	0.2572	0.231	0.2362	0.229	0.239	0.227	0.2364	0.23	0.23613	0.227	0.238	0.229	0.23613	0.227	0.23688	0.229	0.23613
0.9723	0.9961	0.9818	0.1947	0.0672	0.4105	0.555	0.2842	0.551	0.285	0.552	0.283	0.545	0.28325	0.552	0.286	0.545	0.27625	0.552	0.28375	0.545	0.27625
0.9823	0.9872	0.9919	0.0726	0.2567	0.3994	0.449	0.404	0.449	0.404	0.449	0.404	0.446	0.40338	0.449	0.405	0.446	0.40338	0.449	0.40438	0.446	0.40338
0.981	0.9809	0.9931	0.0898	0.3154	0.392	0.497	0.424	0.496	0.424	0.495	0.424	0.497	0.42363	0.495	0.424	0.498	0.42263	0.495	0.42363	0.498	0.42263
0.986	0.9842	0.9988	-0.032	0.322	0.3965	0.425	0.503	0.425	0.503	0.425	0.5018	0.426	0.50163	0.425	0.503	0.428	0.50363	0.425	0.50188	0.428	0.50363
0.9834	0.9685	0.9974	0.038	0.4558	0.3507	0.538	0.5349	0.538	0.534	0.537	0.5331	0.534	0.53538	0.537	0.534	0.534	0.53538	0.537	0.53313	0.534	0.53538

Table 7.3.2 Comparison of the results of the MANFIS with the results of fuzzu-neuro, neural and fuzzy controller analysis

7.4 Discussions

Results obtained for the fault diagnosis from the developed MANFIS, triangular fuzzy-neuro controller, gaussian fuzzy-neuro controller, trapezoidal fuzzy-neuro controller, neural controller, triangular fuzzy controller, gaussian fuzzy controller, trapezoidal fuzzy controller, numerical and experimental analysis, following discussions are drawn.

Fig. 7.2.1 shows the Bell shaped membership function used as membership functions in layer-1 of ANFIS controller. Fig. 7.2.2 represents Multiple ANFIS (MANFIS) architecture for crack detection. The architecture of ANFIS for crack detection is shown in Fig. 7.2.3. Table 7.3.1 shows the comparison of results between the developed MANFIS, numerical analysis and experimental analysis. Table 7.3.2 represents comparison of results between the developed MANFIS, triangular fuzzy-neuro controller, gaussian fuzzy-neuro controller, trapezoidal fuzzy-neuro controller, neural controller and triangular fuzzy controller, gaussian fuzzy controller and trapezoidal fuzzy controller analysis. It is evident from the Tables 7.3.1 and 7.3.2 that the average percentage deviation of the results of MANFIS is 0.5%.

7.5 Summary

Following conclusions are drawn on the basis of analysis and results obtained from multiple adaptive neuro-fuzzy inference system;

Using the above analysis and MANFIS methodology condition monitoring of dynamic structures can be addressed effectively. The crack size and its location have got significant effect on the natural frequencies and mode shapes of the vibrating structures. MANFIS can predict the crack location and its size with the help of the natural frequencies and mode shape differences of the dynamic structures. The developed controller predicted the results are in close proximity with theoretical and experimental results.

Publications

- Parhi D.R. and Das H.C., Diagnosis of fault and condition monitoring of dynamic structures using MANFIS technique, *Journal of Aerospace Engineering Proceedings of the Institution of Mechanical Engineers, Part G, Vol. 223*, In Press.

Chapter 8

ANALYSIS AND DESCRIPTION OF EXPERIMENTAL SETUP

In order to justify the validation of the theoretical analysis and numerical analysis discussed in chapter-3 and different artificial intelligence methodologies proposed for prediction of crack location and crack depth discussed in chapter-3 to chapter-7, experimental investigations have been carried out. For the experimental investigations an experimental set-up has been developed in order to measure the dynamic response of the cantilever beam with a transverse crack. The details of the instruments used in the experimental set-up, test specimens and experimental procedure are presented in the subsequent sections.

8.1 Description of Instruments used in the Experimental Analysis

A (800 x 50 x 6mm) aluminum beam specimen is selected for the experimental investigations. The schematic block diagram of the whole experimental setup is shown in Fig. 3.3.1. It can be noted from the Fig. 3.3.1 that the electro-dynamic exciter is driven by a function generator connected to a signal amplifier. Vibration indicator connected to a vibration analyzer shows the vibration responses of cracked cantilever beam through the signal which comes from the accelerometer. The detailed specifications of the instruments used in this investigation are given below.

1. Vibration pick-up (Accelerometer)	-	Delta Tron Accelerometer
		Type : 4513-001
		Make : Bruel & kjaer
		Sensitivity : 10mv/g-500mv/g
		Frequency
		Range : 1Hz-10KHz
		Supply voltage: 24volts
		Operating
		temperature
		Range : -50 ⁰ C to +100 ⁰ c

2. Vibration Analyzer - Type : 3560L
Product Name : Pocket front end
Make : Bruel & kjaer
Frequency Range : 7 Hz to 20 Khz
ADC Bits : 16
Simultaneous Channels : 2 Inputs,
2 Tachometer
Input Type : Direct/CCLD
3. Vibration indicator - PULSE LabShop Software Version 12
Make : Bruel & kjaer
4. Function Generator - Model : FG200K
Frequency Range : 0.2Hz to 200 KHz
VCG IN connector for Sweep Generation
Sine, Triangle, Square, TTL outputs
Output Attenuation up to 60dB
Output Level : 15Vp-p into 600 ohms
Square Wave
Rise/Fall Time : <300nSec
Make : Aplab
5. Power Amplifier - Type : 2719
Power Amplifier : 180VA
Make : Bruel & kjaer

6. Vibration Exciter - Type : 4808
 Permanent Magnetic Vibration Exciter
 Force rating 112N (25 lbf) sine peak
 (187 N (42 lbf) with cooling)
 Frequency
 Range : 5Hz to 10 kHz
 First axial
 resonance : 10 kHz
 Maximum bare table
 Acceleration : 700 m/s² (71 g)
 Continuous 12.7 mm (0.5 in)
 peak-to-peak displacement
 with over travel stops
 Two high-quality, 4-pin
 Neutrik® Speakon® connectors
 Make: Bruel & kjaer
7. Specimen - cantilever type cracked aluminum
 beam specimen of dimension
 (800 x 50 x 6mm)

8.2 Experimental Set-up

A cracked cantilever beam has been rigidly clamped to the concrete foundation base as shown in the Fig.8.1. The free end of the beam is excited with a vibration exciter. The vibration exciter is excited by the signal from the function generator. The signal is amplified by a power amplifier before being fed to the vibration exciter. The amplitude of vibration of the uncracked and cracked cantilever beam is taken by the accelerometer and is fed to the vibration indicator (PULSE LabShop Software Version 12) for vibration analysis. The vibration signatures are analyzed graphically by PULSE LabShop Software loaded in the laptop. The views of the instruments used in the experimental set-up are shown in Figs. 8.2(a) - 8.2(g) .



Fig. 8.1 View of complete assembly of the experimental set-up



Fig.8.2 (a) Concrete foundation with beam specimen

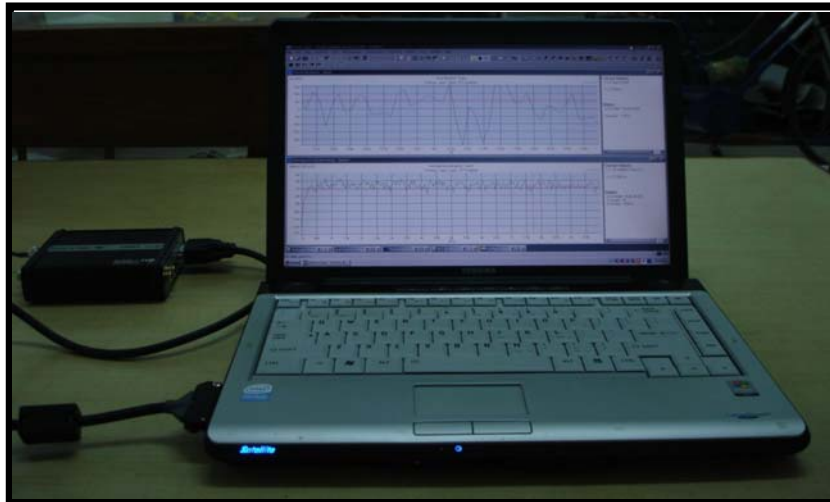


Fig.8.2 (b) Vibration indicator (PULSE labShop software) with lap top



Fig.8.2 (c) Vibration exciter



Fig.8.2 (d) Vibration pick-up (accelerometer)



Fig.8.2 (e) Vibration analyser



Fig.8.2 (f) Function generator



Fig.8.2 (g) Power amplifier

Fig.8.2 View of the instruments used in the experimental set-up

8.3 Experimental Procedure

Several tests are conducted using the experimental setup (Fig. 8.1) on Aluminum beam specimens (800 x 50 x 6mm) with a transverse crack for determining the natural frequencies and mode shapes for different crack locations and crack depths. These specimens are set to vibrate under 1st, 2nd and 3rd mode of vibrations and the corresponding amplitudes are recorded in the vibration indicator. Experimental results for amplitude of transverse vibration at various locations along the length of the beam are recorded by positioning the vibration pick-up and tuning the vibration generator at the corresponding resonant frequencies.

8.4 Experimental Results and Discussions

The experimental results of relative amplitude for different relative crack locations (0.026, 0.05128) and different crack locations (0.3, 0.4) for 1st, 2nd and 3rd modes of vibration are presented graphically in Fig.3.3.2, Fig.3.3.3 and Fig.3.3.4 in section 3.3.1 of chapter 3. Corresponding results of numerical analysis are also presented in the same graph for cracked and uncracked beam for immediate comparison. The experimental results for relative crack location and relative crack depth are compared with the corresponding results of the triangular, gaussian and trapezoidal fuzzy controller in Table 4.3.6 of chapter-4 and are found to be in good agreement. The experimental results for relative crack location and relative crack depth are compared with the corresponding results of the back propagation neural controller in Table 5.3.4 of chapter-5 and are found to be in agreement. The experimental results for relative crack location and relative crack depth are also compared with the corresponding results of the triangular, gaussian and trapezoidal fuzzy-neuro controllers in Table 6.2.1 of chapter-6 and are found to be in good agreement. The experimental results for relative crack location and relative crack depth are also compared with the corresponding results of the multiple adaptive neuro-fuzzy controller in Table 7.2.1 of chapter-7 and are found to be in good agreement.

Chapter 9

RESULTS AND DISCUSSIONS

9.1 Introduction

In this section the results obtained from different analyses performed on the cracked cantilever beam have been analyzed and discussed. The effects of crack parameters on the dynamic response of the structure have been elaborated.

9.2 Discussions of Results

The current research has been carried out in seven stages. The stages comprised of are 1) Literature survey. 2) Analysis of dynamic characteristics of beam with a transverse crack. 3) Analysis of fuzzy logic technique for crack detection. 4) Analysis of artificial neural network for crack detection. 5) Analysis of hybrid fuzzy neuro system for crack detection. 6) Analysis of MANFIS for crack detection 7) Analysis and description of experimental setup. These stages are presented in chapter forms from chapter two to chapter eight. The outcomes of results of different chapters during analysis are presented below systematically.

Chapter two depicts the various methodologies adapted since last five decades for crack detection in damaged structures. Many condition monitoring tools used by authors for fault detection in different domain of engineering applications with the help of artificial intelligence techniques have been discussed.

In chapter three theoretical analysis has been carried out on the cracked cantilever beam (Fig. 3.2.1). During analysis it is observed that the crack position and crack depth have a considerable effect on the dynamic response of the beam. The variation of the mode shapes for the 1st three modes of vibration and the significant changes in the mode shapes at the crack location can be seen with magnifying views in Fig. 3.2.4 to Fig. 3.2.27. From the analysis it is found that with the increase in relative crack depth there is an increase in

dimensionless compliances (Fig. 3.2.2), which clearly shows the relationship between relative crack depth and vibration parameters of the structure. The results from the numerical analysis have been validated with the results obtained from the developed experimental set up (Fig. 3.3.1). The comparisons of results from theoretical and experimental analysis for the cracked and uncracked beam are presented in Fig.3.3.2 to Fig.3.3.4, which shows a close agreement. The variation of relative natural frequencies, relative mode shapes with respect to relative crack locations and relative crack depth in three dimensional forms, along with the contour plots are depicted in Fig.3.2.28 and Fig.3.2.29 respectively.

Fuzzy controllers have been designed for prediction of crack location and its severity using three different types of membership functions such as triangular function (Fig. 4.2.1(a)), Gaussian function (Fig. 4.2.1(b)) and trapezoidal function (Fig. 4.2.1(c)) and are presented in chapter four. The fuzzy controllers developed here take the 1st three natural frequencies and mode shape differences as input parameters and relative crack depth and relative crack location as output parameters as shown in Fig. 4.2.2. Several fuzzy rules and fuzzy linguistic terms have been developed to design the fuzzy controller, some of them are described in Table 4.3.1 and Table 4.3.2. The complete architecture of triangular, Gaussian, trapezoidal fuzzy controller are presented in Fig. 4.3.1, Fig. 4.3.2 and Fig. 4.3.3 respectively. Fig. 4.3.4 to Fig. 4.3.6 exhibits the fuzzy results after defuzzification when rule 1 and 19 of the Table 4.3.2 are activated for triangular, Gaussian and trapezoidal membership function respectively. Table 4.3.3 gives the comparison among the results obtained from numerical, experimental, fuzzy controller with triangular membership function, fuzzy controller with gaussian membership function and fuzzy controller with trapezoidal membership functions. Results obtained from gaussian membership function fuzzy controller is more accurate in comparison to other two controllers and the computational time for crack prediction is considerably lower as compared to numerical analysis. The predicted results from fuzzy controllers for crack location and crack depth are compared with the theoretical and experimental results for cross verification. A close agreement between the results is found.

Chapter five describes the design of neural network controller with back propagation method (Fig.5.2.5) for prediction of crack location and its size for the cracked cantilever beam. The details of neural network technique (Fig.5.2.1), reasons for using neural network, activation

function (Fig.5.2.2), modeling of multi layer perceptron have been depicted in section 5.2. Neural network approach has been used to develop the controller so as to take the advantage of neuron for high accuracy results and faster computation. The neural network controller has been trained with eight hundred patterns of data of different crack location and crack depth gives out put such as relative crack depth and relative crack location. Few of the examples of training patterns out of several hundreds to train the controller are given in the Table 5.3.1. The working principle of the ten layer feed forward controller and a schematic diagram of multi layer neural network controller is depicted in Fig.5.3.2 and Fig.5.3.1 respectively. The controller is made of ten layers with one input layer, eight numbers of hidden layer and one output layer. The input layer takes the relative natural frequencies and relative mode shapes as input parameters where as relative crack location and relative crack depth are the results from the output layer. The controller is designed in a diamond shape for convergence of results. It is observed that the error in the output of the controller is considerably reduced from the desired output by employing error back propagation method. The result from the controller is compared with the outputs from numerical, fuzzy and experimental analysis for checking the robustness of the developed system. The comparison of the results from neural controller, fuzzy controllers, numerical analysis and experimental analysis are expressed in Table 5.3.2. The prediction of crack location and its intensity from the neural network controller is very close to the actual results.

Fuzzy neuro controllers have been developed in chapter six by integrating the capabilities of fuzzy logic and neural network for prediction of crack in damaged structures. Fig. 6.2.1, Fig. 6.2.2 and Fig. 6.2.3 represent the developed fuzzy-neural controllers with triangular, gaussian and trapezoidal membership functions respectively. These three controllers are used for prediction of crack location and crack depth. The fuzzy-neuro controller is based on the natural frequencies and mode shape differences of the structures with crack. Table 6.2.1 and Table 6.2.2 show the comparison of the results of triangular, gaussian and trapezoidal fuzzy-neuro controllers with the results from numerical, experimental, neural controller and triangular, gaussian and trapezoidal fuzzy controllers. The predicted values from the designed hybrid controller of crack location and its size are compared with the numerical, experimental, neural and fuzzy controllers results and are found to be well in agreement. This

fuzzy-neuro controller can be used as an effective tool for fault diagnosis of vibrating structures.

Multiple adaptive neuro fuzzy inference system (MANFIS) has been developed for effective condition monitoring in dynamically vibrating structures and is discussed in chapter seven. Bell shaped membership function has been adapted for designing the MANFIS controller. Fig. 7.2.1 shows the Bell shaped membership function used in layer-1 of ANFIS controller. Relative natural frequencies and relative mode shapes are the input parameters for the controller and relative crack depth and relative crack location are the output parameters from the controller. Fig. 7.2.2 represents multiple ANFIS (MANFIS) controller for crack detection. The architecture of Adaptive neuro-fuzzy inference system (ANFIS) for crack detection is shown in Fig. 7.2.3. Table 7.3.1 shows the comparison of results between the developed MANFIS controller, numerical analysis and experimental analysis. From the comparison it is evident that the results from the MANFIS controller have higher accuracy with respect to numerical analysis. Table 7.3.2 represents comparison of results between the developed MANFIS controller, triangular fuzzy-neuro controller, gaussian fuzzy-neuro controller, trapezoidal fuzzy-neuro controller, neural controller and triangular fuzzy controller, gaussian fuzzy controller and trapezoidal fuzzy controller analysis. From the analysis of the Table 7.3.2 it is observed that the results obtained from the MANFIS technique yields better results with least amount of error as compared to the other methods cited in the Table 7.3.2.

Chapter eight discusses on various instruments used in the experimental setup for carrying out the experimental analysis. The instruments used are 1. Concrete foundation with beam specimen 2. Vibration indicator (PULSE labShop software) with lap top 3. Vibration exciter 4. Vibration pick-up (accelerometer) 5. Vibration analyzer 6. Function generator 7. Power amplifier and are given in Fig. 8.2(a) to Fig. 8.2(g) respectively. This chapter also discusses the experimental procedure in section 8.3. During experimental analysis care has been taken to reduce error and noise signal.

The contributions, conclusions and scope for future work of the above analysis have been given in the next chapter.

Chapter 10

CONCLUSIONS AND FURTHER WORK

The aim of this research has been to develop an efficient methodology for diagnosis of crack in a vibrating structure. To achieve the above objective a comprehensive investigation has been carried out to study the effect of crack on the vibration signatures of a dynamically vibrating uniform cracked cantilever beam. The vibration analysis has been carried out in several stages, such as theoretical, numerical, and experimental analysis. The influence of cracks on the dynamic behavior of the beam is found to be very sensitive in regards to crack location, crack depth and mode number. A number of inverse methods have been developed comprising of artificial intelligence techniques such as fuzzy logic, neural network, fuzzy neuro and MANFIS techniques for predicting the crack location and its severity based on changes in the vibration signatures (natural frequencies, mode shapes).

On the basis of analyses and discussions done in previous chapters, the following contributions and conclusions of the research are drawn.

10.1 Contributions

Theoretical analysis of the cracked beam on the basis of strain energy release rate has been carried out to find out the effect of crack depth and crack location on vibration signatures of the beam.

Numerical analysis has been carried out on the basis of above theoretical and experimental analysis for studying the influence of crack depth and crack location on the dynamic response of the cracked beam. Four inverse methods comprising of artificial intelligence techniques such as fuzzy logic, neural network, fuzzy neuro and MANFIS have been developed for diagnosis of crack depth and crack location.

10.2 Conclusions

- Small crack depth ratios have little effects on the natural frequencies of the cracked cantilever beam. Deviations in mode shapes are noticeable due to presence of crack. Analysis of change in natural frequencies and mode shape in combination is effective for prediction of crack in beam structure containing small crack.
- A clearcut deviation in the mode shapes and natural frequencies at the vicinity of crack location has been observed from the comparison of the results of the un cracked and cracked beam during the vibration analysis.
- Unique changes have been observed in the natural frequencies and mode shapes with the change of crack depth and crack location. The changes in the vibration signatures become more prominent as the crack grows bigger. It is observed that the results from theoretical, numerical and experimental analysis are in good agreement.
- Three types of fuzzy controllers have been designed with triangular, gaussian and trapezoidal membership functions to predict the crack location and its size with the help of natural frequencies and mode shape differences. During this design several rules are formed and are used with various membership functions.
- It has been observed that the developed fuzzy controllers can predict the relative crack location, relative crack depth of the beam with a considerably less amount of computational time.
- Comparisons of fuzzy controller results with the experimental results show the effectiveness of the proposed methods towards the identification of location and extent of damage in vibrating structures. Fuzzy controller with gaussian membership function is found to be more suitable.
- The neural network controller has been developed using back propagation algorithm to predict the crack location and size by using relative deviation of first three natural frequencies and first three mode shapes as inputs. The neural network controller predicted results are reasonably acceptable and in agreement with the experimental

data. The successful detection of crack and its intensity in cantilever beam demonstrates that the new technique developed can be used as a smart fault detecting tool for different types of vibrating structures.

- From the comparison of fuzzy and neural network controller results, the neural controller is found to deliver closer result with respect to actual result.
- The fuzzy neuro hybrid intelligent systems have been designed with relative deviation of first three natural frequencies and first three mode shapes as input parameters and relative crack depth and relative crack location as output parameters. The predicted results are found to be of higher accuracy than the results obtained from independent fuzzy and neural controller.
- The multiple adaptive neuro fuzzy inference system (MANFIS) has been designed and is used as an effective tool for diagnosis of crack in vibrating structures. The results obtained from MANFIS controller are found to be of higher accuracy than fuzzy and neural controllers results. The developed MANFIS controller predicted results are in close proximity with theoretical and experimental results.
- After analysis the errors obtained from various methodologies developed using artificial intelligence techniques, it can be stated that the fuzzy-neuro hybrid intelligence controller based on Gaussian membership function and the MANFIS controller are two most efficient controllers for fault diagnosis.

10.3 Applications

- The developed controllers can be used as effective tools for online condition monitoring of engineering systems.
- The present study can be utilized for inverse engineering application/problems, and can also be used in biomedical engineering system for fault detection.

- The methodologies formulated using artificial intelligence techniques can be used for prediction of fatigue crack of offshore structure, flow lines, turbo machinery, nuclear plants, ship structures etc.

10.4 Scope for Future Work

- In this research fault diagnosis and structural health monitoring systems have been derived using vibration signatures. These developed techniques can be extended to predict the health of complex structures with multiple cracks.
- Genetic algorithm can be hybridized with the current developed controller for design of more robust fault diagnosis system.
- Systems can be developed for fault diagnosis of structures subjected to moving load.

REFERENCES

1. Ayre, R.S. and Jacobsen, L.S., 1950. Natural frequencies of continuous beams of uniform span length, *Journal of Applied Mechanics* **17**, pp. 391–395.
2. Miles, J.W., 1956. Vibration of beams on many supports, *Proceedings of the American Society of Civil Engineers, Engineering Mechanics Division* **82**, pp. 1–9.
3. Bollinger, J.G and Geiger, G., 1964 Analysis of the static and dynamic behavior of lathe spindles, *International Journal of Machine Tool Design and Research*, **3(4)**, pp.193-209.
4. Gladwell, G.M.L., 1964. Branch mode analysis of vibrating systems. *Journal of Sound and Vibration*, **1**, pp 41-59.
5. Mercer, C.A and Seavey. C., 1967. Prediction of natural frequencies and normal modes of skin-stringer panel rows, *Journal of Sound and Vibration* **6**, pp.149–162.
6. Watrasiewicz, B.M., 1968. Mechanical vibration analysis by holographic methods, *Optics Technology*, 1(1), pp.20-23.
7. Lin, Y.K. and Donaldson, B.K., 1969. A brief survey of transfer matrix techniques with special reference to the analysis of aircraft panels, *Journal of Sound and Vibration* **10**, pp. 103–143.
8. Chun, K.R., 1972. Free vibrations of a beam with one end spring hinged and the other free, *Transactions of the American Society of Mechanical Engineers, Journal of Applied Mechanics* **39** pp. 1154–1155.
9. Lee, T.W., 1973. Vibration frequencies for a uniform beam with one end spring-hinged and carrying a mass at the other free end, *Transactions of the American Society of Mechanical Engineers, Journal of Applied Mechanics* **40**, pp. 813–815.
10. Thomas, D.L. and Wilson, R.R., 1973. The use of straight beam finite elements for analysis of vibrations of curved beams, *Journal of Sound and Vibration*, **26(1)**pp. 155-158.
11. Venkateswara, R. G. and Kanaka R.K., 1974. A galerkin finite element analysis of a uniform beam carrying a concentrated mass and rotary inertia with a spring hinge. *Journal of Sound and Vibration*, **37(4)**,pp. 567-569.

12. Rayleigh J.W.S., 1894. Theory of sound, Dover Publ., New York.
13. Ritz, W. Crelle's journal, **85**, 1909.
14. Donaldson, J.M. 1968. Reduction of noise radiated from ship structures, *Applied Acoustics*, **1**(4) pp. 275-291.
15. Henderson, J.P and McDaniel, T.J., 1971. The analysis of curved multi-span structures, *Journal of Sound and Vibration* **18** , pp. 203–219.
16. Tottenham, H. and Shimizu.K., 1972. Analysis of the free vibration of cantilever cylindrical thin elastic shells by the matrix progression method, *International Journal of Mechanical Sciences*, **14**(5)pp. 293-310.
17. Petyt, M. and Fleischer, C.C., 1974. Vibration of multi-supported curved beams, *Journal of Sound and Vibration*, **32**(3)pp. 359-365.
18. Gorman, D.J. Free lateral vibration analysis of double-span uniform beams, *International Journal of Mechanical Sciences*, **16**(6)pp. 345-351.
19. Irwin G.R., 1957. Relation of stresses near a crack to the crack extension force, *Actes IX congress International Mechanical Application*, T.8 Universities Bruxelles, pp. 245-251.
20. Tada, H., Paris, P.C and Irwin G.R., 1973. The stress analysis of cracks hand book. *Del Research Corp. Hellertown, Pennsylvanian.*
21. Pafertias T., 1979. Dynamic behavior of a cracked rotor, Technical Information Series, General electric No DF-74-LS-79.
22. Gash, R., 1993. A survey of dynamic behavior of a simple rotating shaft with a transverse crack, *Journal of Sound and Vibration*, **160**(2), pp.313-332.
23. Henry T.A. & Okah Ave B.E., 1976. Vibration in cracked shaft, *IME conference of publication, Vibration in rotating machinery*, pp.c162/76.
24. Mayes, I.W. and Davies, W.G.R, 1976. The vibrational Behavior of a Rotating shaft System Containing a Transverse crack, *IME Conference Publication , Vibration of Rotating Machinery*, **c/168**(76), pp.53-64.
25. Freund, L.B. and Herrmann, G., 1976. Dynamic Fracture of a Beam or Plate in Plane Bending, *Trans ASME, Journal of Applied Mechanics*, pp.112-116.

26. Adeli, H., Herrmann, G. and Freund, L.B., 1977. Effect of Axial Force on Dynamic Fracture of a Beam or Plate in Pure Bending. *A.S.M.E. Journal of Applied Mechanics*, **47**, pp.647-651.
27. Dentsoras, A.J. and Dimarogonas, A.D., 1983. Resonance Controlled Fatigue crack Propagation in a Beam Under Longitudinal Vibration. *International Journal of Fracture*, **23** pp.15-22.
28. Wong, E and Zu, J.W., 1999. Dynamic Response of a Coupled Spinning Timoshenko Shaft System, *Trans ASME, Journal of Vibration and Acoustics*, **121**, pp.110-113.
29. Nian, G.S., Lin, Z.J., Sheng, J.J and An, H.C. , 1989. A Vibration Diagnosis Approach to Structural fault. *A.S.M.E., Journal of Vibration, Acoustics, stress, and Reliability in Design*, **111**, pp.88-93.
30. Quain, G.L., Gu, S. N. and Jiang, J.S., 1990, The dynamic behavior and crack detection of a beam with a crack, *Journal of Sound and Vibration*, **138**(2), pp. 233-243.
31. Ismail, F., Ibrahim, A. and Martin, H.R., 1990, Identification of Fatigue cracks from vibration testing, *Journal of Sound and Vibration*, **140**(2), pp. 305-317.
32. Sekhar, A.S. and Prabhu, B.S., 1992 Crack detection and vibration characteristics of a cracked shaft, *Journal of Sound and Vibration*, **157**(2), pp. 375-381.
33. Sorkin. G, Pohler. C.H, Stavovy, .A.B and Borriello.F.F., 1973. An overview of fatigue and fracture for design and certification of advanced high performance ships, *Engineering Fracture Mechanics*, **5**(2)pp. 307-352.
34. Rao, V.G., Sundararamaiah.V., and Raju, I.S., 1974. Finite element analysis of vibrations of initially stressed thin shells of revolution, *Journal of Sound and Vibration*, **37**(1) pp.57-64.
35. Wood H. A., 1975. Application of fracture mechanics to aircraft structural safety, *Engineering Fracture Mechanics*, **7**(3) pp. 557-558.
36. Dimarogonas, A.D. and Papadopoulos, C.A., 1983. Vibration of cracked shafts in bending, *Journal of Sound and Vibration*, **91**, pp- 583-593.
37. Kitipornchai, S. and Chan, S.L., 1987. Nonlinear Finite Element Analysis of Angle and Tee Beam-Columns, *Journal of Structural Engineering*, ASCE, **113**(4), 721-739.

38. Rizos, P.F., Aspragathos, N. and Dimarogonas, A.D., 1989. Identification of cracked location and magnitude in a cantilever beam from the vibrational modes, *Journal of Sound and Vibration*, **138** (3), pp.381 – 388.
39. Ostachowicz, W. M. and Krawczuk, M. 1990. Vibration analysis of a cracked beam, *Computers & Structures*, **36**(2) pp. 245-250.
40. Shen, M. H. H. and Taylor, J. E., 1991. An identification problem for vibrating cracked beams, *Journal of Sound and Vibration*, **150** (3), pp. 457-484.
41. Shen, M.H.H. and Chu, Y.C., 1992. Vibrations of beams with a fatigue crack, *Computers & Structures*, **45** (1), pp. 79-9317.
42. Narkis, Y., 1994. Identification of Crack Location in Vibrating Simply Supported Beams. *Journal of sound and vibration*, **172**(4), pp. 548-558.
43. Müller, P. C., Bajkowski, J. and Söffker, D., 1994. Chaotic motions and fault detection in a cracked rotor, *Nonlinear Dynamics*, **5**(2) pp.233-254.
44. Dimarogonas, A., 1996. Vibration of Cracked Structures: A State of the Art Review. *Engineering Fracture Mechanics*. **55**, pp. 831-857.
45. Tsai, T. C. and Wang, Y. Z., 1996. Vibration Analysis and diagnosis of a cracked beam, *Journal of Sound and Vibration*, **192**(3), pp.607-620.
46. Gounaris, G.D. and PapadoPoulos, C.A., 1997. Analytical and experimental crack identification of beam structures in air or in fluid, *Computers and Structures*, **65**(5) , pp.633-639.
47. Chondros, T.G. and Dimarogonas, A.D., 1998. Vibration of a Cracked Cantilever Beam, *Journal of Vibration and Acoustic*, **120**, pp. 742-746.
48. Chondros, T.G, Dimarogonas, A.D. and Yao, J. A., 1998. Continuous cracked beam vibration theory, *Journal of Sound and Vibration*, **215**, pp.17-34.
49. Yokoyama, T. and Chen, M. C., 1998.Vibration analysis of edge-cracked beams using a line-spring model, *Engineering Fracture Mechanics*, **59**(3), pp. 403-409.
50. Kisa, M. and Brandon J., 2000. The Effects of closure of cracks on the dynamics of a cracked cantilever beam, *Journal of Sound and Vibration*, **238**(1), pp.1-18.
51. Fabrizio, V. and Danilo, C., 2000. Damage detection in beam structures based on frequency measurements, *J. Engrg. Mech* , **126**(7), pp. 761-768.

52. Xia, Y. and Hong, H., 2000. Measurement Selection for vibration based Structural damage identification, *Journal of Sound and Vibration*, **236**(1), pp. 89-104.
53. Duffey, T.A., Doebling, S.W., Farrar, C.R., Baker, W.E. and Rhee, W.H., 2001. Vibration-Based Damage Identification in Structures Exhibiting Axial and Torsional Response. *Journal of Vibration and Acoustic*. **123**, pp. 84-91.
54. Viola, E., Federici, L. and Nobile, L., 2001. Detection of crack location using cracked beam element method for structural analysis. *Theoretical and Applied Fracture Mechanics*. **36**, pp. 23-35.
55. Saavedra, P.N. and Cuitono, L.A., 2001. Crack detection and vibration behavior of cracked beams. *Computers and Structures*. **79**, pp. 1451-1459.
56. Yang, X. F., Swamidas, A. S. J. and Seshadri, R., 2001. Crack Identification in vibrating beams using the Energy Method, *Journal of Sound and vibration* **244**(2), pp.339-357.
57. Gounaris, G., Papadopoulos, C. A., 2002. Crack identification in rotating shafts by coupled response measurements *Engineering Fracture Mechanics*, **69**, pp.339-352.
58. Fernandez-saez, J., Rubio, L. and Navarro, C., 2002. Approximate calculation of the fundamental frequency for bending vibrations of cracked beams. *Journal of Sound and Vibration* **225** (2), pp. 345-352.
59. Yang, B., Suh, C. S. and Chan, A. K., 2002. Characterization and Detection of Crack-induced Rotary Instability, *Journal of Vibration and Acoustics*, **124**(1), pp. 40-49.
60. Saavedra, P. N. and Cuitiño, L. A., 2002. Vibration Analysis of Rotor for Crack Identification, *Journal of Vibration and Control*, **8**(1), pp.51-67.
61. Kim, J.T. and Stubbs, M., 2002. Improved Damage Identification Method based on modal information, *Journal of Sound and Vibration*, **252** (2), pp. 223-238.
62. Patil, D.P., Maity, S.K., 2003. Detection of multiple cracks using frequency measurements. *Engineering Fracture Mechanics*. **70**, pp. 1553-1572.
63. Darpe, A.K., Gupta K. and Chawla A., 2003. Dynamics of a two-crack rotor, *Journal of Sound and Vibration*, **259** (3), pp.649-675.
64. Zheng, D.Y. and Fan, S.C., 2003. Vibration and stability of cracked hollow sectional beam, *Journal of sound and vibration*, **267**(4), pp.933-954.

65. Zou, J., Chen, J., Niu, J.C. and Geng, Z.M., 2003. Discussion on the local flexibility due to the crack in a cracked rotor system,” *Journal of sound and vibration*, **262**(2), pp.365-369.
66. Owolabi, G. M., Swamidas , A. S. J. and Seshadri, R. 2003. Crack detection in beams using changes in frequencies and amplitudes of frequency response functions,” *Journal of Sound and Vibration*, **265** (1), pp. 1-22.
67. Hwang, H.Y. and Kim, C., 2004. Damage detection in structures using a few frequency response measurements. *Journal of Sound and Vibration*. **270**, pp. 1-14.
68. Loutridis, S., Douka, E. and Trochidis, A., 2004. Crack identification in double-cracked beams using wavelet analysis. *Journal of Sound and Vibration*. **277**, pp. 1025-1039.
69. Wang, Q., 2004. A comprehensive stability analysis of a cracked beam subjected to follower compression. *International Journal of Solids and Structures*. **41**, pp. 4875-4888.
70. Kishen, C. J.M., and Kumar, A., 2004. Finite element analysis for fracture behavior of cracked beam-columns, *Finite Elements in Analysis and Design*, **40**, pp.1773 – 1789.
71. Hwang, H.Y. and Kim C., 2004. Damage detection in structures using a few frequency response, *Journal of Sound and Vibration*, **270**, pp. 1–14.
72. Dharmaraju, N., Tiwari, R. and Talukdar, S., 2004. Identification of an open crack model in a beam based on force–response measurements, *Computers and Structures* **82**, pp.167–179.
73. Khiem, N. T. and Lien, T. V., 2004. Multi-crack detection for beam by the natural frequencies, *Journal of Sound and Vibration*, **273** (1-2), pp.175-184.
74. Kyricazoglou, C., Le Page, B.H. and Guild, F. J., 2004. Vibration damping for crack detection in composite laminates, *Composites Part A: Applied Science and Manufacturing*, **35**(7-8), 2004, pp.945-953.
75. Zheng, D.Y. and Kessissoglou, N.J. 2004. Free vibration analysis of a cracked beam by finite element method, *journal of sound and vibration*, **273**(3), pp.457-475.

76. Mackerle, J., 2004. Finite-element modelling of non-destructive material evaluation, an addendum: a bibliography (1997–2003), *Modelling and Simulation in Materials Science and Engineering*, **12**, pp.799-834.
77. Wang, K., Inman, D.J. and Farror, C. R., 2004. Modeling and analysis of a cracked composite cantilever beam vibrating in coupled bending and torsion,” *journal of sound and vibration*, **284**(1-2), pp.23-49.
78. Cerri, M.N. and Ruta, G.C., 2004. Detection of localized damage in plane circular arches by frequency data, *Journal of Sound and vibration*, **270**(1-2), pp.39-59.
79. Nobile, L., Carloni, C. and Nobile, M., 2004. Strain energy density prediction of crack initiation and direction in cracked T beams and pipes, *Theoretical and Applied fracture mechanics*, **41**(1-3), pp.137-145.
80. Luh, G.C. and Cheng, W.C., 2005. Immune model-based fault diagnosis, *Mathematics and Computers in Simulation*, **67**(6), pp.515-539
81. Chondros, T.G. ,2005. Variational formulation of a rod under torsional vibration for crack identification, *Theoretical and Applied Fracture Mechanics*,**44**(1), pp. 95-104.
82. Escobar, J.A., Sosa, J.J. and Gomez, R., 2005. Structural damage detection using the transformation matrix. *Computers and Structures*. **83**, pp. 357-368.
83. McAdams, D.A., Tumer, I.Y., 2005. Toward Intelligent Fault Detection in Turbine Blades: Variational Vibration Models of Damaged Pinned-Pinned Beams. *Journal of Vibration and Acoustic*. **127**, pp. 467-474.
84. Binici, B., 2005. Vibration of beams with multiple open cracks subjected to axial force. *Journal of Sound and Vibration*. **287**, pp. 277-295.
85. Chang, C.C., Chen, L.W., 2005. Detection of the location and size of cracks in the multiple cracked beam by spatial wavelet based approach. *Mechanical Systems and Signal processing*. **19**, pp. 139-155.
86. Wang, K., Inman, D.J. and Farrar, C.R., 2005. Crack-induced Changes in Divergence and Flutter of Cantilevered Composite Panels. *Structural Health Monitoring*. **4**, pp.377-392.
87. Law, S.S. and Lu, Z.R., 2005. Crack identification in beam from dynamic responses”. *Journal of Sound and Vibration*. **285**, pp. 967-987.
88. Cam, E., Orhan, S. and Luy, M., 2005. An analysis of cracked beam structure using

- impact echo method. *NDT & E International*. **38**, pp. 368-373.
89. Sekhar, A.S., Mohanty A.R. and Prabhakar, S., 2005. Vibrations of cracked rotor system: transverse crack versus slant crack, *Journal of Sound and Vibration* **279**, pp. 1203–1217.
 90. Çam, E., Sadettin, O. and Murat, L., 2005. An analysis of cracked beam structure using impact echo method, *NDT and E International*. **38**, pp. 368–373.
 91. Loutridis S., Douka E. and Hadjileontiadis L.J., 2005. Forced vibration behaviour and crack detection of cracked beams using instantaneous frequency, *NDT & E International*, **38**(5), pp. 411-419.
 92. Patil D.P. and Maiti S.K., 2005. Experimental verification of a method of detection of multiple cracks in beams based on frequency measurements, *Journal of Sound and Vibration* **281**, pp. 439–451.
 93. Behzad, M., Meghdari, A., and Ebrahimi, A., 2005. A new approach for vibration analysis of a cracked beam. *International Journal of Engineering, Transactions B: Applications*, **18** (4), pp.319-330.
 94. Nahvi, H. and Jabbari, M., 2005. Crack detection in beams using experimental model data and finite element model,” *International Journal of Mechanical Sciences*, **47**(10), , pp.1477-1497.
 95. Leontios, H. J., Douka, E. and Trochidis, A., 2005. Crack detection in beams using Kurtosis, *Computers and structures*. **83**(12-13), pp.909-919.
 96. Mei, C., Karpenko, Y., Moody, S. and Allen, D., 2006. Analytical approach to free and forced vibrations of axially loaded cracked Timoshenko beams. *Journal of Sound and Vibration*. 291, pp. 1041-1060.
 97. Chasalevris, A. C. and Papadopoulos, C. A., 2006. Identification of multiple cracks in beams under bending, *Mechanical Systems and Signal Processing* **20**, pp.1631-1673.
 98. Loya, J.A., Rubio, L., and Fernandez, J., 2006. Natural frequencies for bending vibrations of timoshenko cracked beams. *Journal of Sound and Vibration*, **290** (3-5), pp. 640-653.
 99. Humar, J., Bagchi, A. and Xu, H., 2006. Performance of vibration based techniques for the identification of structural damage,” *structural health monitoring*, **5**(3), pp-215-241.

100. Shih, H.W., Thambiratnam, D.P. and Chan, T.H.T., 2007. Vibration based structural damage detection in flexural members using multi-criteria approach. *Journal of Sound and Vibration*. **328**, pp. 127-144.
101. Dash, P.K. and Chatterjee, A.K., 2004. Effect of Environment on Fracture Toughness of woven Carbon / Epoxy Composite, *Journal of the Institution of Engineers (I), Aerospace Division*, 35, pp. 16- 21.
102. Harsha, S.P. 2006. Nonlinear dynamic response of a balanced rotor supported by rolling element bearings due to radial internal clearance effect, *Mechanism and Machine Theory*, 41(6), pp. 688-706.
103. Panda, L. N. and Kar, R. C., 2007. Nonlinear dynamics of a pipe conveying pulsating fluid with parametric and internal resonances, *Nonlinear Dynamics*, 49(1-2), pp.9-30.
104. Hu, N., Fukunga, H., Kameyama, M., Mahapatra, D.R. and Gopalakrishnan, S., 2007. Analysis of Wave Propagation in Beams With Transverse and Lateral Cracks Using a Weakly Formulated Spectral Method. *Journal of Applied Mechanics*. **74**, pp.119-127.
105. Yang, J., Chen, Y., Xiang, Y. and Jia, X.L., 2007. Free and forced vibration of cracked inhomogeneous beams under an axial force and moving mass. *Journal of Sound and Vibration*. **312**, pp. 166-181.
106. Yoona, H., Sona, I. and Ahn, S., 2007. Free Vibration Analysis of Euler-Bernoulli beam with double Cracks, *Journal of Mechanical Science and Technology*, **21**, pp. 476-485.
107. Wang, J. and Qiao, P., 2007. Improved damage detection for beam-type structures using a uniform load surface. *Structural Health Monitoring*, **6**(2), pp. 99-110.
108. Lissenden, C. J., Tissot, S. P. M., Trethewey, W. and Maynard, K. P., **2007**. Torsion response of a cracked stainless steel shaft, *Fatigue & Fracture of Engineering Materials & Structures*, **30**(8), pp.734 – 747.
109. Al-Said, S. M., 2007. Crack identification in a stepped beam carrying a rigid disk, *Journal Sound and Vibration*, **300** (3), pp. 863-876.

110. Kisa, M. and Gurrel, A. M., 2007. Free vibration analysis of uniform and stepped cracked beams with circular cross sections,” *International Journal of Engineering Science*, **45**(2-8), pp. 364-380.
111. Karthikeyan, M., Tiwari, R. and Talukdar, S., 2007. Crack localization and sizing in a beam based on free and forced response measurements. *Journal of mechanical systems and signal processing*, **21**(3), pp.1362-1385.
112. Orhan, S., 2007. Analysis of free and forced vibration of a cracked cantilever beam, *NDT & E International*, **40** (6), pp. 443-450.
113. Darpe, A. K., 2007. A novel way to detect transverse surface crack in a rotating shaft, *Journal of sound and vibration*, **305** (1-2), pp. 151-171.
114. Voila, E., Dilena, M. and Tornabene, F., 2007. Analytical and Numerical Results for Vibration Analysis of multi-stepped and multi-damaged circular arches. *Journal of Sound and vibration*, **299**(1-2), pp. 143-163.
115. Sinha, J. K., 2007. Higher order spectra for crack and misalignment identification in the shaft of rotating machine. *Structural health Monitoring*, **6**(4), pp. 325-334.
116. Peng, Z. K., Lang , Z.Q and Billings, S.A. 2007. Crack detection using non linear output frequency response functions (NOFRFS). *Journal of sound and vibration*, **301** (3-5), pp.777-788.
117. Peng, Z.K., Lang, Z.Q., Billings , S.A. and Lu, Y. 2007. Analysis of bilinear oscillators under harmonic loading using nonlinear output frequency response functions. *International Journal of Mechanical Sciences*, **49**(11), pp.1213-1225.
118. Tandon, N., Yadava, G.S. and Ramkrishna, K.M., 2007. A comparison of some condition monitoring techniques for the detection of defect in induction motor ball bearing. *Mechanical system and signal processing*, **21**(1), pp.244-256.
119. Friswell, M. I., 2007. Damage identification using inverse methods. *Philosophical transactions of the royal society A: physical and engineering sciences*, **365**(1851), pp.393-410.
120. Yan, Y.J., Cheng, L., Wu, Z.Y. and Yam, H., 2007. Development in vibration-based structural damage detection technique. *Mechanical Systems and Signal Processing*, **21**(5), pp. 2198-2211.

121. Naniwadekar, M.R., Naik, S.S. and Maiti, S.K., 2008. On prediction of crack in different orientations in pipe using frequency based approach. *Mechanical Systems and Signal Processing*, **22**(3), pp. 693-708.
122. Trendafilova, I., Cartmell, M.P. and Ostachowicz, W., 2008. Vibration-based damage detection in an aircraft wing scaled model using principal component analysis and pattern recognition. *Journal of Sound and Vibration*, **313**, (3-5), pp. 560-566.
123. Courtney, Charles R.P., Drinkwater, Bruce W., Neild, Simon A. and Wilcox, Paul D., 2008. Factors affecting the ultrasonic intermodulation crack detection technique using bispectral analysis. *NDT & E International*, **41**(3), pp. 223-234.
124. Park, J., 2008. Identification of damage in beam structures using flexural wave propagation characteristics. *Journal of Sound and Vibration*. **318**, pp. 820-829.
125. Sekhar, A.S., 2008. Multiple cracks effects and identification. *Mechanical Systems and Signal Processing*. **22**, pp. 845-878.
126. Qiao, P. and Cao, M., 2008. Waveform fractal dimension for mode shape-based damage identification of beam-type structures. *International Journal of Solids and Structures*. **45**, pp. 5946-5961.
127. Li, J., Hua, H. and Shen, R., 2008. Dynamic Stiffness Analysis of a Beam Based on Trigonometric Shear Deformation Theory. *Journal of Vibration and Acoustic*, **130**, pp. 1-7.
128. Ostachowicz, W.M., 2008. Damage detection of structures using spectral finite element method. *Computers and Structures*. **86**, pp. 454-462.
129. Grabowska, J., Palacz, M., and Krawczuk, M., 2008. Damage identification by wavelet analysis. *Mechanical Systems and Signal Processing*. **22**, pp. 1623-1635.
130. Reddy, R. M., and Rao, B. N., 2008. Continuum Shape Sensitivity Analysis of Mixed-Mode Fracture Using Fractal Finite Element Method. *Engineering Fracture Mechanics*, **75**(10), pp. 2860-2906.
131. Hearndon, J.L., Potirniche, G.P., Parker, D., Wevas, P.M., Rinehart, H., Wang, P.T. and Meyer, M.F.H., 2008. Monitoring structural damage of components using an effective modulus approach. *Theoretical and applied fracture mechanics*, **50**, (01), pp.23-29.

132. Al-said, S. M., 2008. Crack detection in stepped beam carrying slowly moving mass. *Journal of sound and vibration*, **14**(12), pp.1903-1920.
133. Shin, Y., Kwon, K. and Yun, J., 2008. Vibration analysis of a circular arch with variable cross section using differential transformation and generalized differential quadrature. *Journal of Sound and Vibration*, **309**(1-2), pp. 9-19.
134. Cerri, M.N., Dilena, M., and Ruta, G.C., 2008. Vibration and damage detection in undamaged and cracked circular arches: Experimental and Analytical results. *Journal of sound and vibration*, **314**(1-2), pp.83-94.
135. Ebersbach, S., and Peng, Z., 2008. Expert system development for vibration analysis in machine condition monitoring. *Expert systems with Applications*, **34**(1), pp. 291-299.
136. Babu, T.R., and Sekhar, A.S., 2008. Detection of two cracks in a rotor-bearing system using amplitude deviation curve. *Journal of Sound and Vibration*, **314**(3-5), pp. 457-464.
137. Peng, Z.K., Lang, Z.Q. and Chu, F.L., 2008. Numerical analysis of cracked beams using nonlinear output frequency response functions. *Computers & Structures*, **86**(17-18), pp. 1809-1818.
138. Yaghin, M.A. L. and Hesari, M.A., 2008. Using Wavelet Analysis In Crack Detection at the arch Concrete Dam Under Frequency Analysis With FEM. *Journal of Wavelet Theory and Applications*, **2**(1), pp. 61–81.
139. Bayissa, N.L., Haritos, N. and Thelandersson, S., 2008. Vibration based structural damage identification using wavelet transform. *Mechanical systems and signal processing*, **22**(5), 2008, pp. 1194-1215.
140. Sukla, S., 2009. Free vibrations and stability of stepped columns with cracks. *Journal of Sound and Vibration*, **319**(3-5), pp. 1301-1311
141. Dilena, M. and Morassi, A., 2009. Structural health monitoring of rods based on natural frequency and antiresonant frequency measurements. *Structural health monitoring*, **8**(2), pp. 149-173.
142. Mazanoglu, K., Yesilyurt, I. and Sabuncu, M., 2009. Vibration analysis of multiple cracked non-uniform beams. *Journal of sound and vibration*. **320**(45), pp.977-989.

143. Lee, J. H., 2009. Identification of multiple cracks in a beam using natural frequencies. *Journal of sound and vibration*, **320**(3), pp. 482-490.
144. Faverjon, B. and Sinou, J.J., 2009. Identification of open crack in a beam using an a posteriori error estimator of the frequency response functions with noisy measurements. *European journal of machines*, **28**(1), pp.75-85.
145. He, Y., Ye, J., Chen, X. and He, Z., 2009. Discussion on calculation of local flexibility due to crack in a pipe. *Mechanical systems and signal processing*, **23**(3), pp. 804-810.
146. Douka, E., Bammios, G. and Trochidis, A., 2009. A method for determining the location and depth of cracks in double cracked beams. *Applied Acoustics*, **65**(10), pp.997-1008.
147. Labuschagne, A., Van Ren S burg, N.F.J. and Vander Merwe, A.J., Comparison of linear beam theories. *Mathematical and Computer Modelling*, **79**, pp. 20-30.
148. Gan, Z., Zhao, M. and Chow, T.W.S., 2009. Induction machine fault detection using clone selection programming. *Expert Systems with Applications*, **36**(4), pp. 8000-8012.
149. Ribeiro A.M.R., Maia N.M.M. and Silva J.M.M, 1999. Experimental evaluation of the transmissibility matrix, International modal analysis conference, No17, 3727 (2), pp-1126-1129.
150. Fontul, M., Ribeiro, A.M.R. and Silva, J.M.M., 2004. Transmissibility matrix in harmonic and random processes, Journal Shock and Vibration, 11(5-6), pp. 563-571.
151. John McCarthy., 1959. In *Mechanisation of Thought Processes, Proceedings of the Symposium of the National Physics Laboratory*, pp.77-84, London, U.K., Her Majesty's Stationery Office.
152. Zadeh L.A., 2001. A new direction in AI—Toward a computational theory of perceptions, *AI Magazine*, **22**(1), 73–84.
153. Negoită, C.V., 1973. On the application of the fuzzy sets separation theorem for automatic classification in information retrieval systems, *Information Sciences*, **5**pp. 279-286.
154. Kandel Abraham, 1973. Comment on an algorithm that generates fuzzy prime implicants by Lee and Chang , *Information and Control*, **22**(3)pp.279-282

155. Fox, J., 1977. Some observations on fuzzy diagnosis and medical computing. *International Journal of Bio-Medical Computing*, **8**(4), pp. 269-275.
156. Gologlu and Cevdet, 2004. Machine capability and fixturing constraints-imposed automatic machining set-ups generation, *Journal of Materials Processing Technology*, **48**(1), pp. 83-92.
157. Zimmermann, H. J., 1978. Fuzzy programming and linear programming with several objective functions. *Fuzzy Sets and Systems*, **1**(1), pp. 45-55.
158. Wada, K., Hayano, N. and Oka, H., 1991. Application of the fuzzy control method for level control of a hopper. *Advanced Powder Technology*, **2**(3), pp. 163-172.
159. Rao S.S. and Sawyer J.P., 1995. A fuzzy element approach for the analysis of imprecisely defined system. *AIAA Journal*, **33**(12), pp. 2364–2370.
160. Hanss, M. and Willner K., 2000. A fuzzy arithmetical approach to the solution of finite element problems with uncertain parameters. *Mechanics Research Communications*, **27**(3), pp. 257–272.
161. Boutros, T. and Liang, M., 2007. Mechanical fault detection using fuzzy index fusion. *International Journal of Machine Tools and Manufacture*, **47**(11), pp.1702-1714.
162. Akpan, U.O., Koko, T.S., Orisamolu, I.R., and Gallant, B.K., 2001. Fuzzy finite-element analysis of smart structures. *Smart Materials and Structures*, **10**, pp.273–284.
163. Skarlatos, D., Karakasis, K. and Trochidis, A., 2004. Railway wheel fault diagnosis using a fuzzy-logic method. *Applied Acoustics*, **65**(10), pp. 951-966.
164. Liu, Q., Chen, X. and Gindy, N., 2005. Fuzzy pattern recognition of AE signals for grinding burn. *International Journal of Machine Tools and Manufacture*, **45**(7-8),pp. 811-818.
165. Parhi, D.R., 2005. Navigation of mobile robot using a fuzzy logic controller, *Journal of Intelligent and Robotic Systems: Theory and Applications*, **42**, pp. 253-273.
166. Angelov, P. and Xydeas, C., 2006 Fuzzy Systems Design: Direct and Indirect Approaches, *Soft Computing*, special issue on New Trends in the Fuzzy Modelling part I: Novel Approaches, **10**(9), pp.836-849.
167. Loutas, T.H., Sotiriades, G., Kalaitzoglou, I. and Kostopoulos, V., 2009. Condition monitoring of a single-stage gearbox with artificially induced gear cracks utilizing

- on-line vibration and acoustic emission measurements. *Applied Acoustics*, **70**(9), pp. 1148-1159.
168. Saravanan, N., Cholairajan, S. and Ramachandran, K.I., 2009. Vibration-based fault diagnosis of spur bevel gear box using fuzzy technique. *Expert Systems with Applications*, **36**(2), Part 2, pp. 3119-3135.
 169. Chen, L. and Rao, S.S., 1997. Fuzzy finite-element approach for the vibration analysis of imprecisely-defined systems. *Finite Elements Analysis and Design*, **27**, pp.69–83.
 170. Pawar, P. M. and Ganguli, R., 2003. Genetic fuzzy system for damage detection in beams and helicopter rotor blades. *Computer Methods in Applied Mechanics and Engineering*, **92**(16-18), pp. 2031-2057.
 171. Taha, M.M. and Lucero, J., 2005. Damage identification for structural health monitoring using fuzzy pattern recognition. *Engineering Structures*, **27**(12), pp. 1774-1783.
 172. Packianather, M. S. and Drake, P. R. 2004. Modelling neural network performance through response surface methodology for classifying wood veneer defects. *Proceedings of Institution of Mechanical Engineers, Part B: Journal of Engineering, Manufacture*, 218 (4). pp. 459-466.
 173. Dwivedy, S.K. and Eberhard, P., 2006. Dynamic analysis of flexible manipulators, a literature review, *Mechanism and Machine Theory*, 41(7), pp. 749-777.
 174. Pawar, P.M., Reddy, K.V and Ganguli, R., 2007. Damage Detection in Beams using Spatial Fourier Analysis and Neural Networks. *Journal of Intelligent Material Systems and Structures*, **18**(4), pp. 347-360.
 175. Kim, Y. M., Kimand, C.K., Hong, G. H., 2007. Fuzzy set based crack diagnosis system for reinforced concrete structures. *Computers & Structures*, **85**(23-24), pp. 1828-1844.
 176. Sasmal, S. and Ramanjaneyulu, K., 2008. Condition evaluation of existing reinforced concrete bridges using fuzzy based analytic hierarchy approach. *Expert Systems with Applications*, **35**(3), pp. 1430-1443.

177. Chandrashekar, M. and Ganguli, R., 2009. Damage assessment of structures with uncertainty by using mode-shape curvatures and fuzzy logic. *Journal of Sound and Vibration*, **326**(3-5), pp. 939-957.
178. Zadeh, L., 1996. Fuzzy logic = computing with words, *IEEE Transactions on Fuzzy Systems* **4**(2) pp.103–111.
179. Pitts, W., 1943, A Logical Calculus of Ideas Immanent in Nervous Activity, In: *Bulletin of Mathematical Biophysics*, **5**, pp 115–133.
180. Hebb Donald, 1949. *The Organization of Behavior*, New York: Wiley, **4** pp.60-78.
181. Little, W. A. and Shaw, G. L., 1978. Analytic study of the memory storage capacity of a neural network. *Mathematical Biosciences*, **39**(3-4), pp. 281-290.
182. Urban, F. K., Park, D. C. and Tabet, M. F., 1992. Development of artificial neural networks for real time, in situ ellipsometry data reduction. *Thin Solid Films*, **220**(1-2), pp. 247-253.
183. Athanasiu, G., Pavlopoulos, P. and Vlachos, S., 1993. Real time track identification with artificial neural networks”, *Nuclear Instruments and Methods in Physics Research Section A: Accelerators, Spectrometers, Detectors and Associated Equipment*, **324**(1-2), pp. 320-329.
184. Hagan, M.T., Demuth, H.B. and Beale, M.H 1995, *Neural Network Design*, 1st edn, PWS Publications, Boston.
185. Sette, S., Luc, B. and Langenhove, Van., 1996. Optimising a production process by a neural network/genetic algorithm approach. *Engineering Applications of Artificial intelligence*. **9**(6), pp. 681-689.
186. Mohanty, K.K. and Majumdar, T. J., 1996. An artificial neural network (ANN) based software package for classification of remotely sensed data. *Computers & Geosciences*, **22**(1), pp. 81-87.
187. Taib, M. N., Andres, R. and Narayanaswamy, R., 1996. Extending the response range of an optical fibre pH sensor using an artificial neural network. *Analytica Chimica Acta*, **330**(1), pp. 31-40.
188. Kermanshahi, B., 1998. Recurrent neural network for forecasting next 10 years loads of nine Japanese utilities. *Neurocomputing*, **23**(1-3), pp. 125-133.

189. Haykin, S., 1999, *Neural Networks – A Comprehensive Foundation*, 2nd edn, Prentice-Hall Inc., USA.
190. Ghiassi, M., Saidane, H. and Zimbra, D.K., 2005. A dynamic artificial neural network model for forecasting time series events. *International Journal of Forecasting*, **21**(2), pp. 341-362.
191. Hines, J.W. and Uhrig, R.E., 2005. Trends in computational intelligence in nuclear engineering *Progress in Nuclear Energy*. **46**(3-4), pp. 167-175.
192. Song, J. H., Venkatesh, S. S., Conant, E. A., Arger, P. H. and Sehgal, C. M., 2005. Comparative analysis of logistic regression and artificial neural network for computer-aided diagnosis of breast masses. *Academic Radiology*, **12**(4), pp. 487-495.
193. Kadi, H. E., 2006. Modeling the mechanical behavior of fiber-reinforced polymeric composite materials using artificial neural networks—A review, *Composite Structures*, **73**(1), pp. 1-23.
194. Lucon, P.A. and Donovan, R. P., 2007. An artificial neural network approach to multiphase continua constitutive modeling. *Composites Part B: Engineering*, **38**(7-8) pp. 817-823.
195. Assaad, M., Boné, R. and Cardot, H., 2008. A new boosting algorithm for improved time-series forecasting with recurrent neural networks. *Information Fusion*, **9**(1), pp. 41-55.
196. Carbonneau, R., Laframboise, K. and Vahidov, R., 2008. Application of machine learning techniques for supply chain demand forecasting. *European Journal of Operational Research*, **184**(3), pp. 1140-1154.
197. Lolas, S. and Olatunbosun, O.A., 2008. Prediction of vehicle reliability performance using artificial neural networks. *Expert Systems with Applications*, **34**(4), pp. 2360-2369.
198. Ozerdem, M. S. and Kolukisa, S., 2009. Artificial neural network approach to predict the mechanical properties of Cu–Sn–Pb–Zn–Ni cast alloys. *Materials & Design*, **30**(3), pp.764-769.
199. Reddy, N.S., Krishnaiah, J., Hong, S. and Lee, J. S., 2009. Modeling medium carbon steels by using artificial neural networks. *Materials Science and Engineering: A*, **508**, (1-2), pp. 93-105.

200. Panigrahi, B.K. and Pandi, V. R., 2009. Congestion management using adaptive bacterial foraging algorithm, *Energy Conversion and Management*, **50**(5), pp.1202-1209.
201. Sun, Q., Nahon, M. and Sharf, I., 2000. An Inverse Dynamics Algorithm for Multiple Flexible-Link Manipulators, *Journal of Vibration and Control*, **6**(4), pp.557-569.
202. Uhrig, R. E., 1993. Use of neural networks in nuclear power plants. *ISA Transactions*, **32**(2), pp. 139-145.
203. Sreedhar, R., Fernandez, B. and Masada, G.Y., 1995. A neural network based adaptive fault detection scheme. *American Control Conference*, **5**, pp. 3259-3263.
204. Uhrig, R. E. and Tsoukalas, L. H., 1999. Soft computing technologies in nuclear engineering applications. *Progress in Nuclear Energy*, **34**(1), pp. 13-75.
205. Gao, X. Z. and Ovaska, S. J., 2002. "Genetic Algorithm Training of Elman Neural Network in Motor Fault Detection. *Neural computing and application*, **11**(1), pp. 37-44.
206. Ferentinos, K. P. and Albright, L. D., 2003. Fault Detection and Diagnosis in Deep-trough Hydroponics using Intelligent Computational Tools. *Biosystems Engineering*. **84**(1), pp. 13-30.
207. Samanta, B. K., Al-Balushi, R. and Al-Araimi, S. A., 2004. "Bearing Fault Detection Using Artificial Neural Networks and Genetic Algorithm. *EURASIP Journal on Applied Signal Processing*, **3**, pp. 366-377.
208. Fang, X., Luo, H., and Tang J., 2005. Structural damage detection using neural network with learning rate improvement, *Computers and structures*. **83**, no.(25-26), pp. 2150-2161.
209. Choi, S. and Li. C. J., 2006. Estimation of gear tooth transverse crack size from vibration by fusing selected gear condition indices. *Meas. Sci. Technol.* **17**, pp. 2395-2400.
210. Rajakarunakaran, S. P., Venkumar, Devaraj, D. and Rao, K. S. P., 2008, Artificial neural network approach for fault detection in rotary system, *Applied Soft Computing*, **8**(1), pp.740-748

211. Zhou, Z., Hu, C., Yang, J., Xu, D. and Zhou, D., 2009. Online updating belief rule based system for pipeline leak detection under expert intervention. *Expert Systems with Applications*, **36**(4), pp. 7700-7709.
212. Nishith V., Sanjeev, S. T. and Bhaskar D. K., 1997. Counterpropagation neural networks for fault detection and diagnosis, *Computers & Chemical Engineering*, **21**(2), pp. 177-185.
213. Stavroulakis, G. E. and Antes, H., 1998. Neural crack identification in steady state elastodynamics. *Computer Methods in Applied Mechanics and Engineering*, **165**(1-4), pp. 129-146.
214. Suh, M.W., Shim, M. B. and Kim, Crack, M. Y., 2000. Identification using hybrid neuro – genetic technique, *Journal of Sound and vibration*. **238**(4), pp.617-635.
215. Zubaydi, A., Haddara, M. R. and Swamidas, A. S. J., 2002. Damage identification in a ship's structure using neural networks. *Ocean Engineering*, **29**(10), pp. 1187-1200.
216. Kao, C.Y. and Hung, S.L., 2003. Detection of structural damage via free vibration responses generated by approximating artificial neural networks”, *Computers & Structures*, **81**(28-29),pp.631-2644.
217. Yam, L. H., Yan, Y. J. and Jiang, J. S., 2003. “Vibration-based damage detection for composite structures using wavelet transform and neural network identification *Composite Structures*, **60**(4), pp. 403-412.
218. Yam, L H., Yan, Y J., Cheng, L. and Jiang, J S., 2003. Identification of complex crack damage for honeycomb sandwich plate using wavelet analysis and neural networks, *Smart Mater. Struct.* **12**, 661-671.
219. Sahin, M. and Sheno, R.A., 2003. “Quantification and localisation of damage in beam-like structures by using artificial neural networks with experimental validation, *Engineering Structures*, **25**, pp.1785–1802.
220. Zacharias, J., Hartmann, C. and Delgado, A., 2004. Damage detection on crates of beverages by artificial neural networks trained with finite-element data. *Computer Methods in Applied Mechanics and Engineering*, **193**(6-8), pp. 561-574.
221. Suresh, S., Omkar, S.N., Ganguli, R. and Mani, V., 2004. Identification of crack location and depth in a cantilever beam using a modular neural network approach. *Smart Materials and Structures*, **13**(4), pp. 907-916.

222. Maity, D. and Saha, A., 2004. Damage assessment in structure from changes in static parameter using neural networks. *Sadhana*. **29**, pp. 315-327.
223. Lee, J. J., Lee, J. W., Yi, J. H., Yun, C. B. and Jung, H. Y., 2005. Neural networks-based damage detection for bridges considering errors in baseline finite element models. *Journal of Sound and Vibration*, **280**(3-5), pp. 555-578.
224. Yeung, W.T. and Smith, J.W. 2005. Damage detection in bridges using neural networks for pattern recognition of vibration signatures. *Engineering Structures*, **27**(5), pp. 685-698.
225. Li, H., He, C., Ji, J., Wang, H. and Hao, C., 2005. Crack Damage Detection in Beam-Like Structures using RBF Neural Networks with Experimental Validation. *International Journal of Innovative Computing, Information and Control*. **1**, pp. 625-634.
226. Hesheng, T., Songtao, X., Rong, C. and Yuangong, W., 2005. Analysis on structural Damage Identification Based on Combined Parameters. *Applied Mathematics and Mechanics*. **26**, pp. 44-51.
227. Choubey, A., Sehgal, D.K. and Tandon, N., 2006. Finite element analysis of vessels to study changes in natural frequencies due to cracks. *International Journal of Pressure Vessels and Piping*, **83**(3), pp. 181-187.
228. Li, C. J. and Lee, J. H., 2006. Non-contact rotating beam crack size estimation from vibro-acoustic signals. *Meas. Sci. Technol.* **17**, 1529-1536 .
229. Yu, L., Cheng, L., Yam, L.H., Yan, Y.J. and Jiang, J.S., 2007. Experimental validation of vibration-based damage detection for static laminated composite shells partially filled with fluid. *Composite Structures*, **79**(2), pp. 288-299.
230. Wang, B.S. and He, Z.C., 2007. Crack detection of arch dam using statistical neural network based on the reductions of natural frequencies. *Journal of Sound and Vibration*, **302**(4-5), pp.1037-1047.
231. Pawar, P.M., Reddy, K.V. and Ganguli, R., 2007. Damage Detection in Beams using Spatial Fourier Analysis and Neural Networks. *Journal of Intelligent Material Systems and Structures*. **1** pp. 347-359.
232. Reddy, K.V. and Ganguli, R., 2007. Fourier Analysis of Mode Shapes of Damaged Beams. *Computers, Materials and Continua*, **5**(2), pp. 79-98.

233. Bakhary, N., Hao, H. and Deeks, A.J., 2007. Damage detection using artificial neural network with consideration of uncertainties. *Engineering Structures*, **29**, pp. 2806-2815.
234. Jantunen, E., 2000 Flexible Hierarchical Neuro-Fuzzy System for Prognosis. Proceedings of COMADEM 2000, 13th *International Congress on Condition Monitoring and Diagnostic Engineering Management*. Houston, USA.pp.699-708
235. Ichihashi, H., Shirai, T., Nagasaka, K. and Miyoshi, T., 1996. Neuro-fuzzy ID3: a method of inducing fuzzy decision trees with linear programming for maximizing entropy and an algebraic method for incremental learning. *Fuzzy Sets and Systems*, **81**(1), pp. 157-167.
236. Wang, W. Q., Golnaraghi, M. F. and Ismail, F., 2004. Prognosis of machine health condition using neuro-fuzzy systems. *Mechanical Systems and Signal Processing*, **18**(4), pp. 813-831.
237. Singh, G. K. and Al Kazzaz, S. A. S., 2003. Induction machine drive condition monitoring and diagnostic research—a survey. *Electric Power Systems Research*, **64**(2), pp. 145-158.
238. Xu, Z.D., and Guo, Y.Q., 2008. Neuro-fuzzy control strategy for earthquake-excited nonlinear magnetorheological structures. *Soil Dynamics and Earthquake Engineering*, **28**(9), pp. 717-727.
239. Wang, W. and Kanneg, D., 2009. An integrated classifier for gear system monitoring. *Mechanical Systems and Signal Processing*, **23**(4), pp. 1298-1312.
240. Saridakis, K.M., Chasalevris, A.C., PapadoPoulos, C.A. and Dentsoras, A.J., 2008. Applying neural networks, Genetic algorithms and Fuzzy logic for the identification of cracks in shafts by using coupled response measurements. *Computer and Structures*, **86**(11-12), pp.1318-1338.
241. Rafiee, J., Tse, P.W., Harifi, A. and Sadeghi, M.H., 2009. A novel technique for selecting mother wavelet function using an intelligent fault diagnosis system. *Expert Systems with Applications*, **36**(3), Part 1, pp. 4862-4875.
242. Jovanovic, B.B., Reljin, I.S. and Reljin, B.D., 2004. Modified ANFIS architecture - improving efficiency of ANFIS technique, Fac. of Electr. Eng., Belgrade Univ.,

- Serbia; *Neural Network Applications in Electrical Engineering*, NEUREL 2004, pp. 215-220.
243. Jang, J.S.R. (1993) 'ANFIS: adaptive-network-based fuzzy inference systems', *IEEE Transactions on Systems, Man, and Cybernetics*, May, **23**(3) pp. 665-685.
 244. Chen De-wang and Zhang Jun-ping., 2005. Time series prediction based on ensemble ANFIS, *Proceedings of the Fourth International Conference on Machine Learning and Cybernetics*, Gangzhou pp. 18-21.
 245. Hinojosa J. and Doménech-Asensi G., 2007. Space-mapped neuro-fuzzy optimization for microwave device modeling, *Microwave and Optical Technology Letters*, **49**(6) pp.1328 – 1334.
 246. Jassar, S., Liao, Z. and Zhao, L., 2009. Adaptive neuro-fuzzy based inferential sensor model for estimating the average air temperature in space heating systems. *Building and Environment*, **44**(8), pp. 1609-1616.
 247. Domenech-Asensi, Hinojosa.G, Ruiz.J, Diaz-Madrid., .R.J.A., 2008 Accurate and reusable macromodeling technique using a fuzzy-logic approach, *Circuits and Systems*, ISCAS 2008. *IEEE International Symposium*, pp. 508-511.
 248. Zhang J., Dai, W., Fan, M., Chung, H., Wei, Z. and Bi.D., 2005. An Investigation into the Use of Delay Coordinate Embedding Technique with MIMO ANFIS for Nonlinear Prediction of Chaotic Signals Book: *Lecture notes on computer science*, Springer Berlin, **3614**, pp.677-688.
 249. Nguyen, N. and Lee, H., 2007. Bearing fault diagnosis using adaptive network based fuzzy inference system. *International Symposium on Electrical & Electronics Engineering*, pp. 280-285 .
 250. Elbaset, A. A. and Hiyama, T., 2009. Fault detection and classification in transmission lines using ANFIS. *IEEJ Transactions and Industry Applications*, **129**(7), pp.705-713.
 251. Ye, Z., Sadeghian, A., and Wu, B., 2006. Mechanical fault diagnostics for induction motor with variable speed drives using Adaptive Neuro-fuzzy Inference System. *Electric Power Systems Research*, **76**(9-10), pp. 742-752.
 252. Yeo, S. M., Kim, C. H., Hong, K. S., Lim, Y. B., Aggarwal, R. K., Johns, A. T. and Choi, M. S., 2003. A novel algorithm for fault classification in transmission lines

- using a combined adaptive network and fuzzy inference system. *International Journal of Electrical Power & Energy Systems*, **25**(9), pp. 747-758.
253. Sadeh, J. and Afradi, H., 2009. A new and accurate fault location algorithm for combined transmission lines using Adaptive Network-Based Fuzzy Inference System *Electric Power Systems Research*, **79**(11), pp. 1538-1545.
254. Razavi-Far, R., Davilu, H., Palade, V., Lucas, C., 2009. Model-based fault detection and isolation of a steam generator using neuro-fuzzy networks. *Neurocomputing*, **72**(13-15), pp. 2939-2951.
255. Tran, V. T., Yang, B., Oh, M. and Tan, A.C. C., 2009. Fault diagnosis of induction motor based on decision trees and adaptive neuro-fuzzy inference. *Expert Systems with Applications*, **36**(2), Part 1, pp.1840-1849.
256. Lei, Y., He, Z., Zi, Y. and Hu, Q., 2007. Fault diagnosis of rotating machinery based on multiple ANFIS combination with Gas. *Mechanical Systems and Signal Processing*. **21**(5), pp. 2280-2294.
257. Lei, Y., He, Z. and Zi, Y., 2008. A new approach to intelligent fault diagnosis of rotating machinery. *Expert Systems with Applications*, **35**(4), pp.1593-1600.
258. Takagi, T. and Sugeno, M., 1985. Fuzzy identification of systems and its application to modelling and control. *IEEE Trans. on Systems, Man, Cybernetics*. **15**(1), pp.116-132.

Published Papers

- Das H.C. and Parhi D.R., Modal analysis of vibrating structures impregnated with crack, *International Journal of Applied Mechanics & Engineering*, 13(3), 2008, 639-652.
- Parhi D.R. and Das H.C., Diagnosis of fault and condition monitoring of dynamic structures using MANFIS technique, *Journal of Aerospace Engineering Proceedings of the Institution of Mechanical Engineers, Part G* (Accepted for publication).
- Das H.C. and Parhi D.R., Damage Analysis of Cracked Structure Using Fuzzy Control Technique, *International Journal of Acoustics and Vibration*, 13(2) , 2008 , 3-14.
- Parhi D.R. and Das H.C., Structural damage detection by fuzzy- gaussian technique, *International Journal of Applied Mathematics and Mechanics*, 4(2), 2008, 39-59.
- Das H.C. and Parhi D.R., Identification of Crack Location and Intensity in a Cracked Beam by Fuzzy Reasoning, *International Journal of Intelligent Systems Technologies and Applications* (In Press).
- Das H.C. and Parhi D.R., Online fuzzy logic crack detection of a cantilever beam, *International Journal of Knowledge-Based and Intelligent Engineering Systems*, 12(2), 2008, 157-171.
- Parhi D.R. and Das H.C. Smart crack detection of a beam using fuzzy logic controller, *International Journal of Computational Intelligence: Theory and Practice*, 3(1), 2008, 9-21.
- Das H.C. and Parhi D.R., Detection of crack in cantilever structures using fuzzy-gaussian interface technique, *American Institute of Aeronautics and astronautics journal*, 47(1), 2009, 105-115.
- Das H.C. and Parhi D.R., Fuzzy-Neuro Controller for Smart Fault Detection of A Beam, *International Journal of Acoustics and Vibration*, 13(2), 2009, 55-66.
- Das H.C. and Parhi D.R., Application of Neural network for fault diagnosis of cracked cantilever beam, *IEEE International Symposium on Biologically Inspired Computing and Applications (BICA-2009)*, Bhubaneswar, India, December 21-22, 2009, 353-358.

MODAL ANALYSIS OF VIBRATING STRUCTURES IMPREGNATED WITH CRACK

HARISH CH. DAS*

Department of Mechanical Engineering
I.T.E.R, Bhubaneswar
Orissa, India, 751010
e-mail: harishdas1965@gmail.com

DAYAL R. PARHI

Department of Mechanical Engineering
N.I.T. Rourkela
Orissa, India, 769008
e-mail: dayalparhi@yahoo.com

In the current investigation a dynamic analysis of the cracked cantilever beam is carried out. Local flexibility is being introduced due to the presence of a crack in the structural member that affects its dynamic response. For finding out the deviation in mode shapes and natural frequencies of the cracked cantilever beam the local stiffness matrices are taken into account. Theoretical expressions have been developed to calculate the natural frequencies and mode shapes of the cracked cantilever beam using local stiffness matrices. The strain energy release rate has been used for calculating the local stiffnesses of the beam. Suitable boundary conditions are taken into account at the crack location. Comparisons made between the numerical results and the corresponding experimental results show very good agreement and authenticate the theory developed.

Key words: cantilever beam, vibration, crack, mode shape, natural frequency.

1. Introduction

Many researchers now are focusing on vibration characteristics of cracked beam structures. The most advance researches going on now on cracked structures are addressed below.

The natural frequencies for bending vibrations of Timoshenko cracked beams with simple boundary conditions have been obtained by Loya *et al.* (2006). The beam is modeled as two segments connected by two massless springs (one extensional and another one rotational). This model promotes discontinuities in both vertical displacement and rotation due to bending, which are proportional to shear force and bending moment transmitted by the cracked section, respectively. Their results show that their method provides simple expressions for the natural frequencies of cracked beams and it gives good results for shallow cracks. Karthikeyan *et al.* (2007) discussed a method of crack localization and sizing in a beam from the free and forced response measurements. Their method has been illustrated through numerical examples. Their prediction for the crack location and size are in agreement taking the noise and measurement error into account. Wang *et al.* (2006) showed that the local effect of softening at the crack location can be simulated by an equivalent spring connecting the two segments of the beam. This model uses the transfer matrix method in conjunction with the Bernoulli-Euler theories of beam vibration, modal analysis and fracture mechanics principle to derive a characteristic equation, which relates the natural frequencies. Their approach has been verified experimentally by taking one-side crack in a cantilever beam. A damage identification approach applied aptly in bridges and continuous beams, based on the curvature mode shapes, was studied

* To whom correspondence should be addressed

Diagnosis of fault and condition monitoring of dynamic structures using multiple adaptive-neuro-fuzzy inference system technique

DR K Parhi* and H Das

Mechanical Engineering Department, National Institute of Technology, Rourkela, Orissa, India

Q1

The manuscript was received on 27 May 2009 and was accepted after revision for publication on 15 September 2009.

DOI: 10.1243/09544100JAERO632

Abstract: Fault diagnosis and condition monitoring of dynamic structures are analysed and discussed in the current article. To diagnose the crack in the structure, the multiple adaptive-neuro-fuzzy inference system (MANFIS) methodology has been applied. The adaptive neuro-fuzzy controller has an input layer, hidden layers, and an output layer. The input layer is the fuzzy layer. The other layers are neural layers. The inputs to the fuzzy layer are relative deviation of the first three natural frequencies and relative values of percentage deviation for the first three mode shapes. The interim outputs of the fuzzy layer are inputs to the neural layers of the neuro-fuzzy controller. The final outputs of the MANFIS controller are relative crack depth and relative crack location. Several hundreds of fuzzy rules and neural network training patterns are derived using natural frequencies, mode shapes, crack depths, and crack locations. Real results have been obtained using the experimental setup. Comparison of the simulation and experimental results showed that there is good agreement between them. This methodology can be effectively used for condition monitoring of dynamic structures.

Q2

Keywords: fault, condition monitoring, multiple adaptive-neuro-fuzzy inference system, vibration

1 INTRODUCTION

Condition monitoring and crack identification in dynamic structures are key areas of engineering research. Scientist are focusing their attention and analysing various methodologies for fault identification and condition monitoring. Some of the recent efforts made by engineers for fault identification are described below.

Several researchers have used neural network technique for prediction of damage present in dynamic structures. Sahoo and Maity [1] have stated that artificial neural networks (ANN) can be used as an alternative effective tool for solving the inverse problems for damage assessment, because of their pattern-matching capability. They have stated that the results of ANN are quite encouraging and can be used as

Q3

a damage assessment algorithm. Chen *et al.* [2] in their article have studied Fault detection and diagnosis for railway track circuits using neuro-fuzzy systems. They have stated that their hybrid fault detection and diagnosis system combines the benefits of both fuzzy logic and neural networks. Akpan *et al.* [3] have proposed a fuzzy finite element approach for modelling smart structures with vague or imprecise uncertainties. Reddy and Ganguli [4] have used the neural network for fault detection of a helicopter blade. In their method, the radial basis function neural network has been used and several combinations of modes are investigated for training and testing the neural network. Tan *et al.* [5] have used a hybrid neural network model for rule generation and its application to process fault detection and diagnosis. Their hybrid neural network model is based on the integration of fuzzy ARTMAP (FAM) and the rectangular basis function network, which is capable of learning and revealing fuzzy rules. A damage detection algorithm has been developed by Sahin and Shenoj [6] using ANNs for prediction of the location and severity of damage in

Q4

Q5

*Corresponding author: Mechanical Engineering Department, National Institute of Technology, Rourkela, Orissa 769008, India. email: parhidr@yahoo.com

A Quarterly Publication of the IIAV

ISSN 1027-5851

International Journal of Acoustics and Vibration



- Damage Analysis of Cracked Structure Using Fuzzy Control Technique
- Optimum Design of Vibro-acoustic Systems using SEA
- Adaptive Disturbance Rejection and Stabilisation for Rotor Systems with Internal Damping
- Performance Measures of Comfort and Rattlespace Usage for Limited-Stroke Vehicle Suspension Systems

June 2008

Volume 13, Number 2

STRUCTURAL DAMAGE DETECTION BY FUZZY- GAUSSIAN TECHNIQUE

D. R. Parhi¹ and H. C. Das²

¹*Department of Mechanical Engineering, N.I.T. Rourkela, Orissa, India, 769008,
Email: dayalparhi@yahoo.com*

²*Department of Mechanical Engineering, I.T.E.R, Bhubaneswar, Orissa, India, 751010,*

Received 11 December 2007; accepted 3 March 2008

ABSTRACT

The method of detecting crack location and its intensity in beam structures by fuzzy logic techniques has been considered in this paper. The fuzzy logic controller used here comprises of six input parameters and two output parameters. Gaussian membership functions are used for the fuzzy controller. The input parameters to the fuzzy- Gaussian controller are relative deviation of first three natural frequencies and relative value of first three mode shapes percentage deviation. The output parameters of the fuzzy inference system are relative crack depth and relative crack location. At the beginning theoretical analyses have been outlined for cracked cantilever beam to calculate the vibration parameters such as natural frequencies and mode shapes. The local stiffnesses at the crack location are influenced by crack intensity and are calculated using strain energy release rate. A set of boundary conditions are considered involving the effect of crack location. A series of fuzzy rules are derived from vibration parameters which are finally used for prediction of crack location and its intensity. The proposed approach is verified by comparing with the results obtained from the developed experimental setup.

Key words: Vibration, crack, natural frequency, mode shape, fuzzy-gaussian controller.

NOMENCLATURE

a_1	= depth of crack
A	= cross-sectional area of the beam
A_i $i = 1$ to 12	= unknown coefficients of matrix A
B	= width of the beam
B_1	= vector of exciting motion
C_u	= $\left(\frac{E}{\rho}\right)^{1/2}$
C_y	= $\left(\frac{EI}{\mu}\right)^{1/2}$
E	= young's modulus of elasticity of the beam material
f_{md}	= relative first mode difference
f_{nf}	= relative first natural frequency
F_i $i = 1, 2$	= experimentally determined function

For readers

[Subscription](#)

[information](#)

[Order articles](#)

[Sample journals](#)

[Latest issues](#)

[Books](#)

[Published proceedings](#)

For authors

[Submission of papers](#)

[Notes for authors](#)

[Calls for papers](#)

Services

[Search](#)

[Newsletter](#)

[Blog](#)

[TOC alerts](#)

[RSS feeds](#)

[Twitter](#)

[OAI repository](#)

[Library form](#)

[Register with](#)

[Inderscience](#)

[Feedback](#)

Noticeboard

[New journals](#)

[Conference](#)

[announcements](#)

Researchers:

Please take this survey
about reference linking.

Start Survey ▶

Complete the survey
before October 31 and
enter draw for a Flip
Video recorder

Forthcoming Papers for IJISTA

This page lists papers submitted for IJISTA via the web that have been reviewed and accepted but not yet published. Please note: article title authors, abstracts and keywords may change upon publication.

Our TOC e-mail alerting service will notify you immediately when new issues of IJISTA are published on-line. [Click here](#) to register for our TOC E-Mail Alerting. We also offer the convenience of RSS feeds which provide a means to view new content timely posted to your web site or desktop. [Click here](#) to start to use our free RSS news feeds.

10 PAPERS IN PRESS:

Identification of Crack Location and Intensity in a Cracked Beam by Fuzzy Reasoning

by Harish Das, Dayal Parhi

Abstract: In this paper a soft-computing-fuzzy-logic approach for crack identification in cantilever beam has been considered. The fuzzy controller consists of six input parameters and two output parameters. The input parameters are first three relative natural frequencies and first three relative mode shape differences in dimensionless forms. The output parameters are relative crack location and relative crack depth. Theoretical analyses have been done including the effects of crack depths and crack locations on natural frequencies and mode shapes. Several fuzzy rules are outlined for the fuzzy controller. Gaussian membership functions are used for the fuzzy controller. The local stiffnesses at crack location of the beam have been calculated using strain energy release rate. The fuzzy rules are used to identify the location and depth of the crack. Finally the effectiveness of the developed fuzzy controller has been verified by results obtained from the developed experimental setup.

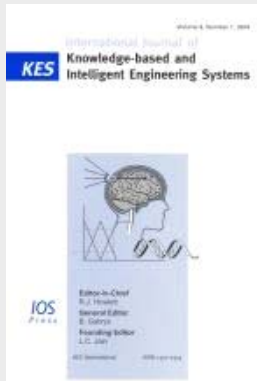
Keywords: beam, vibration, crack, natural frequency, strain energy, mode shape, fuzzy gaussian controller

The Design of H8 control methodology for Nonlinear Systems to Guarantee the Tracking Behavior in the Sense of Input-Output Spheres

by Shun-Min Wang

Abstract: A general nonlinear system usually contains some

Journal Article

6		<h3>Online fuzzy logic crack detection of a cantilever beam</h3>
Journal	International Journal of Knowledge-Based and Intelligent Engineering Systems	
Publisher	IOS Press	
ISSN	1327-2314 (Print) 1875-8827 (Online)	
Issue	Volume 12, Number 2 / 2008	
Pages	157-171	
Subject Group	Computer & Communication Sciences	
Pay-Per-View Copyright Statement		

1.3.1.1.1 Authors

Harish Ch. Das¹, Dayal R. Parhi²

¹Department of Mechanical Engineering, I.T.E.R, Bhubaneswar, Orissa, 751010, India

²Department of Mechanical Engineering, N.I.T. Rourkela, Orissa, 769008, India

1.3.1.1.2 Abstract

Premature failure of beam structure is observed due to presence of crack. In the current analysis a fuzzy inference system has been developed for detection of crack location and crack depth of a cracked cantilever beam structure. The six input parameters to the fuzzy membership functions are percentage deviation of first three natural frequencies and first three mode shapes of the cantilever beam. The two output parameters of the fuzzy inference system are relative crack depth and relative crack location. Strain energy release rate at the crack section of the beam has been used for calculating its local stiffnesses. Different boundary conditions for the cracked beam structure are outlined during theoretical analysis for deriving the vibration signatures (mode shapes and natural frequencies). These signatures are subsequently used for deriving the fuzzy rules. Several fuzzy rules are derived and the Fuzzy inference system has been designed accordingly. Experimental setup has been developed for verifying the robustness of the developed fuzzy inference system. The developed fuzzy inference system can predict the location and depth of the crack in a close proximity to the real results.

Smart Crack Detection of a Beam Using Fuzzy Logic Controller

Dayal R. Parhi, Harish Ch. Das

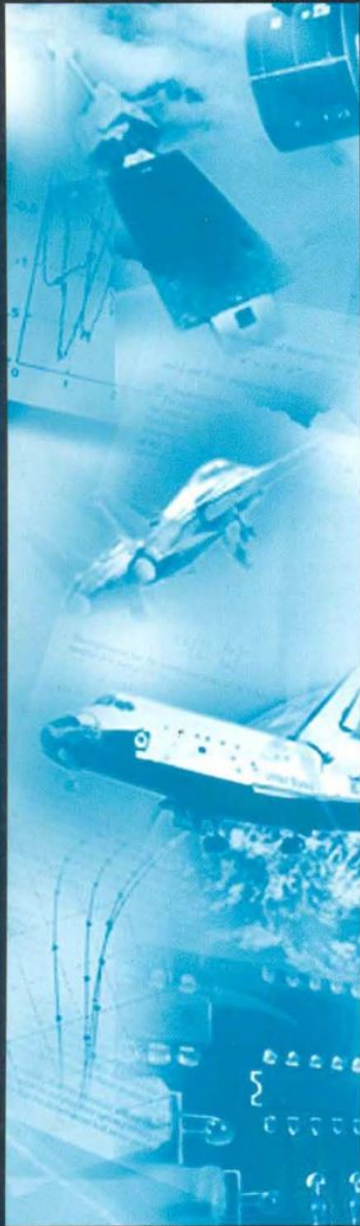
Abstract

Smart detection method to find out the fault in a cracked beam is addressed here. In the present investigation a fuzzy logic approach is used. In the fuzzy inference system six input parameters and two output parameters are used. The input parameters to the fuzzy membership functions are percentage deviation of first three natural frequencies and first three mode shapes. The output parameters of the fuzzy inference system are relative crack depth and relative crack location. For deriving the fuzzy rules for natural frequencies, mode shapes, crack depths and crack locations theoretical expressions have been developed. Strain energy release rate has been used for calculating the local stiffnesses of the beam. The local stiffnesses are dependent on the crack depth. Different boundary conditions are outlined which take into account the crack location. Several fuzzy rules are derived and the Fuzzy controller has been designed accordingly. An experimental setup has been developed for verifying the effectiveness of the developed fuzzy controller. The location and intensity of the crack can be predicted by the developed fuzzy inference system in a close proximity to the actual results.

AIAA JOURNAL

VOLUME 47, NUMBER 1

JANUARY 2009



Announcements, Comments, and Acknowledgments	E. Oran	1
Reviewers for 1 October 2007–30 September 2008		13
Editorial Policy Statement on Numerical and Experimental Accuracy		16
Ethical Standards for Publication of Aeronautics and Astronautics Research		17
AIAA Manuscript Review Process		18

AIRCRAFT TECHNOLOGY, CONVENTIONAL, STOL/VTOL

Detection of the Crack in Cantilever Structures Using Fuzzy Gaussian Inference Technique	H. C. Das and D. R. Parhi	105
Extremum-Seeking Control of Subsonic Cavity Flow	K. Kim, C. Kasnakoğlu, A. Serrani, M. Samimy	195

FLUID DYNAMICS

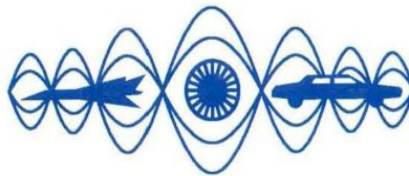
High-Resolution Reynolds-Averaged Navier–Stokes Flow Predictions over Axisymmetric Bodies with Tapered Tails	T. L. Jeans, G. D. Watt, A. G. Gerber, A. G. L. Holloway, C. R. Baker	19
Bluff Body Noise Control Using Perforated Fairings	K. Boorsma, X. Zhang, N. Molin, L. C. Chow	33
Evaluation of Euler Fluxes for Hypersonic Flow Computations	K. Kitamura, P. Roe, F. Ismail	44
Cross-Spectral Analysis of the Pressure in a Mach 0.85 Turbulent Jet	J. W. Hall, A. M. Hall, J. T. Pinier, M. N. Glauser	54
Geometric Installation and Deformation Effects in High-Lift Flows	J. W. van der Burg, H. F. von Geyr, R. Heinrich, P. Eliasson, T. Delille, J. Krier	60
Active Control of a High Reynolds Number Mach 0.9 Axisymmetric Jet	J.-H. Kim, J. Kastner, M. Samimy	116
Laplacian Equivalents to Subsonic Potential Flows	B. J. German	129
Direct and Large-Eddy Simulations of Merging in Corotating Vortex System	L. Nybelen and R. Paoli	157
Flow Separation Control by Plasma Actuator with Nanosecond Pulsed-Periodic Discharge	D. V. Roupassov, A. A. Nikipelov, M. M. Nudnova, A. Y. Starikovskii	168
Algorithm for the Nonlinear Propagation of Broadband Jet Noise	S. Saxena, P. J. Morris, K. Viswanathan	186

Table of Contents continued on back cover



A Publication of the American Institute of Aeronautics and Astronautics Devoted to Aerospace Research and Development
AIAJAH 47(1) 1–288 (2009)
ISSN 0001-1452

International Journal of Acoustics and Vibration



- **Noise and Blood Pressure: a Cross Sectional and Longitudinal Study of the Effects of Exposure to Loud Noise on Residents in Calabar, Cross River State, Nigeria**
- **Fuzzy-Neuro Controller for Smart Fault Detection of a Beam**
- **The application of Fault Simulation to Machine Diagnostics and Prognostics**
- **Source Identification and Noise Reduction of a Reciprocating Compressor; a Case History**
- **Gearbox Noise and Vibration Prediction and Control**

June 2009

Volume 14, Number 2

Application of Neural network for fault diagnosis of cracked cantilever beam

H.C. Das

Deptt. of Mechanical Engg.
I.T.E.R. Bhubaneswar, India
Harishdas1965@gmail.com

Dayal R. Parhi

Deptt. of Mechanical Engg.
N.I.T. Rourkela, India
dayalparhi@yahoo.com

Abstract— This paper discusses neural network technique for fault diagnosis of a cracked cantilever beam. In the neural network system there are six input parameters and two output parameters. The input parameters to the neural network are relative deviation of first three natural frequencies and first three mode shapes. The output parameters of the neural network system are relative crack depth and relative crack location. To calculate the effect of crack depths and crack locations on natural frequencies and mode shapes, theoretical expressions have been developed. Strain energy release rate at the crack section of the beam has been used for calculating the local stiffnesses of the beam. The local stiffnesses are dependent on the crack depth. Different boundary conditions are outlined which take into account the crack location. Several training patterns are derived and the Neural Network controller has been designed accordingly. Experimental setup has been developed for verifying the robustness of the developed neural network. The developed neural network system can predict the location and depth of the crack in a close proximity to the real results.

Keywords— crack, neural network, beam, vibration, strain energy, stiffness, stress intensity factor, natural frequency, mode shape

1. INTRODUCTION

Dynamics of structures with crack has been studied for last four decades intensively. Natural frequencies and modes shapes undergo variation due to presence of crack. The deviations of natural frequencies and modes shapes mainly dependant on location and intensity of the crack. Scientists are focusing their thoughts to find out the damage location and its intensity. The investigations reported in this regards are jotted below. Measurement of flexural vibrations of a rectangular cross-section cantilever beam having a transverse surface crack extending uniformly along the width of the beam and analytical results are used to relate the measured vibration modes to the crack location and depth [1]. From the measured amplitudes at two points of the structure vibrating at one of its natural modes, the respective vibration frequency and an analytical solution of the dynamic response, the crack location can be found and depth can be estimated with satisfactory accuracy. The method of crack localization and sizing in a beam can be obtained from free and forced response measurements [2]. This method has been illustrated through numerical examples. An iterative algorithm is used to identify the

locations and extent of damage in beams using only the changes in their first several natural frequencies [3]. A method using singular value decomposition is developed to handle the ill-conditioned system equations that occur in the experimental investigation by using the measured natural frequencies of the modified structure. An extensive study has been done on diagnosis of fracture damage in structure [4]. The concept of 'fracture hinge' is developed analytically and the same is applied to a cracked section for detecting fracture damage in simple structures. It is experimentally verified that the structural effect of a cracked section can be represented by an equivalent spring loaded hinge.

A nondestructive evaluation procedure is presented for identifying a crack in a structure using modal test data. [5]. The structure is discretized into a set of elements and the crack is assumed to be located within one of the elements. Measured vibration frequencies and mode shapes are used in an identification process to identify the cracked element based on a simple reduced stiffness model. A simple model is proposed that describes the flexural vibration characteristics of a rotating cracked Timoshenko beam [6]. The cracked beam is modeled using two uniform segments connected by a mass less torsional spring at the crack location. The proposed method is verified by finite element analysis. An experimental investigation of the identification of crack location and size has been carried out [7]. By providing the first three natural frequencies through vibration measurements, curves of crack equivalent stiffness versus crack location are plotted, and the intersection of the three curves predicts the crack location and size. Curvature mode shape can be used as a possible candidate for identifying and locating damage in a structure [8]. By using a cantilever and a simply supported analytical beam model, it is shown that absolute changes in the curvature mode shapes are localized in the region of damage and hence can be used to detect damage in a structure.

Artificial neural networks (ANN) can be used as an alternative effective tool for solving the inverse problems because of the pattern-matching capability [9]. The results of ANN are quite encouraging and prove the robustness of the proposed damage assessment algorithm. An artificial neural network-based model has been developed for the fault detection of centrifugal pumping system [10]. The fault detection model is developed by using two different artificial neural network approaches, namely feed forward network with back propagation algorithm and binary adaptive resonance network (ART1). The performance of the developed back propagation and ART1 model is tested for a total of seven categories of faults in the centrifugal pumping system. The modal frequency parameters for the